

**Experimental and computational study of  
indirect expansion solar assisted heat pump  
system with latent heat storage for domestic hot  
water production**

**A thesis submitted for the degree of  
Doctor of Philosophy (PhD)**

**by**

**Walid Mohamed Khalil Abdalla Youssef**

**College of Engineering, Design, and Physical Sciences**

**Brunel University London**



## ***Abstract***

Solar assisted heat pump (SAHP) systems have been widely applied in domestic hot water (DHW) production due to their sustainability and stability in operations. However, their performance efficiency requires further improvement using advanced technologies such as energy storage with phase change materials (PCM) and optimal system controls. Undoubtedly, employing PCMs for latent heat storage (LHS) application has a great potential to improve a solar thermal application performance. Despite this fact, the use of PCM in this area is quite limited due to the poor thermal conductivity of available PCMs. Therefore, heat transfer enhancement is one of the essential strategies that can overcome this obstacle. Accordingly, a test rig of a new indirect expansion solar assisted heat pump (IDX-SAHP) system has been designed, built and instrumented. The system can handle heating capacity up to 9 kW. The IDX-SAHP system consists of three operational loops: solar thermal, solar-air assisted heat pump and load profile. A 2 kW PCM heat exchanger (HX) was purposely designed and installed in the system solar thermal loop to store solar energy, when applicable, and release heat when required by the heat pump. The PCM HX is employed with a novel heat transfer enhancement method. The maximum coefficient of performance (COP) of the IDX-SHAP system reached 4.99 during the sunny day with the PCM (HX) integration. However, the maximum energy saving was achieved during the cloudy day with the PCM HX integration. Moreover, the proposed heat transfer enhancement method has been modelled through CFD package and validated with the experimental results. This allows a clear understanding of the reasons for the longer discharging process compared with the charging process. Furthermore, the inlet flow rate and temperature variation of the PCM HX was simulated during charging and discharging processes. The optimum inlet flow rate for this application was found at 0.1 kg/s while the optimum inlet temperature was found at 40°C. Meanwhile, the whole system was modelled by the coupling of TRNSYS, EES and CFD to investigate the potential and advantages of using the system in locations with rich solar intensity such as Cairo and Madrid. The simulation shows that the solar thermal operation loop was called more frequently in these locations. This had a significant impact on the system energy consumption, especially during winter. The maximum COP and solar performance factor (SPF) of the modelled system were 5.3 and 0.83 respectively.

## *Acknowledgements*

I would like to express my appreciation and gratitude to my supervisors, Dr Yunting Ge and Professor Savvas Tassou, for allowing me to work on this project, and for extending and guiding my potential; both intellectually and tactfully. I was blessed to have their support and encouragement during my PhD research.

I also would like to extend my appreciation to Centre for Sustainable Energy Use in Food Chains (CSEF) – Brunel University, Tridium Europe, Spirotech b.v and Kingspan UK for their contribution with the necessary material and equipment for my research. I am also to thank Brunel University Technician team; Costa Xantho, Eamon Wyse, John Fosbery and Guy Fitch for their support and help in my experimental study.

I would like to thank CSEF members; Dr Konstantinos Tsamos, Dimitri Parpa, Hassan Moure, Thiago Santos and Maureen Senatore for being always side by side. Special thanks to my dear friend Dr Evangelia Topriskas who was always there for me whenever needed.

A very special thanks to my father Mohamed Khalil for his moral, emotional and financial support. Also, I could not achieve what I have reached now without the support of my mother's Zanoouba and my sisters' Nashwa and Nehal.

Finally, I would like to thank my wife Dr Kalliopi Koutsou from the deepest of my heart for her unlimited support all the way. I would like to award this success I have achieved to my future baby who will light our life in October 2017.

# *Contents*

<b>Chapter 1. Introduction.....</b>	<b>1</b>
1.1. Research motivation.....	2
1.2. Objective of the research.....	5
1.3. Thesis structure .....	5
1.4. Publication .....	8
<b>Chapter 2. Background Information .....</b>	<b>10</b>
2.1. Introduction .....	11
2.2. Domestic water heating.....	11
2.3. Heat pumps .....	12
2.4. Solar assisted heat pumps .....	14
2.5. SAHP Control strategies .....	20
2.6. Phase change materials .....	21
2.7. The use of PCM in solar and heat pump systems .....	26
2.8. Summary of Chapter 2 .....	28
<b>Chapter 3. Experimental Components and Processes.....</b>	<b>29</b>
3.1. Introduction .....	30
3.2. Experiment setup and test rig components.....	30
3.3. Instrumentation .....	46
3.4. Phase change material heat exchanger.....	49
3.5. Control strategy.....	53
3.6. Building management system .....	56
3.7. Logic block connection graphics design .....	63
3.8. Summary of Chapter 3 .....	64
<b>Chapter 4. Experimental Findings and Analysis .....</b>	<b>65</b>
4.1. Introduction .....	66
4.2. Start-up measurements and procedure .....	66



4.3.	Thermodynamic analysis .....	69
4.4.	Experiment finding and discussion .....	70
4.5.	Uncertainty analysis .....	78
4.6.	Summary of Chapter 4 .....	79
	<b>Chapter 5. Numerical Model Development .....</b>	<b>80</b>
5.1.	Introduction .....	81
5.2.	Introduction to numerical simulation .....	81
5.3.	Model development strategy .....	82
5.4.	Numerical model validation .....	97
5.5.	Summary of Chapter 5 .....	102
	<b>Chapter 6. Analysis of Numerical Model.....</b>	<b>103</b>
6.1.	Introduction .....	104
6.2.	PCM model applications .....	104
6.3.	Coupled model case studies .....	115
6.4.	Summary of Chapter 6 .....	122
	<b>Chapter 7. Conclusion and Further Recommendation .....</b>	<b>123</b>
7.1.	Concluding remarks .....	126
7.2.	Recommendation and further work.....	129
	<b>References .....</b>	<b>130</b>
	<b>Appendices.....</b>	<b>141</b>
	Appendix A .....	142
	Appendix B.....	152
	Appendix C.....	156
	Appendix D .....	160
	Appendix E.....	163
	Appendix F.....	165

## *List of figures*

Figure 1.1. left – CO <sub>2</sub> emission by energy use, Right – DEC by Fuel (BEIS, 2017a)	3
Figure 1.2. System boundaries for solar heat pump (SHP) system in heating mode (D’Antoni, Fedrizzi and Sparber, 2012)	4
Figure 1.3. Research methodology diagram.	7
Figure 2.1. Daily DHW profile (Energy Savings Trust, 2008)	12
Figure 2.2. Sales of the domestic applications in the UK(Dawson, 2012)	13
Figure 2.3. P-h diagram for ideal vapour compression cycle - modified from (Wang, 2000)	14
Figure 2.4. Schematic diagram of the DX-SAHP system (Kong et al., 2011)	16
Figure 2.5. Schematic diagram of parallel SAHP (a. DHW, b. Space heating)(Chu and Cruickshank, 2013)	17
Figure 2.6. Schematic diagram of a dual SAHP for space heating (Chu and Cruickshank, 2013)	17
Figure 2.7. Schematic diagram of series SAHP (a. DHW, b. Space heating)(Chu and Cruickshank, 2013)	18
Figure 2.8. Schematic diagram of Chow et al (Chow et al., 2012)	20
Figure 2.9. The operation modes developed by Yang and Wang (Yang and Wang, 2012)	21
Figure 2.10. PCM classifications [modified from (Abhat, 1983; Zalba et al., 2003)]	23
Figure 2.11. Schematic drawings of three different dual-tank latent heat storage system configurations (Qu et al., 2015).	27
Figure 3.1. Test rig Schematic layout	31

Figure 3.2. Test rig Brunel University TB104 .....	32
Figure 3.3. Heat source loop .....	33
Figure 3.4. Evacuated Tube Collector.....	34
Figure 3.5. Deaerator set up (Left) and interiors / 3D cross section (Right).....	34
Figure 3.6. Air-water Fan HX (Left) and 3-way valve (right) .....	35
Figure 3.7. selected expansion tank (Left) and expansion tank cross-section (Right) .....	36
Figure 3.8. Solar/heat source circulation pump .....	37
Figure 3.9. Heat pump loop.....	38
Figure 3.10. compressor installation (left), starting capacitor and adjustable pressure switch (right) .....	39
Figure 3.11. Evaporator and condenser HX – Preinstalled (left) and installed (right) .....	39
Figure 3.12. Actual TXV (left) and TXV cross-section (right) .....	40
Figure 3.13. Heat sink loop .....	41
Figure 3.14. WST .....	42
Figure 3.15. Load simulation loop .....	43
Figure 3.16. Fan assisted air cooler.....	44
Figure 3.17. Motor driven pump with a digital inverter .....	44
Figure 3.18. Direct solar loop .....	45
Figure 3.19. thermistor (temperature sensor) type 10K .....	46
Figure 3.20. Pressure transmitter .....	47

Figure 3.21. pulsed screwed flow meter .....	47
Figure 3.22. Pyranometer (irradiance meter) and signal amplifier .....	48
Figure 3.23. Copper Spiral pipe .....	51
Figure 3.24. 3D drawing in mm for PCM HX – Isometric (left) – front (middle) – top and bottom (right) .....	52
Figure 3.25. PCM HX design process.....	53
Figure 3.26. Flowchart of system control strategy.....	55
Figure 3.27. BMS control box before wiring (left) and after wiring (right) .....	58
Figure 3.28. Resistance temperature calibration curve .....	59
Figure 3.29. Pressure -Voltage Calibration.....	59
Figure 3.30. flow rate calibration.....	60
Figure 3.31. load voltage profile .....	61
Figure 3.32. writeable schedule function for load voltage profile .....	62
Figure 3.33. Load simulation pump and fan cooler block connection.....	62
Figure 3.34. Control logic block connection.....	63
Figure 4.1. Variations of solar irradiances during four test days 4.....	67
Figure 4.2. Variations of ambient and feed water temperatures during two sunny test days 5 .....	67
Figure 4.3. Variations of ambient and feed water temperatures during two cloudy test days 6 .....	68
Figure 4.4. Variations of load profiles during all four test days 7 .....	69

Figure 4.5. Variations of WST water temperatures and temperature T4 during two sunny test days 8 .....	70
Figure 4.6. Variations of WST water temperatures and temperature T4 during two cloudy test days 9 .....	71
Figure 4.7. Variations of PCM HX inside temperatures during two test days 10.....	72
Figure 4.8. Variations of system power consumption during four test days 11.....	72
Figure 4.9. Variations of system heating capacities during four test days 12.....	73
Figure 4.10. Variations of system COPs during four test days 13.....	74
Figure 4.11. Variations of compressor and AWHX fan control signals during two sunny test days 14 .....	75
Figure 4.12. Variations of compressor and AWHX fan control signals during two cloudy test days 15 .....	76
Figure 5.1. Graphical model for the proposed test rig .....	83
Figure 5.2. Energy balance of each node in the thermal storage tank (modified from (Klein et al., 2014)) .....	84
Figure 5.3. Controller Function (Klein et al., 2014) .....	85
Figure 5.4. Heat pump performance curves .....	87
Figure 5.5. PCM HX sections assumption .....	89
Figure 5.6. spiral tube element analysis .....	90
Figure 5.7. PCM HX numerical model development .....	92
Figure 5.8. Mesh Comparison of PCM HX horizontal cross-section - coarse and fine, respectively .....	93
Figure 5.9. PCM HX Model Validation for discharging process .....	94

Figure 5.10 PCM HX Model Validation for charging process .....	95
Figure 5.11. Simulation coupling process diagram.....	97
Figure 5.12. Tank temperatures (Top-Mid-Bottom) validation with experimental results .....	98
Figure 5.13. Source temperature validation with experimental results.....	99
Figure 5.14. Heating Capacity validation with experimental results .....	100
Figure 5.15. COP validation with experimental results .....	101
Figure 6.1. Mass fraction, Temperature and total energy at the middle of operation – a) charging.....	105
Figure 6.2. PCM discharging - the temperature at the middle of PCM HX for fixed inlet temperature (10°C) and different flow rates. ....	110
Figure 6.3. PCM discharging - mass fraction at the middle of PCM HX for fixed inlet temperature (10°C) and different flow rates. ....	110
Figure 6.4. PCM charging- temperature at the middle of PCM HX for fixed inlet temperature (40°C) and different flow rates. ....	111
Figure 6.5. PCM charging – mass fraction at the middle of PCM HX for fixed inlet temperature (40°C) and different flow rates. ....	111
Figure 6.6. PCM discharging - the temperature at the middle of PCM HX for fixed inlet flow rate (0.1 kg/s) and different inlet temperature. ....	112
Figure 6.7. PCM discharging – mass fraction at the middle of PCM HX for fixed inlet flow rate (0.1 kg/s) and different inlet temperature. ....	113
Figure 6.8. PCM charging - temperature at the middle of PCM HX for fixed inlet flow rate (0.1 kg/s) and different inlet temperature.....	113
Figure 6.9. PCM charging – mass fraction at the middle of PCM HX for fixed inlet flow rate (0.1 kg/s) and different inlet temperature. ....	114

Figure 6.10. Typical irradiance during day in Cairo and Madrid for summer and winter .....	116
Figure 6.11. Typical ambient temperature during day in Cairo and Madrid for summer and winter.....	116
Figure 6.12. Variation WST water temperature during summer and winter in Cairo. ....	117
Figure 6.13. Variation WST water temperature during summer and winter in Madrid. ....	117
Figure 6.14. PCM HX inside temperature during summer and winter in Cairo and Madrid.....	118
Figure 6.15. System power consumption during summer and winter in Cairo and Madrid.....	119
Figure 6.16. System COP and SPF during summer and winter in Cairo.....	120
Figure 6.17. System COP and SPF during summer and winter in Madrid .....	121

### **In Appendices**

App-Fig 1. Evacuated tube collector heat pipe and manifold.....	142
App-Fig 2. Heat pipe details of single evacuated tube.....	142
App-Fig 3. Heat pipe collector efficiency by the manufacture .....	142
App-Fig 4. WST dimensions (in mm) and configuration .....	144
App-Fig 5. a quote of the required components to refurbishment the heat pump ..	148
App-Fig 6. App-Fig 5. a quote of another AWHX .....	149
App-Fig 7. Initial quote of the purchased AWHX (page 1).....	150

App-Fig 8. Initial quote of the purchased AWHX (page 2).....	151
App-Fig 9. NTC Thermistor tolerance.....	152
App-Fig 10. Flow meter dimension .....	154
App-Fig 11. Flow meter pressure loss (bar).....	154
App-Fig 12. Flow meter error margin.....	154
App-Fig 13. PCM A16 temporal variation during melting/solidification cycle .....	156
App-Fig 14. PCM A16 phase change cycle .....	156
App-Fig 15. PCM A16 properties .....	157
App-Fig 16. Copy of Heat transfer enhancement design report (page 1) .....	158
App-Fig 17. Copy of heat transfer enhancement design report (page 2) .....	159
App-Fig 18. JACE-NDIO layout .....	160
App-Fig 19. Earthling connection for the control box.....	161
App-Fig 20. Thermistor input connection diagram.....	161
App-Fig 21. 0-10 voltage input connection diagram .....	162
App-Fig 22. Digital output connection diagram .....	162
App-Fig 23. Analogue output connection diagram.....	162
App-Fig 24. Print screen of the error set up in EES.....	163
App-Fig 25. Print screen of the uncertainty analysis results in EES .....	164



## ***List of Tables***

Table 1. components list .....	32
Table 2. Instruments types, operation range and accuracy .....	49
Table 3. PCM-A16 properties .....	49
Table 4. Proxy Point setting for flow meter .....	60
Table 5. Proxy point setting for Pyranometer .....	60
Table 6. System Performance for the four test days .....	78
Table 7. Mesh selection - coarse and fine .....	93
Table 8. Charging temperature (°C) timeline at flow rate 0.1 kg/s.....	107
Table 9. Discharging temperature (°C) timeline at flow rate 0.1 kg/s .....	108
Table 10. System Performance for the simulated days .....	121

## **In Appendices**

App-Tab 1. The proposed solar collector specifications (marked in red).....	143
App-Tab 2 the water-glycol properties used in the source load, heat sink loop and direct solar loop.....	145
App-Tab 3. Pressure Transmitter Specifications .....	153
App-Tab 4. pressure transmitter operation range.....	153
App-Tab 5. Sensitivity of the Pyranometer.....	155
App-Tab 6. Control box configuration.....	160

### *Abbreviations*

AWHX	Air-water heat exchanger
BMS	Building management system
BTES	Borehole thermal energy storage
CFD	Computational fluid dynamics
COP	Coefficient of performance
DC	Direct current
DEC	Domestic energy consumption
DHW	Domestic hot water
DX	Direct expansion
EES	Engineering equation solver
EST	Energy saving trust
HTF	Heat transfer fluid
HVAC	Heating, ventilation and air-conditioning
HX	Heat exchanger
IDX	Indirect expansion
IP	Internet protocol
LAN	Local area network
NTC	Negative temperature coefficient
PCM	Phase change material
PVC	Poly (vinyl chloride)
SAHP	Solar assisted heat pump
SHP	Solar heat pump
SPF	Solar performance factor

TES	Thermal energy storage
TRNSYS	Transient system simulation tool
TXV	Thermal expansion valve
UK	United Kingdom
WST	Water storage tank

*List of Symbols*

A	Area	(m <sup>2</sup> )
C <sub>p</sub>	Specific heat	(kJ/kg.k)
E	Voltage	(V)
f	Friction factor	
h	Enthalpy	(kJ/kg)
$\bar{h}$	Convection heat transfer coefficient	(W/m <sup>2</sup> .k)
k	Thermal conductivity	(W/m.k)
l	Latent heat	(kJ/kg)
L	Total length of the spiral tubes	(m)
l <sub>mtd</sub>	Logarithmic mean temperature difference	(°C)
m <sup>·</sup>	Flow rate	(kg/s)
m	Mass	(kg)
Nu	Nusselt number	
P	Pressure	(pa)
Pr	Prandtl number	
$\dot{Q}$	Capacity	(kW)
r	Radius	(m)

Re	Reynolds number	
S	Shape factor	
T	Temperature	(°C)
t	Time	(sec)
U	The overall heat transfer coefficient	(W/m <sup>2</sup> K)
V	Volume	(m <sup>3</sup> )
$\dot{W}$	Power consumption	(kW)
w	Width	(m)
x	Length	(m)
$\beta$	Thermal expansion	(K <sup>-1</sup> )
$\gamma$	Control signal	
$\Delta$	Change	

### *Subscripts*

awhx	Air-water heat exchanger
c	Cross section
C	Copper
coll	Collector
comp	Compressor
D	Radial
env	Environmental
evap	Evaporating
h	Heating
H	Upper band

hx	Heat exchanger
i	Inner / Node number
in	Inlet
L	Lower band
o	Outer
out	Outlet
pcm	Phase change material
pum	Pumps
ref	Refrigerant
s	Surface
sol	Solar
sys	System
w	Water

---

*Chapter 1. Introduction*

---

### ***1.1. Research motivation***

In the United Kingdom (UK), up to 29% of total energy consumption is caused by the domestic sector. Mainly, the biggest portion of this energy is consumed by space and water heating purposes by direct burning of fossil fuels, in particular, natural gas (BEIS, 2017b). The extensive consumption of fossil fuels or natural gas has caused significant atmospheric pollution, global warming, rising energy costs and threatens future energy shortage. In such circumstances, meeting CO<sub>2</sub> emission reduction targets remain a challenge for the country, if alternative energy resources or technologies cannot be applied for heating. Moreover, running out of non-renewable energy sets a solar thermal system one of the most important applications for producing DHW and space heating nowadays. The world recent trends on energy consumption and CO<sub>2</sub> have raised by 49% and 43% respectively, during the last decades. Social activities and life routine of nations play a significant role in their energy consumption. For example, developed nations such as; Japan, America and Western European have a rise in the energy consumption rate of 1.1%. On the other hand, growing countries such as the Middle East and Africa have a rise of the energy consumption rate of 3.2% (IEA, 2016). This increase of the fossil fuel consumption has seriously affected the energy supply chain. It also has an environmental impact on the nation by increasing its CO<sub>2</sub> emission (Waters, Wilkes and Goodright, 2015).

In the Europe, Building sector consumes nearly 40% of the energy consumption and it is in charge of the same percentage of CO<sub>2</sub> emissions. Mainly, HVAC (heating, ventilation and air-conditioning) systems, lighting and appliances consume nearly 60%, 15% and 10% respectively of this portion. Therefore, developing optimising HVAC systems and water heating systems will significantly achieve noticeable savings in the energy consumption (IEA, 2016). In the UK, up to 15 % of the total CO<sub>2</sub> emission was produced by domestic heat. Three-quarter of this percentage was mainly produced by homes that use direct emission heating application. This is because almost three-quarters of domestic energy consumption (DEC) in the UK is produced by gas as shown in Figure 1.1 (The CCC, 2016) (BEIS, 2017b).

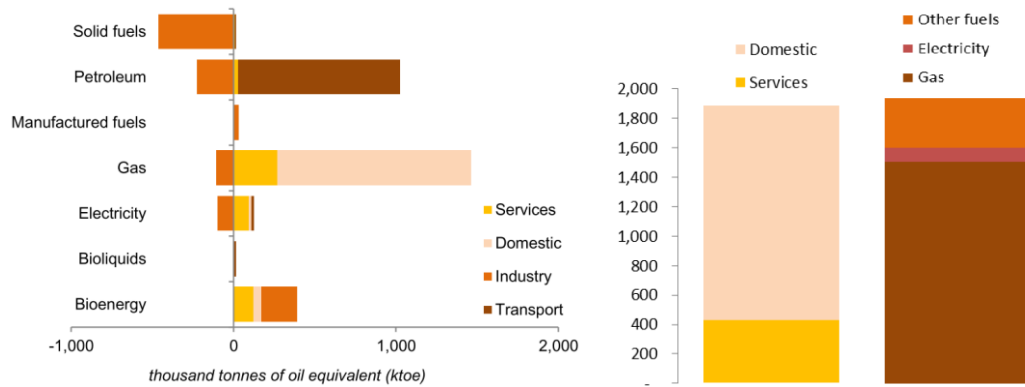


Figure 1.1. left – CO<sub>2</sub> emission by energy use, Right – DEC by Fuel (BEIS, 2017a)

The heating demand can be met by green technologies and advanced systems such as a solar thermal, air-water heat pump, geothermal heat pump and their integration. Solar domestic water heaters (SDWHs) have been increasing in popularity in the UK and other countries worldwide and can greatly save energy for water heating in the summer since the 90s (Freeman, 1997). However, the large temperature difference between the solar collector and ambient temperatures during winter has greatly reduced system performance that assistant heaters such as gas, wood boilers or electric heaters must be added (Weiss, 2003) (Ayompe *et al.*, 2011). The air source heat pump water heaters are compact, simpler and economic but also work less efficiently over the cold winter period (Aguilar, White and Ryan, 2005). These situations may be improved with the integration of geothermal heat sources, as heat is being drawn from the warmer earth in winter. However, the high capital costs and property alterations expected for these geothermal heat pumps make them less attractive for existing homes (Aguilar, White and Ryan, 2005). Of these alternative substitutes, a SAHP (SAHP) system has been deemed the more feasible option when taking into consideration important factors such as cost, application area limitation and constant water heating.

The development of combining solar energy and heat pump application has developed rapidly during that last decade. Therefore, the effect carried by the IEA to set standardization to combine such complex systems was crucial which is concluded in Task 44. The main objectives of this task are (D’Antoni, Fedrizzi and Sparber, 2012):

- Evaluating the performance factor of such systems.
- Studying possible combination method
- Simulation of different developed system in various communal conditions.



- Developing a component model for creating new systems or combining existing ones as shown in Figure 1.2.

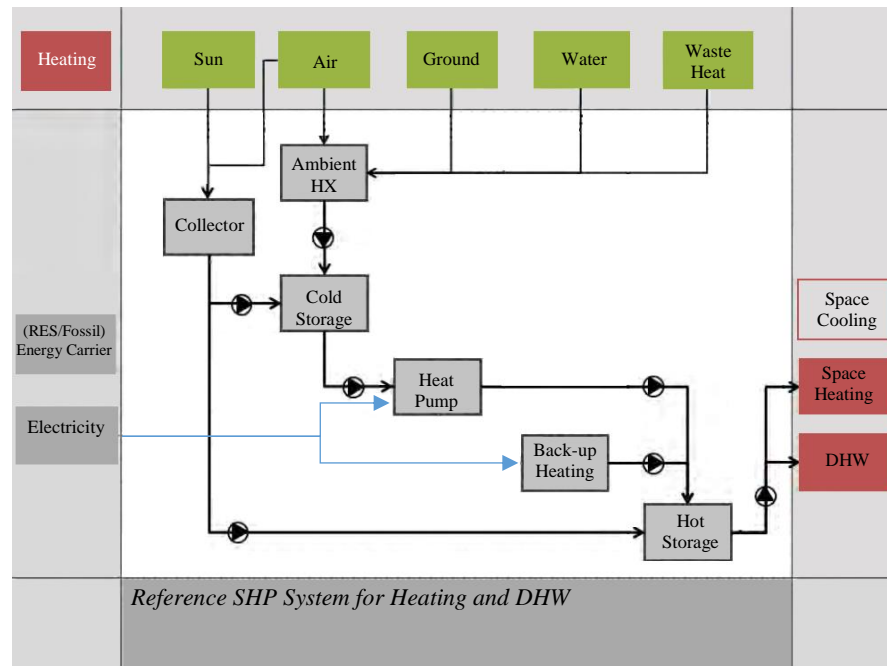


Figure 1.2. System boundaries for solar heat pump (SHP) system in heating mode (D’Antoni, Fedrizzi and Sparber, 2012)

In summary, DHW production with new innovative systems is a critical area for research in order to meet the current demand withdrawal with the lowest CO<sub>2</sub> emissions. Therefore, after conducting the literature review, it was found that SAHP has become more common during the last decade. However, optimising the system configuration is still a potential area to be researched. Evaluating the optimal control for such SAHP systems still big challenges in terms of energy saving. As the system involves with solar thermal energy, integrating a latent heat storage application to such system could have a great impact on the system performance. As latent heat storage, PCM has become widespread in use nowadays. However, its poor thermal conductivity elements its use. Therefore, studying novel ways of enhancing its heat transfer is also an area to be studied. Simulation development has become very advanced. However, coupling different software simulations together is still an area of development. Investigating the performance of such systems in different locations open the eye for a new market potential.

Therefore, in this study, a novel IDX-SAHP system configuration was developed in order to investigate an original control strategy for the system operation. The study

also includes the potential benefit of integrating a latent heat storage application to improve the system performance and get the optimal solar energy operation. Also, the study includes a CDF simulation for the PCM HX to provide a full understanding of the charging/discharging process of PCM. In addition, a novel coupled-simulation modelling method is introduced to investigate the system performance in locations with high solar intensity. The main objectives of this research will be described in the following section.

### ***1.2. Objective of the research***

- Conducting a literature review on SAHP and its classifications in addition to a focused review of PCM classification and its application.
- Design and build a novel test rig for an IDX-SAHP system.
- Design and manufacture a novel PCM HX and integrating it to the proposed test rig.
- Develop and implement optimal control strategy to ensure reliable and energy saving operation for the system.
- Model the PCM HX using CFD to test different flow rates and inlet temperatures.
- Modelling the constructed IDX-SAHP using TRNSYS and validate the model with experimental results.
- Couple the PCM HX CFD model with the IDX-SAHP TRNSYS model and simulate the system in different locations with high irradiance.

### ***1.3. Thesis structure***

***Chapter 1*** gives a brief description of the research motivation and expectation outcomes of this study in addition to a brief general introduction.

***Chapter 2*** is conducting reviews of the previous work that has been achieved in SAHP, similar system control strategy, PCM types and its application. It will also include a brief theory review for some of the concepts that used in this study.

***Chapter 3*** describes the test rig design and system components. It also illustrates system loops configuration. The PCM HX sizing, design and manufacturing process is also included. A fully detailed control strategy and experimental implementation method via building management system (BMS) are provided in this chapter.

**Chapter 4** includes the pre-measurements for the tested days and test procedures. It also includes the thermodynamic analysis of produced results. And finally, the analysed experimental finding is covered.

**Chapter 5** demonstrates the methodology that has been used for the system numerical simulation. In addition, it includes; the setup for the novel TRNSYS model, the setup for the developed EES heat pump model, the setup for CFD model of PCM HX and a creative method of coupling all these models together.

**Chapter 6** shows the validation of the numerical models. It also includes findings and discussion of a PCM HX CFD simulation of different inlet temperatures and flow rates. It shows the final finding and discussion of the coupled models in different climates locations and the effect of PCM HX.

**Chapter 7** discusses the conclusion further recommendation for further improvements

Figure 1.3 shows the research methodology diagram that used to develop this research.

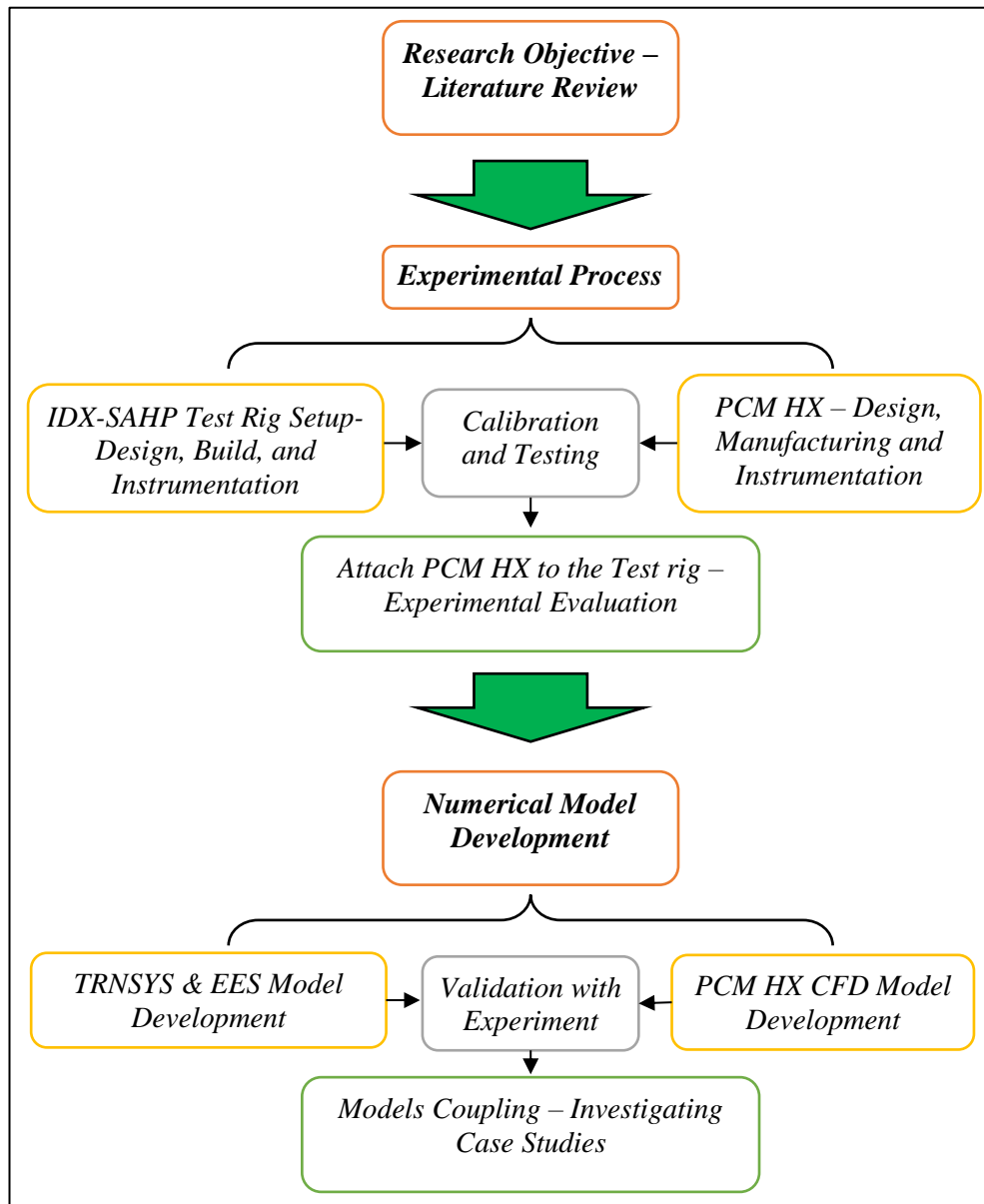


Figure 1.3. Research methodology diagram.

Experimentally, the novelty of this research is to introduce an original IDX-SAHP configuration and control strategy which will contribute to the development potential in this field. Another innovation is getting the optimal advantages of the solar energy by employing a latent heat storage with a novel heat transfer enchantment method to the proposed system. The research also adds to the literature significant experimental data for the control behaviours during different climate conditions in London. In addition, experimental data of the melting/solidification behaviour of the proposed PCM are provided.

Numerically, PCM HX is modelled via CFD FLUENT simulation tool to provide a detailed understanding of the charging/discharging process of the PCM and the effect of variation of the inlet flow rate and temperature. This study also includes a novel simulation coupling method to model the proposed system including the PCM HX and custom-made heat pump. The simulation is aiming to investigate the system benefits in different locations with high solar intensity in terms of energy saving and control validity.

#### ***1.4. Publication***

The effect of this research led to the following publications:

##### ***Journal Publications***

- W. Youssef, Y.T. Ge, S.A. Tassou, Effects of latent heat storage and controls on stability and performance of a solar assisted heat pump system for domestic hot water production, *Solar Energy*, Volume 150, 1 July 2017, Pages 394-407, ISSN 0038-092X, d:10.1016/j.solener.2017.04.065.
- W. Youssef, Y.T. Ge, S. A. Tassou, Indirect expansion solar assisted heat pump system for hot water production with latent heat storage and applicable control strategy, ICSEF International conference, Windsor, UK – Apr'17. *Energy Procedia*, 123, 180–187. <https://doi.org/10.1016/j.egypro.2017.07.258>
- W. Youssef, Y.T. Ge, S.A. Tassou, CFD modelling development and experimental validation of a phase change material heat exchanger with spiral-wired tubes. Submitted (Pending)
- W. Youssef. Y.T. Ge, S.A. Tassou, Performance evaluation and comparison of an indirect solar assisted heat pump system at different weather conditions using a combined TRNSYS-EES-CFD model. (Submitted to Supervisor)

##### ***Conference Publications***

- W. Youssef, Y.T. Ge, S. A. Tassou, Phase Change Material Heat Exchanger for Excess Thermal Solar Energy Storage, SOLARIS International Conference, London, UK Jul'17
- W. Youssef, Y.T. Ge, Investigation of Optimal Control Strategies for an Indirect Solar Assisted Heat Pump (i-SAHP) System, SUSTEM International Conference, Newcastle, UK Jul, 15

*Poster Presentations*

- W. Youssef, Y.T. Ge, Investigation of Energy Storage Technology using Phase Change Materials for a Solar Thermal System, CSEF Centre launch, July 2014, Brunel University London, UK
- W. Youssef, Y.T. Ge, Investigation of Optimal Control Strategies for an Indirect Solar Assisted Heat Pump (i-SAHP) System, SUSTEM International Conference, Newcastle, UK Jul, 15.

---

***Chapter 2. Background Information***

---

### ***2.1. Introduction***

The background concept of the heat pump and UK typical load profile are illustrated in this section. Different methods of SAHPs are presented with a focus in the indirect type. A review also has been carried out in the operation on the thermal solar panel and its control strategies. Furthermore, a focused review has been conducted on the PCM classification and its applications. In addition, a heat transfer enhancement method for the use of PCM is included.

### ***2.2. Domestic water heating***

DHW and space heating are the largest portion of the domestic sector energy consumption of 29% of the total energy consumption in the UK, taking into account that domestic energy sector is causative of 15% of the CO<sub>2</sub> emissions in the UK (BEIS, 2016, 2017a). Therefore, it was a fateful role from Energy Saving Trust (EST) to measure the DHW consumption based on sampling of 120 dwellings. The key goals of these measurements were to determine the volumetric DHW consumption and measure the associated energy demand for these measured profiles (Energy Savings Trust, 2008). According to the British standard guide, the hot water should be supplied at least 50°C within 1 minute running and feed water should be below 20°C after running the water for 2 minutes (BS, 2015). As it shows in Figure 2.1, the DHW consumption profile was evaluated and the daily peak periods are between 7-10 am and 6-9 pm. However, this profile can vary depending on the season of the year (Lomet, Suard and Chèze, 2015). Another forecasting study has validated the EST measurements by developing a demand-side management program to predict the DHW of a dwelling (Gelažanskas and Gamage, 2015).



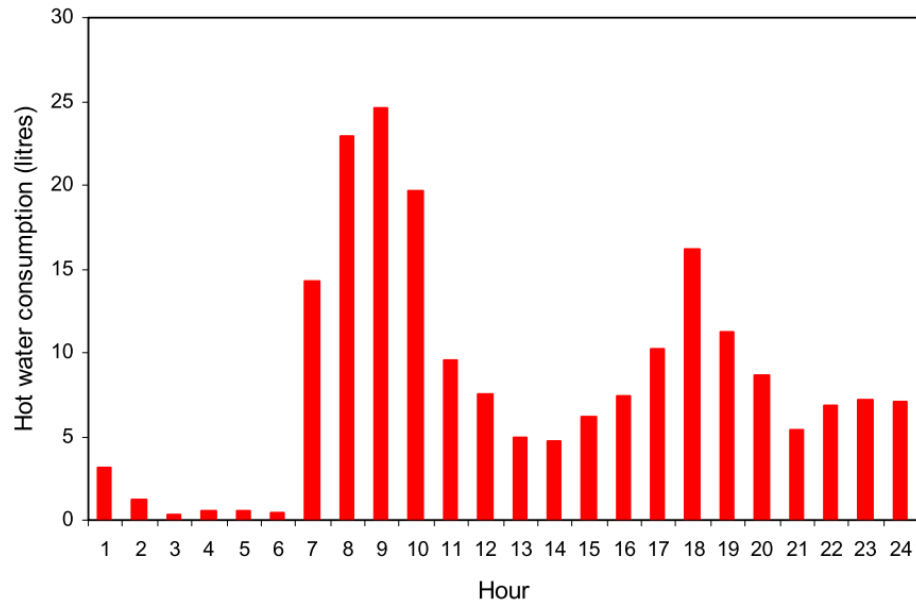


Figure 2.1. Daily DHW profile (Energy Savings Trust, 2008)

Another effort was carried out in Belgium to measure DHW consumption for 12 apartment buildings of various apartments' capacities. The study proved that the average DHW temperature for the whole sample was 55.5°C and cold feed water was 15.3°C (Gerin, Bleys and Cuyper, 2015). In North America, a model has been developed for estimating DHW consumption which took into account occupancy, inlet feed water temperature, and age of occupants. The model proved that the age of the occupant has a significant effect on the DHW consumption (Parker, Fairey and Lutz, 2015). In South Africa, a measurement analysis was conducted by measuring the DHW consumption for 90 households over a year period. The DHW profile matched the profile by EST in terms of peak periods. It was also found that the DHW consumption increased by 70% from summer to winter (Meyer and Tshimankinda, 1998) (Meyerl, 2000).

### 2.3. Heat pumps

Heat pumps are one of the applications that can be used for water heating in both DHW and space heating. Heat pumps became a successful application for DHW due to their cheap and available heat source which can cover the cooling rejected from their evaporator side. Therefore, the trend nowadays is to use the low-carbon technology such as; solar thermal and heat pump for residential water heating purposes. Consequently, the use of these applications is expected to reduce the CO<sub>2</sub> emissions by up to 6.5% and 15% by 2030 and 2050 respectively (DTI, 2006). In 2007, Only about 2000 installations for the heat pump system was counted in the UK

(Element Energy, 2008). In 2009 and 2010, the market witnessed a rapid increase of the heat pump installations to reach 8000 ground source heat pumps and 30,000 air source heat pumps (Fritsch, 2011). During that time, the heat pumps occupied only 10% of the market sales for newly built buildings (2010) as a primary water heating application. Since the heat pump became more popular application, its development is significantly increasing and it counts a large portion of the market today, It is expected to be increased to up to 51% by 2020 (Dawson, 2012), as it is shown in Figure 2.2.

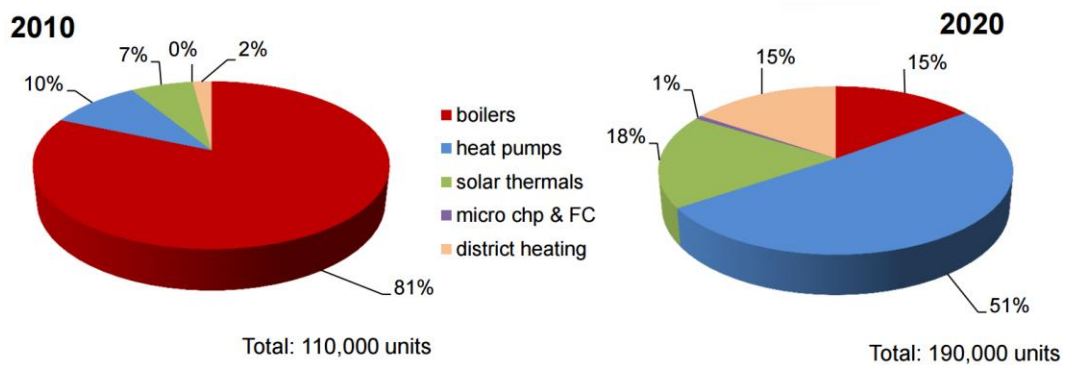


Figure 2.2. Sales of the domestic applications in the UK(Dawson, 2012)

The use of heat pumps nowadays became very popular which makes it an area of interest for research and development. In theory, the heat pump is a device which can extract heat from source with high temperature to a sink with lower temperature (Tassou, 2010). The thing that distinguishes heat pump is that it has a high COP which can consume less energy compared with electrical immersed heater systems (Kalogirou, 2004). Any typical heat pump consists of four essential components; compressor, condenser, expansion valve and evaporator. The refrigerant of the heat pump is the key element of evaluating the performance of the heat pump. The refrigerants have unique properties which undergo phase transition from liquid to gas and vice versa. This phase change allows a latent heat storage between the condenser and evaporator (Wang, 2000). The gas phase takes place after evaporation at low pressure (Evaporating Pressure) and the liquid phase takes place after the condenser at high pressure (Condensing Pressure) as shown in Figure 2.3.

The COP of heat pump applications relies on many parameters, such as evaporating temperature, condensing temperature, working refrigerant and its configurations(Hepbasli and Kalinci, 2009).

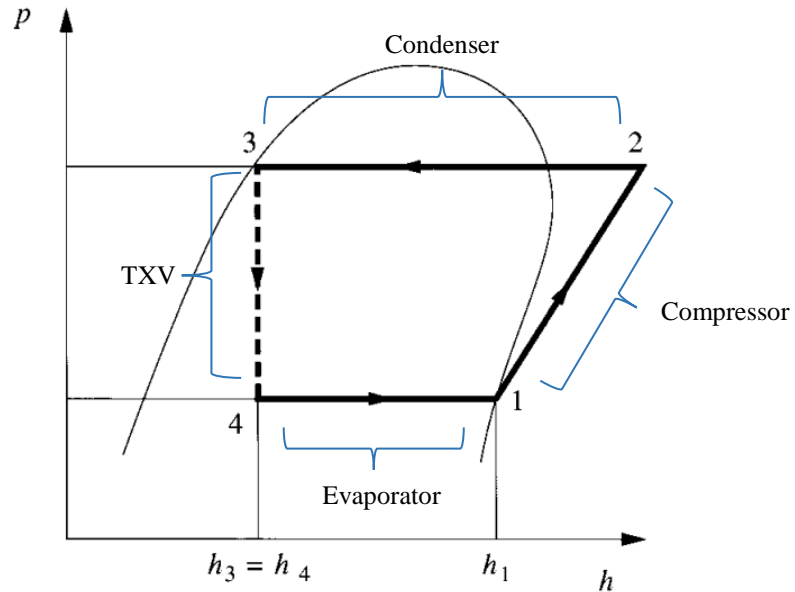


Figure 2.3. *P-h diagram for ideal vapour compression cycle - modified from (Wang, 2000)*

According to the British standards, The Seasonal Coefficient of Performance measured equivalent to the system when determined in the manufacturer test conditions and average climate for outdoor air units, and with the maximum load profile declared by the manufacturer (BS, 2017).

## 2.4. Solar assisted heat pumps

### 2.4.1. Early work

After Jordan & Threlkeld and (Jordan and Threlkeld, 1954) and Sporn & Ambrose (Sporn and Ambrose, 1955) fired the intention of combining solar energy with heat pump, this area became one of the most interesting studies in the energy sector. In the late 1970s, Lior (Lior, 1977) tried to combine solar-powered, fuel superheated steam Rankine cycle with heat pump by driving the heat pump compressor with a steam turbine. This study achieved 50-60% resource energy saving in cooling mode and 3 to 4 fold reduction in energy consumption compared with a conventional boiler. Andrews (Andrews, 1978) simulated the series configuration SAHP SAHP and studied the effect of using air heating collector with air to water HX and without. MacArthur et al (MacArthur, Palm and Lessmann, 1978) simulated SAHP system compared with a conventional system and calculated the backup heating required and a payback period of the system. The significant outcome of this study concluded that collector area and storage capacity are key factors to size the system. Also, the economic analysis concluded that payback period of the system will be a little less

than the mortgage time. Freeman et al (Freeman, Mitchell and Audit, 1979) were investigating a breakthrough study involving three types of configuration which are series, parallel, and duel which will be explained later in this chapter. The important outcome of this study showed that parallel system is the most practical as the other two systems essentially depend on the collector area.

Chandrashekar et al (Chandrashekar *et al.*, 1982) simulated six different models of SAHP system compared with resistance heating system and air-to-air heat pump. The outcome of this study recommended the SAHP system for building blocks rather than single family as the SAHP system will be cost effective for large scale. Morgan (Morgan, 1982) carried one of first experimental investigation for direct expansion SAHP (DX-SAHP) system. The experiment used Freon 11 as working fluid for the heat pump and it concluded that there was excessive superheat due to oversizing the collector but the system did well under various test conditions. Further investigation on a larger scale was recommended.

In the early 90s, Nilufer Egrican (Nilufer Egrican, 1991) simulated a series of connected SAHP and he verified the outcome of Freeman; that the collector size and storage capacity are significant factors for designing the system.

#### ***2.4.2. SAHP classifications***

SAHP can be classified based on various factors. One of the most important factors is the heat pump evaporator expansion which can be concluded simply into two categories, DX-SAHP and IDX-SAHP.

##### ***Direct Solar Assisted Heat Pump (DX-SAHP)***

According to Chaturvedi et al.(Chaturvedi, Chiang and Roberts, 1982) and Morgan (Morgan, 1982), the refrigerant of the heat pump circulates and directly through the solar collector allowing the highest possible evaporating temperature that can be achieved using solar power. Since the early 80s to late 90s in last century, Chaturvedi et al. carried several effective investigations for DX-SAHP (Chaturvedi and Shen, 1984; Chaturvedi and Abazeri, 1987; Chaturvedi, Chen and Kheireddine, 1998). The description of type is illustrated in Figure 2.4 (Kong *et al.*, 2011) which shows a simple schematic diagram of the system.

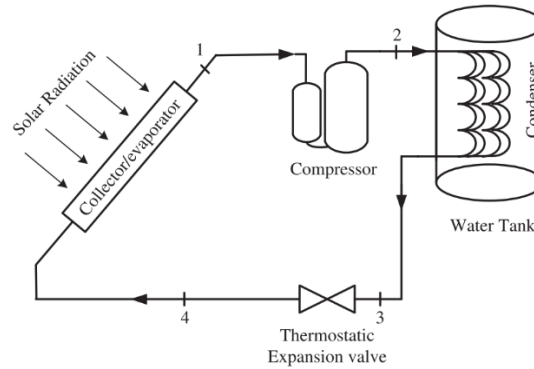


Figure 2.4. Schematic diagram of the DX-SAHP system (Kong et al., 2011).

Omojaro & Breitkopf (Omojaro and Breitkopf, 2013) carried a review over the DX-SAHP application and area of research. This work concluded that the evaporator-collector counts as the most interesting area of research. The same study also was mentioned that most of the work was involved with commercial heating and was recommended to carry further investigating in the cooling application.

DX-SAHP system is a very interesting area of study and many publications were very useful to read and study but we will not search it deeply as our area of interest focuses at IDX-SAHP which it will be illustrated in the following section.

#### ***Indirect Solar Assisted Heat Pump (IDX-SAHP)***

As mentioned earlier, Freeman et al. (Freeman, Mitchell and Audit, 1979) were one of the first introduced the IDX-SAHP and this work also introduced another two types which are parallel SAHP and dual SAHP. The configurations of this kind of systems significantly depend on the application that it is used for. Focusing on thermal storage, the literature will focus on the DHW application and space heating. Chu & Cruickshank (Chu and Cruickshank, 2013) carried a review of SAHP system that used in Canada for the residential sector which illustrates various types of SAHP which are easy to understand and simply illustrated.

In all indirect types, the system extracts the heat from the heat source via working fluid and transfers it to the evaporator via a HX. There are three different configurations for IDX-SAHP which are parallel, dual and series.

**In Parallel SAHP**, the system combines a traditional heat pump system with tradition solar heating system. The ambient air is the heat source for heat pump and solar energy is the heat source for an indirect solar system which both contribute to cover the load demand separately (Buker and Riffat, 2016). The arrangement of system

component depends on the application either DHW or Space heating as shown in Figure 2.5 (Chu and Cruickshank, 2013). In the space heating applications the heat pump can be air-to-air or water-to-air heat pump but in the DHW applications, the heat pump can be air-to-water or water-to-water heat pump.

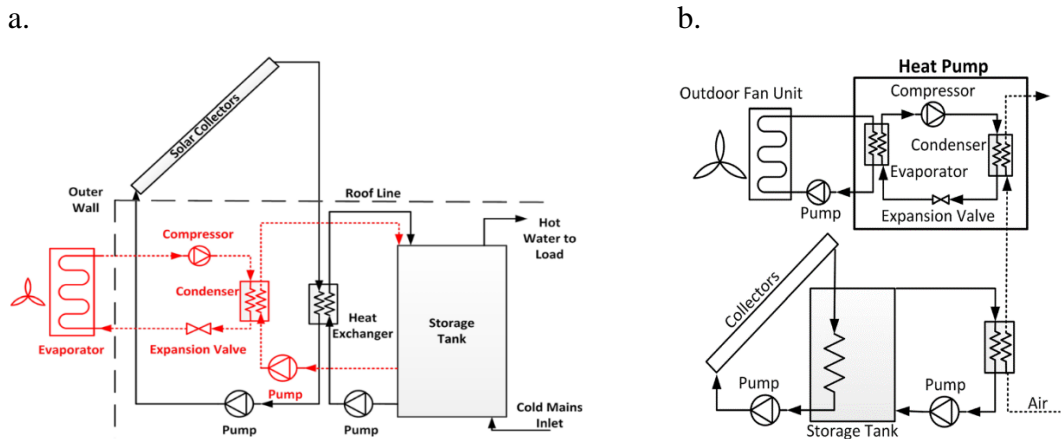


Figure 2.5. Schematic diagram of parallel SAHP (a. DHW, b. Space heating)(Chu and Cruickshank, 2013)

**In dual SAHP**, the heat pump includes two evaporators, one connected to the solar source and the other connected to an ambient air source. That allows the heat pump to extract heat from either source. The configuration of this type again depends on the application (space heating or DHW). Figure 2.6 shows the configuration of this type in space heating application.

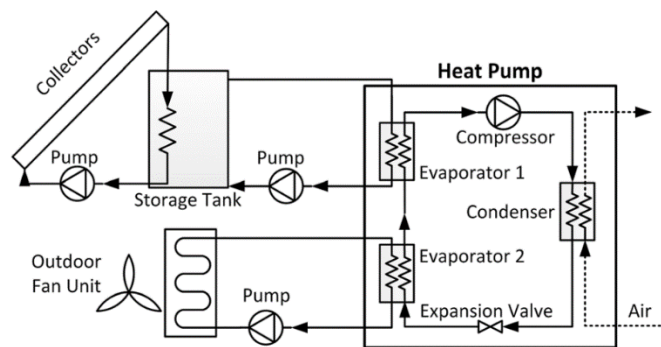


Figure 2.6. Schematic diagram of a dual SAHP for space heating (Chu and Cruickshank, 2013)

**In indirect series SAHP**, the solar loop, heat pump, and the application are connected in series together. The heat pump in this type has only solar energy as a heat source where the evaporator is connected to the solar source and the condenser is connected to the application. The configuration of this type also depends on the application as shown in Figure 2.7.

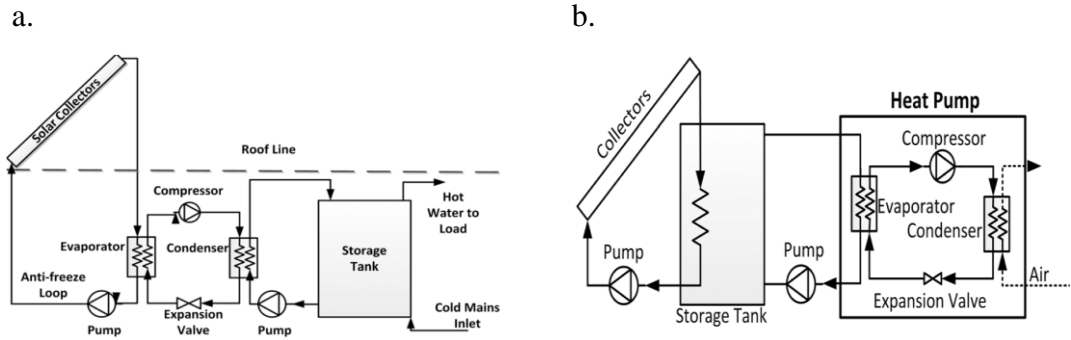


Figure 2.7. Schematic diagram of series SAHP (a. DHW, b. Space heating)(Chu and Cruickshank, 2013)

### 2.4.3. IDX-SAHP development and applications

Many researchers have conducted studies for these types or combination between them and the previous types of applications. Wang et al (Wang *et al.*, 2011) have simulated and experimentally validated a multifunctional IDX-SAHP which can supply space heating load, space cooling load, and DHW by switching between its operating modes. The heating mode was implemented by a dual source system while the space cooling was achieved via a liquid to air HX placed indoor. The study proved to be well operated and energy efficient. Furthermore, it was recommended that the system's performance can be enhanced during winter in an area with high solar irradiance. Sterling and Collins (Sterling and Collins, 2012) started a feasibility analysis of dual tank IDX-SAHP system compared with a traditional thermal solar system using numerical simulation. The analysis outcome verifies that dual tank is the most efficient configuration of the IDX-SAHP and the potential of the use of SAHP system in DHW. That encourages to push the research forward by investigating an experimental study of a multi-configuration SAHP test apparatus (Banister, Wagar and Collins, 2014a). The idea was to have a validation tool for numerical methods, control strategy and reliability of the system. The study was very effective to identify the modes of operation and further numerical validation which focused on thermal storage stratification (Banister, Wagar and Collins, 2014b). The work of this study continued to develop a possible control strategy that can optimize the performance of the system numerically (Banister and Collins, 2015). The model has been validated using the built test apparatus (Banister, Wagar and Collins, 2014a). Panaras et al (Panas, Mathioulakis and Belessiotis, 2014) have developed a method for testing the performance of SAHP based on the dynamic system testing. The configuration of

the presented SAHP in this work was a typical parallel SAHP configuration. The key parameter of this method is the COP of the heat pump and how the condenser is fitted to the storage tank. Carbonell et al (Carbonell, Haller and Frank, 2014) simulated a parallel SAHP system. The simulation compared two different sources heat pumps, ground source and air source heat pump. The ground source heat pump appeared to be promising for absolute electricity saving when it was combined with solar energy (in parallel) which achieved 2.51 MWh but when combined with the air source achieved only 1.98 MWh. Şevik et al (Şevik *et al.*, 2013) experimented a series SAHP used for mushroom drying. It's relatively similar to series SAHP system that is used for space heating. The overall COP of the system including all powered components was fluctuating between 2.1 to 3.1 and it was mentioned that heat pump performance was much better due to the assist of solar energy. Çağlar & Yamalı (Çağlar and Yamalı, 2012) experimented IDX-SAHP system used for space heating. The novelty of this work concludes at the configuration of the evaporator which was designed as a helical coil and was immersed inside the solar storage tank. The author described the heat pump as an air-to-air heat pump; however, it should have been classified as water to air heat pump because the heat source was from waterside while the space heating was the air side. Taken into account the power consumption of the whole system including the fan and other powered components, the overall COP of the system was calculated at 5.56 with a maximum heat transfer rate of 5.87 kW. Bakirci & Yuksel (Bakirci and Yuksel, 2011) experimented series SAHP system used for space heating in Turkey. The innovation of this study was limited to the storage tank configuration. During solar gain, the energy was stored first in the storage tank then it passed through a HX to the evaporator while during cloudy or night mode, the energy was extracted directly from the storage tank to evaporator. As this study was carried out for a year period, the average COP of the system was 2.9. Chow et al (Chow *et al.*, 2012) designed and simulated SAHP used for hot water demand and space heating of swimming pool in Hong Kong. The configuration of this system was a relatively different as it allows solar energy from the solar collector to be stored directly in the storage tank and used as heat source for heat pump at same time. It also stores the excess energy from the heat pump back to the storage tank via HX placed between the compressor and condenser (desuperheater) as shown in Figure 2.8. The simulation showed that system's COP was 4.52 with energy saving a factor of 79% and a payback period of 5 years.



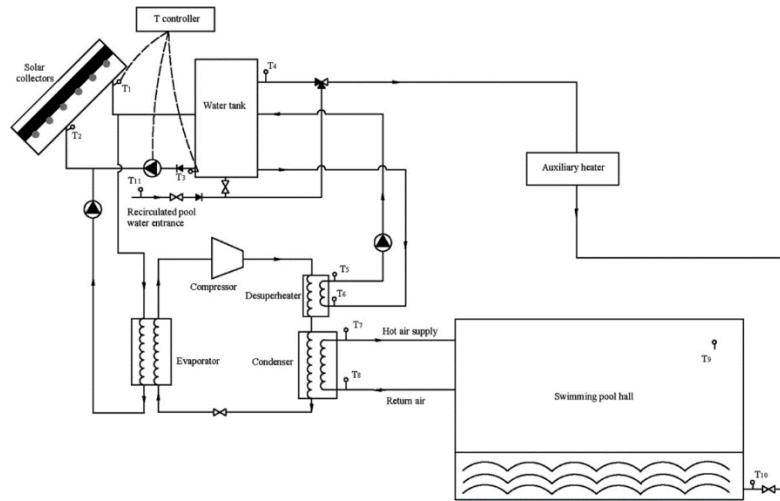


Figure 2.8. Schematic diagram of Chow *et al* (Chow *et al.*, 2012).

Jie *et al.* (Jie *et al.*, 2015) have conducted recent research for multi-functional IDX-SAHP system. The solar irradiance was simulated using a solar simulator (range between 0-1200 W/m<sup>2</sup>) at lab facility in China. The configuration of this test rig contained two storage tanks, one for solar storage (200L capacity) and the other for DHW (300L capacity). The system was built to cover DHW, Space heating and space cooling demand. Worth mentioning, the heat transfer rate for both evaporator and condenser have increased by 37.4% and 32.3% respectively when the solar irradiance was 500 W/m<sup>2</sup>. This study was validated via dynamic model in further work (Cai *et al.*, 2016).

Consequently, the system configuration is still a massive area of research. The literature stated in section 2.4.3 shows there is a still gap on evaluating the best system configuration. Therefore, this research is aiming to propose a novel configuration for IDX-SAHP systems. The following section will discuss the recent development of controlling this type of systems.

### 2.5. SAHP Control strategies

System control is a significant element for energy consumption, reliability, and stability of the system. Yang and Wang (Yang and Wang, 2012) developed three different modes to control heating demand of dwelling using ground source SAHP and borehole thermal energy storage (BTES). The first mode was developed to cover heating demand using only solar energy and charge BTES. The second mode was

developed to use solar energy and the stored energy in the BTES while the third mode used the ground source heat pump to cover the heating load. The operation of this system is illustrated in Figure 2.9. The study recommended independent charging/discharging network to use the stored solar energy during winter.

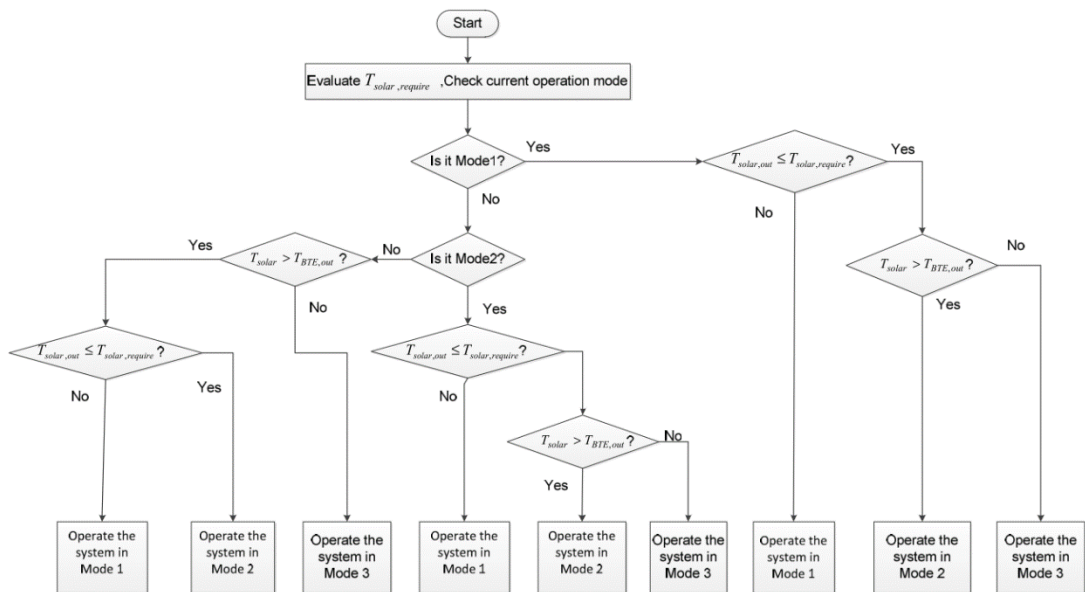


Figure 2.9. The operation modes developed by Yang and Wang (Yang and Wang, 2012)

Thermal solar collector flow rate was also found an interesting area to study. Nhut and park (Nhut and Park, 2013) simulated an automatic operation of the solar DHW system. The study concluded that variable speed mass flow rate is only 1.54% higher than constant mass flow rate from heat gain point of view but it decreased 65.61% on the pump power consumption. Shirazi et al (Shirazi *et al.*, 2016) also simulated different control strategies to solar collector pump and recommended that variable speed pump achieved higher solar friction.

Consequently, the development of the control of IDX-SAHP systems was very limited. However, the control of such systems plays a critical role in its performance in terms of energy saving and system reliability.

## 2.6. Phase change materials

Solar thermal systems have been widely applied in DHW production due to their sustainability and stability in operations. In these kinds of systems, thermal energy storage (TES) technologies and utilization are essential considering the intermittent

nature of solar energy resource. Their storage technologies can be classified as sensible heat storage, thermochemical storage, latent heat storage (Ibrahim *et al.*, 2017). For sensible heat storage, the amount of heat stored is dependent on the production of material's mass, specific heat and temperature change such that a larger vessel and bigger installation space are normally required. On the other hand, the thermochemical storage consists of reversible reactions to store and release heat energy (Edem N 'tsoukpoe *et al.*, 2009). This technology offers higher energy density than sensible or latent heat storage systems. However, it is still at the stage of research and development. As to the latent heat storage, it involves PCM changed from one state to another such as solid to liquid when heat is added or released. The applicable PCMs include organic, inorganic and eutectics with different melting/solidification points (Abhat, 1983; Zalba *et al.*, 2003). Organic PCMs, such as fatty acids and paraffin, have self-nucleating properties but a lower thermal conductivity and higher cost (Bruno, 2004). Such PCMs have been successfully applied to many domestic and commercial applications such as space heating in building, solar air/water heating and refrigeration etc. (Alva *et al.*, 2017). Inorganic materials such as salt hydrates have good availability at a lower cost but exhibit difficulties in phase separation and their abilities to melt incongruently. The eutectic PCM is a mixture of two or more components of organic and inorganic PCMs. It is therefore important to select the optimal PCM in any particular application to satisfy terms of operation and cost. Due to the high latent heat values, the solid-liquid latent heat storage system with PCMs can be more compact comparing to that of sensible heat storage. It also has the ability to store the energy at nearly constant temperature. However, the most undesirable property of the PCMs is the low thermal conductivity which can affect their wide applications in latent heat storage systems such that heat transfer enhancement in a PCM is essential. This will be explained further in section 2.6.3.

PCM is vastly used in many applications nowadays due to its high latent heat of fusion. That is because of its ability to charge or discharge of excess energy from or to any application. Abhat (Abhat, 1981, 1983) conducted studies in the early 80s for TES. He classified the technique of TES into two ways, sensible heat storage, and latent heat storage. Energy can be stored in latent heat of the material in four forms, gas-liquid, solid-gas, solid-solid, and solid-liquid. Mostly and commonly used is a solid-liquid phase which it can be classified into three categories, organic materials,

inorganic materials and eutectics. The sub-sets structure of the material is shown in Figure 2.10.

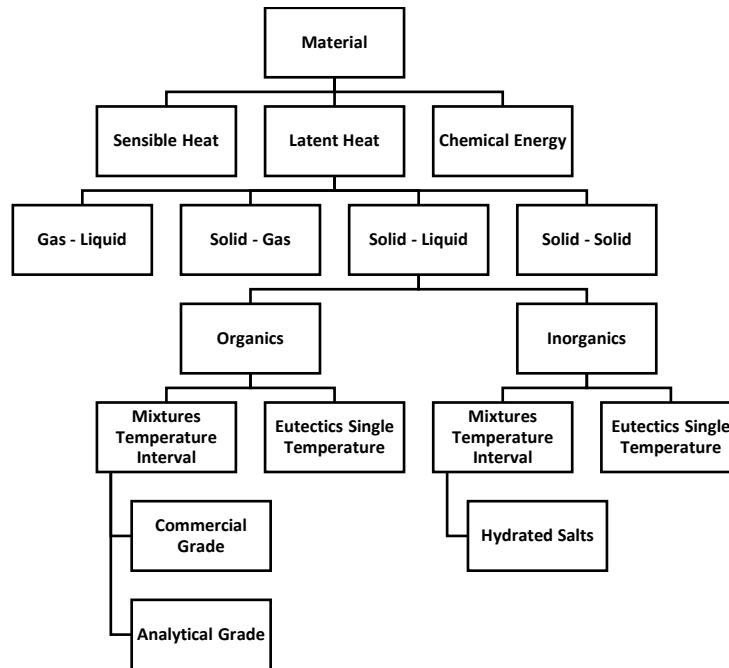


Figure 2.10. PCM classifications [modified from (Abhat, 1983; Zalba *et al.*, 2003)]

### 2.6.1. PCM classifications

#### ➤ Organic PCMs

Organic material is commonly known as paraffin waxes and fatty acids (non-paraffins) (Abhat, 1983). Chemically speaking, paraffin waxes have a straight hydrocarbons chain without much branching. All paraffin waxes have a major component which called alkanes, chemically described by  $C_nH_{2n+2}$  (Lane, 1983); it constitutes usually 75-100 % of the paraffin content. Fatty acids are an organic material which can be described chemically as  $CH_3(CH_2)_{2n}COOH$ . Organic material is either commercially graded or analytically graded.

#### ➤ Inorganic PCMs (Salt hydrate)

Salt hydrates were widely used as PCM since 1947 (Telkes, 1947). The chemical characterization of salt hydrate is  $M.nH_2O$ , where M is the inorganic composite. The main problem for this kind of PCMs is incongruently melting (Abhat, 1983). This happens due to the density difference in the process of the solid phase which makes

solid partials settle at the bottom of the container that can interrupt the liquid-solid cycle.

➤ Eutectics PCMs

Eutectic PCM is a combination of two or more components of PCM to achieve minimum melting point temperature which is usually below zero. It can be composed of organic-organic materials, organic-inorganic materials, and inorganic-inorganic materials. It is not vastly used due to poor data availability of its thermos-physical properties.

**2.6.2. Selection criteria**

As heat storage material, no material can satisfy all desirable features for the application. However, the selection of PCM that will be used to design thermal storage system must meet certain criteria which are governed by its thermos-physical properties, kinetic properties, and chemical properties as following (Tyagi and Buddhi, 2007):

➤ Thermos-physical properties

- 1) PCM melting point temperature must meet the operation temperature range of the application.
- 2) The storage volume plays a key role in the design cost. This means that the higher latent heat of selected PCM per unit volume, the less container volume needed; which allows energy storage in less volume.
- 3) Sensible heat storage can be increased by selecting high specific heat PCM.
- 4) Charging and discharging of the material stored energy significantly depends on the thermal conductivity of the material. Thus, higher is better.
- 5) Slight change of volume during transformation phase and small vapour pressure at operating temperature.
- 6) Congruent melting of PCM for each melting/freezing cycle will consistent storage capacity.

➤ Kinetic properties

- 1) To avoid supercooling of the liquid phase, PCM must have high nucleation rate.

- 2) To enhance heat recovery, PCM is preferred to have a high rate of crystal growth.
- Chemical properties
- 1) Reversible at freeze/melt cycle.
  - 2) Stable in large life-cycles.
  - 3) Non-corrosive to its container.
  - 4) For safety. PCM preferred to be non-toxic, non-flammable and non-explosive.

In this research, the proposed PCM material for this investigation is selected according to the above criteria. The temperature of the PCM is selected according to the optimal evaporating temperature, solar thermal operation and ambient condition. This will be explained further in section 3.4.1.

### **2.6.3. Heat transfer enhancement**

Different heat transfer enhancement methods for PCMs were proposed by researchers (Kenisarin and Mahkamov, 2007; Jegadheeswaran and Pohekar, 2009; Rathod and Banerjee, 2011; Tian and Zhao, 2011). Some of these methods suggested the use of fins while the others recommended mixing randomly the PCM with high thermal conductivity particles such as carbon fibre and metal beads. Of these possible heat transfer enhancement methods, enhancement with fins was found to be a feasible solution due to their simpler design, easier manufacturing, low-cost and higher efficiency (Rathod and Banerjee, 2011). Evidently, the enhancement with longitudinal fins showed 12.5% decrease in melting time for 80°C inlet temperature. On the other hand, the use of triplex tube HX with different fin configurations demonstrated that the parameters of fin length, number and pitch had strong effects on the melting time of PCM (Liu, Sun and Ma, 2005; Al-Abidi *et al.*, 2013). PCM heat transfer enhancement was compared experimentally when circular and longitudinal fins were applied (Agyenim, Eames and Smyth, 2009). Accordingly, the PCM with longitudinal fins presented better performance. Nonetheless, the heat transfer enhancement performance for a particular application depends on some other parameters such as application configuration, heat transfer fluid (HTF) and type of PCM etc. In one of the relevant studies, different types of PCM HX designs were selected (Medrano *et al.*, 2009). These included double pipe HX with PCM in the annular space or embedded in a graphite matrix, double pipe HX with external fins on the copper tube

and PCM in the annular space, compact HX, with PCM between coil and fins, and plate and frame HX, with PCM in half of the passages. The experimental investigations showed that the double pipe HX with PCM embedded in graphite matrix presented the highest overall heat transfer coefficient which the compact HX could provide the highest average thermal power due to its highest ratio of heat transfer area to external volume. Subsequently, there are many designs and operating options which can affect the PCM heat transfer enhancements. Therefore, it is necessary to find out an efficient method to evaluate, compare and optimise these options.

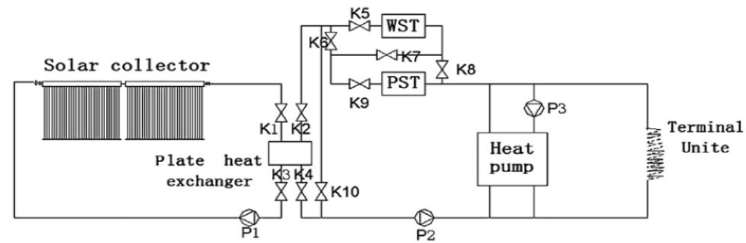
#### ***2.6.4. PCM Computational Fluid Dynamic (CFD)***

Of those applicable design and evaluation methods, CFD modelling can be an efficient simulation tool to predict the melting/solidification behaviour of PCM by numerically solving Navier-Stokes partial differential equations of mass, energy and momentum (Fluent INC, 2016). Comparing to the experimental investigations, the CFD modelling strategies have a number of advantages in terms of less time consuming and more designed options to be evaluated. With a validated CFD model, some significant and detailed simulation results can be obtained. These include dynamic profiles of PCM temperature, melting/solidification rate, heat transfer rate and energy stored/released etc. However, to set up an accurate CFD model for the PCM exchangers, some important parameters need to be specified such as the equivalent thermal conductivity when some heat transfer enhancement materials are mixed with the PCM. In addition, an appropriate phase change model to characterise the PCM melting and solidification behaviours needs to be selected in the CFD model of which the model of “volume of fluid” was commonly applied (Assis *et al.*, 2006; Zhou *et al.*, 2017). Even so, some other phase change models may be evaluated and compared.

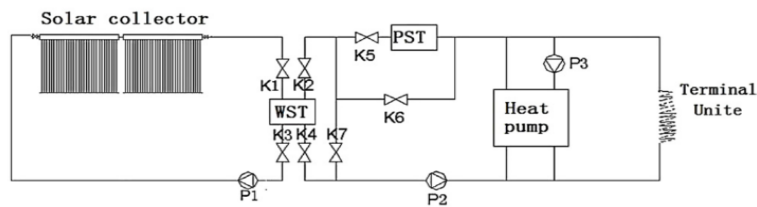
#### ***2.7. The use of PCM in solar and heat pump systems***

Kaygusuz *et al.* (Kaygusuz, Ayhan and Arslan, 1993) (Kaygusuz, Gültekin and Ayhan, 1993) (Kaygusuz and Ayhan, 1999) (Kaygusuz *et al.*, 1993) experimented and simulated different series of studies on the effect of combining SAHP with PCM. They compared series, parallel and dual configurations. The COPs of the heat pump for series, parallel and dual were 4, 5, and 3.5, respectively while average storage efficiency were 50%, 50% and 60%. The quality of the storage was not as good as

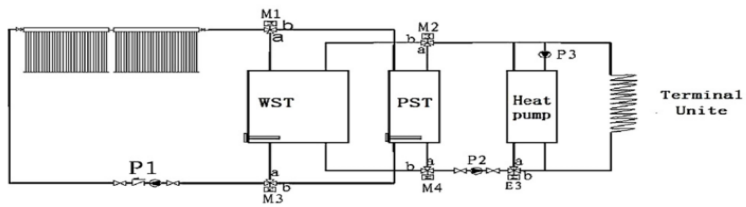
expected as the PCM was encapsulated in Poly vinyl chloride (PVC) containers with really poor thermal conductivity. Qu et al (Qu *et al.*, 2015) studied three different configurations of SAHP combined with dual tank latent heat storage which are illustrated in Figure 2.11. The dual tank latent heat storage appeared to be successful as the COP of the system was 10.03 which is approximately 3.5 higher than water storage system.



(a) Design I



b) Design II



(c) Design III

Figure 2.11. Schematic drawings of three different dual-tank latent heat storage system configurations (Qu *et al.*, 2015).

In this study, for an application of an indirect solar assistant heat pump (IDX-SAHP) test system, a PCM HX tank was purposely designed, manufactured and integrated into the system to store excessive solar energy and be used as heat source for the IDX-SAHP when needed. To enhance the thermal conductivity of the PCM, a number of spiral-wired tubes were utilised and installed in PCM tank which has not been applied before for the PCM heat transfer enhancement. Meanwhile, a detailed CFD model has been developed for the PCM HX with spiral-wired tubes and special treatments are considered in the CFD modelling such as the equivalent thermal conductivity



calculations etc. The developed CFD model has been validated with experimental measurements and simulations are therefore carried out at different operating conditions. The simulation results are significant to understand the working mechanism of PCM melting/solidification process and effect of operating conditions on the PCM HX performance and thus optimising the HX operation.

### ***2.8. Summary of Chapter 2***

SAHP development was found to be an interesting area for research. However, combining this technology with latent heat storage was found still limited. Moreover, finding optimal controlling for such system was another challenge to overcome.

This chapter went through the background concepts of SAHP. The types of the SAHP depends on its configurations which were found to be classified into three categories; DX-SAHP, IDX-SAHP and dual SAHP. The literature focused on the IDX-SAHP in terms of its configuration, previous work, development and its control strategies. Furthermore, a brief review of PCM material was conducted in terms of its classification, selection criteria, advantages and disadvantages. The DHW temperature was selected at 55°C as the minimum DHW operation temperature is 50°C according to the British standards. The literature shows there is no optimal configuration yet for IDX-SAHP system. This is because of the lack of the control development in this area. The literature illustrated a clear understanding of the PCM types and selection criteria. As PCM poor thermal conductivity was a major challenge to its use, a focused literature on the heat transfer enhancement techniques was performed; numerically and experimentally. The literature showed the radial fins solution was the most practical in terms of efficient heat transfer and cost-effective. Consequently, the literature of the previous use of latent heat storage was focused on SAHP applications.

In the following chapter, a detailed illustration will be performed about the experimental setup, system components, PCM HX design and system control strategies.

---

*Chapter 3. Experimental Components and  
Processes*

---

### ***3.1. Introduction***

In this chapter, we will illustrate the procedures, components, equipment and instruments that were used for the experiment. This setup will be used on the numerical development and model validation.

The aim of this part is to investigate an actual hot water consumption withdrawal profile for dwelling between 300L-350L per day using the presented system. This is suitable for large houses (more than 4 bedrooms) or small buildings (2-3 apartments). This size was recommended for the solar thermal system provider as the water storage tank (WST) is part of the solar thermal system. In addition to the above, this section will describe how the system works and the configuration of the test rig components. It will also demonstrate the procedures of designing, manufacturing and installing the PCM HX.

Moreover, the test rig is controlled by BMS which allows an automatic operation of the system. It also permits logging the data needed to study system performance.

### ***3.2. Experiment setup and test rig components***

The test rig was designed, constructed and instrumented at Brunel University laboratory facilities for the sake of this study. The test rig consists of five different circulation loops; heat source loop, heat sink loop, heat pump loop, direct solar loop and load simulator loop. Figure 3.1 and Figure 3.2 illustrate the test rig schematic layout and actual setup, respectively. All components are numbered and listed in Table 1. The components and its function will be briefly explained in this section according to the operation function of each loop.

The system configuration is aiming to allow different heat sources to the heat pump as well as direct solar thermal operation through an original control strategy. For the operation conditions, the condensation temperature range at the waterside is between 50-60°C. The evaporating temperature can vary depending on the heat source selected. For the solar collector operation, at a minimum of 650 W/m<sup>2</sup> irradiance, the temperature difference across the collect can reach 5K at 0.1 kg/s flow rate. The solar collector efficiency for this system can vary between 0.6 – 0.75 depending on the irradiance and operation temperature. Appendix A includes more details regarding the collector performance. This system can supply heating capacity for up to 9 kW.

This should be suitable for large houses (more than 4 bedrooms) or small buildings (2-3 apartments). The cost of the system is relatively high but it is expected to have low energy consumption and CO<sub>2</sub> emissions. Due to the project time limit, further economic analysis needs to be performed on the system as it is not included in this study.

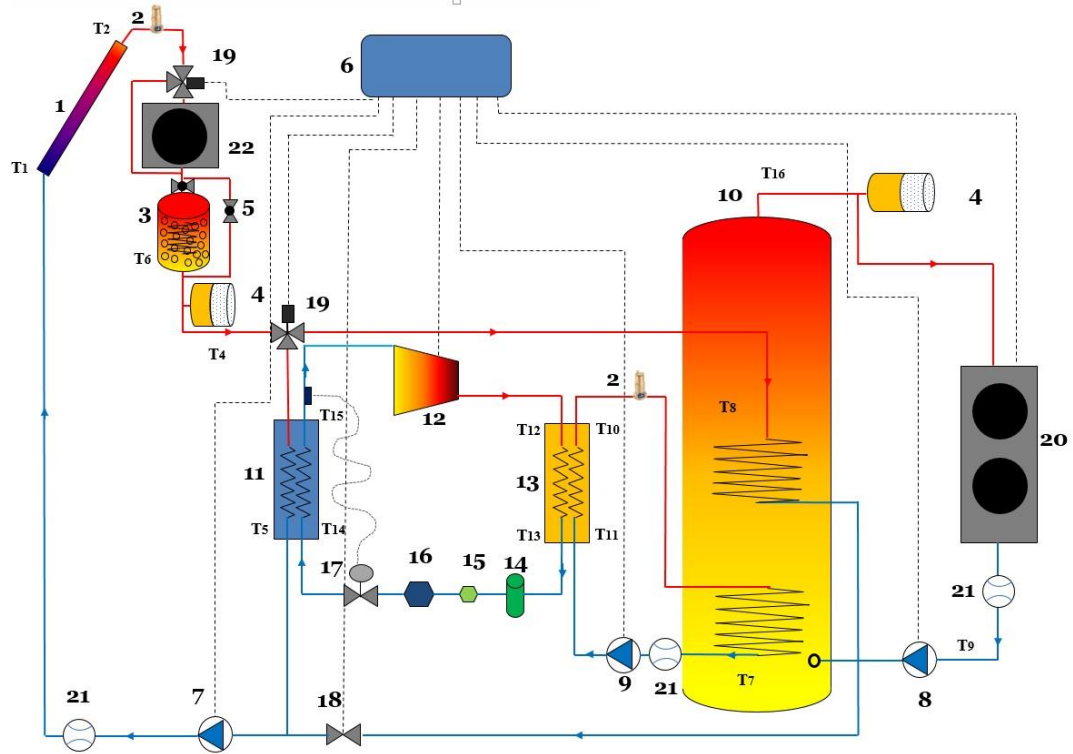


Figure 3.1. Test rig Schematic layout

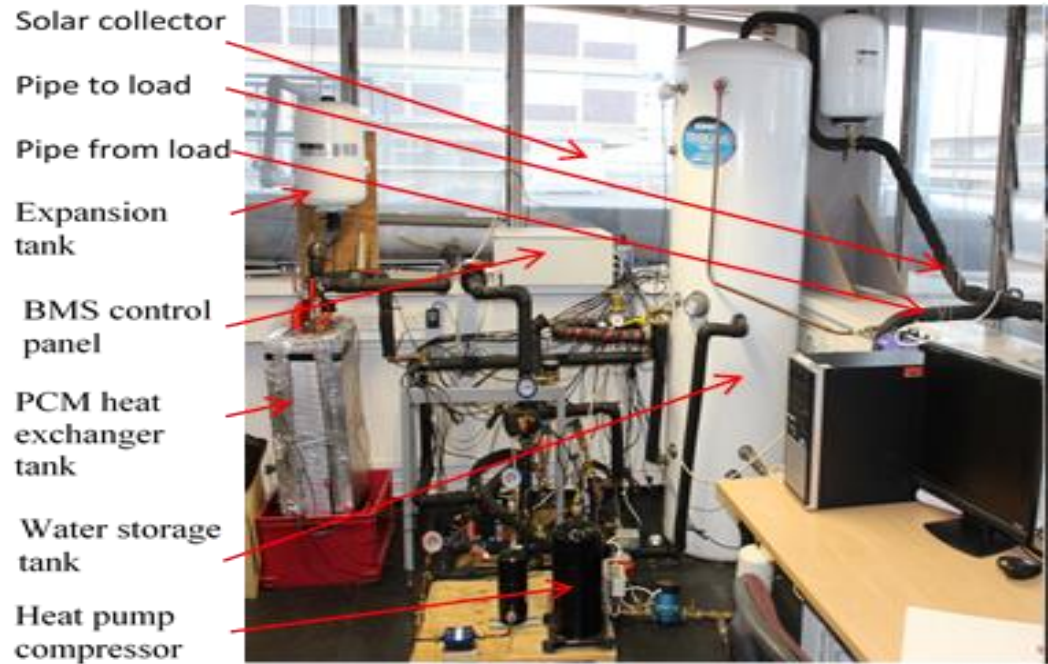


Figure 3.2. Test rig Brunel University TB104

Table 1. components list

<i>No</i>	<i>Name</i>	<i>No</i>	<i>Name</i>
1	Evacuated Tube Collector	12	Compressor
2	Deaerator	13	Condenser
3	PCM HX	14	Receiver
4	Expansion Tank	15	Filter
5	Bypass- ball valve	16	Sight Glass
6	BMS Controller	17	TXV
7	Solar / Heat Source Pump	18	2-Way Valve
8	Load simulation Pump	19	3-Way Valve
9	Heat Sink Pump	20	Fan Cooler
10	Storage Tank	21	Flowmeter
11	Evaporator	22	AWHX

### 3.2.1. Heat source loop

In a typical water-to-water heat pump system, the working fluid circulates in this loop to reject cooling capacity by the heat pump to the heat source. This loop allows the system to dump the heat pump is cooling capacity via three different sources; solar collector, air fan or to the stored latent heat from the PCM HX. The components of this loop are coloured and numbered in Figure 3.3 and Table 1, respectively. The control of the switch between these sources and the mechanism of selection between

them will be illustrated in details at section 3.5. The PCM HX will be illustrated in detail in section 3.4.

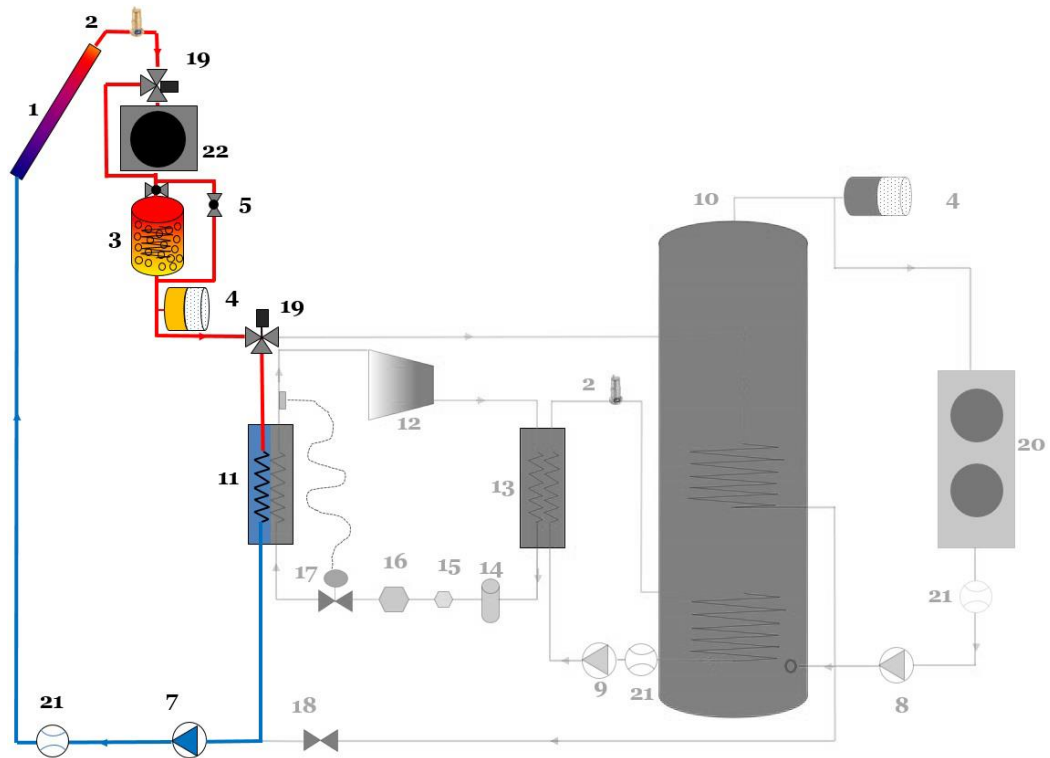


Figure 3.3. Heat source loop

#### *Evacuated Tube Collector (1)*

The solar collector that was chosen for this study was a Thermomax HP400 Evacuated tube collector. The reason for selecting this type of collector is because of its high performance and the ability to produce hot water in poor solar climate condition like in the UK. Especially, the control includes a solar mode operation which allows direct thermal solar operation as explained in section 3.5.1. The collector consists of a 30 heat pipe vacuumed into glassed tube at  $10^{-8}$  bar. At the top of the collector, there is a manifold that allows a cross heat exchange between the heat pipe bulb and water-glycol circulating in this loop as it is shown in Figure 3.4. The collector has a total area of  $3.021\text{m}^2$  and the stagnation temperature is  $183.6\text{ }^\circ\text{C}$ . The collector was located south facing with fixed tilting angle of  $52^\circ$ .



Figure 3.4. Evacuated Tube Collector

**Deaerator (2)**

As this loop is closed looped, it was very important to install a deaerator to allow the air bubble generated due the circulating for the water-glycol to be vented. Figure 3.5 shows the interior and a 3D cross-section of the deaerator used. It also shows the flow direction for the water-glycol. The location of the deaerator was set after the collector outlet as water-glycol gets heated and the pressure inside this loop is slightly increased which allows the trapped air bubbles to be vented.

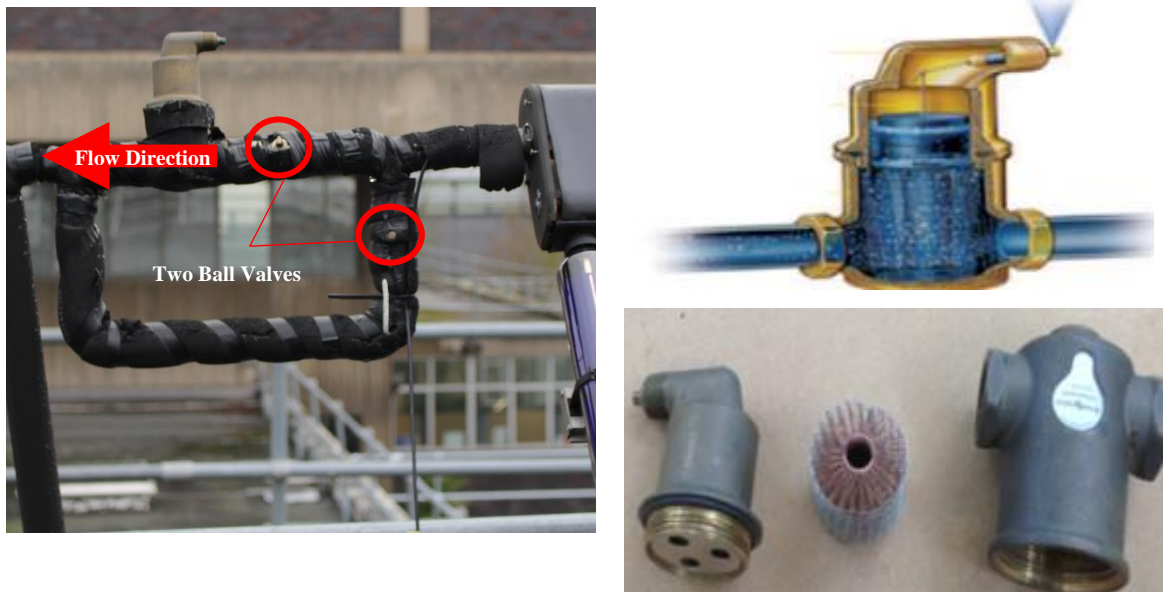
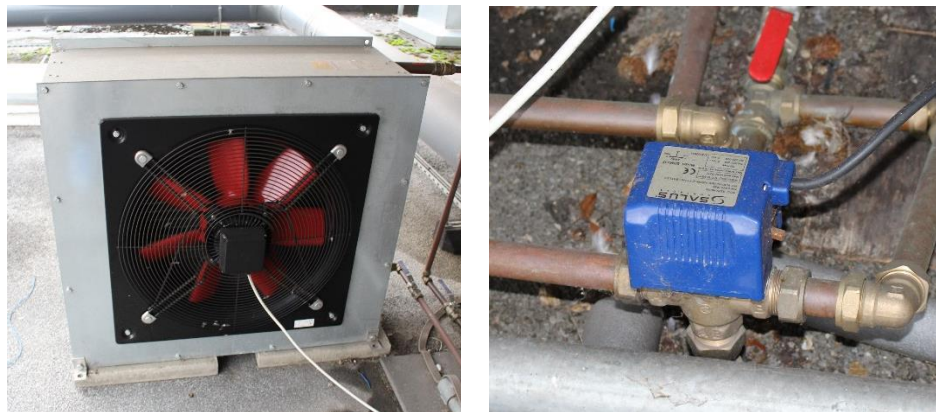


Figure 3.5. Deaerator set up (Left) and interiors / 3D cross section (Right)

**Air-water heat exchanger (22)**



The air-water heat exchanger (AWHX) is a significant element for the system as it allows air heat source for the operation of the heat pump when it is needed. It also allows a cooling down for the collector when it is over-heated. The operation and control of this component will be illustrated in detail in section 3.5. Figure 3.6 shows the actual unit that was selected for the system and the motorised 3-way valve that controls the direction of the working fluid. The tubes and fins of this components are made from copper and aluminium respectively. The heat transfer duty of this component is up to 10 kW with a single phase fan. This capacity can vary according to the evaporator capacity by controlling the fan speed from the BMS system. The maximum cooling capacity of the evaporator is 5 kW. After conducting market search, it was found that the nearest AWHX that covers that capacity was 10 kW. The power supply for AWHX and 3- motorised valve are connected to BMS control which will be covered in detail in section 3.5. The full specification of the AWHX is included in the quotation form in Appendix A. The expected evaporating temperature during that the operation of AWHX is almost as same as the ambient temperature. This evaporating temperature is not controlled and can vary when the system switches between the modes of operation.



*Figure 3.6. Air-water Fan HX (Left) and 3-way valve (right)*

#### ***Expansion tank (4)***

Due to the high-temperature change in this loop, it was necessary to fit an expansion tank as is a closed circuit. Figure 3.7 shows the actual expansion tank installed in the system (left figure) and the internal cross-section of a typical expansion tank (right figure). The tank is divided into two parts via a rubber diaphragm; one part directly connected to the loop and the other is pressured with air at 3 bars. As the temperature



rises in this loop, the pressure also increases which moves the diaphragm and compressing the air inside the expansion tank.



Figure 3.7. selected expansion tank (Left) and expansion tank cross-section (Right)

**Solar / Heat source circulation pump (7)**

As this working fluid is water-glycol 25% Wt, a circulation pump was an essential component of this loop. The selected pump for this loop is a variable speed circulation pump which was recommended by the solar system supplier. The pump is a single phase – 240V with three manual adjusted speeds. The power supply for this pump is connected to the BMS control as the operation of this pump is automated. As Figure 3.8 shows, the pump outlet is attached to a temperature gauge and a pressure gauged relief valve for safety consideration. The inlet of this pump is attached to a manifold with two ball valves to enable charging or discharging of this loop. The manifold has a check valve and flow rate meter in between these two ball valves as shown in Figure 3.8 (left). There are two functions for the check valve; a) it is really important for charging the loop with water-glycol by keeping it fully closed while charging the water-glycol from the upper ball valve and let all the air inside this loop to be vented from the lower ball valve. b) It helps to regulate the flow rate of the system at desired setup. The tank size was determined according to equation (1), where  $\Delta V$  is the change in volume,  $V$  is the original volume,  $\beta$  is thermal expansion coefficient of water-glycol,  $T_{max}$  is maximum operating temperature and  $T_{min}$  is minimum operating temperature.

$$\Delta V = V\beta (T_{max} - T_{min}) \tag{L} \tag{1}$$

The evaporator (11) will be explained in section 3.2.2.

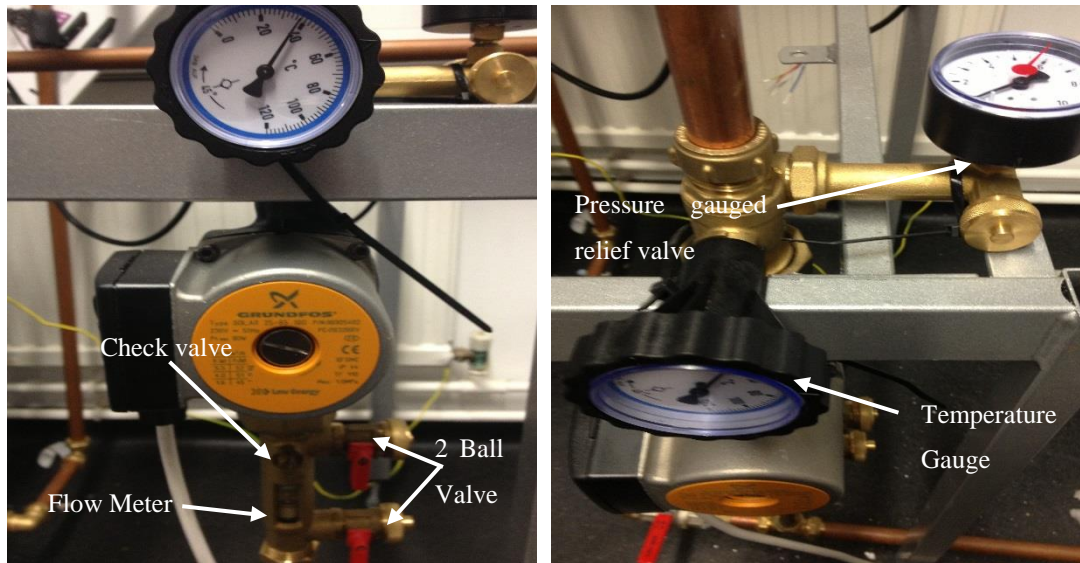


Figure 3.8. Solar/heat source circulation pump

The charging procedure for this loop is as follows:

- Visually check all connections and components
- Pressurize the loop with water and leave it overnight to check for leaks
- Discharge all water and refill the loop with water- glycol antifreeze
- Keep the loop circulating the water for a while to get rid of all bubbles trapped in the loop (it should vent from the deaerator)

This loop was charged with 25% Wt glycol in water to allow a minimum temperature in this loop at  $-15^{\circ}\text{C}$ . The reason for this low temperature is to prevent freezing resulted from sudden temperature drop from the evaporator waterside during winter operation. Especially, as the AWHX is located at the return line of the solar collector, the water will travel a long distance in low temperature before it reaches the AWHX.

### 3.2.2. Heat pump loop

Due to the poor solar energy in the UK, the heat pump is a primary heating source for the system. A customised water-to-water heat pump was selected for the system. A previous experiment was conducted using a heat pump with R-404a refrigerant. R-404a was not suitable for the system as it has a critical temperature of  $72.1^{\circ}\text{C}$  which the system may run above this point. That led to changing the heat pump with R-134a working fluid which has a critical temperature of  $101.1^{\circ}\text{C}$ . The components of this

loop are typical water-to-water heat pump components which are coloured and numbered in Figure 3.9 and Table 1, respectively.

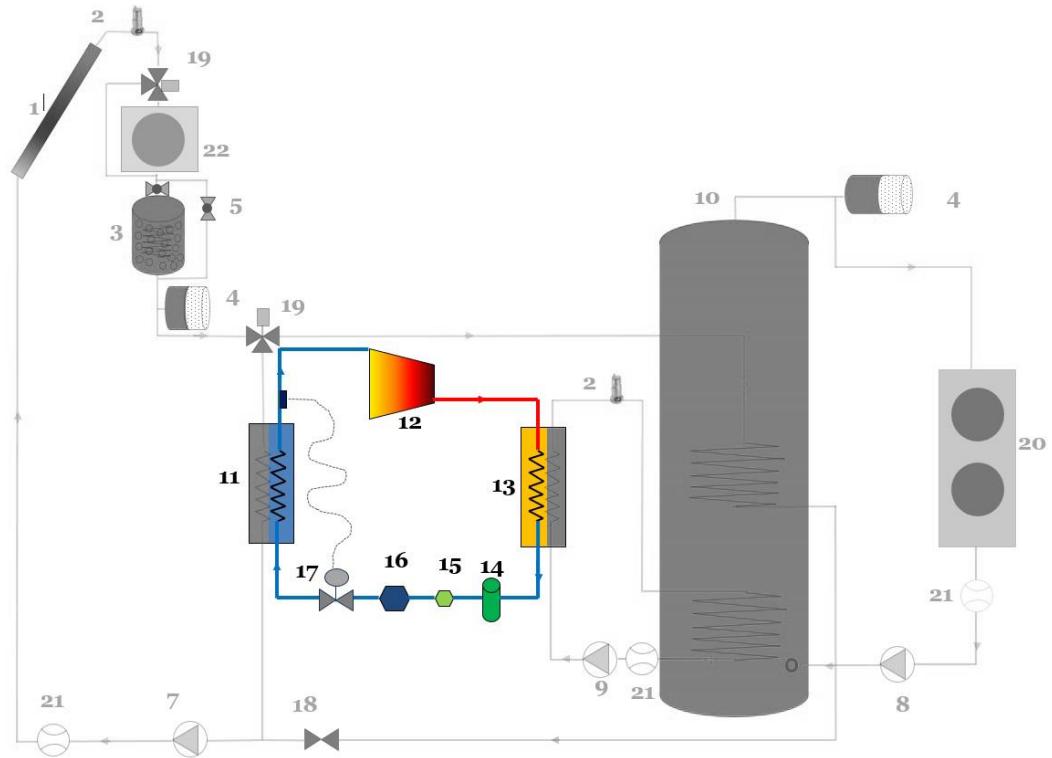


Figure 3.9. Heat pump loop

### Compressor (12)

The compressor is the key element for any refrigeration system. Therefore, the selection of suitable compressor is really important as its performance is directly affecting the whole system performance. The selected compressor of this project is a scroll compressor. The compressor suction and discharge connections are 1/2 inch and 3/4 inch respectively. As shown in Figure 3.10, there are two ball valves at suction and discharge connections. This arrangement facilitates the maintenance of refrigeration circuit without losing the compressor oil. The maximum high pressure is 29.5 bar and maximum low side temperature is 50°C. The compressor is single phased and working with a start capacitor to increase the starting torque of the compressor. There is also a dual adjustable pressure switch is connected to the high and low-pressure sides of the system. This switch function is to protect the compressor from low suction pressure and running dry conditions which lead to a mechanical

damage for the compressor. The power supply for the compressor is firstly connected to the pressure switch then to BMS control.

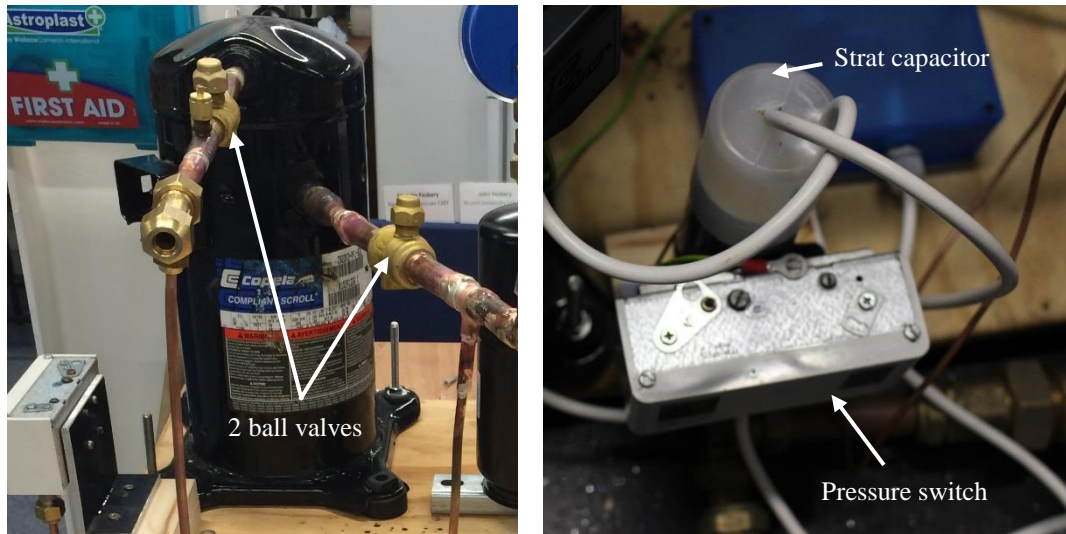


Figure 3.10. compressor installation (left), starting capacitor and adjustable pressure switch (right)

#### **Evaporator (11) and Condenser (13)**

The evaporator and condenser are water-refrigerant brazed plate HX. There are made of stainless steel with copper brazing. The evaporator and condenser are covered with insulating to reduce the heat losses in the cycle. As Figure 3.11 shows, the refrigerant side of the HX is soldered to the refrigerant pipes and the water side has a compression fitting to connect to the water-glycol circuit.

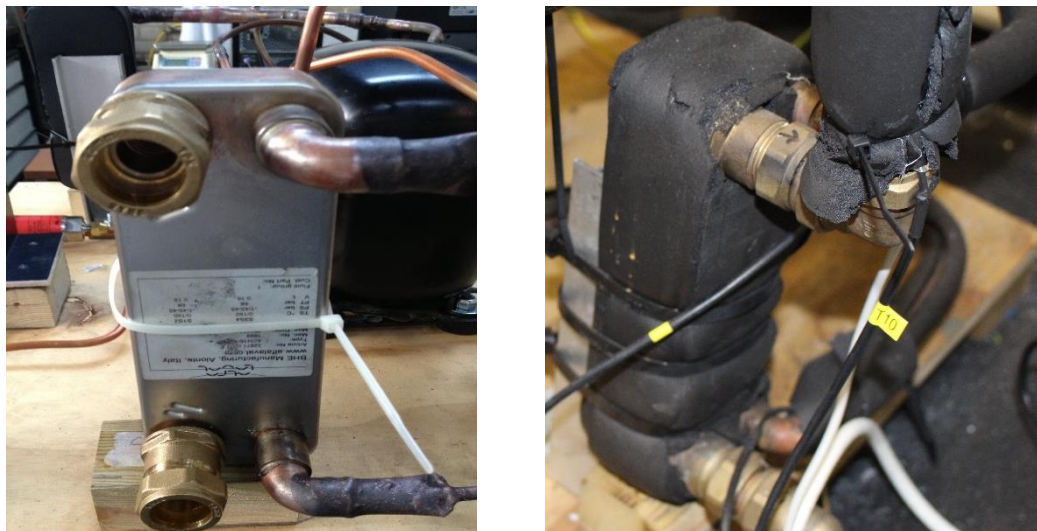


Figure 3.11. Evaporator and condenser HX – Preinstalled (left) and installed (right)

#### **Thermal Expansion Valve (TXV) (17)**



The selected TXV is TEN2 R134a with interchangeable orifice. As it is shown in Figure 3.12 (right), the valve consists of the valve body with flared; a) inlet and b) outlet, c) bulb with capillary tube d) adjustable superheat e) diaphragm connected to needle and f) interchangeable orifice. The bulb is filled with R-134a refrigerant which is the same as the refrigerant in the system. The bulb is placed horizontally at the evaporator outlet to sense the outlet temperature of the refrigerant. When the temperature rises after the evaporator, the gas in bulb expands and pushes the diaphragm and needle down to shut the valve. When the temperature drops after the evaporator, the gas inside the bulb contracts and pulls the diaphragm and needle up to open the valve. In this way, the superheat can be regulated at certain difference by adjusting the screw of the superheat.

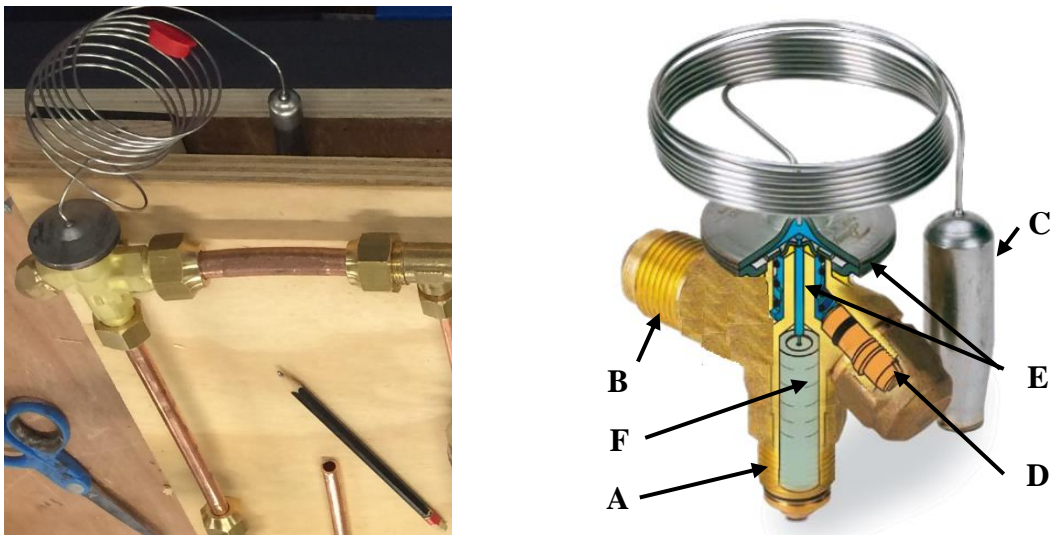


Figure 3.12. Actual TXV (left) and TXV cross-section (right)

#### ***Other components of heat pump loop***

The loop also has some components which are important to maintain the system such as sight glass to check the refrigerant condition, a filter to clean the cycle from any contaminants and a receiver to separate the oil from the refrigerant. These components have to be monitored from time to time to keep healthy running for the cycle.

The charging procedure for the heat pump as follows:

- Charging the system with nitrogen to check for any leaks
- Vacuum the system properly
- Weight the refrigerant cylinder before charging

- Charging the system and calculating the amount of the refrigerant charged which was recommended by the compressor manufacturer.

### 3.2.3. Heat sink loop

As the general concept of any heat pump, this loop transfers the extracted by the heat pump from the heat source to the WST. The components of this loop are; circulation pump, condenser, deaerator and WST. The components of this loop are simple and most of these components have been explained earlier. The specification of the WST will be explained further in this section.

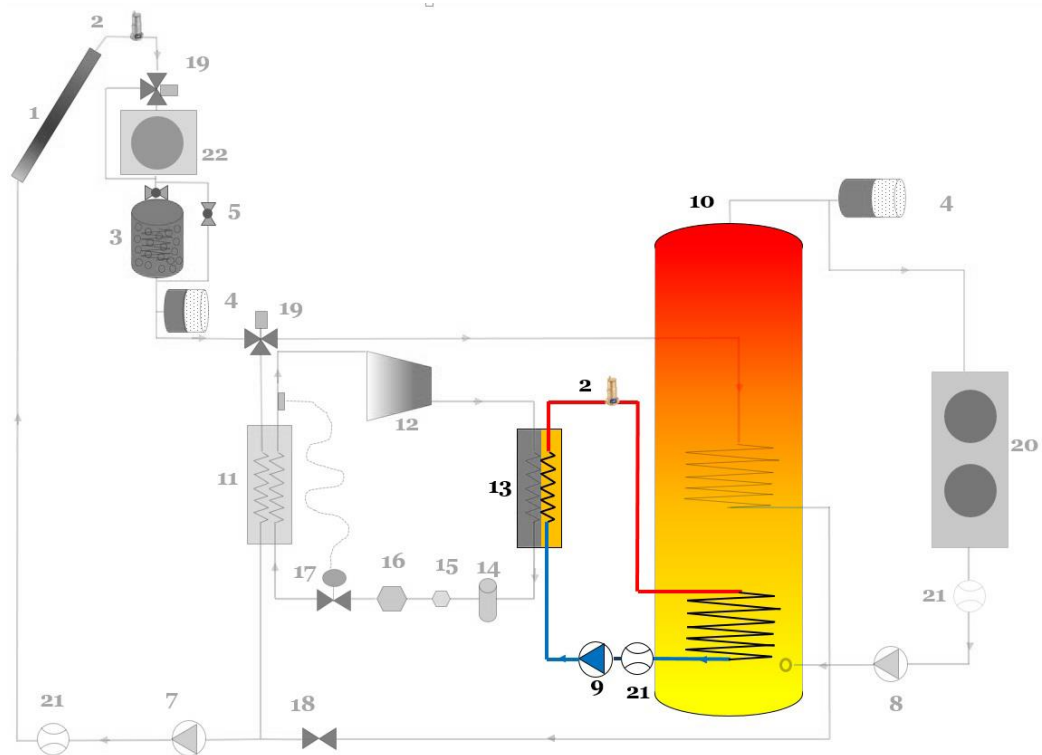


Figure 3.13. Heat sink loop

#### Water Storage Tank (10)

The WST is the main heat storage in the system. It is made of stainless steel and has a capacity of 300 litres. The dimension of the tank is 2032mm height and 550mm diameter. The maximum pressure the tank can hold is 15 bar. However, it has a temperature and pressure relief valve which opens at 90°C and 7 bars respectively. All the connections are 22mm compression fitting. As Figure 3.14 shows, the tank has two immersion coil HXs placed at middle and bottom of the tank which have fluid content of 4.826 litres and total surface area of 0.86 m<sup>2</sup>. The inlet and outlet of the coil HXs are at the same level which is 979mm and 365 mm measured from the

ground for the middle and bottom coil respectively. The exterior of the tank is insulated with 50mm thick foam which has standing heat loss of 2.1 kWh/day. The hot drawn outlet is located at the very top of the tank and the cold water feed inlet is located at 465mm from the ground. The cold water feed is connected to the diffuser pipe which sends the supplied cold water to the very bottom of the tank. There is also an Auxiliary heater placed at 1030mm from the ground but this heater is not in use. There are 3 dry stat pockets to place the temperature sensors at different heights of 1831mm, 1034mm and 420mm measured from the ground.

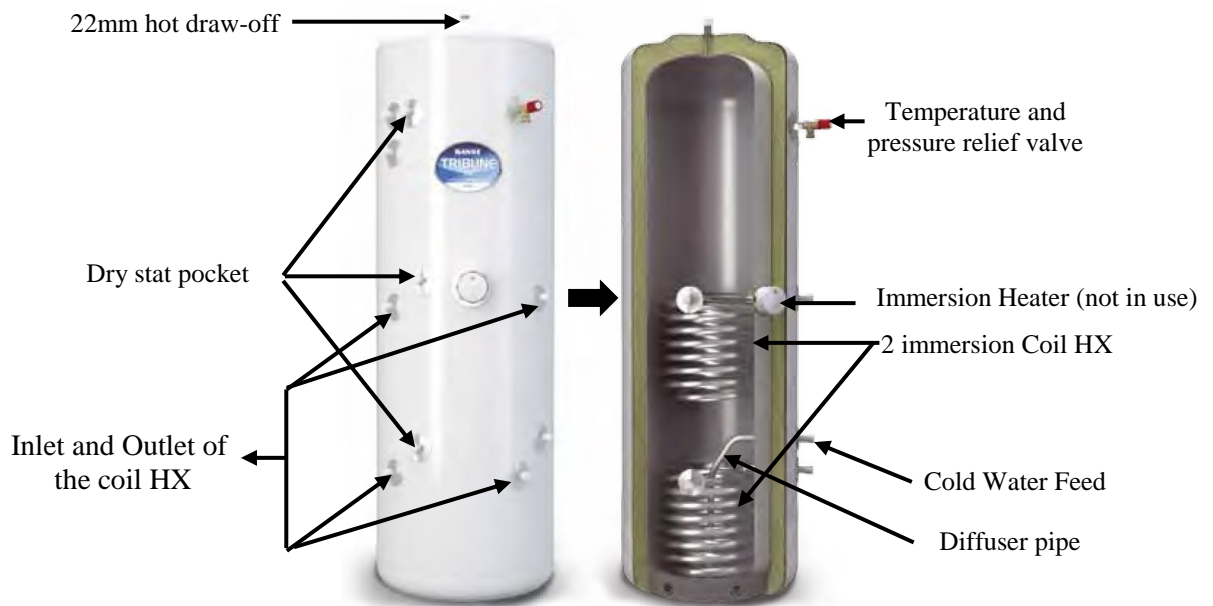


Figure 3.14. WST

The rest of the components have been explained earlier. Since the heat pump is the primary heat source for the system, this loop is connected to the bottom immersion coil of the WST to avoid tank stratification effect. This loop is also occupied with a manifold with two ball valves as same as the ones in the source loop to allow charging and discharging of the working fluid. The charging process of this loop is the same as the charging process of source loop (section 3.2.1). The previous details of the tank are important as it will be used for system modelling at section 5.3.1. More details regarding the WST dimensions and configuration is included in Appendix A.

### 3.2.4. Load simulation loop

One of the challenges that this research has faced is to connect the system to an actual domestic house. Since that option was not available, this loop simulates a typical water withdraw load profile of UK dwelling by sending the hot water to cool down to

the ambient temperature and send it back as feed water to the tank via controlled speed pump. Figure 3.15 illustrates the configuration of this loop which consists of WST, thermal expansion tank fan assisted cooler and controlled speed pump. The storage tank and thermal expansion tank has been explained earlier.

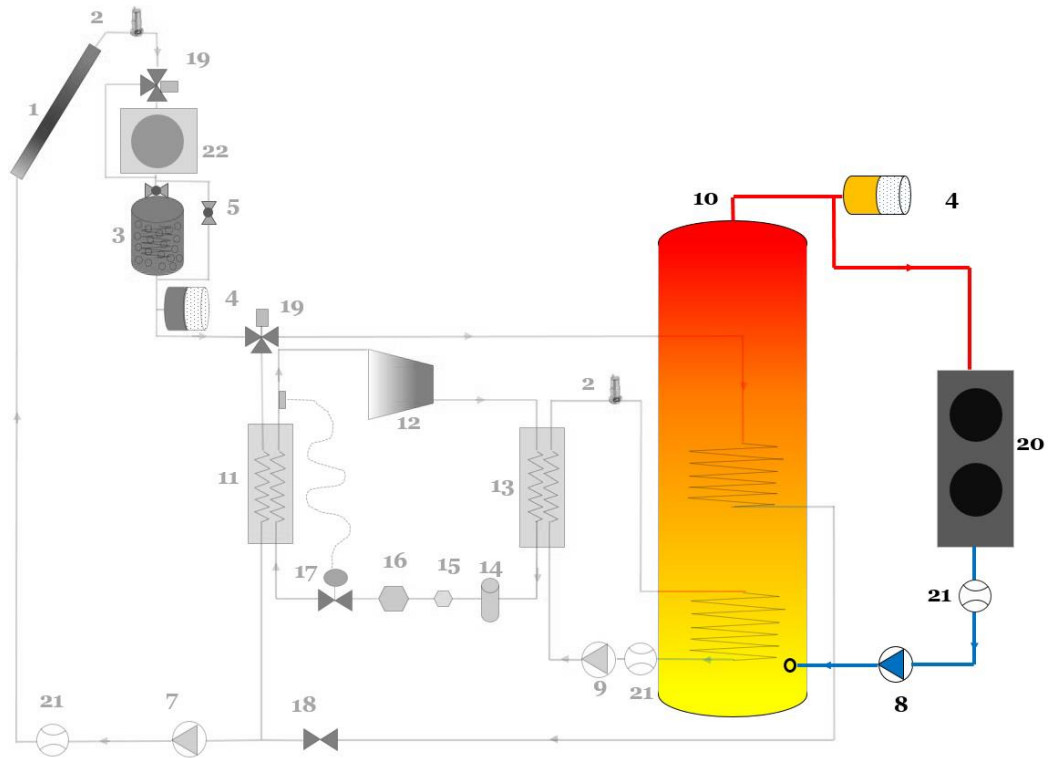


Figure 3.15. Load simulation loop

**Fan assisted cooler (20)**

This component is similar to the fan assisted HX used in the source loop. The main difference is this component is assisted with two fans which single phased and connected in series as shown in Figure 3.16. The component can dump cooling capacity for up to 44.9 kW. The total surface area is 93 m<sup>2</sup>. There are two ball valves at the inlet and outlet of the component to control the flow rate range and to do maintenance for a component if needed. There are also two drains off points to charge and discharge the loop as shown in Figure 3.16. The power supply for this fan is connected a digital inverter which receives an analogue signal from the BMS control to control the fan speed if needed (Figure 3.17).





Figure 3.16. Fan assisted air cooler

### Controlled speed pump (8)

In order to circulate the water in this loop, a motor driven pump is used. The pump has max flow rate of  $12 \text{ m}^3/\text{h}$  and the working temperature range is  $0\text{-}90^\circ\text{C}$ . The pump is single phased and usually has a single speed. In this experiment, the power supply of the pump's motor is connected to a digital inverter which receives an analogue signal from the BMS control as shown in Figure 3.17.



Figure 3.17. Motor driven pump with a digital inverter

The expansion tank was necessary since it is a closed loop when the water expands in high temperature. The charging and discharging procedures of this loop the same as the heat source loop and the heat sink loop.

### 3.2.5. Direct solar loop

This loop is used for direct solar heating when the irradiance is sufficient to heat up the storage tank. It works as a traditional solar thermal system. The components of this loop which was described earlier are solar collector, expansion tank, 3-way

motorized valve, storage tank with immersion coil, 2-way motorized valve and circulation pump. The key components of this loop are 3way valve and 2 ways valve as they can enable or disable this loop via BMS control. Figure 3.18 shows the configuration of this loop.

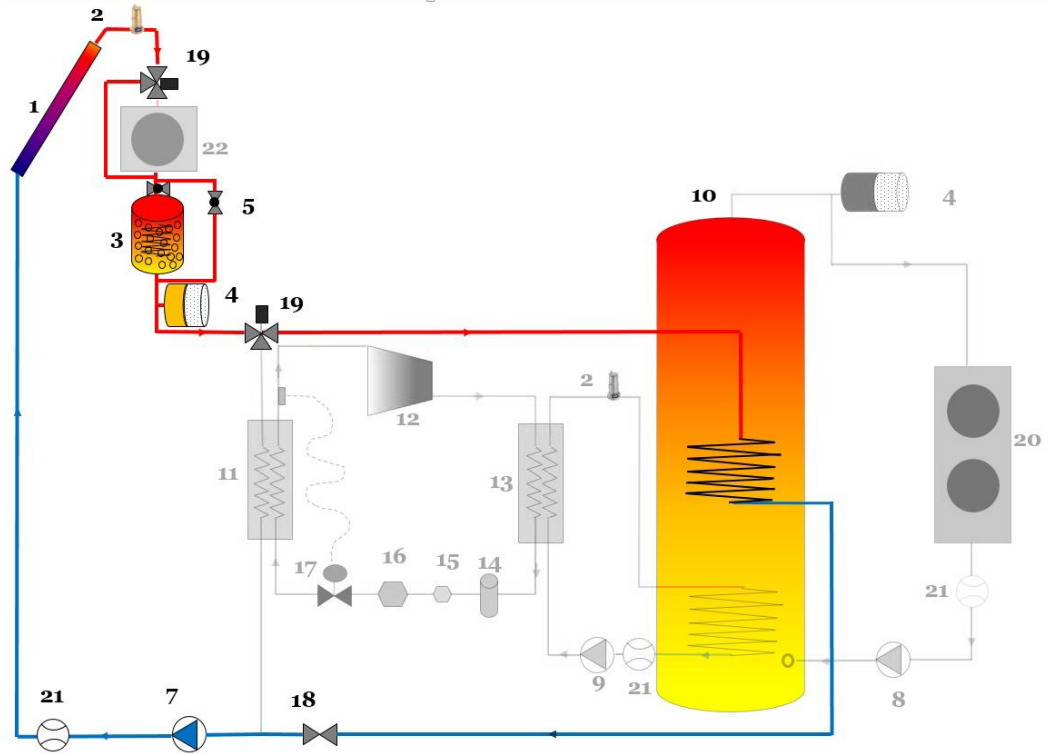


Figure 3.18. Direct solar loop

### ***3.3. Instrumentation***

In this section, a brief description of the equipment used to measure the system performance will be provided as well as the degree of accuracy for each one. This will include; the temperature sensors, pressure transmitters, flow meters, Pyranometer and power analyser.

#### ***Temperature sensors***

The temperature sensors used are Negative Temperature Coefficient (NTC) thermistor type 10K ohms at 25°C (test condition) manufactured by AVX (AVX, 2016). The thermistor's bulbs were soldered to double shielded wire and covered with heat shrink wrap as it is shown in Figure 3.19. The thermistor accuracy and operation range are stated in Table 2. The temperature sensor locations are shown in Figure 3.1. More details are included in Appendix B

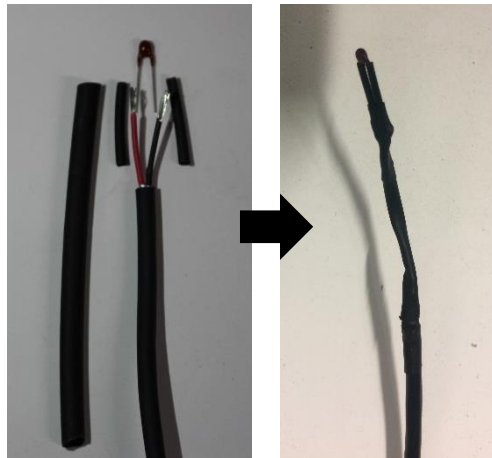


*Figure 3.19. thermistor (temperature sensor) type 10K*

#### ***Pressure transmitter***

In order to measure the pressure before and after the compressor, a pressure transmitter was used with output signal 1-5V DC and supply voltage of 8-30V DC. The product is manufactured by Danfoss (Danfoss, 2014). The transmitter sends signals and receives power supply through a 3 pin socket located at the top of it while the lower part has a flare fitting to be connected to the heat pump cycle as it is shown in Figure 3.20. The transmitter operation range and accuracy can be found in Table 2. More details are included in Appendix B.



Figure 3.20. Pressure transmitter

### ***Flowmeter (21)***

The flow meters used in this test rig are pulsed screwed water meter manufactured by Sontay (Sontay, 2012). The flow meter sends a signal every 10 pulses to indicate a litre of water. The flow meter has inlet and outlet of 1 inch so a compression fitting adaptor was fitted at both inlet and outlet. As it is shown in Figure 3.21, the flow meter has gauge reading as well to enabling visual recording if it is necessary. There are three flow meters at the test rig located at Solar/Source Loop, heat sink loop and load simulation loop. More details are included in Appendix B.



Figure 3.21. pulsed screwed flow meter

### ***Pyranometer***

A Pyranometer is used to measure the irradiance intensity which is manufactured by Kipp & Zonen (Kipp & Zonen, 2015). The Pyranometer comes with a handheld display and data logger. The sensor output signal to handheld display is measured as  $10\mu\text{V}$  per  $\text{W}/\text{m}^2$ . This did match the input signal to BMS unit as it can only read volts higher than one. Therefore, a custom-made amplifier has been made to amplify the  $\mu\text{V}$  output signal from the sensor and send it to the BMS as shown in Figure 3.22. The

accuracy and operation range are stated in Table 2. It should be mentioned also that the sensor is located horizontally at building roof fence to avoid any shading effect. More details are included in Appendix B.



*Figure 3.22. Pyranometer (irradiance meter) and signal amplifier*

### ***Power Analyser***

A power quality analyser was used to monitor the compressor power consumption during operation. The device is manufactured by Fluke type 435 (Fluke, 2016). The power analyser can measure and analyse lots of function depends on the initial setup. The following parameters have been set up to be monitored.

- Average Input Voltage
- Average Input Current
- Average Active Power
- Power Factor

The accuracy and operational range are shown in Table 2.

Table 2. Instruments types, operation range and accuracy

Parameters	Type	Range	Accuracy
Temperatures	Thermistor 10K	-55 to 125 °C	± 0.1 °C
Pressures	Pressure Transmitter	-1 to 34 bar	± 0.3 %
Flow rate	Pulsed Screwed Water Meter	35 to 7000 L/h	± 5 %
Solar irradiance	Pyranometer	0 to 2000 W/m <sup>2</sup>	± 10 W/m <sup>2</sup>
Power	Power Quality Analyser	0 to 20 MW	± 1 %

### 3.4. Phase change material heat exchanger

In this section. Includes a brief introduction on how the PCM material was selected and the PCM HX was initially sized in addition to the proposed method for enhancing the heat transfer between the PCM and working fluid. It also describes the design process of the HX.

#### 3.4.1. PCM material selection

Based on previous literature, organic PCM materials show more stability and efficiency in the charging /discharging lifecycle. The selected material is organic paraffin type A16 which has a melting point 16°C. This temperature was selected based on few considerations; A) the UK weather is not always sunny and solar irradiance is high, therefore, the PCM can be charged with as little as possible from solar collector especially during winter. B) During summer, the temperature in the UK during the night was found above 18°C. This will allow charging from ambient source. After searching the market, the properties of the material chosen for this research are listed in Table 1. More details regarding the PCM A16 is included in Appendix C.

Table 3. PCM-A16 properties

<i>Properties</i>	<i>Values</i>	<i>Units</i>
Melting Area	15-17	°C
Congealing area	17-15	°C
Latent heat	213	kJ.kg <sup>-1</sup>
specific heat	2.37	kJ.(kg.K) <sup>-1</sup>
Density Solid (at 10°C)	840	kg.m <sup>-3</sup>
Density Liquid (at 25°C)	760	kg.m <sup>-3</sup>
Thermal Conductivity	0.18	W.(m.K) <sup>-1</sup>

Flash Point	>250	°C
Max Operation Temp	200	°C

---

#### **3.4.2. Simple calculation and initial sizing**

After selecting the PCM material, it was quite challengeable to find out the matched weight charge of PCM for the experimental rig based on the required energy to be stored. The aim of the PCM HX was to store excessive solar or ambient energy and to be used as a heat source for the IDX-SAHP system. The designed evaporator cooling capacity of the heat pump unit was 2 kW so as to produce sufficient heating to the WST through the heat pump condenser. With this capacity, the PCM energy (dominantly latent energy) was expected to be stored or released within a specified time period and calculated as equation (2).

$$\dot{Q} = \frac{mL}{t} \quad (\text{kW}) \quad (2)$$

The time period was set to 1 hour such that the required PCM weight charge was 33.8 kg. Subsequently, 35 kg PCM was ordered and charged in the PCM HX.

#### **3.4.3. Heat transfer enhancement & detailed design**

One of the most common PCM disadvantages is the poor thermal conductivity. This will directly affect the charging /discharging time of PCM. In order to achieve the targeted storage time, a novel design was developed to enhance the heat transfer between the PCM and HTF in the heat source or sink loop. The HTF used in the experiment and CFD modelling is a mixture of glycol water with glycol concentration of 25% (Wt.) as it is part of the source loop explained earlier in section 3.2.1. The enhancement design was based on a spiral-wired tube which had copper wires soldered around the main copper tube as shown in Figure 3.23. More details for design specifications is included Appendix C.



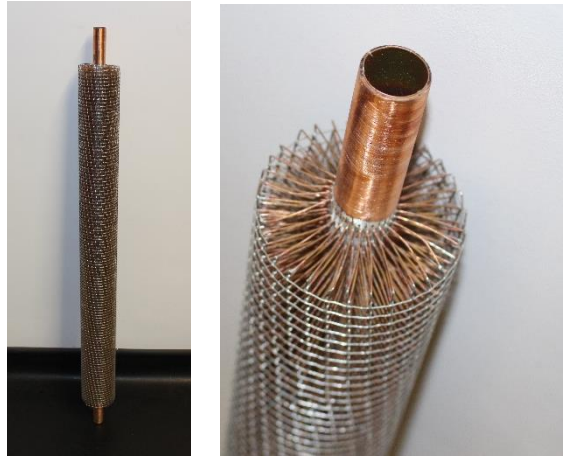


*Figure 3.23. Copper Spiral pipe*

After calculating the amount of PCM mass, the PCM volume was determined by the density of the PCM. A full detailed tank structure has been designed using SolidWorks. After trying a few ideas using 3D drawing, the best feasible design was determined. As the manufacturing process was conducted via the lab facilities at Brunel University, a rectangular mild steel container was found reasonable and easy to make as exterior for the PCM HX. The reason to choose mild steel is because it is cheap and has low thermal conductivity. A mild steel sheet was folded and welded according to the detailed drawing using SolidWorks. The container was designed to contain eight of the proposed spiral-wired tubes. As shown in Figure 3.24 (left), the container has eight 22mm diameter holes at both top and bottom in order to fit the spiral-wired tubes through it. The container top cover was designed to be removable so as to fill or discharge the PCM material. The spiral-wired tubes at both top and bottom ends were connected by a number of U-shape silicon connectors, as shown in Figure 3.24. This silicon connector was selected because it is flexible and it can withstand high pressure and temperature.



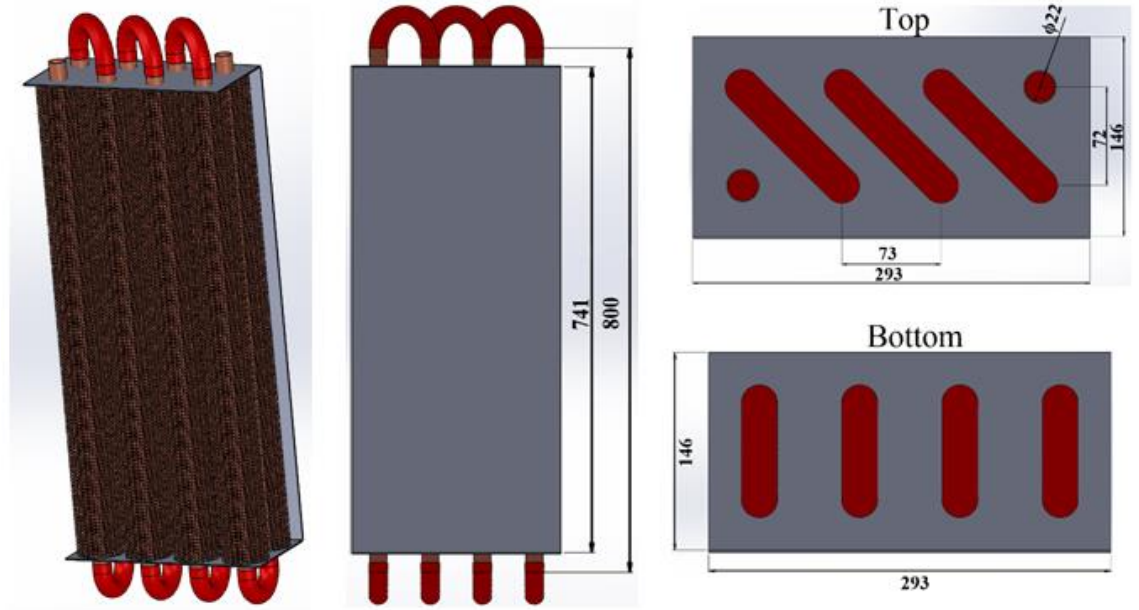


Figure 3.24. 3D drawing in mm for PCM HX – Isometric (left) – front (middle) – top and bottom (right)

After a fully detailed drawing was completed based on the proposed design, the manufacturing process took place. As it is shown in Figure 3.25, after folding and welding the mild steel sheet, eight holes were drilled at the bottom of the container. The spiral-wired tubes were laid off in the container and the bottom ends of the spiral-wired tubes were soldered to the container body. A thermistor was placed inside the tank close to the middle to measure the internal temperature of the PCM. Then a black rubber sealant was placed between the top cover and container body. After that, the U-shape silicone connections were fitted at both bottom and top of the container. Another thermistor was placed at the exterior front of the container to measure the temperature change at different places of the HX. Finally, it was really important to insulate that exterior of the PCM HX to minimize the heat losses, so a 50 mm thick insulation was attached to the HX exterior. The PCM was filled into the PCM HX during the previous process. The tank was fitted to the test rig as it is shown in Figure 3.2.

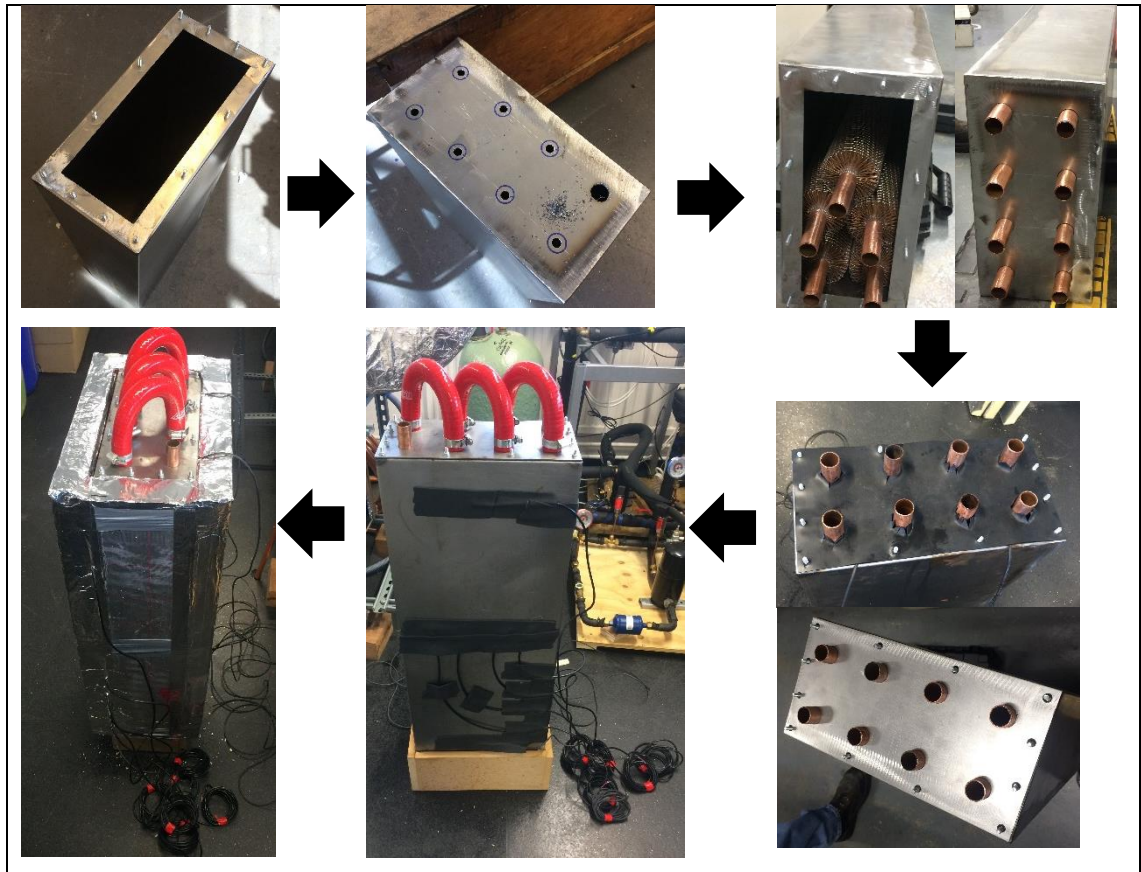


Figure 3.25. PCM HX design process

### 3.5. Control strategy

In this section is included a description of the control strategy and of the modes of operation in addition to brief details of the BMS system and how it is used to control the system and data logging.

#### 3.5.1. Test rig modes of operation

In order to increase the system efficiency, the system should utilize the solar energy as much as possible corresponding to the DHW load demand and weather condition. The operation modes can be classified as below:

##### *Solar and PCM Charging Modes*

In these two modes, the system works as a conventional solar thermal system to cover the DHW load demand and simultaneously charge the PCM HX when applicable. These two modes operate in the same loop which has the following sequence (Figure 3.18):

*Solar collector → V19 ( after the solar collector, left port open and down port closed to bypass the AWHX) → PCM HX → expansion tank → V19 (after the PCM*

*HX, right port open and down port closed) → WST middle immersed coil → V18 (open) → pump 7 (on) → flowmeter → solar collector.*

#### ***IDX-SAHP Mode***

In this mode, the heat pump will take responsibility to meet the DHW load demand. It consists of three related circulation loops: heat source, heat pump and heat sink loops. In the heat sink loop, the glycol-water is the HTF circulating around the heat pump condenser water side and the bottom immersed coil of the WST. The circulation of this loop operates in the following sequence:

*Pump 9 → condenser (water side) → WST bottom immersed coil → flowmeter → pump 9.*

In the heat pump loop, the heat is extracted from the heat source and delivered to the heat sink via a vapour compression heat pump cycle. The refrigerant in the cycle circulates in the following sequence:

*Compressor → condenser (refrigerant side) → receiver → sight glass → filter → TEV → evaporator (refrigerant side) → compressor.*

In the heat source loop, one of the following applicable loop circulations can be selected and controlled based on relevant heat source utilisation:

- 1) AWHX is off- this operation will be enabled if there is enough heat source from solar energy of either solar irradiance or the PCM HX. The circulation of this loop operates in the following sequence:

*Solar collector → V19 (after the solar collector, left port open and down port closed to bypass the AWHX) → PCM HX → expansion tank → V19 (after the PCM HX, right port closed and down port open towards the evaporator) → evaporator (water side) → pump 7 → flowmeter → solar collector.*

- 2) AWHX is on- this operation will be enabled if there is not enough heat source from either solar irradiance or the PCM HX. The circulation of this loop operates in the following sequence:

*Solar collector → V19 (after solar collector, left port closed and down port open towards the AWHX) → PCM HX → expansion tank → V19 (after PCM HX, right port closed and down port open towards the evaporator) → evaporator (water side) → pump 7 → flowmeter → solar collector.*

It should be noted that in Figure 3.1 two bypass- ball valves 5 were installed respectively at the inlet and by-pass pipes of the PCM HX. These two valves are utilised and controlled to measure and compare the performance of the system with and without PCM HX integrated. Also, this loop can be used to charge the PCM.

### 3.5.2. System control strategy

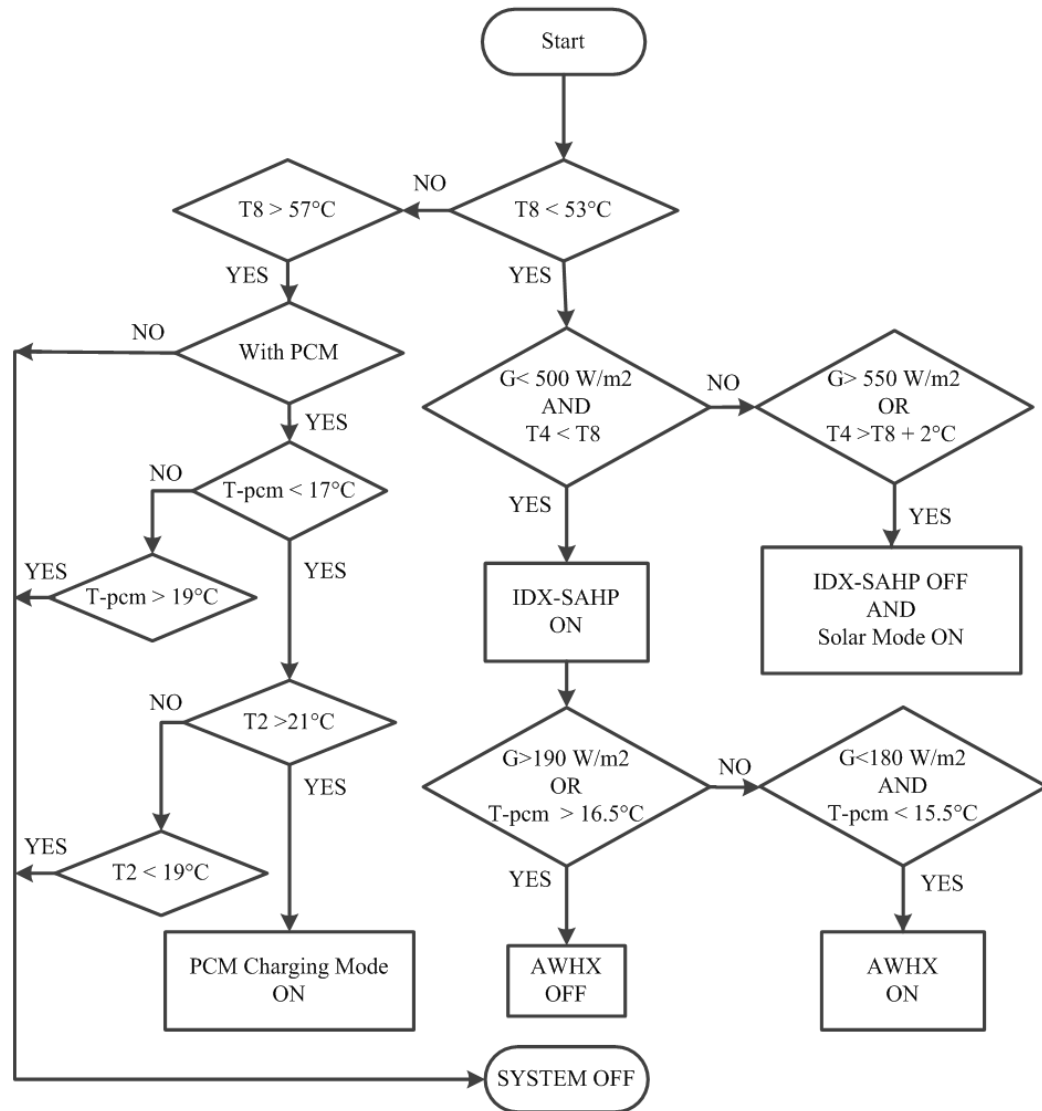


Figure 3.26. Flowchart of system control strategy

As shown in Figure 3.26, the system control strategy has been purposely designed to maintain the water temperature at the middle of the WST ( $T_8$ ) at  $55^\circ\text{C}$  with  $\pm 2\text{ K}$  dead band during a 24-hour operational day. If the  $T_8$  is less than its permitted lower value ( $53^\circ\text{C}$ ), the control will check the instant solar irradiance  $G$  and the supply water temperature ( $T_4$ ) to the WST. If there is not enough solar irradiance ( $G < 500\text{ W/m}^2$ )

and the  $T_4$  is less than  $T_8$ , the IDX-SAHP should be switched on. The control will then check the applicable heat source for the IDX-SAHP. If  $G$  is greater than  $190 \text{ W/m}^2$  or PCM HX temperature  $T_{\text{pcm}}$  is larger than  $16.5^\circ\text{C}$ , either the solar irradiance or heat stored in the PCM HX can be used as the heat source such that the AWHX should be turned off. Otherwise, the AWHX needs to be switched on considering a specific dead band for each parameter so that the ambient air can be utilised as the heat source. On the other hand, if the solar irradiance is sufficient ( $G > 550 \text{ W/m}^2$ ) or  $T_4$  is greater than  $T_8$  plus a 2 K dead band, the IDX-SAHP should be off and the solar mode will be on. When the  $T_8$  is controlled within the setting point band ( $55 \pm 2^\circ\text{C}$ ), the system maintains its operating state. If  $T_8$  is above its higher band, the control will switch off the whole system if the PCM HX is not applied. Otherwise, it needs to determine if the PCM HX needs to be charged with assessing the PCM HX temperature ( $T_{\text{pcm}}$ ) and water temperature at the solar collector outlet ( $T_2$ ). If the  $T_{\text{pcm}}$  is less than  $17^\circ\text{C}$ , the PCM charging mode needs to be turned on when  $T_2$  is greater than  $21^\circ\text{C}$ , otherwise, the whole system will be off (2 K dead band for  $T_2$ ). Alternatively, if the  $T_{\text{pcm}}$  is greater than  $17^\circ\text{C}$  and less than  $19^\circ\text{C}$ , nothing will be changed. However, if the  $T_{\text{pcm}}$  is higher than  $19^\circ\text{C}$ , the whole system will be off.

### ***3.6. Building management system***

In this section, a brief description of the BMS and its component is provided. It also includes a description of how all the system components and instruments are connected and calibrated to the BMS in addition to a description of how the proposed control strategy was implemented to the system using BMS control.

#### ***3.6.1. BMS description***

The selected BMS is developed by Tridium Company. There are two major components of the BMS are:

##### ***1. The controller***

This component is also called JACE by the developer and it is type 6. It is based on a Java programming language developed by Tridium. The controller uses internet protocol (IP) for communication through direct local area network (LAN) connection to a network or through the internet. This promotes a remote control and management for the system through external devices. The controller is operated by a software call Niagara<sup>AX</sup> framework. This framework provides a BMS control elements and

recording the data history which can be used to evaluate the system performance. There two main concepts worth defining to understand the programming of the controller which “platform” and “station”:

Platform: is a local host of the controller which contains all the data required to operate the controller. It has the concept of typical computer host which enables the display and operation of different application and data.

Station: is a customised application created by the developer to control and manage a specific system

## 2. NDIO Module

The NDIO module is the actuator device that can connect actual system components or instruments to the controller. NDIO module types are defined as IO-N which IO refers to its input/output type and N is the number of points that NDIO can take. The selected BMS has 3 modules; one is large type IO-34 and two small type IO-16. The modules are connected in series with a controller as it is shown in Figure 3.27. The typical NDIO module points can be classified to:

- Universal input
- Digital output
- Analogue output

The number of each type of these points depends on the size of the modules. The universal input can read Boolean signal, resistance input or voltage input which can be calibrated to the appropriate unit. The digital output can send a Boolean signal (true/false) and the analogue output can send voltage signal from 0-10 Volts. More details are available in Appendix D.

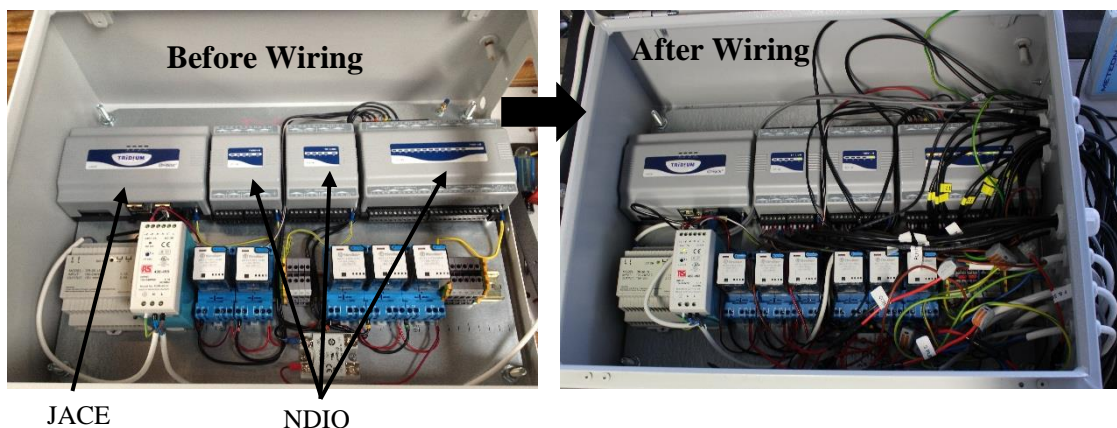


*Figure 3.27. BMS control box before wiring (left) and after wiring (right)*

### **3.6.2. Components connection and instruments calibration**

All powered components and instruments were connected successfully to NDIO modules. The wiring instructions are included at Appendix D. All the output connections are connected to digital output points (Boolean output ) apart from the air cooler and Pump 8 which are connected to analogue output points (voltage output) to control the load profile for DHW consumption. All sensors, transmitters and flow meters are connected to the Universal inputs. All points connected to NDIO module are defined by the station as something call proxy point. As mentioned earlier, the proxy point reads the outputs connected which can be either digital output (Boolean output point) or analogue output (voltage output point). On the other hand, the proxy point has a significant effect on the universal inputs. When the station reads the proxy point connected to the universal inputs, the user has to specify the type of input which can one of the following:

- Voltage input pint
- Resistive input point
- Thermistor input point
- Counter input point
- Boolean input point

Some of these options require further calibration after selecting it. The framework has a built-in calibration function for the popular sensors, meters and gauges. However, if the calibration settings are not included, the user can calibrate these devices linearly or by introducing a new calibration curve.

#### ***Temperature Sensors***

As mention earlier at section 3.3, the selected temperature sensor was a thermistor type 10K $\Omega$ . This type was selected practically because it has a built-in calibration function as shown in Figure 3.28.



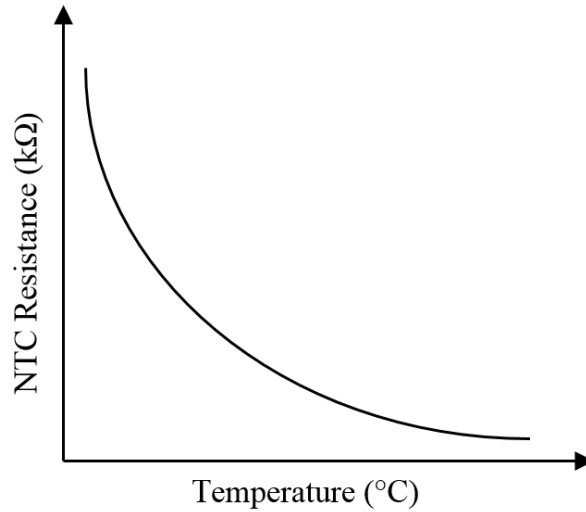


Figure 3.28. Resistance temperature calibration curve

**Pressure Transmitter**

The selected pressure transmitter selected for this experiment has no default calibration setting on the framework. Therefore, the calibration setting was added manually to the framework. The governing equation and block connection diagram between the voltage and pressure is shown in equation (3) and Figure 3.29, respectively.

$$P = \frac{35E-39}{4} \quad (\text{bars}) \quad (3)$$

Where V is output voltage from the pressure transmitter.

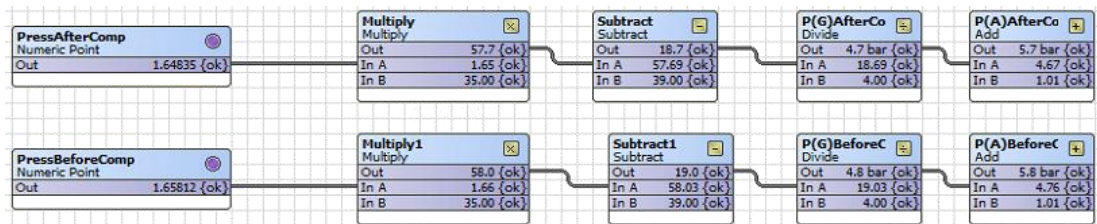


Figure 3.29. Pressure -Voltage Calibration

**Flow Meter**

As mentioned earlier at section 3.3, the flow meter selected for this study is a pulsed screwed flow meter. It sends a pulse signal every 0.1 L. therefore, the scale can be adjusted when the proxy point is imported. The proxy point settings are shown in Table 4.



Table 4. Proxy Point setting for flow meter

Type	Counter Input Point
Conversion	Linear
Scale	10
offset	0
Facets Unit	L
Precision	1

The selected flow meter counts only the litres passing through but it does not record the time. In order to calculate the flow rate, the framework has an extension function all discrete totalize extension which can record the time of operation of any proxy point. This extension has been added to the proxy point of the digital output point of the pumps. In this way, the flow rate is calculated by dividing litre counted by the flow meter by the time of the pumps' operation as shown in Figure 3.30.

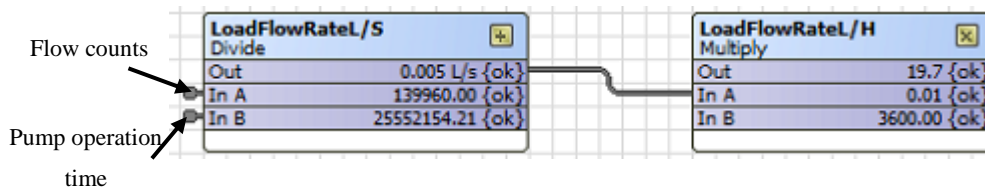


Figure 3.30. flow rate calibration

**Pyranometer**

The proposed Pyranometer can send a very small output signal in  $\mu V$ . As mentioned in section 3.3, a custom-made amplifier was developed in order to increase the voltage in range 0.0-4.35 V which the NDIO can read. The Pyranometer has operation range of 0-2000  $W/m^2$ . Therefore, the scale of the Pyranometer proxy point was calculated according to equation (4) which was 460. The Pyranometer proxy point settings are shown in Table 5.

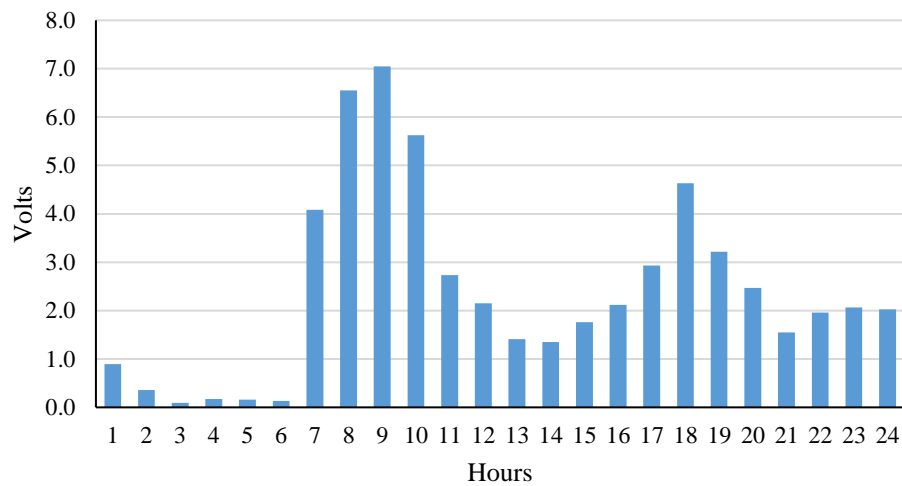
$$Scale = \frac{operation\ Range}{Output\ Range} \tag{4}$$

Table 5. Proxy point setting for Pyranometer

Type	Voltage Input Point
Conversion	Linear
Scale	460
offset	0
Facets Unit	$W/m^2$
Precision	1

### *Load Simulation Pump*

The load simulation pump is connected to a digital inverter, this inverter receives a voltage signal in a range of 0-10 V from the analogue output of the NDIO where 0V indicate the pump if off and the 10 V indicate a full speed. As per the DHW consumption profile per day is shown in Figure 2.1 (Energy Savings Trust, 2008), the maximum consumption per day is 25 l/h. Therefore, the maximum flow rate at the load simulation loop has to be set to be 35 l/h through a ball valve. The load profile voltage scale was evaluated using an equation (4) which found that the profile needs to be reduced by 3.5 times. The load voltage profile is shown in Figure 3.31.



*Figure 3.31. load voltage profile*

The load voltage profile was inserted to the framework through a writeable schedule function which can change the voltage each hour as it is shown in Figure 3.32. The output connection of this function was further connected to an analogue voltage output to the pump. This output signal it was also checked; if it is higher than zero to operate the fan cooler on signal and if it is equal to zero to switch off the fan cooler as it is shown in Figure 3.33.

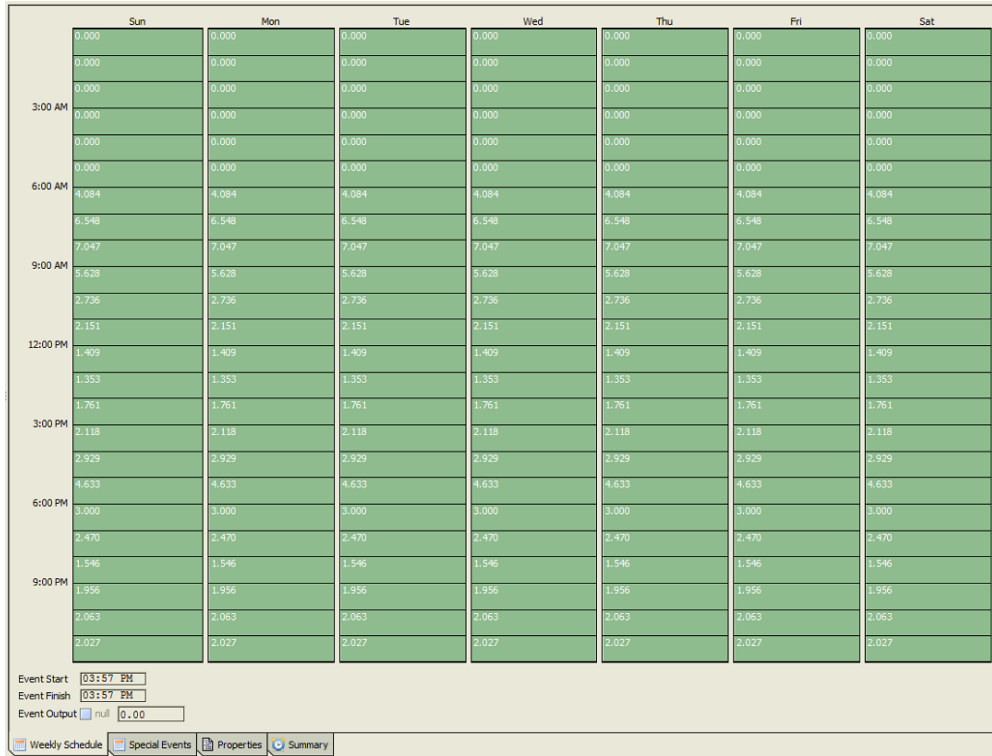


Figure 3.32. writeable schedule function for load voltage profile

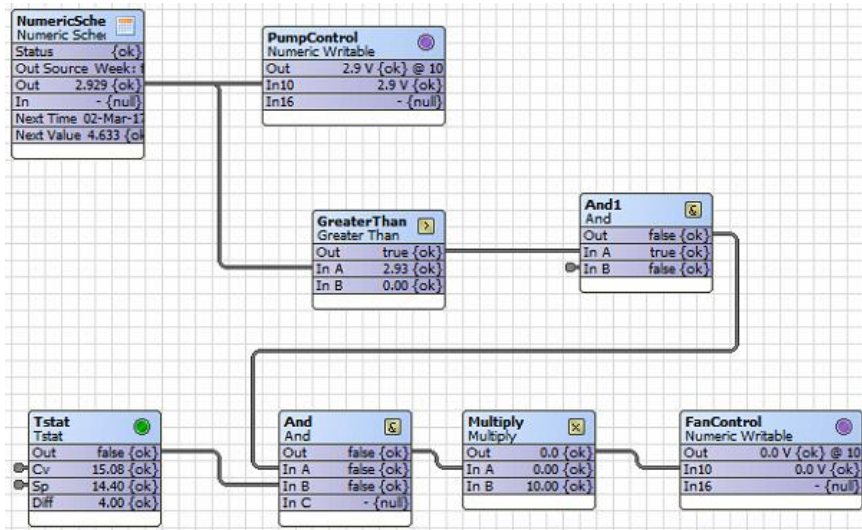


Figure 3.33. Load simulation pump and fan cooler block connection diagram

### 3.7. Logic block connection graphics design

In order to implement the proposed control strategy at section 3.5.2, a block connection was developed using the framework of the BMS system. As it is shown in Figure 3.34, the block connection diagram consists of several blocks wired together. Each block has its own settings based on its function and it can have several of single inputs but it can only have a single output. The most important function used in this logic is the Tstat function that this software has. This function allows a dead band range to avoid a fluctuation of the signal. All Tstat blocks are marked with a green dot in Figure 3.34.

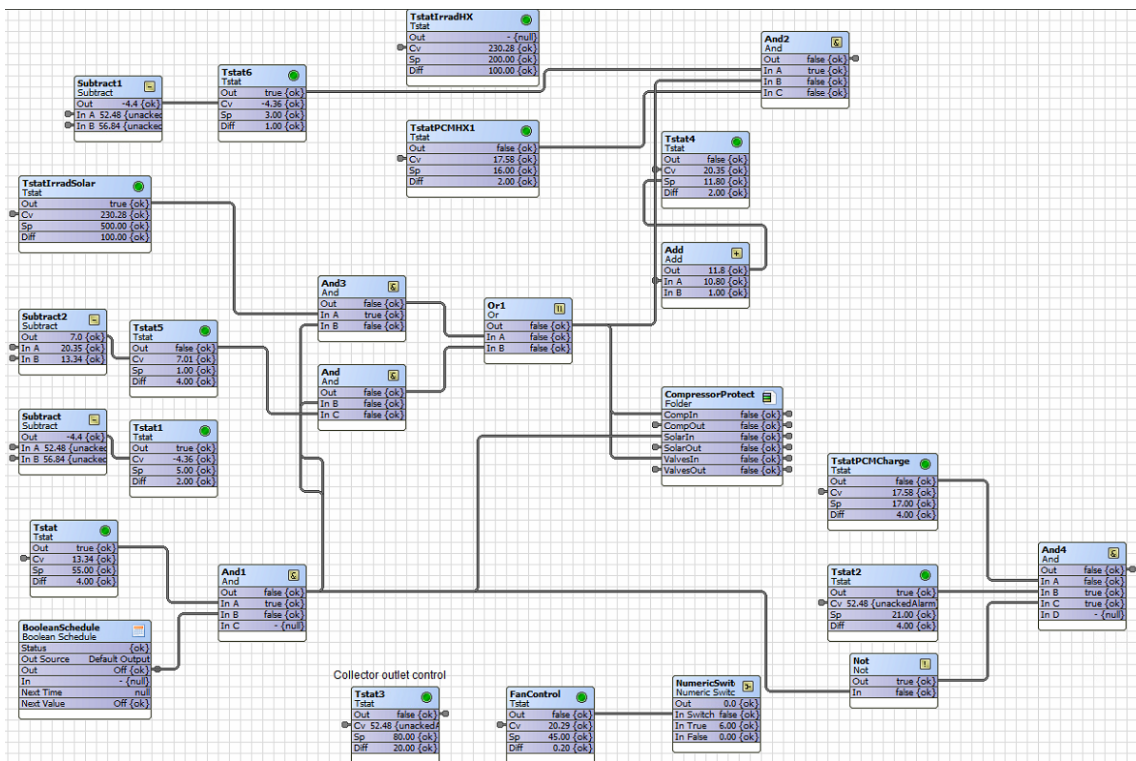


Figure 3.34. Control logic block connection

### ***3.8. Summary of Chapter 3***

This chapter illustrates the procedures, equipment and instrument used for the experimental investigation of this research. The design consideration and thermodynamic analysis were presented in detail. The key points of the experimental process are:

- Design and construct IDX-SAHP test rig
- Identify system operation modes
- Create and implement optimal control strategy for the system
- Design, manufacture and install PCM HX for excess energy storage.

The system heating output capacity is 9 kW. The system is designed for large houses (4-5 bedrooms) or small buildings (2-3 apartments). The solar collector efficiency is expected to be between 0.6-0.75 depending on the solar irradiance and operation temperature. For the heat pump operation, the condensation temperature is expected to be between 50-60°C. Meanwhile the evaporating temperature can vary depending on the selected heat source and operation time. For the PCM HX, the organic PCM material was selected for this project with a melting point at 16°C. The AWHX capacity is 10 kW. This capacity could be reduced by controlling the fan speed depending on the cooling capacity. The COP of the system is expected to reach 5 by using the PCM HX. The original control strategy applied to the system aims to reduce the system energy consumption and reliable operation of the system. The system is expected to operate at the ambient conditions during summer and winter including sunny and cloudy conditions.

The next chapter discusses the experimental outcomes after we tested the system with and without the effect of PCM HX. The experiment focuses on testing the proposed control strategy and the effect of PCM HX on the system performance and stability.

---

***Chapter 4. Experimental Findings and Analysis***

---

### ***4.1. Introduction***

In this chapter, the findings of the experimental part of this project will be presented. The experimental components, configuration and the proposed control strategy are illustrated in Chapter 3. The outcome of this chapter will be used in the development and validation of the dynamic simulation models to be presented in Chapter 5. The results included in this chapter will demonstrate a comparison of the system's operation during different climate conditions. This will include the system performance with and without the effect of PCM HX which operation was described in section 3.4.

### ***4.2. Start-up measurements and procedure***

In order to examine experimentally the effect of the PCM HX on system stability and performance, four test days have been conducted in 24 hours each at four combined climate conditions and PCM integrations. These included sunny with and without PCM HX and cloudy with and without PCM HX. As shown in Figure 4.1, the solar irradiances during two sunny test days with and without PCM HX were almost steady with maximum values of  $621 \text{ W/m}^2$  and  $625 \text{ W/m}^2$  respectively while the irradiances during those two cloudy test days had too many fluctuations. It is also noticed that the solar energy was only available during the daytime when the solar irradiance was greater than zero.

Figure 4.2 and Figure 4.3 show the variations of ambient and WST load feed water (T9) temperatures during all these four test days. It should be noted that all temperature, power, irradiance and pressure logging data were based on five minutes interval whereas any other logging data was based on the change of each sensed value. As explained earlier, the feed water supply to the WST is mainly from domestic tap water. Therefore, the minimum temperature it could achieve was the same as the ambient temperature due to the heat transfer limitation of the AWHX.

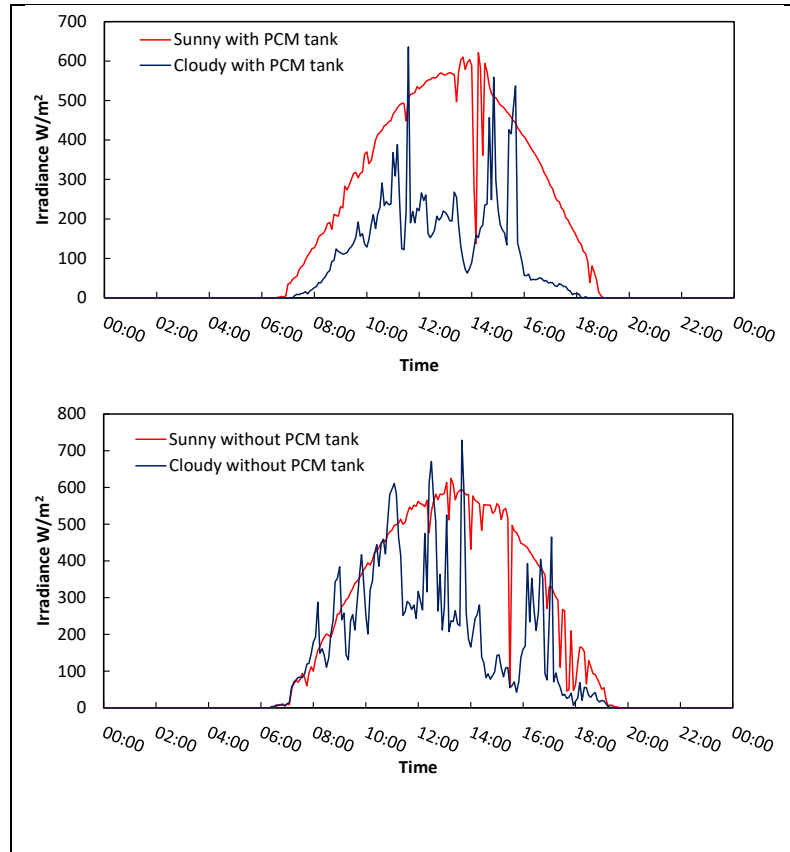


Figure 4.1. Variations of solar irradiances during four test days 4

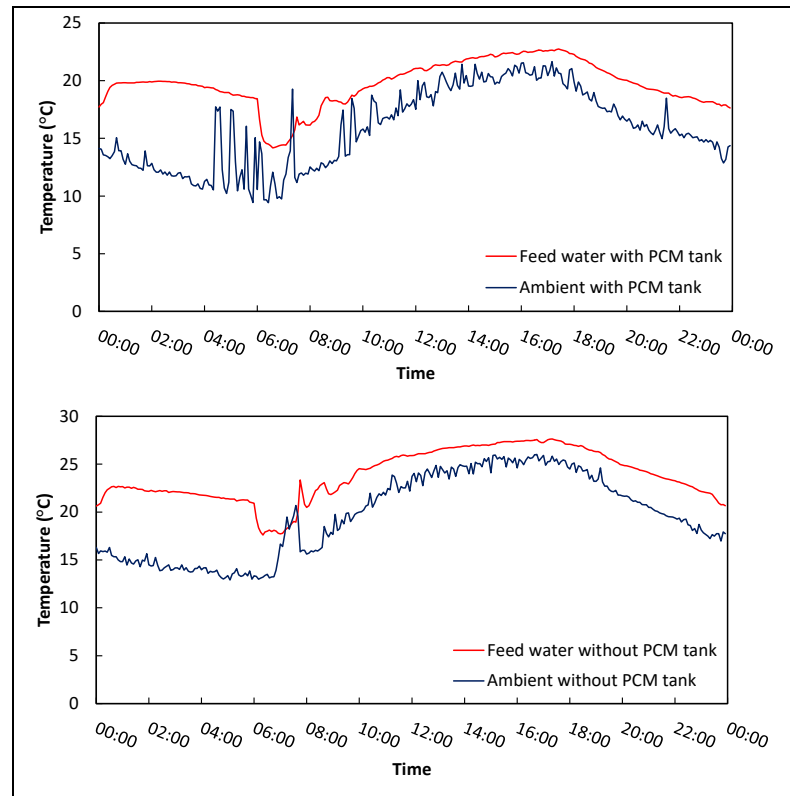


Figure 4.2. Variations of ambient and feed water temperatures during two sunny test days 5



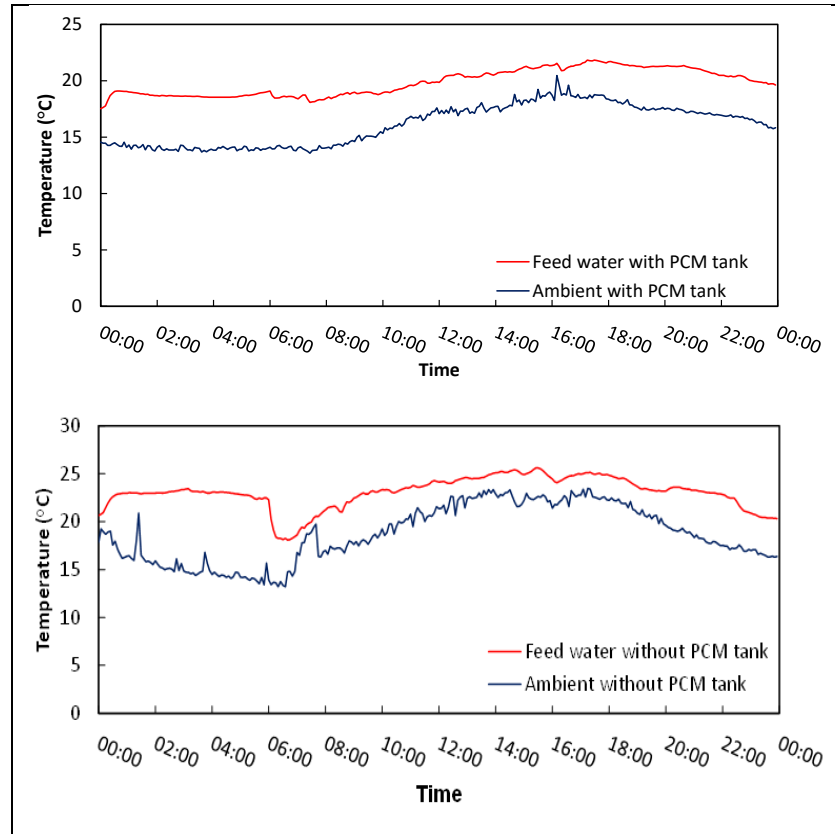


Figure 4.3. Variations of ambient and feed water temperatures during two cloudy test days 6

Figure 4.4 shows the feed water flow rate or load profile supplied to the WST for each operational day. Each flow rate was controlled by a variable circulation pump speed which was regulated by BMS according to the specified load profile (Energy Savings Trust, 2008). It is seen that the load profile for each test day was controlled almost the same with each other which of course should be independent of weather conditions and system designs.

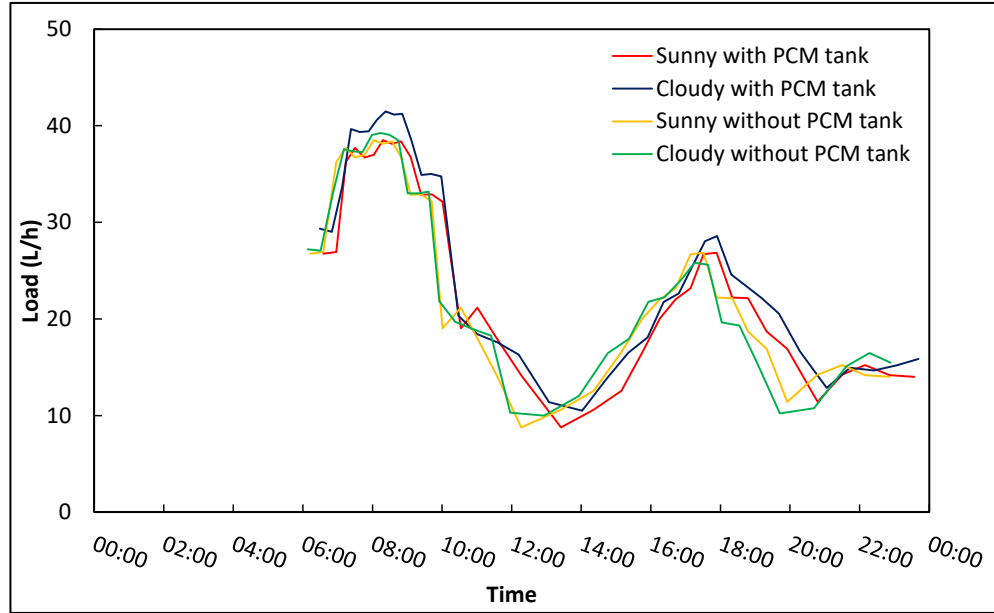


Figure 4.4. Variations of load profiles during all four test days 7

### 4.3. Thermodynamic analysis

The mass flow rate of refrigerant is calculated by the energy balance of water and refrigerant sides across the condenser assuming there is no heat loss to ambient:

$$\dot{m}_{ref}(\Delta h)_{ref} = \dot{m}_w C_{p,w}(\Delta T)_w \quad (\text{kW}) \quad (5)$$

The thermo-physical properties of R134a used for thermodynamic analysis are calculated using Engineering Equation Solver (EES<sup>®</sup>) (Klein and Alvarado, 2016).

The heating capacity of the system in IDX-SAHP mode is calculated based on water side inlet and outlet parameters of the condenser:

$$\dot{Q}_h = \dot{m}_w C_{p,w}(\Delta T)_w \quad (\text{kW}) \quad (6)$$

The heating COP of the system is calculated as the ratio of the total heating capacity to the total power consumption of the system:

$$COP_{sys} = \frac{\dot{Q}_h}{\dot{W}_{comp} + \dot{W}_{awhx} + \dot{W}_{pum}} \quad (7)$$

The SPF for direct solar loop is calculated by equation (8)

$$SPF = \frac{\dot{Q}_{coll}}{\dot{Q}_{sol} + \dot{W}_{pum}} \quad (8)$$

#### 4.4. Experiment finding and discussion

Based on the proposed system control strategy described previously, experimental investigations were carried out on the IDX-SAHP system during those four test days and some of the test results are demonstrated and evaluated in this section. As illustrated in Figure 4.5 and Figure 4.6 for the temperature development inside the WST, the system could meet the DHW demand by supplying hot water flow from the WST top with temperatures between 52°C and 57°C during all these four test days. To understand clearly the system controls, the variation of water temperature from the PCM HX outlet (T4) is also presented in each plot.

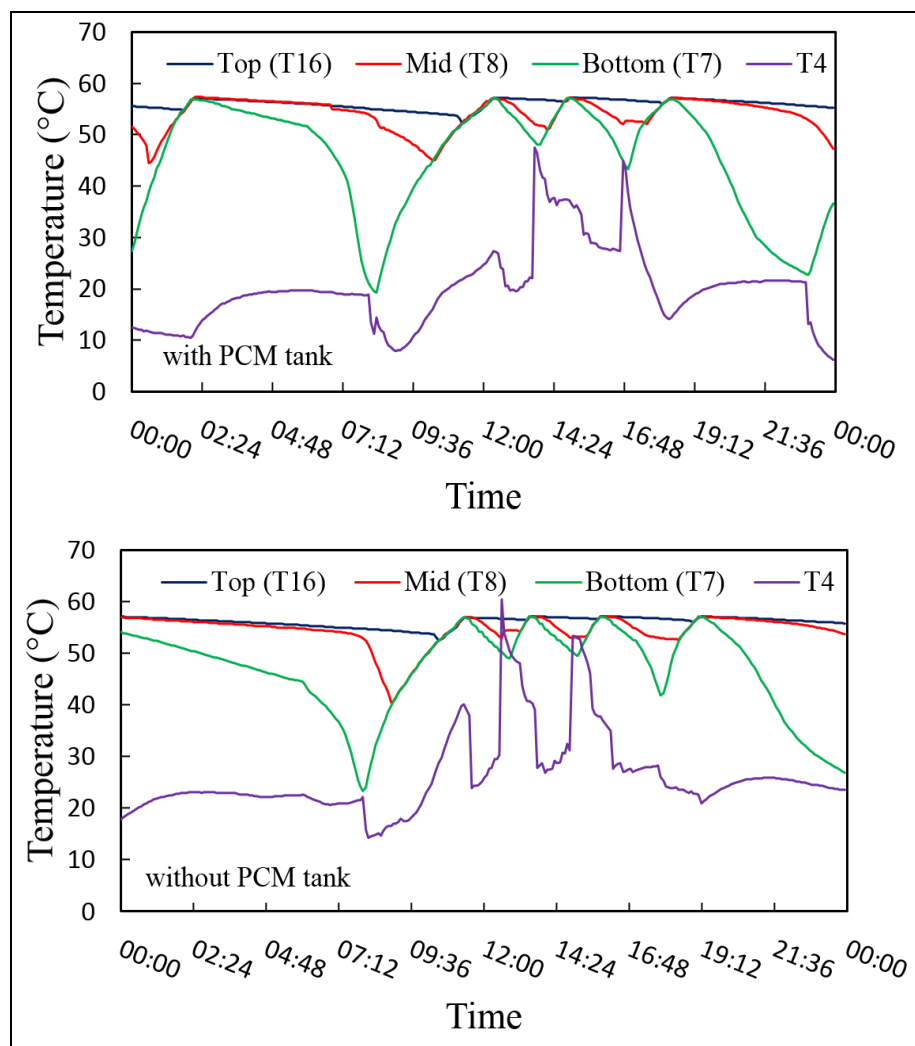


Figure 4.5. Variations of WST water temperatures and temperature T4 during two sunny test days 8

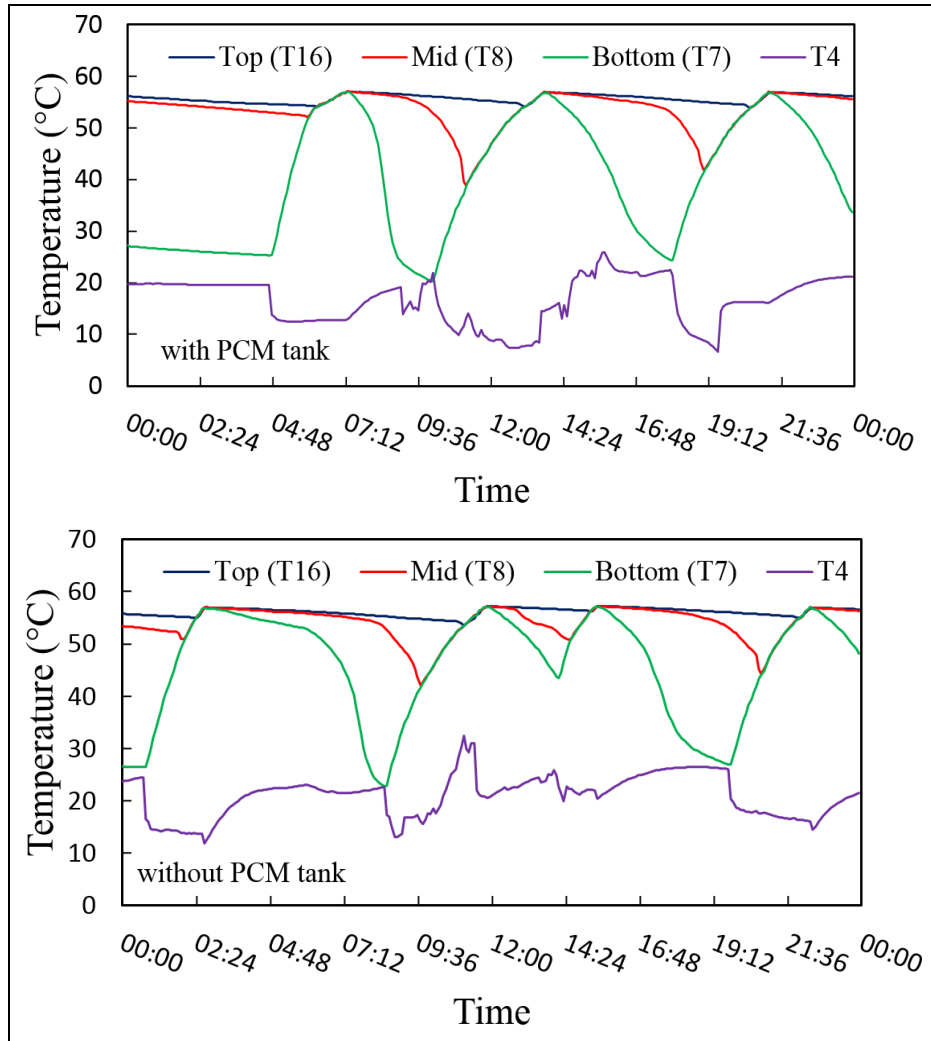


Figure 4.6. Variations of WST water temperatures and temperature T4 during two cloudy test days 9

As indicated in Figure 3.26, the temperatures of T8 and T4 and solar irradiance will determine the operation of the IDX-SAHP. It is observed that for each test day around 8 am there was a big temperature drop at the tank bottom (T7) before the water temperature T8 dropped below the lower band of its setting point. This abrupt decrease in the bottom tank water temperature T7 was due to the starting of DHW load demand in the morning on that day as shown in Figure 4.4. Meanwhile, the feed water temperature for each operational day was different due to various ambient air temperatures. Consequently, there were different lowest bottom tank water temperatures for these four test days. To fully understand the system performance, the test results of these four operating days are explained separately in the following parts.

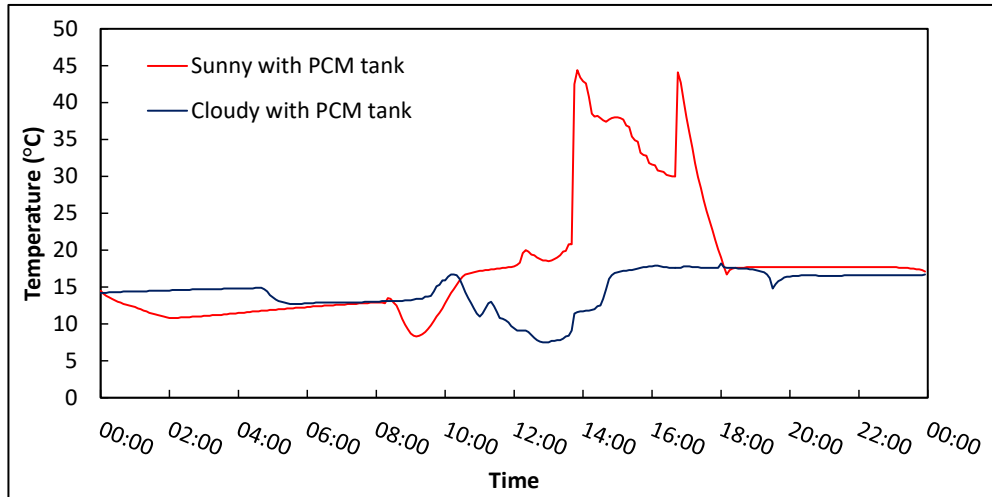


Figure 4.7. Variations of PCM HX inside temperatures during two test days 10

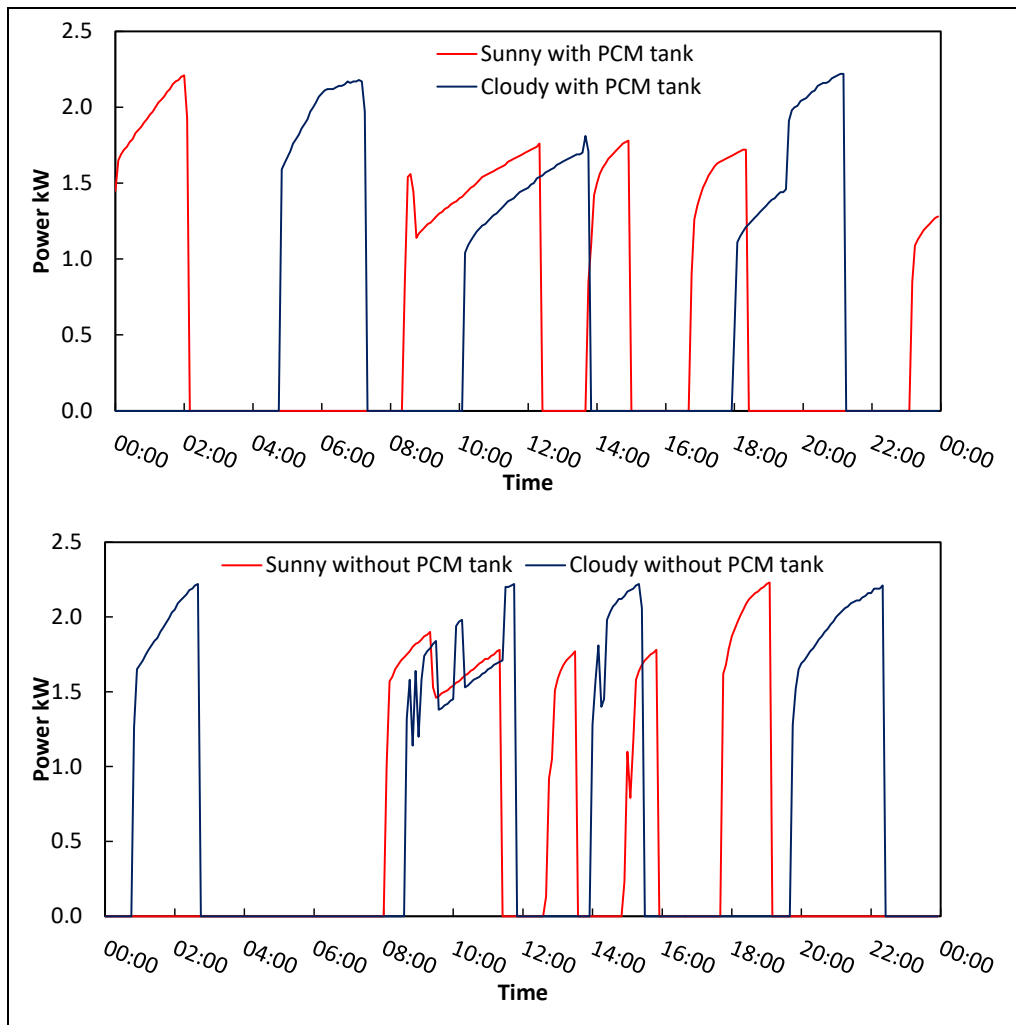


Figure 4.8. Variations of system power consumption during four test days 11

For the sunny test day with PCM HX, the compressor started at midnight with no heat stored in the PCM HX as the PCM temperature ( $T_{\text{pcm}}$ ) inside the PCM HX was  $14.5^{\circ}\text{C}$ , as shown in Figure 4.7, which was below its melting point. That resulted in switching the AWHX on during that period to utilise the heating source from the ambient air, as shown later on in Figure 4.11. The heat pump compressor operated until 2:05 pm when  $T_8$  was higher than  $57.0^{\circ}\text{C}$  and the system then started in PCM charging mode. During this period the maximum value for the total power consumption, condenser capacity and COP were 2.2 kW, 9.632 kW and 4.7 respectively as shown in Figure 4.8, Figure 4.9 and Figure 4.10 each.

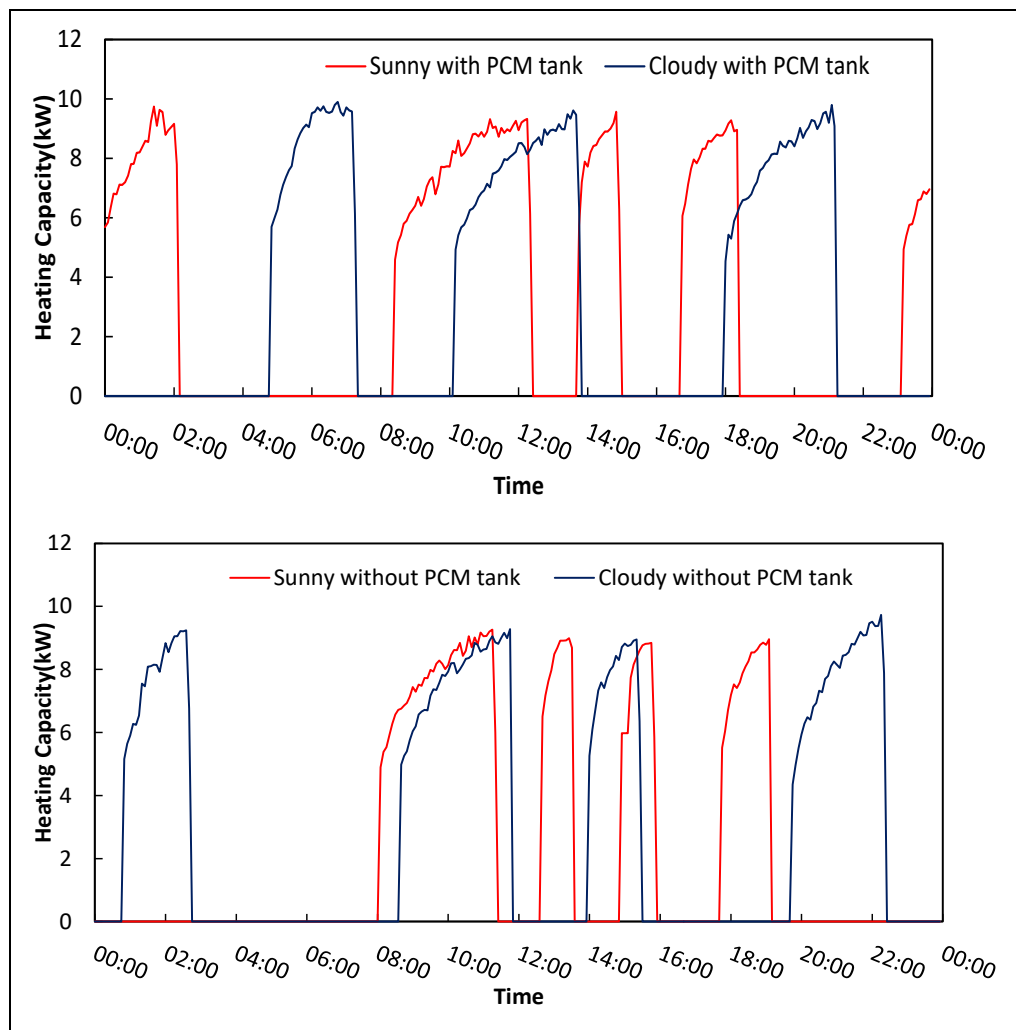


Figure 4.9. Variations of system heating capacities during four test days 12

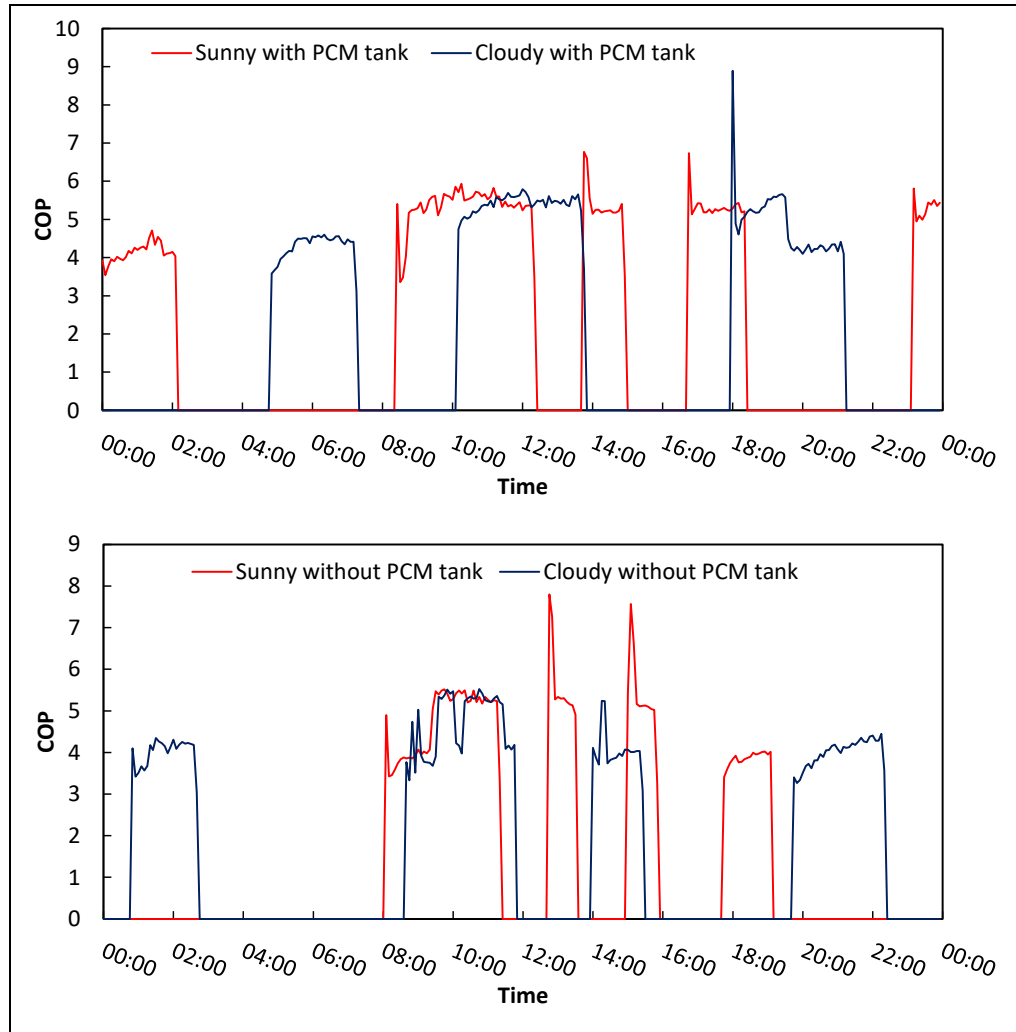


Figure 4.10. Variations of system COPs during four test days 13

The PCM charging mode operated until 8:20 am when  $T_8$  started to drop below  $53^\circ\text{C}$  and the heat pump compressor was switched on again. Up to that point, the PCM inside the tank was still not charged significantly since its temperature was only at  $12.8^\circ\text{C}$  such that the AWHX needed to operate. The AWHX operated until at 8:35 am when the solar irradiance  $G$  reached above  $190\text{ W/m}^2$  and could be utilised as the heat source for the IDX-SAHP. Correspondingly, at that instant, the system power consumption thus dropped abruptly and the COP increased sharply, as shown in Figure 4.8 and Figure 4.10 respectively.

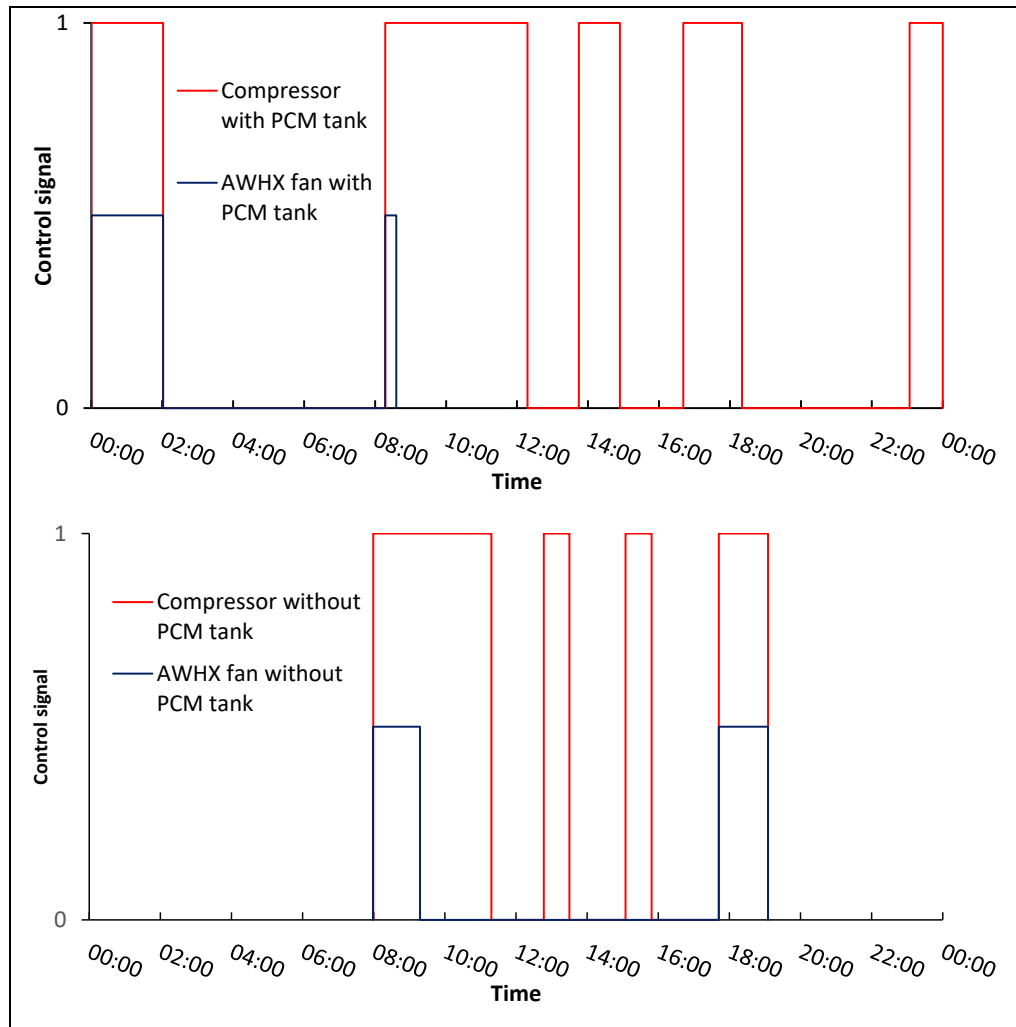


Figure 4.11. Variations of compressor and AWHX fan control signals during two sunny test days 14

After that, the system power consumption and condenser heating capacity increased gradually but COP varied. The heat pump compressor kept running until 12:20 when T8 started to be higher than 57°C again. During this period, the PCM temperature T-pcm started to drop to its minimum temperature at 8.3°C at 9:10 am since the AWHX was on at the beginning. The T-pcm was then picked up at different rates when the AWHX was off and more solar irradiances were available. These included significant 8.7°C increase from 9:10 am to 10:50 am due to sensible PCM heating process and only 1 °C increase from 17°C to 18°C at the time period between 10:55 am to 12:05 because of the latent PCM heating process involved. At 12:05, the PCM was totalled melted and from there only sensible PCM heating existed such that the T-pcm increased abruptly from 12:05 to 12:20.



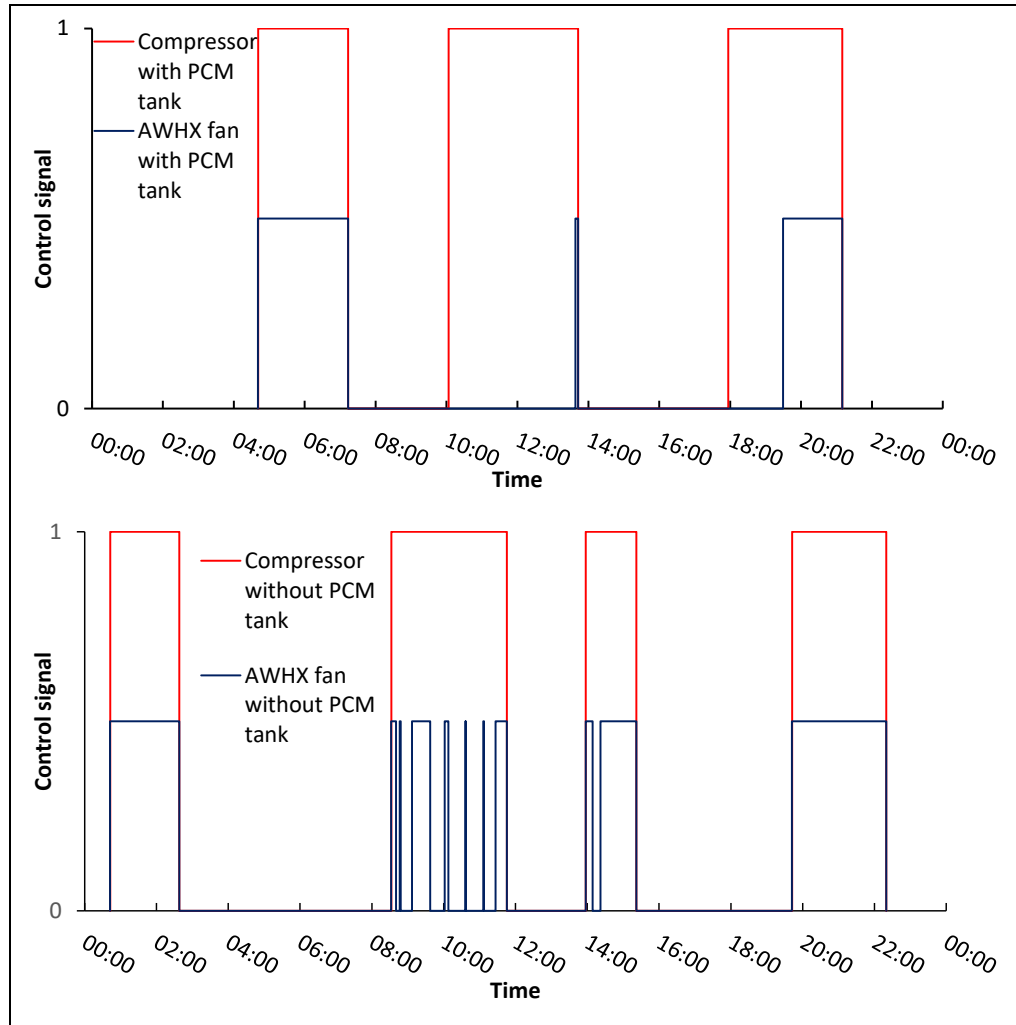


Figure 4.12. Variations of compressor and AWHX fan control signals during two cloudy test days 15

From there, the whole system was shut down since the  $T_{\text{pcm}}$  was higher than  $19.0^{\circ}\text{C}$ . The tank water temperature at T8 thus started and continued to drop to below  $53.0^{\circ}\text{C}$  at 13:40 when either IDX-SAHP or solar mode needs to be controlled. From that time as shown in Figure 4.5, although the solar irradiance  $G$  was higher than  $500\text{ W/m}^2$ , the water temperature T4 was still lower than T8 such that the IDX-SAHP mode was on and the AWHX was off due to the higher  $G$  values. Meanwhile, the PCM temperature  $T_{\text{pcm}}$  had a big jump due to the high temperature from the solar collector outlet and the PCM sensible heating process. The  $T_{\text{pcm}}$  then followed the changes of the solar collector outlet water temperature and the PCM absorbed and released heat respectively to the water flow depending on the temperature differences between these two temperatures. Correspondingly, from 19:15 the water received heat from the heat stored in the PCM HX. The system was switched off at 14:55 when T8 was above  $57^{\circ}\text{C}$  and the  $T_{\text{pcm}}$  was higher than  $19^{\circ}\text{C}$ . After that, the IDX-SAHP had two on periods starting at 16:45 and 23:10 respectively when T8 were both lower than

53.0 °C and one-off period starting at 18:25 when T8 was above 57°C. It is noted that the AWHX was always off during this period since the T-pcm was continuously higher than 16.5°C.

For the cloudy test day with PCM HX, the same control strategy shown in Figure 3.26 would be followed. As shown in Figure 4.6, from midnight the system was continued off until at 4:45 am when the water temperature T8 dropped below 53.0°C. After that, the heat pump compressor had three times running periods and three times off periods due to the variations of T8, as shown in Figure 4.12. Meanwhile, there was still two longer and one shorter on periods for the AWHX considering of the corresponding lower solar irradiances and lower T-pcm then. Subsequently, the variations of system power consumption, heating capacity and COP could be found from Figure 4.8, Figure 4.9 and Figure 4.10 respectively.

For the sunny test day without PCM HX, the system operation on or off was dependent only on the water temperature T8 and any changes of T-pcm shown in Figure 3.26 would be ignored. As shown in Figure 4.5, from midnight the system was continued off until at 8:00 am when the water temperature T8 dropped below 53.0°C. After that, the heat pump compressor had four times running periods and four times off periods due to the variations of T8, as shown in Figure 4.11. Meanwhile, there were still two longer on periods for the AWHX considering of the corresponding lower solar irradiances then.

Similarly, for the cloudy test day without PCM HX, the system operation on or off was dependent only on the water temperature T8 and any changes of T-pcm shown in Figure 3.26 would be ignored. As shown in Figure 4.6, from midnight the system was continued off until at 0:45 am when the water temperature T8 dropped below 53.0°C. After that, the heat pump compressor had four times running periods and four times off periods due to the variations of T8, as shown in Figure 4.12. Meanwhile, there were still three longer on and a number of shorter on periods for the AWHX considering of the corresponding lower solar irradiances then.

Respectively, for the cloudy days with and without PCM HX, the variations of system power consumption, heating capacity and COP could be found from Figure 4.8, Figure 4.9 and Figure 4.10 respectively.

As the system is automated control, the operation periods are dependent on the ambient condition and load profile correspondence. Since the ambient condition is difficult to control, the feed water temperature to the WST will be affected by this variation, especially during cloudy tested days. Thus, this explains the shift in the profiles during the tested day with and without the PCM HX.

Table 6. System Performance for the four test days

Test day	Total power (kWh)	Heating capacity(kWh)	Heating COP
Sunny day with PCM	15.61	77.90	4.99
Cloudy day with PCM	15.83	75.95	4.80
Sunny day without PCM	11.09	52.15	4.70
Cloudy day without PCM	17.11	72.00	4.21

In summary, the total system power consumption, heating capacity and COP are calculated based on measurements for each of these test days and listed in Table 6. It is noted that the heating capacity is the same as the energy input to the WST for each test day. From the measurements, the heating capacities (energy inputs) for three test days were quite similar to each other considering the similar load profiles and feed water temperatures as shown in Figure 4.2, Figure 4.3 and Figure 4.4. However, the heating capacity (energy input) on the ‘Sunny day without PCM’ was relatively low considering the higher ambient and feed water temperatures on that day as shown in Figure 4.2. From the table, although the total power consumption and heating capacities varied with different test days, the sunny day with PCM had the maximum COP of 4.99, the COP on cloudy day with PCM the second at 4.80, the COP on sunny day without PCM the third at 4.70 while the COP on cloudy day without PCM the least at 4.21. The test results can demonstrate that the system performance can be significantly improved on various weather conditions if the PCM tank could be integrated.

#### 4.5. Uncertainty analysis

Taking into consideration the uncertainty of the experiment measurements including the water/glycol mass flow rates, temperatures, power consumption and pressures, the average uncertainties are calculated for all test days by aid of the EES software(Klein *et al.*, 2014) which are  $\pm 9.32\%$ ,  $\pm 9.28\%$  and  $\pm 9.31\%$  for the COP, the heating capacity

and the refrigerant mass flow rate, respectively. The uncertainty values are relatively high as the calculations are based on heat balance between the water/glycol and refrigerate sides. More details are included in Appendix E.

#### ***4.6. Summary of Chapter 4***

This chapter shows the findings of the performed experimental work of this research. The strategy of the experiment was to test four days during 24 hours operation for combined climate conditions and PCM integrations. These included sunny with and without PCM tank and cloudy with and without PCM tank. Furthermore, the thermodynamic analysis and start-up measurement are included. For all tested day, the system COP, system heating capacity, system power consumption, WST temperatures, PCM temperature and control signal is presented graphically. Also, a brief consideration of the uncertainty of the analysis is included. The experimental results show that the designed IDX- SAHP system can meet the daily hot water load demand with constant hot water supply irrespective of weather conditions and system structures. In addition, the IDX-SAHP system could have various performance improvements at different weather conditions when the PCM tank was integrated. Quantitatively, the average COP of the IDX-SHAP system with the PCM tank could increase 6.1% and 14.0% on sunny and cloudy days respectively comparing to those systems without PCM tank integrations. These are based on the weather conditions for different test days illustrated in this chapter.

The following chapter illustrates the numerical development of the system based on the produced results from this chapter. Moreover, the validation of the developed models is also presented.

---

***Chapter 5. Numerical Model Development***

---

### ***5.1. Introduction***

An introduction to the simulation tool that has been used in this study will be provided. It will also illustrate the methodology and some of the theoretical concepts used to simulate the proposed system. The model development strategy will be also illustrated in detail in this chapter. Moreover, the details of the TRNSYS model for the whole system, the EES model for the heat pump and CFD PCM HX model development will be included. A novel dynamic coupling method for the developed models will be also presented in addition to the validation for developed models with experimental results.

### ***5.2. Introduction to numerical simulation***

TRNSYS<sup>®</sup> is a simulation tool that eases the evaluation of transient systems behaviour. This includes HVAC system, water heating systems, renewable energy systems, evaluating system performance and analysing system control logic. The software consists of two major parts; the Kernel and the library. The Kernel is an engine that reads, solves and processes the project input file (\*.dck). The library contains the pre-developed models of typical energy components. Each of these components is called “TYPE” and each type has a unique number. The library contains almost 150 components ranging from controllers, HVAC, HXs, hydronics and weather data. One of the advantages of TRNSYS is that allows the user to modify these components or even create their own. This can be done via various coding languages such as FORTRAN or C++ which can be integrated with the Dynamic Link Library (DLL). Each component contains a subroutine that carries the function of the component. By changing this subroutine or creating a new one, the TRNSYS modular comply these changes with DLL. This gives the users more reliability and flexibility for simulation.

When the user opens TRNSYS simulation studio, TRNSYS creates a project file (\*.tpf). This file allows the user to select the system components and interlink them through a graphical interface. The Kernel engine obtains a solution for this project file using either one of two methods; Successive Substitution method or Powell’s method (Klein *et al.*, 2014). The first method was based on linking the output of a component to the input of another component with the same property. This method allows calling the component as much as it needs to converge the solution. Powell’s method was

developed later on to enhance the data limitation of the Successive Substitution method (Klein *et al.*, 2014). In this research, TRNSYS will be used as a platform to simulate the whole test rig but the PCM HX and heat pump. Further details are included in section 5.3.1.

To simulate the heat pump, EES<sup>®</sup> is used in this study. This tool eases the solutions of non-linear equations. It has a built-in function for thermodynamic and heat transfer problems. This reduces iterative problems as no coding required to get these properties. Further details are provided in section 5.3.2.

Another simulation tool used in this research is ANSYS FLUENT<sup>®</sup>. This package is a CFD tool that predicts the fluid flow behaviours such as; heat and mass transfer, chemical reactions and related phenomena. Its solver engine is based on the finite volume method. This tool will be used to simulate PCM HX. The reason for selecting this tool is because it can predict the melting and solidification behaviour of the PCM and how it will react with the proposed design. Further details are provided in section 5.3.3.

### ***5.3. Model development strategy***

Modelling of each component of the proposed test rig is really important. The reason to choose TRNSYS as platform modular is because it has most of the system components that are existing at its library. As the PCM HX is a new innovation, it was important to create an accurate model that consider melting and solidification process of the PCM and study the behaviour of the proposed method for enhancing heat transfer. Meanwhile, the proposed heat pump of the system is custom made. Therefore, investigation of the performance of the heat pump experimentally was necessary for the modelling of this component. To summarise the vision of the model strategy, the following steps were taken to develop the final numerical model of the system.

- Develop a platform model in TRNSYS for system most components
- Create heat pump model in EES base on the experimental performance data
- Control the system operation using the same control logic in section 3.5.2.
- Create a CFD model for PCM HX
- Couple these models together to evaluate the whole system performance.

To ensure the quality of the modelling, it was necessary to conduct a validation analysis for the developed models.

The main purpose of creating the numerical model of the system is to study the system performance in different countries that have higher and longer irradiance values and period respectively.

### 5.3.1. IDX-SAHP TRNSYS platform model

The whole test rig was simulated in TRNSYS. However, the heat pump and PCM HX was modelled externally and TRNSYS calls these models when is needed during the simulation. This explains why TRNSYS model is used as a platform to run the whole model including the developed external models for the PCM HX and the heat pump. The graphical model of the system is shown in Figure 5.1.

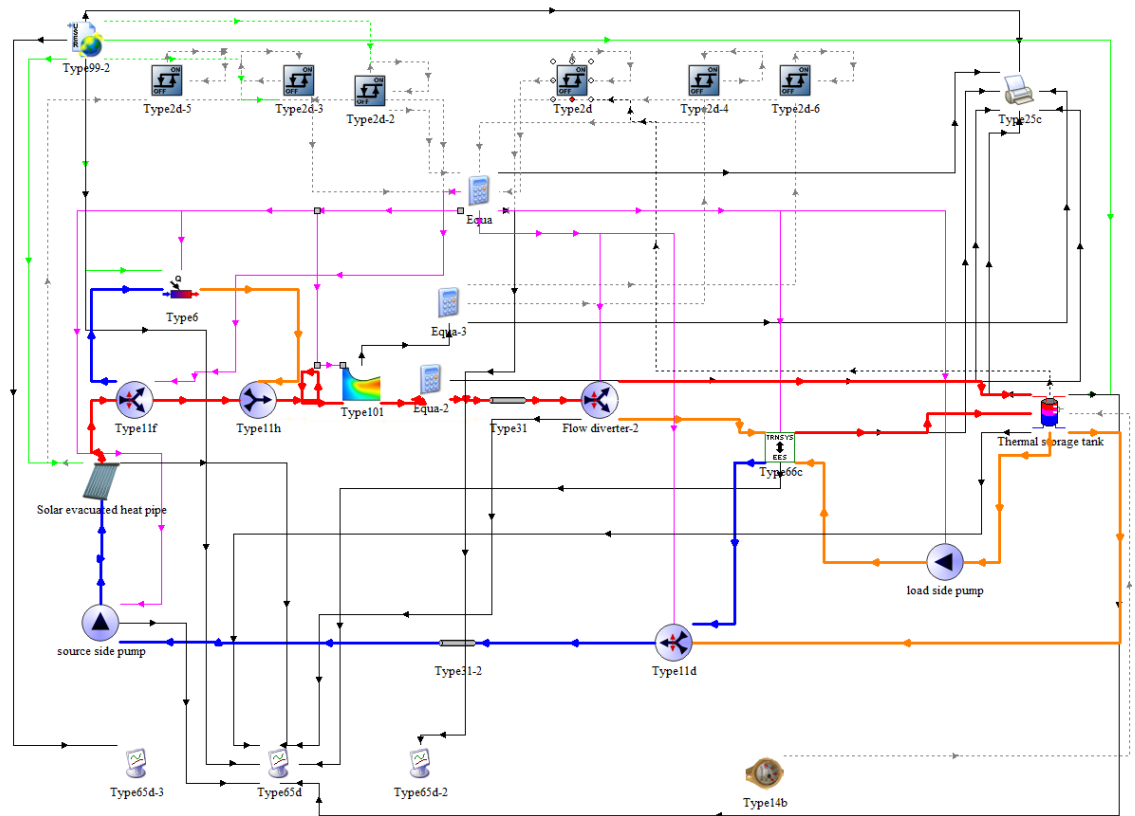


Figure 5.1. Graphical model for the proposed test rig

As TRNSYS is a popular simulation tool, only the theory of the major components of the system will be provided. However, more details regarding the components used from TRNSYS library is presented at Appendix F including parameters setting. The test rig major components are:

- Thermal storage tank



- Control System

### Thermal storage tank

The thermal storage tank of the system was modelled using Type 60d from TRNSYS library. The tank was modelled using 51 nodes which means that the tank will be divided into 51 equal sections. This was necessary to study the effect of the tank stratification and how it affects the performance of the system. This also explains why in equation (9) the first, second and third terms have discretisation. As the temperature changes between the layers, the water thermal conductivity and the overall heat transfer coefficient between the layers will change. The tank has one inlet, one outlet, no auxiliary heating and two internal HXs. At each node, the component balance all energy flow into one equation as it is shown in Figure 5.2 and equation (9) (Klein *et al.*, 2014).

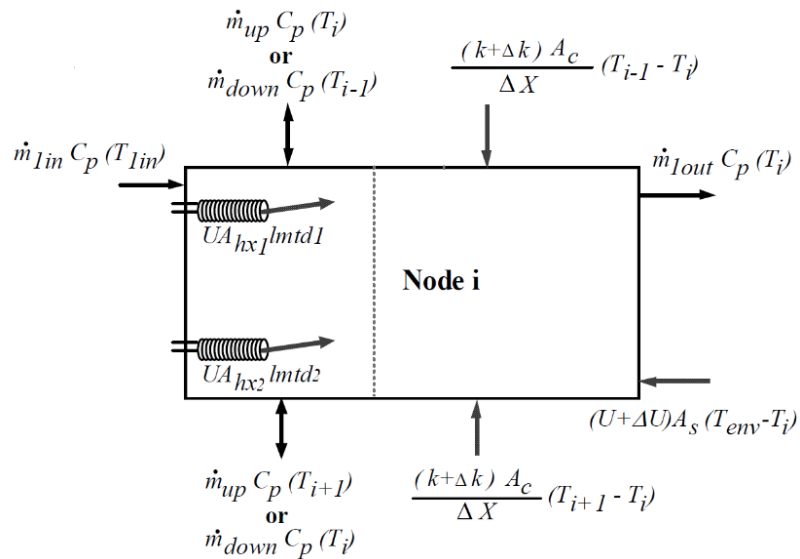


Figure 5.2. Energy balance of each node in the thermal storage tank (modified from (Klein *et al.*, 2014))

$$\begin{aligned}
 (m_i C_p) \frac{dT_i}{dt} = & \frac{(k + \Delta k) A_{c,i}}{\Delta x_{i+1 \rightarrow i}} (T_{i+1} - T_i) + \frac{(k + \Delta k) A_{c,i}}{\Delta x_{i-1 \rightarrow i}} (T_{i-1} - T_i) \\
 & + (U_{tank} + \Delta U_i) A_{s,i} (T_{env} - T_i) \\
 & + m_{down} C_p (T_{i-1}) - m_{up} C_p (T_i) \\
 & - m_{down} C_p (T_i) - m_{up} C_p (T_{i+1}) + UA_{hx1} (lmt d_1) \\
 & + UA_{hx2} (lmt d_2) + m_{in} C_p T_{in} - m_{out} C_p T_{out}
 \end{aligned} \tag{9}$$

From equation (9), the first two terms express the heat transfer by conduction from a certain node to one above or below in addition to the effect of the stratification among the tank. The third term expresses the heat losses from that tank. The fourth, fifth, sixth and seventh terms introduce the vertical heat transferred by the tank fluid from node to another which only one direction can apply at each iteration. The eighth and ninth terms introduce the heat transfer by the immersed HXs. The last two terms show the horizontal heat transfer by the fluid at the node. The component solves these equations using 1-D finite volume method. For the stratification effect, when iteration ends, all temperatures are defined. Therefore, the component checks for the temperature difference between the calculated node and the node above and uses suitable mixing function to evaluate the new temperature at the next node. Despite the simulation has a constant time step, this component uses its own time step to ensure the high a quality outcome (Klein *et al.*, 2014).

### Control System

The proposed control strategy that was introduced in section 3.5 has been implemented on the modelled test rig by TRNSYS. As it is shown in Figure 5.1, the model was mainly controlled using a generic differential control Type2d. This component uses successive substitution method and gives an output signal of value 0 or 1. As it is shown in Figure 5.3, the output control signal is bound by the upper dead band ( $\Delta T_H$ ) and lower dead band ( $\Delta T_L$ ) settings (Klein *et al.*, 2014).

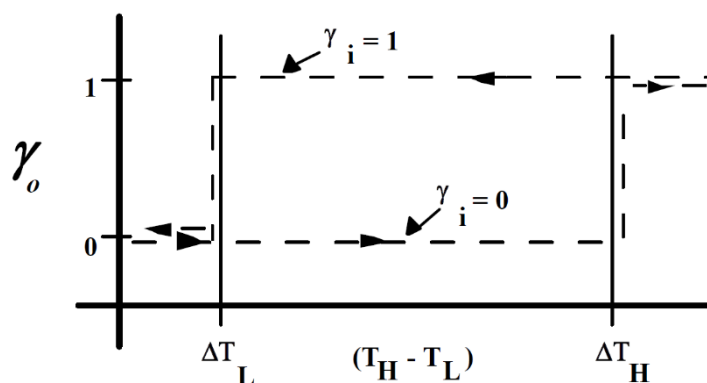


Figure 5.3. Controller Function (Klein *et al.*, 2014)

There are two possible scenarios during operation; the component was previously on or it was previously off:

- If the component was ON ( $\gamma_i = 1$ ):

$$\Delta T_L \leq (T_H - T_L) \text{ then, } \gamma_o = 1 \quad (10)$$

$$\Delta T_L > (T_H - T_L) \text{ then, } \gamma_o = 0 \quad (11)$$

- If the component was OFF ( $\gamma_i = 0$ ):

$$\Delta T_H \leq (T_H - T_L) \text{ then, } \gamma_o = 1 \quad (12)$$

$$\Delta T_H > (T_H - T_L) \text{ then, } \gamma_o = 0 \quad (13)$$

From equations (10), (11), (12) and (13), if the monitoring input value falls between the upper input value and lower input value, the controller checks the difference between then and compares it with upper and lower dead bands.

The control for system modelling was based on the above-illustrated concept which was used to control temperatures and irradiance. The full details of control setup for the system modelling are included in Appendix F.

### **5.3.2. Heat pump EES model**

The heat pump has been developed using EES<sup>®</sup>. As the heat pump is custom-made, it was important to evaluate the performance of the heat pump. An experimental test was conducted in order determine the performance curves of the heat pump. The test procedures were as following:

- 1- Maintain condenser water outlet temperature constant while logging the COP, heating capacity and power consumption values for different evaporator water outlet Repeat the previous step for different condenser water outlet.
- 2- Analyse the data and evaluating the performance curves of the heat pump.
- 3- Evaluating the trend curves and curve equation for the produced curves.

The data analysis was conducted using EES as it was explained earlier in section 4.3 and proceeded in Microsoft Excel.

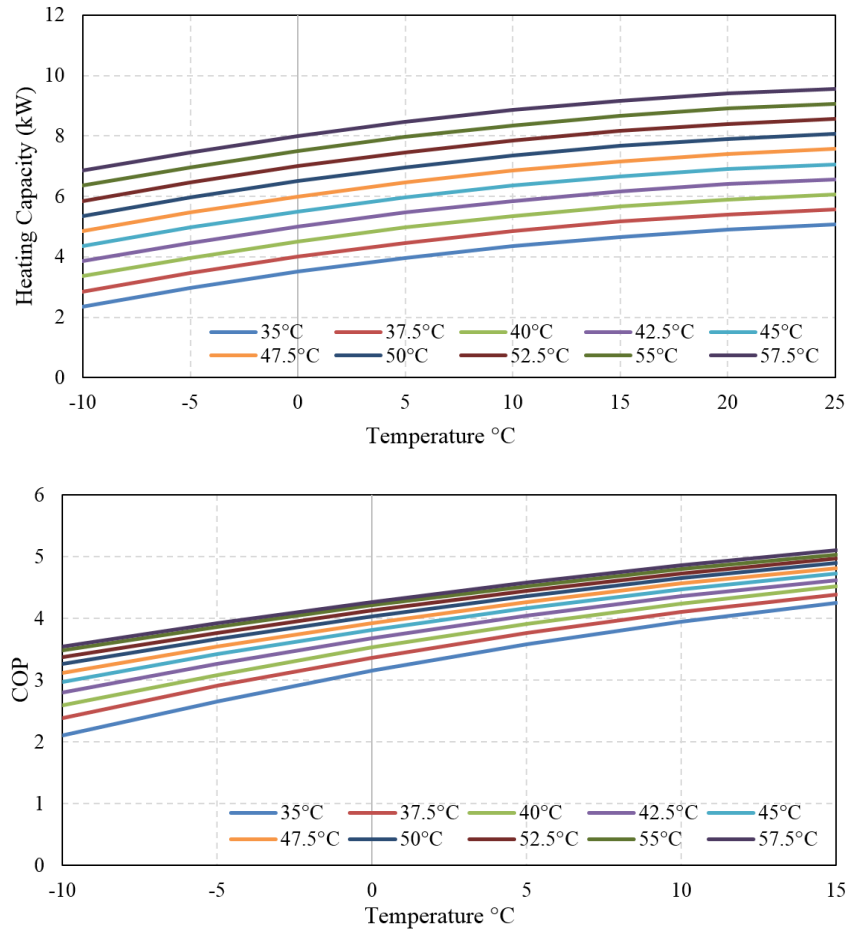


Figure 5.4. Heat pump performance curves

As shown in Figure 5.4, the performance curves of the heat pump were evaluated according to the heat pump COP and heating capacity. Each curve represents the performance of the heat pump at constant condenser water outlet temperature and different evaporator water outlet temperature. Trend lines were evaluated for the performances curves in order to determine each line equation. All curves for COP and heating capacity performance were found to have a second-order polynomial curves which it can be express by equation (14)

$$Y = AT_{evap}^2 + BT_{evap} + C \quad (14)$$

Where A, B and C are dependent on the condensing temperature.

The determined equations were inserted into EES model which performs interpolation between these equations.

Since the condenser water outlet temperature, evaporator water outlet temperature, source loop flow rate and load loop flow rate were imported from TRNSYS.

Therefore, it was important to include in the EES model a few procedures at the beginning of the model to avoid the zero-divide error. The full model included in Appendix F.

### **5.3.3. PCM HX CFD model**

#### *5.3.3.1. Numerical Consideration*

In order to simulate the copper spiral tube and its effect on the heat transfer enhancement between the working fluid and PCM, an estimation method was proposed to evaluate the overall thermal conductivity for the PCM including the spiral wires effect. This method was proposed because of the compact design of the spiral tube which makes the CFD meshing elements enormous and simulation time very long. As it is shown in Figure 3.23, the fin wires are really small in size compared with the main body of the pipe. Therefore, it was considered simpler to evaluate the PCM thermal conductivity coefficient including the effect of the finned wires as one element. It was also assumed that PCM HX is divided into eight rectangle sections. At each section, the water pipe is centred in the middle of this section, as it is shown in the red rectangle in Figure 5.5. Also, the flowing assumption was considered for this calculation:

- Steady-state conditions
- Incompressible liquid and negligible viscous dissipation
- Constant properties
- Neglect natural convection effect for the PCM
- The spiral wires are distributed equally across the PCM

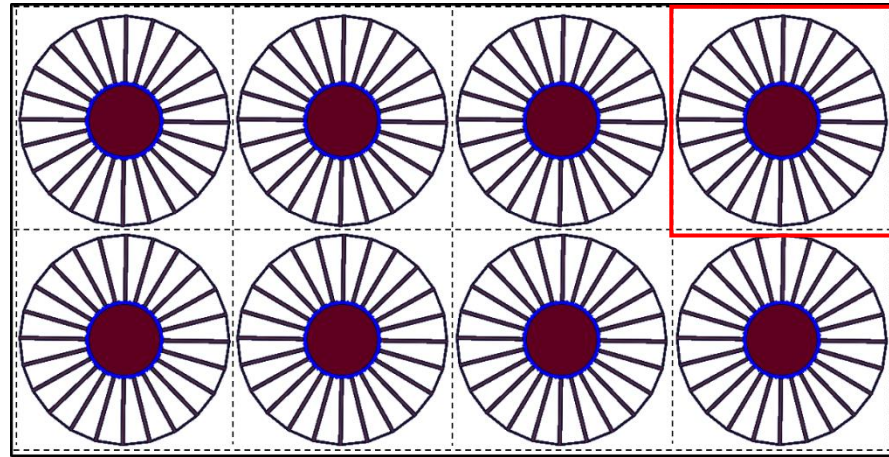


Figure 5.5. PCM HX sections assumption

Figure 5.6 shows a section from the spiral-wired tube and its analysis. During the PCM discharging condition in which the HTF inlet temperature is lower than the PCM temperature inside the PCM HX, the heat will be transferred from the PCM to the pipe wall through conduction and then to the HTF through convection. By knowing the HTF flow rate and inlet and outlet HTF temperatures of the PCM HX from the experimental results, the total amount of thermal power transferred to the tank can be evaluated; this thermal power is transferred constantly between the HTF and the PCM. Therefore, as it listed in equation (15), the overall PCM thermal conductivity ( $k_{pcm}$ ) can be evaluated. During convection heat transfer, the convection heat transfer coefficient was calculated by knowing the Nusselt number, the internal diameter of the pipe and the thermal conductivity of the fluid as listed in equation (16). The Nusselt number depends on the Reynolds number, Prandtl number and internal friction factor ( $f$ ) of the surface as listed in equation (17) in which the friction factor ( $f$ ) is calculated by equation (18). The log-mean temperature difference was calculated using equation (19). The inside surface temperature of the copper pipe can therefore be determined by solving the equations (15- 19). The third term of the equation (15) determines the outside surface temperature of the copper pipe. The last term of the equation (15) determines the overall conduction coefficient of the PCM. This can be evaluated by knowing the shape factor ( $S$ ) which can be calculated using equation (20) (Incropera *et al.*, 2007). The overall PCM thermal conductivity coefficient including the wires effect can thus be calculated at  $11.07 \text{ W} \cdot (\text{m} \cdot \text{K})^{-1}$  when the HX structural data and boundary parameters are given.

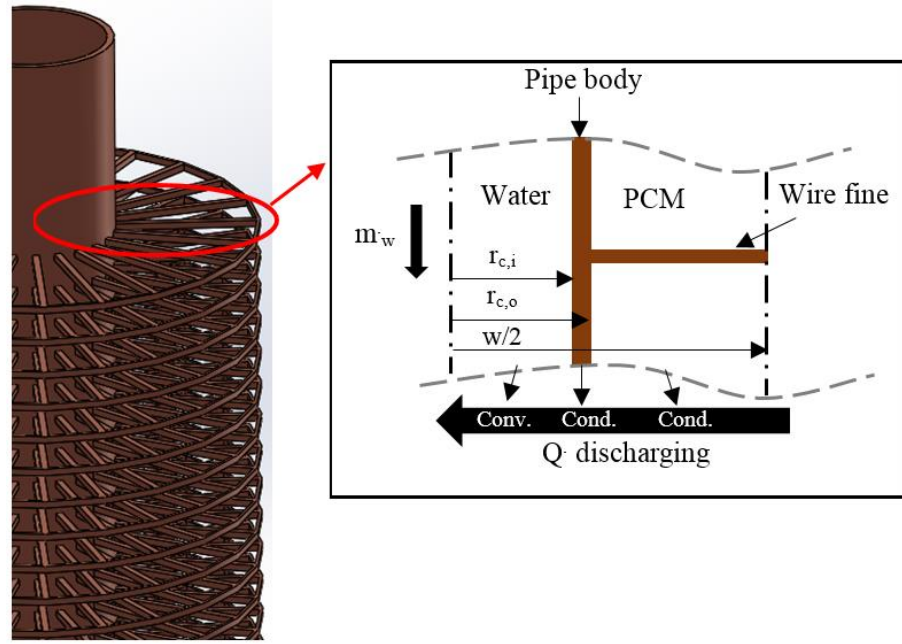


Figure 5.6. spiral tube element analysis

$$\dot{Q} = \underbrace{[m \cdot C_p (T_{in} - T_{out})]}_{\text{main heat transfer}} = \underbrace{[\bar{h} A_s l m t d]}_{\text{Convection}} = \underbrace{\left[ \frac{2\pi k_c L}{\ln\left(\frac{r_{c,o}}{r_{c,i}}\right)} (T_{s,i} - T_{s,o}) \right]}_{\text{Pipe Conduction}} = \underbrace{[S k_{pcm} (T_{s,o} - T_{pcm})]}_{\text{PCM conduction}} \quad (\text{kW}) \quad (15)$$

Where the convection heat transfer coefficient expressed by:

$$\bar{h} = Nu_D \frac{k_w}{2r_{c,i}} \quad (\text{W/m}^2 \cdot \text{K}) \quad (16)$$

$$Nu_d = \frac{\left(\frac{f}{8}\right) (Re_d - 1000) Pr}{1 + 12.7 \left(\frac{f}{8}\right)^{\frac{1}{2}} \left(Pr^{\frac{2}{3}} - 1\right)} \quad (17)$$

$$0.5 \leq Pr \leq 2000 ; 3000 \leq Re_d \leq 5 \times 10^6$$

$$f = (0.790 \ln Re_d - 1.64)^{-2} \quad 3000 \leq Re_d \leq 5 \times 10^6 \quad (18)$$

And the log-mean temperature difference expressed by:

$$lmtd = \frac{(T_{s,i}-T_{out})-(T_{s,i}-T_{in})}{\ln\left(\frac{(T_{s,i}-T_{out})}{(T_{s,i}-T_{in})}\right)} \quad (^\circ\text{C}) \quad (19)$$

$$S = \frac{2\pi L}{\ln\left(1.08\frac{w}{2r_{C,o}}\right)} \quad (20)$$

### 5.3.3.2. Model development and Boundary Conditions

A 3D CFD dynamic model for the PCM HX is developed using ANSYS® Fluent. As shown in

Figure 5.7, the model is set up firstly on Solidworks® before being imported into ANSYS® to be modelled, meshed and posted. The CFD model is developed to study the effects of different HTF flow rates and temperatures on the melting and solidification processes of the PCM with the proposed heat transfer enhancement method. The PCM material properties are defined in Table 1 but its thermal conductivity is revised and calculated by the formulas explained in section 5.3.3.1 considering the heat transfer enhancement of fin wires. The HTF properties are imported from the CFD Fluent built-in database and the standard k-ε turbulence model with standard wall functions is applied. The multiphase function is enabled and “Volume of Fluid” model is selected with implicit volume of faction parameters and pull velocity enabled. The PISO scheme is used for pressure-velocity coupling. The spatial discretization settings for pressure, momentum, volume fraction and energy are PRESTO, first order unwind, compressive and second order unwind respectively. The boundary condition type “Velocity-inlet” is used for the HTF at the PCM HX inlet. The velocity of the inlet HTF flow velocity is determined from the inlet volumetric flow rate and inlet inner pipe diameter. The HTF flow velocity and temperature at the inlet are taken at 0.263-0.789 m/s (0.1-0.3 kg/s) with 0.263 (0.1 kg/s) step and 30-50°C with 10°C interval respectively. The outlet boundary condition is selected as “outflow”.



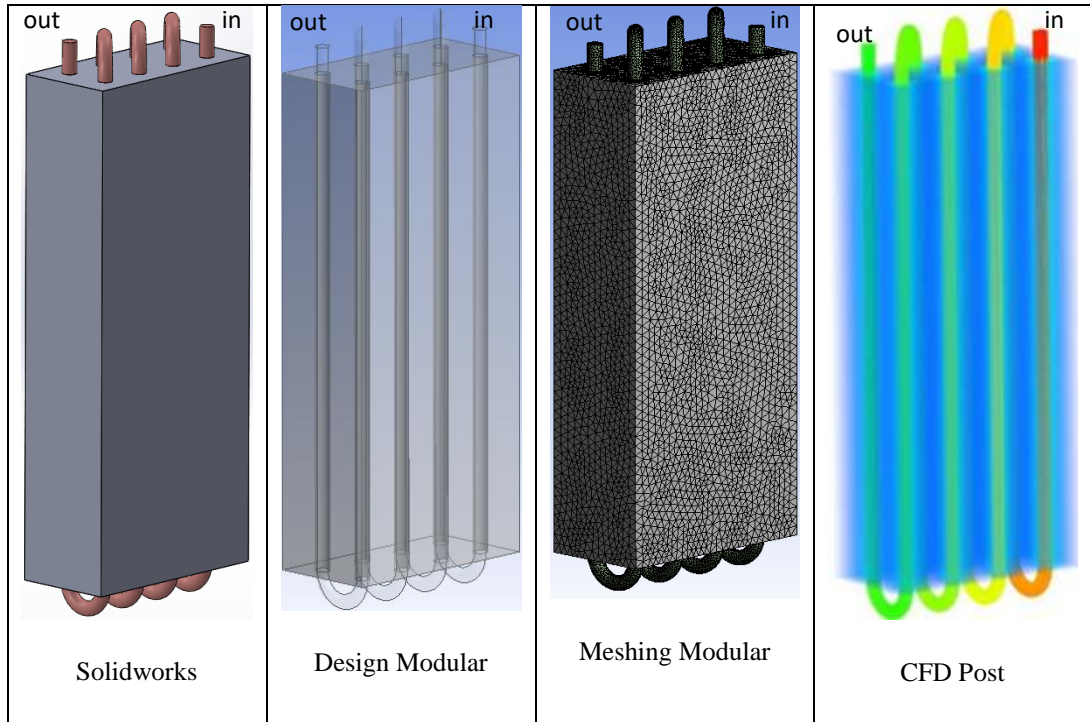


Figure 5.7. PCM HX numerical model development

Being a 3D simulation, it is important to develop a simulation method to minimize the simulation time. As the HTF flow rate is constant for each simulation, the model is first initialized as steady-state to evaluate the flow and turbulence effect. After the solutions are converged, the transient simulation is activated by enabling the energy and volume fraction equations only.

#### 5.3.3.3. Meshing dependency and model validation

To ensure the simulation quality, the mesh selection is necessary to obtain the best results. This is investigated by comparing two different mesh levels: coarse and fine as shown in both Figure 5.8 and Table 7. The cell types used in both meshes are tetrahedron across the whole model but wedge at the inflation layers. The main purpose of the inflation layers is to enhance heat transfer simulation between the HTF and PCM. The fair skewness range of the mesh must not exceed 0.5-0.75 % (Fluent INC, 2016).

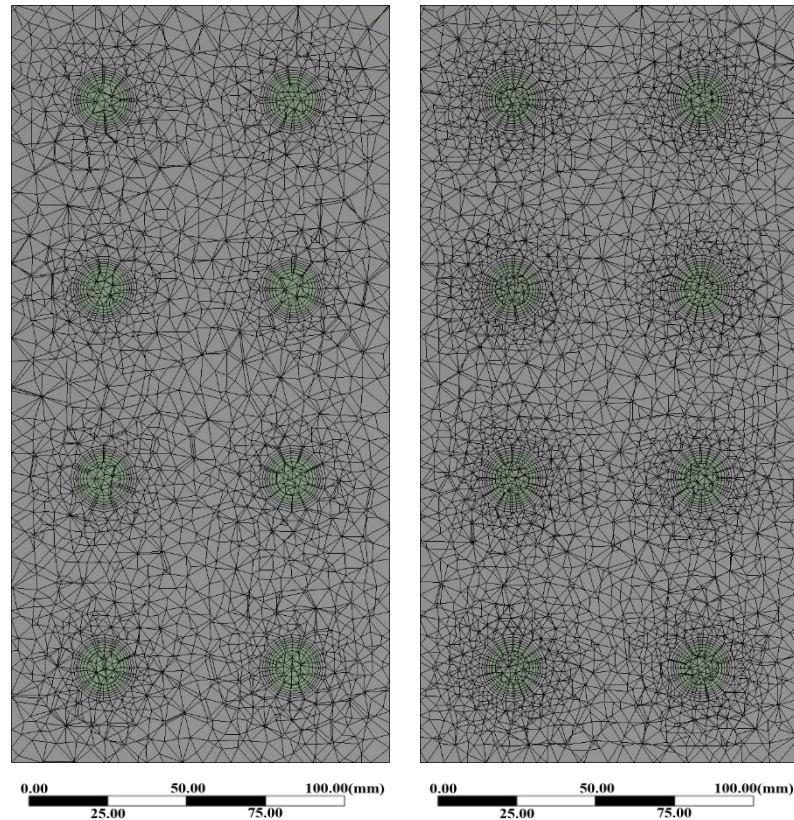


Figure 5.8. Mesh Comparison of PCM HX horizontal cross-section - coarse and fine, respectively

Table 7. Mesh selection - coarse and fine

<b>Level</b>	<b>No of elements</b>	<b>No of Nodes</b>	<b>Skewness</b>	<b>Time per iter.</b>
Coarse	920703	244452	Av. 0.23%, stdev. 0.12%	6-11 s
Fine	1981116	514875	Av. 0.22%, stdev. 0.12%	9-13 s

The simulations for both meshes are conducted to compare the outcome results. The results are quite close to each other where maximum and average relative errors are 1.6 % and 0.08% respectively. Taking the simulation time into consideration, the simulation with coarse mesh is found faster than that with fine mesh to reach convergence during initialization as steady state and also during transient simulation. Therefore, the CFD model with coarse mesh is more suitable to be validated with the experimental results as it has fewer elements number.

Figure 5.9 and Figure 5.10 show the experimental and simulated temperature of a generic thermistor in the middle of the tank during discharging and charging process, respectively. The mass flow for the simulation and experiment during both charging and discharging processes is set at 0.1 kg/s. Meanwhile, the inlet temperatures during charging and discharging processes are set at 40°C and 10°C respectively. During

discharging, it is observed that the PCM was subcooled at the beginning of the phase change process during the test but it does not appear in the simulation result. That is because the solver does not take sub-cooling effect into account. The absolute errors are calculated during the discharging process with the maximum and average values of 3.59 K and 0.75 K respectively. Meanwhile, the absolute errors during charging process are also evaluated with the maximum and average values of 1.38 K and 0.51 K respectively. Since the absolute errors are all less than 3.59 K, the validation of the CFD model can be considered to be acceptable (Zhang *et al.*, 2007).

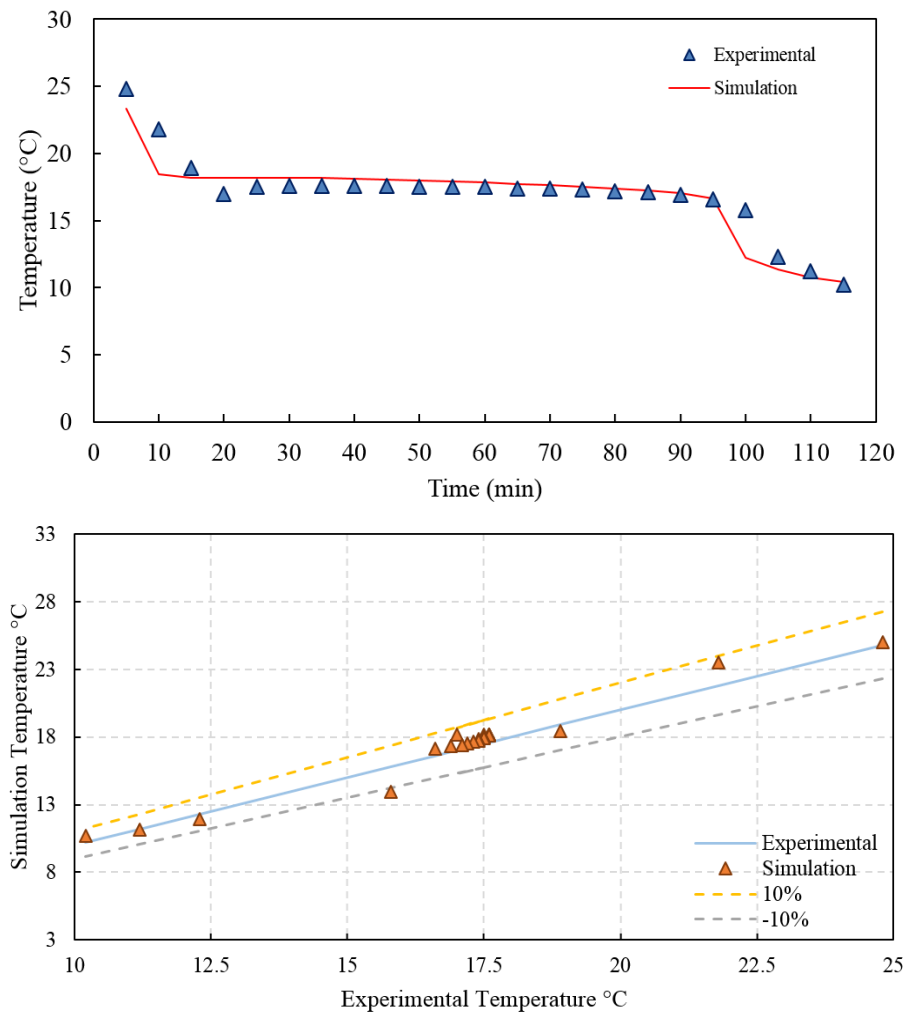


Figure 5.9. PCM HX Model Validation for discharging process

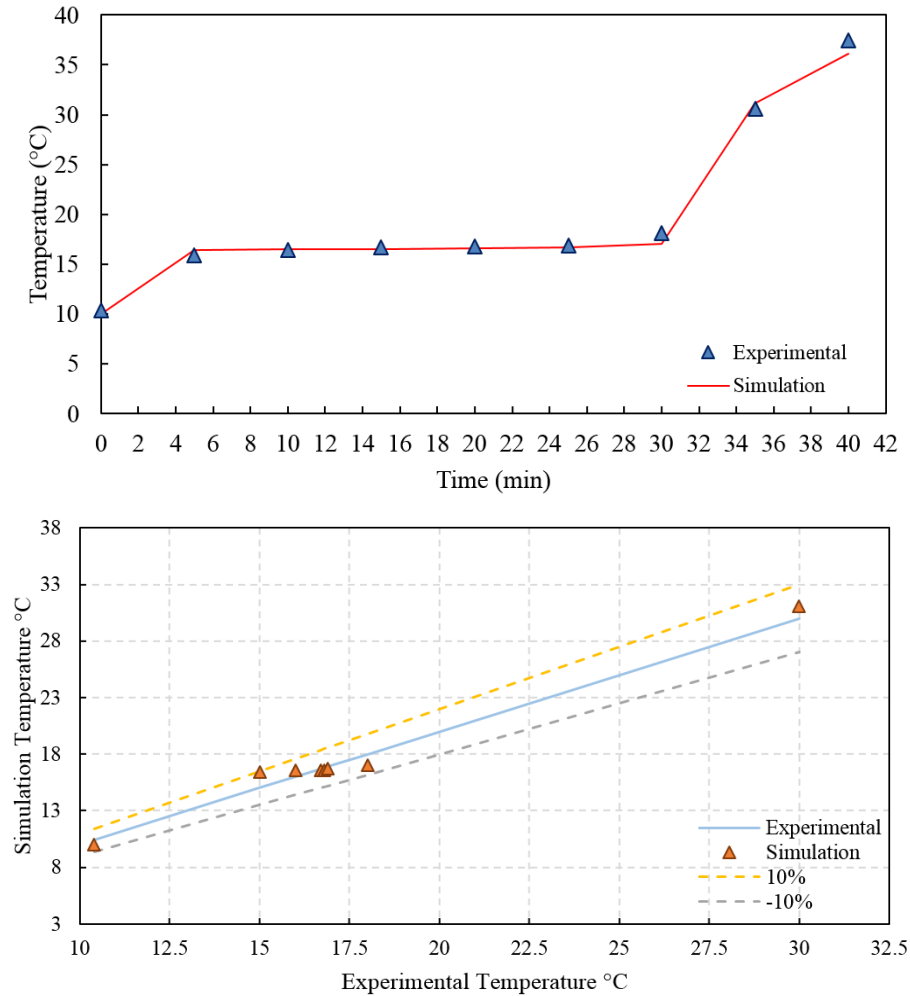


Figure 5.10 PCM HX Model Validation for charging process

#### 5.3.4. Numerical simulation coupling

Simulation tool such as TRNSYS<sup>®</sup> is ideal to simulate the operation and control of the proposed system. However, this simulation tool is more tailored to simulate whole systems rather than focusing on the detailed behaviour of specific component. In this way, the simulation time and computational cost are reduced but the accuracy of evaluating PCM melting and solidification behaviours.

Further, a simulation tool such as ANSYS FLUENT<sup>®</sup> allows more flexibility of the user to study a new innovation by applying the finite element method to predict the thermal, multiphase and turbulence behaviours. Despite that, this simulation tool provides high accuracy results, the simulation time and cost can be high.

Taking into consideration that the heat pump is custom made, it was important to evaluate the performance of the heat pump and integrate it into the whole model. Initially, a water-to-water heat pump from TRNSYS library was used for the simulation but the performance of the simulated heat pump did not match the

experimented performance. Therefore, EES was used to predict the heat pump performance of the actual heat pump used in the system.

Therefore, it can be believed that TRNSYS is an efficient platform to control and simulate the whole system while ANSYS FLUENT provides high accuracy and flexibility to predict a behaviour of certain innovation and EES allows the integration of the custom-made heat pump. Expressly, getting the advantages of these simulation packages will need a coupling between each other (Zhai and Chen, 2005).

In this study, a dynamic link between TRNSYS, EES and CFD FLUENT will be employed. The linking between TRNSYS and EES was implemented by enabling the clipboard function between the two packages. This was a straightforward process as the TRNSYS has EES component at the library and it does not require any further modification. This function imports the TRNSYS inputs to the EES model while the EES model exports the outputs through the same function. Meanwhile, the coupling between TRNSYS and CFD FLUENT was developed through a coupling code written in FORTRAN which it will be explained further. The concept of this coupling is based on creating a script file at each time step generated by TRNSYS to be read by FLUENT. This file contains the boundary condition and settings of the CFD. When FLUENT completes the iterations, it creates a results file. This file contains the output results which are read by TRNSYS.

As transit simulation, a quasi-dynamic coupling was recommended for this type of simulation (Zhai and Chen, 2005). In this method, TRNSYS feeds the CFD with the boundary condition at each time-step. CFD receives the boundary condition from TRNSYS at time-step (t) and returns the results back to TRNSYS at time-step (t+1). In this way, the simulation time can be reduced compared with the other method such as the fully-dynamic (Zhai and Chen, 2005).

In summary, the modelling of the whole system was implemented by coupling TRNSYS, EES and CFD together. TRNSYS is a platform to control and simulation the whole system while EES and TRNSYS are used for modelling the heat pump and PCM tank respectively as shown in Figure 5.11.

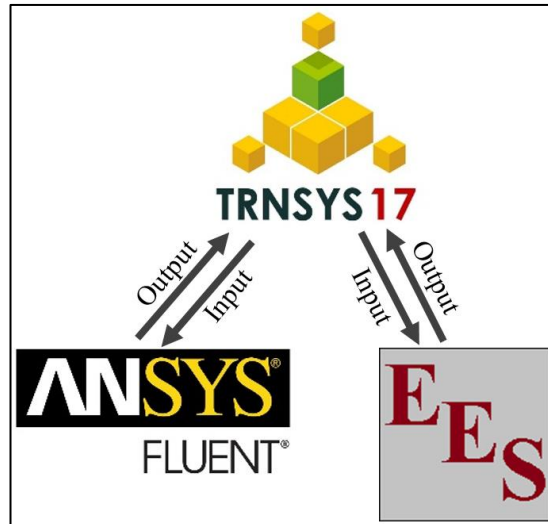


Figure 5.11. Simulation coupling process diagram

#### 5.4. Numerical model validation

The experimental findings evaluated in Chapter 4 were used to validate the developed numerical model. The developed TRNSYS model to simulate the whole system is shown in Figure 5.1. All components of the developed model are described in the TRNSYS file included in Appendix F.

In order to validate the developed model, it was necessary to insert the weather conditions for the tested day to the numerical model. Therefore, the ambient temperature and irradiance readings were inserted via generic data readers and connected to the related components. The output results were generated in the output file which was further exported to Microsoft Excel to be posted.

Figure 5.12 shows the experimental and simulation temperatures at the top, middle and bottom of WST during the first operation period of the selected day in London, UK. The top temperature has the lowest error value during the operation. This is because the stratification effect makes the high temperature always at the top of the tank. As the control WST set point is 55°C, the top temperature will always be around this value. It was observed that the error value between the experimental results and simulation was increased by approaching the bottom of the WST. This is because the number of the node of WST component in TRNSYS was relatively high which allows better accuracy of the simulation results. This also explains why at the lower graph of Figure 5.12 the bottom and mid-temperature simulation errors are higher than 10%.

Figure 5.13 and Figure 5.14 shows a comparison between the experimental results and simulation for the inlet heat pump source temperature and the system heating capacity, respectively. The comparison shows that the source temperature was slightly changed during the mid and end of the operation. Despite the fact that the ambient and irradiance condition was inserted into the simulation the same as the experiment, the solar collector plays a significant role in this temperature difference. Apart from the start of the operation, the heating capacity had relative similarity between the experimental test and simulation. This was because the simulation did not consider the system start-up losses due to cold piping and HTF.

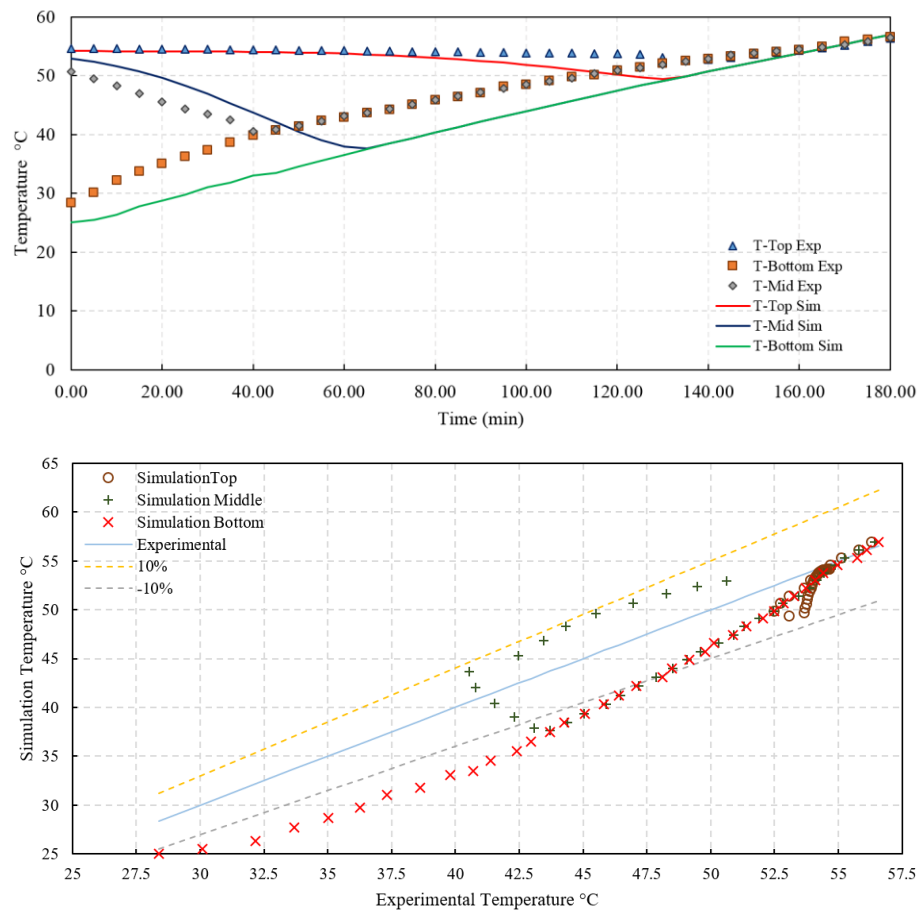


Figure 5.12. Tank temperatures (Top-Mid-Bottom) validation with experimental results



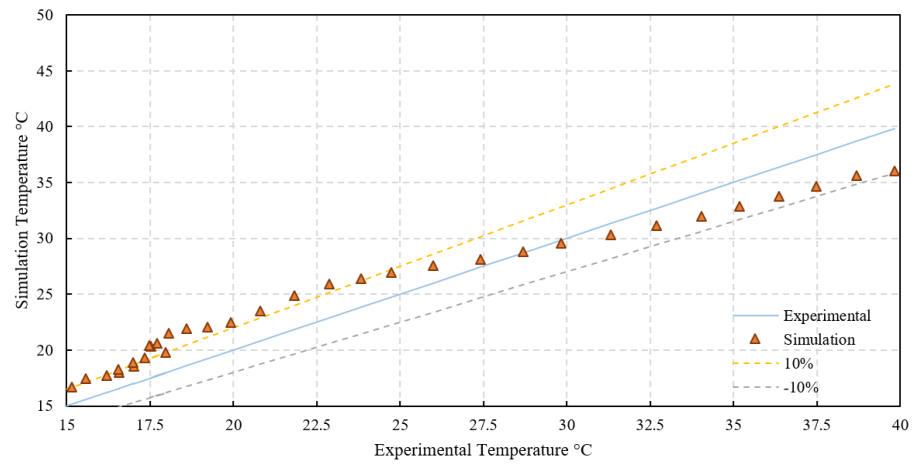
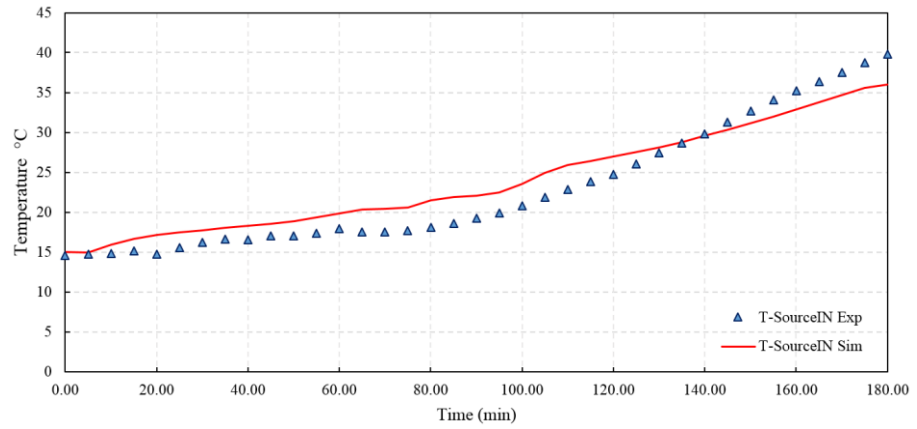
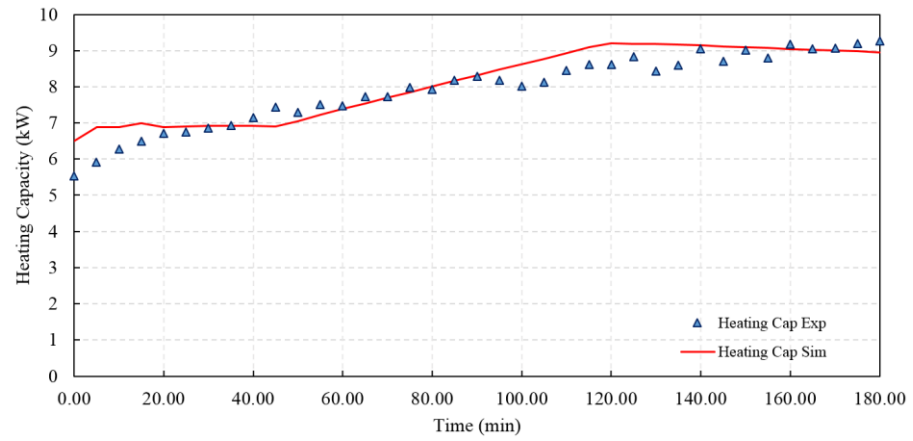


Figure 5.13. Source temperature validation with experimental results





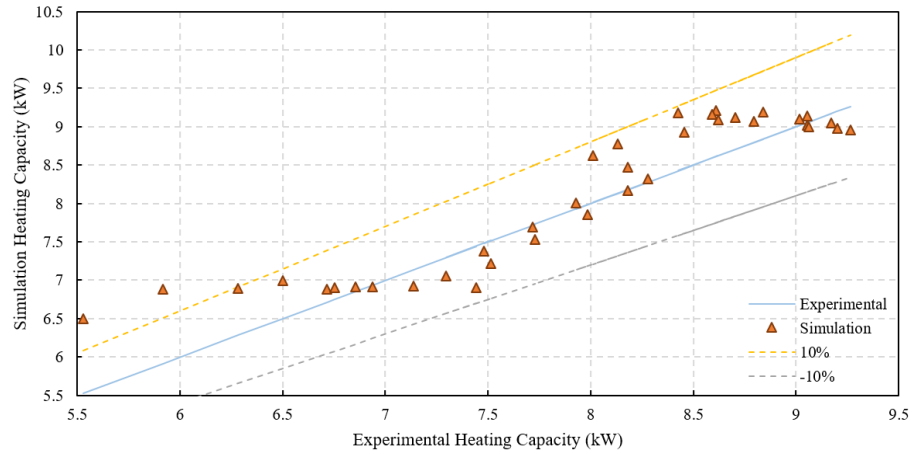
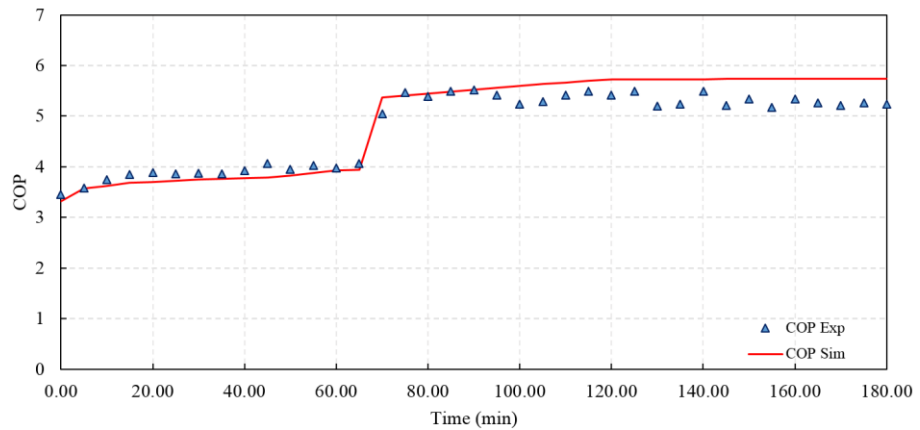


Figure 5.14. Heating Capacity validation with experimental results

Figure 5.15 shows a comparison between the experimental simulation results for the system COP. The figures show the AWHX was operated at the same time and COP values are relatively similar for experiment and simulation. This is because the irradiance profile is the same for both experiment and simulation; on which principle the control logic is based. It was observed that at the end of the operation the COP was slightly higher during simulation compared with the experiment. This was because of the difference between the experimental and theoretical power consumption.



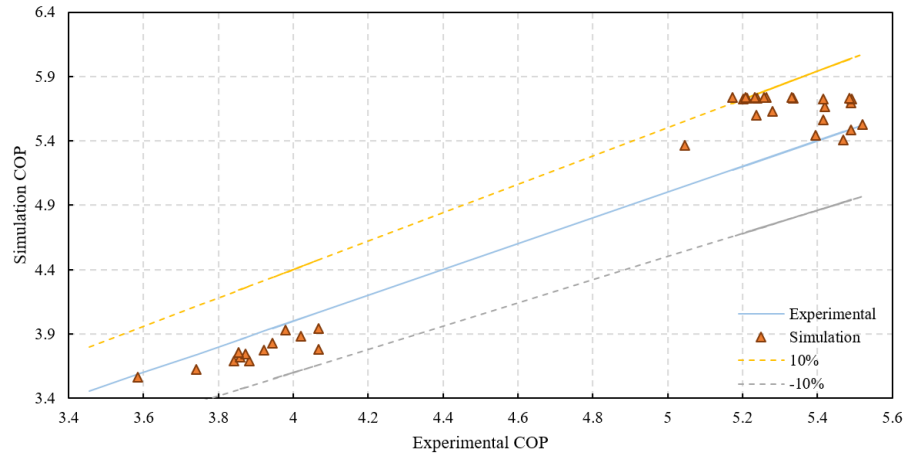


Figure 5.15. COP validation with experimental results

	<i>Maximum</i>		<i>Minimum</i>		<i>Average</i>	
	<i>Abs</i>	<i>Rel.</i>	<i>Abs</i>	<i>Rel.</i>	<i>Abs</i>	<i>Rel.</i>
<i>Top tank temperature °C</i>	3.96	7.38%	0.14	0.25%	1.20	2.24%
<i>Mid tank temperature °C</i>	6.09	13.93%	0.10	0.18%	3.13	6.69%
<i>Bottom tank temperature °C</i>	7.21	18.26%	0.02	0.03%	4.19	10.06%
<i>source inlet temperature °C</i>	3.84	18.98%	0.13	0.46%	2.05	9.66%
<i>Heating capacity (kW)</i>	0.97	17.56%	0.01	0.17%	0.32	4.23%
<i>COP</i>	0.56	10.84%	0.00	0.07%	0.25	5.08%

### ***5.5. Summary of Chapter 5***

This chapter presented the development of the numerical model of the whole system. The development strategy was to use TNRSYS as a platform to simulate the whole system including its control of the system. The heat pump was developed in EES while the PCM HX was developed in CFD FLUENT. All developed model were dynamically coupled to perform the final outcome for the simulation. The developed models were validated with the experimental results by applying same boundary and weather conditions from the experiment. The scope of the numerical model is to study the system's behaviour in different locations. The heat pump performance curves were evaluated through experimental investigation then inserted into the EES. Meanwhile, the PCM thermal conductivity was evaluated at  $11.07 \text{ W} \cdot (\text{m} \cdot \text{K})^{-1}$  including the spiral wire contribution then inserted into the CFD mode as a boundary condition.

The next chapter will discuss the variation of the inlet flow rate and temperature of PCM HX including a demonstration of the behaviours of the charging and discharging process. In addition, the system performance will be studied in two country cases, Egypt and Spain, which were used as case study for a hot climate.

---

***Chapter 6. Analysis of Numerical Model***

---

### **6.1. Introduction**

This chapter presents the results of the numerical model development of this research. The validation of these models with the experimental results is included in Chapter 5. The results in this chapter have a dual propose; a) to investigate the CFD PCM HX melting/solidification behaviours and study the effect of various inlet flow rates and temperatures. b) to simulate the TRNSYS-CFD couples' model for the whole system in different locations with high solar irradiance during different days in summer and winter.

### **6.2. PCM model applications**

#### **6.2.1. PCM temperature contours at charging and discharging processes**

The developed 3D CFD model of the PCM HX is used to predict and analyse the effects of varied HTF inlet flow rate and temperature on the HX charging and discharging processes and behaviours.

Figure 6.1 shows the PCM liquid mass fraction, temperature and total energy at the mid of charging and discharging processes. It is observed that at the specified operating conditions the charging process is much quicker than that of the discharging one. During the charging process, initially, the heat transfers from the HTF to the PCM through pure conduction. When the PCM starts to melt, the natural convection heat transfer between the liquefied PCM and pipe outer surface will directly affect the charging time. Also, the buoyancy effect adds a little convection due to PCM density variation. Again in this Figure, for the charging process, the PCM liquid mass fraction decreases radically from each pipe outer surface while at each cross section more liquid contents are existed close to the inlet pipe due to relatively higher HTF temperature. Correspondingly, similar distribution profile can be found in the total energy. However, the PCM temperatures across the tank are much evenly distributed at a range of 16~17 °C due to the co-existed of liquid and solid phases at that time. Similar parameter distributions can also be established for the discharging process except that the larger liquid mass fraction and total energy are higher at the places close to the outlet pipe due to the higher HTF temperatures. Again, during the discharging process, it is noted that the PCM HX takes a longer time to release the stored energy. This can be further explained by the following. When the stored heat transfers from PCM HX to the HTF, the first solidification layer starts to accumulate

on the outer surface of the copper tube and the spiral wires. This will create an extra conduction thermal resistance in the heat transfer path between the two domains. With the increase of solid content, such thermal resistance will increase as well. On the other hand, neither natural convection nor buoyancy effect exists during the discharging process as the solid content is uniformly accumulated along the spiral-wired tubes.

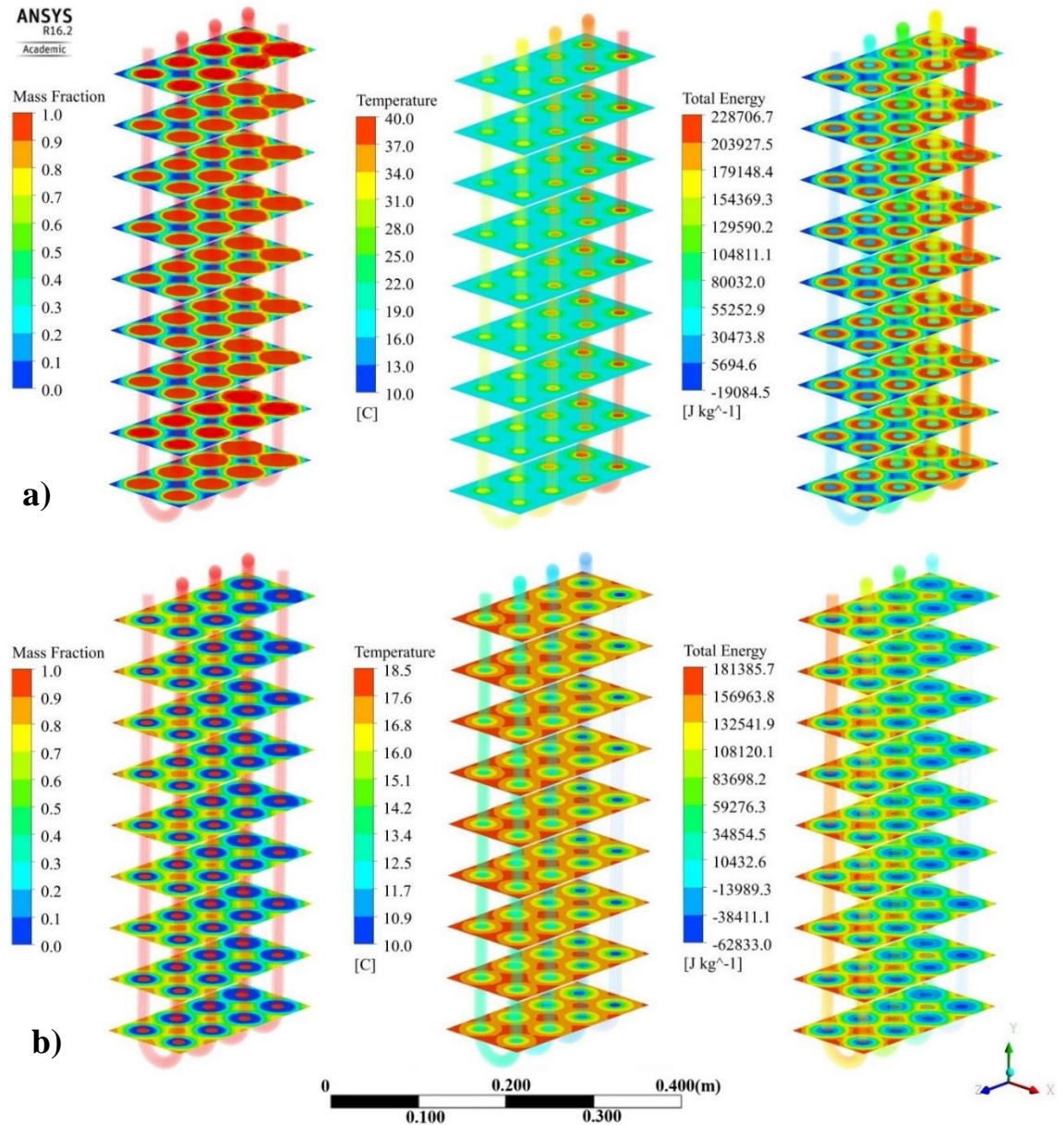
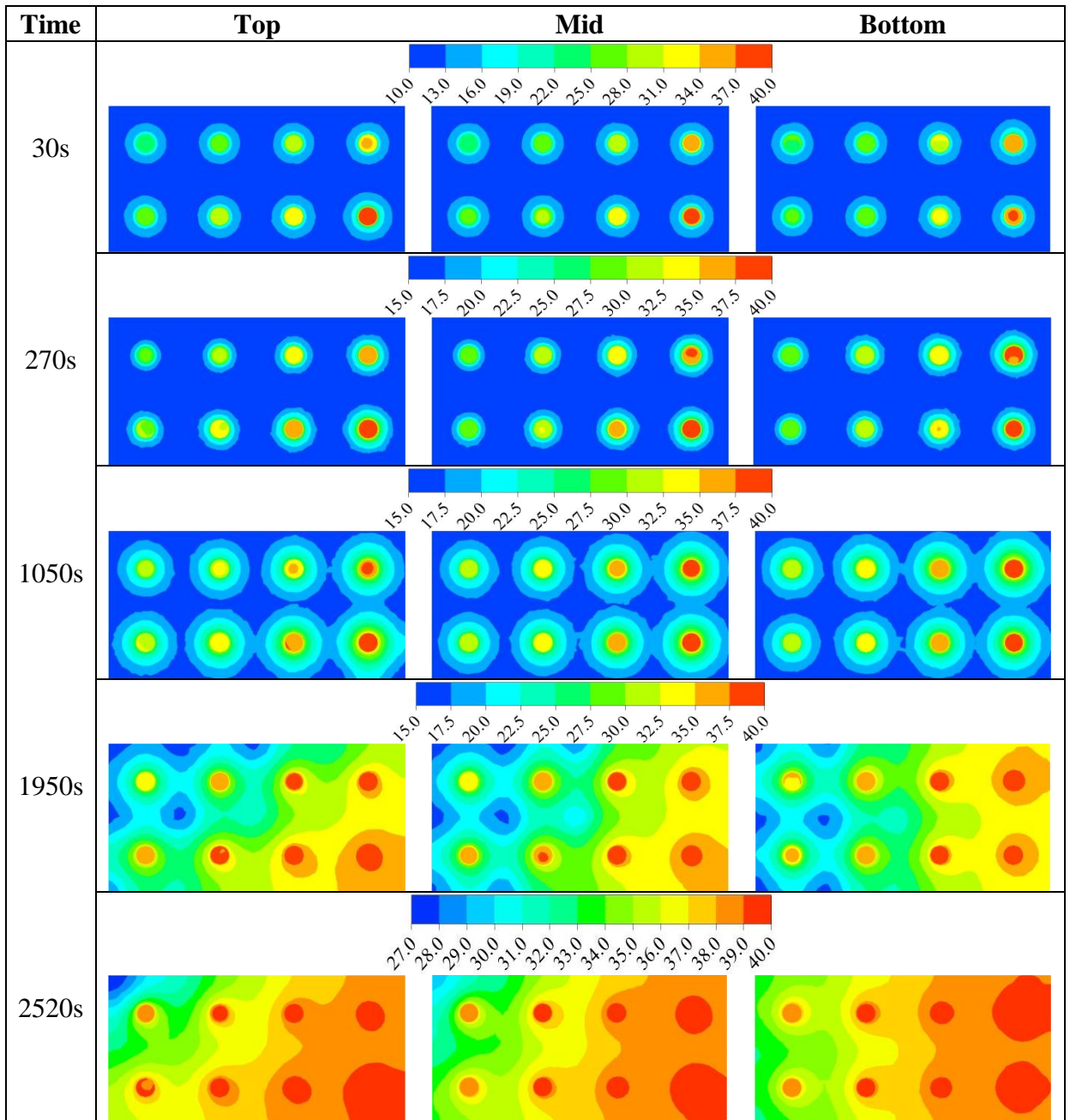


Figure 6.1. Mass fraction, Temperature and total energy at the middle of operation – a) charging

Table 8 shows the CFD temporal variation of the PCM temperature at top, middle and bottom of the PCM HX during charging process at various times from start: 30s, 270s, 1050s, 1950s and 2520s. The inlet HTF (right-bottom of the first figure in each row) temperature and flow rate are maintained at 40°C and 0.1 kg/s respectively. At the

start of the process (at 30s), the temperature distribution across the PCM HX is fairly uniform. At 270s, a sudden rise of the PCM temperature from 10°C to 16°C is observed. That is due to the high-temperature difference at the beginning between the PCM and HTF and the simultaneously sensible heat transfer when the PCM temperature is below its melting point. After that when the PCM reaches its melting temperature, the PCM starts to melt around the spiral-wired tubes and grows radially towards the middle of the tank and the edges. At the mid of the charging time (1050s), more areas around each tube are liquefied and temperatures are well above the melting point although the PCM temperature decreases gradually away from each tube outer surface. Even so, approximately 50% of tank volume is still occupied with solid PCM based on the temperature distributions. At time 1950s, over 90% of the PCM in the tank is liquefied and the liquid PCM temperature follows the HTF temperature distribution inside the pipe. At the end of the charging process (at 2520s), PCM in the tank is completely liquefied. Meanwhile, the PCM temperatures inside the tank reach their highest values and their distributions follow the temperature profile of HTF inside the pipes.

Similarly, Table 9 shows the PCM temperature contours at sections of top, middle and bottom of the PCM HX tank and at times of 30s, 630s, 3050s, 5730s and 6120s during the discharging process. The inlet HTF temperature and flow rate are maintained at 10°C and 0.1 kg/s respectively. At the beginning of the discharging process (at 30s), due to the high temperature difference between the PCM (40°C) and inlet temperature (10°C) and pure sensible heat transfer, the PCM liquid temperatures drop quickly at the areas close to the pipe outer surface especially for the first two pipes from the inlet. At 630s, some areas around the pipes close to inlet have been solidified and the rest are approaching to be solidified.

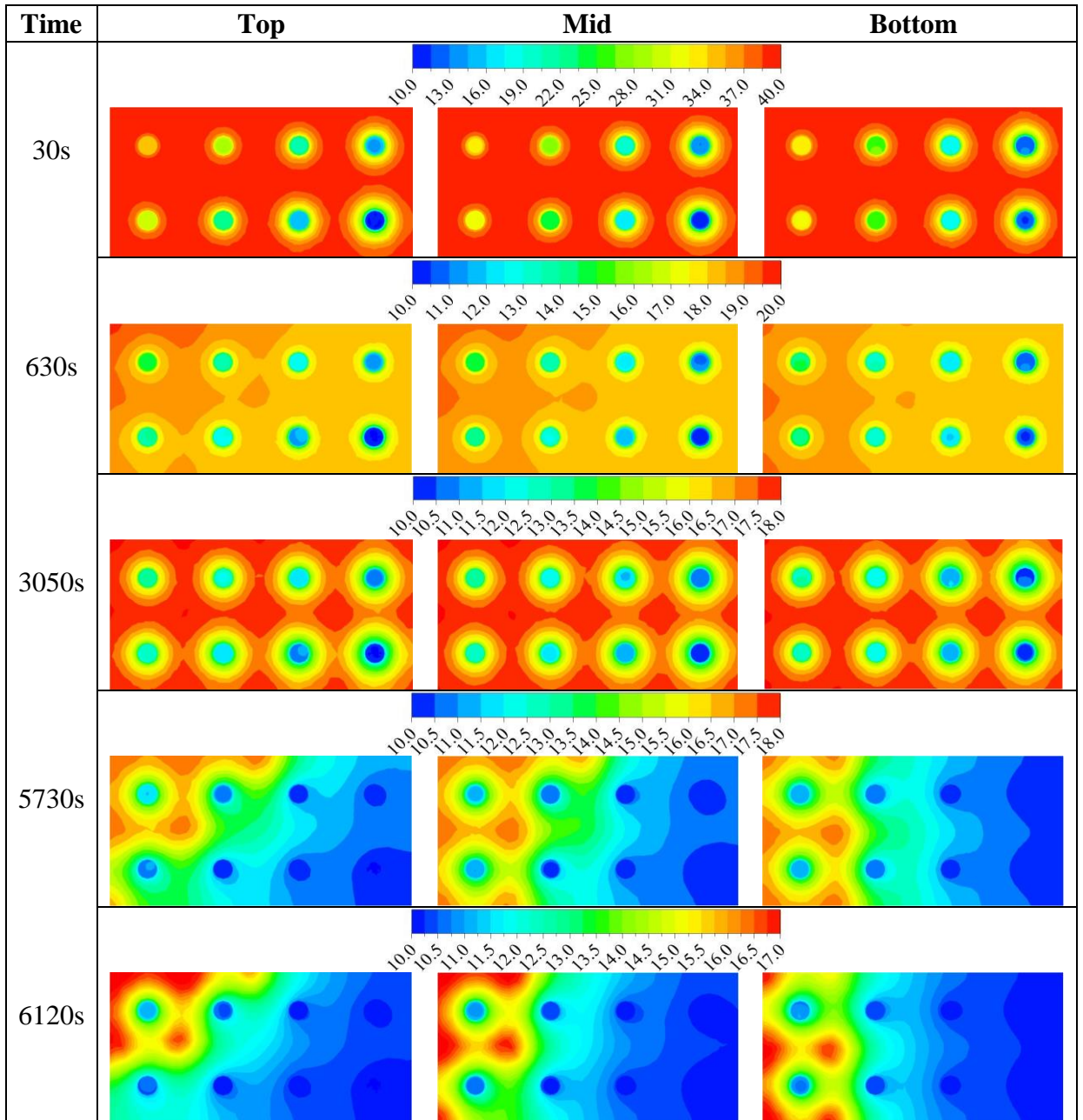
Table 8. Charging temperature ( $^{\circ}\text{C}$ ) timeline at flow rate 0.1 kg/s

In addition, the PCM temperatures increase from left to right for each section following the same temperature profile of HTF flow. At mid of the discharging process (at 3050s), the PCM temperature increases radially from each pipe outer surface and up to 50% around the pipes have been solidified. As explained earlier, this will add more thermal conduction resistance and thus lead to longer process time. By the end of solidification process (at 5730s), it is noticed that over 75% of overall PCM in the tank is solidified and the rest of tank is still in transition states (between 15-17 $^{\circ}\text{C}$ ). At time 6120s when the discharging process ends, the PCM in the tank is



completely solidified while the lowest and highest PCM temperatures are close to the inlet and outlet pipes respectively. Simultaneously, the HTF is heated up to approximately 12°C at the PCM HX outlet.

Table 9. Discharging temperature (°C) timeline at flow rate 0.1 kg/s



### 6.2.2. Effect of HTF flow rate variation

With the developed PCM HX CFD model, simulations are carried out at inlet temperatures of 10°C and 40°C during discharging and charging processes respectively. For each process, three HTF flow rates are applied: 0.1, 0.2 and 0.3 kg/s based on the applicable operation of indirect solar assistant heat pump system where

the PCM HX is fitted. It is expected that the higher HTF flow rate can enhance its convection flow heat transfer and thus speed up both the discharging and charging processes. For the PCM discharging process, the initial PCM temperature inside the tank is set to 40°C. The temporal variations of PCM temperature and liquid fraction at the mid of tank can thus be simulated and shown in Figure 6.2 and Figure 6.3 respectively. From these simulation results, due to the large temperature difference between HTF and PCM and small sensible heat transfer involved, the PCM can all quickly approach to transition temperature point. Although the higher HTF flow rate can speed up a bit this process, the temperature difference between PCM and HTF seems to dominate. In addition, since the main thermal resistance is on the PCM liquid side, the thermal resistance reduction on the HTF flow side due to the flow rate increase has little effect on the overall heat transfer during this period. After that, at each HTF flow rate, the PCM starts to transit phase from liquid to solid by releasing larger latent heat to the HTF and thus taking longer time to complete the phase change. Meanwhile, from heat transfer point of view, due to the phase change involved, the heat transfer coefficient on the PCM is greatly improved such that the PCM side is not the main thermal resistance anymore. Therefore, the heat transfer enhancement on the HTF side due to the flow rate increase can significantly affect the overall heat transfer of the HX and thus greatly reduce the completion time of phase change. Once the PCM is solidified, the PCM temperature drops abruptly at the beginning due to the relatively low solid PCM thermal resistance and limited sensible heat transfer. However, with the reduction of the temperature difference between HTF and PCM, the heat transfer process is also reduced such that the PCM temperature decrease rate is also slowed down as shown in Figure 6.2. Correspondingly, as shown in Figure 6.3 more time is needed for the PCM transition period and the time is greatly reduced when the HTF flow rate increases.

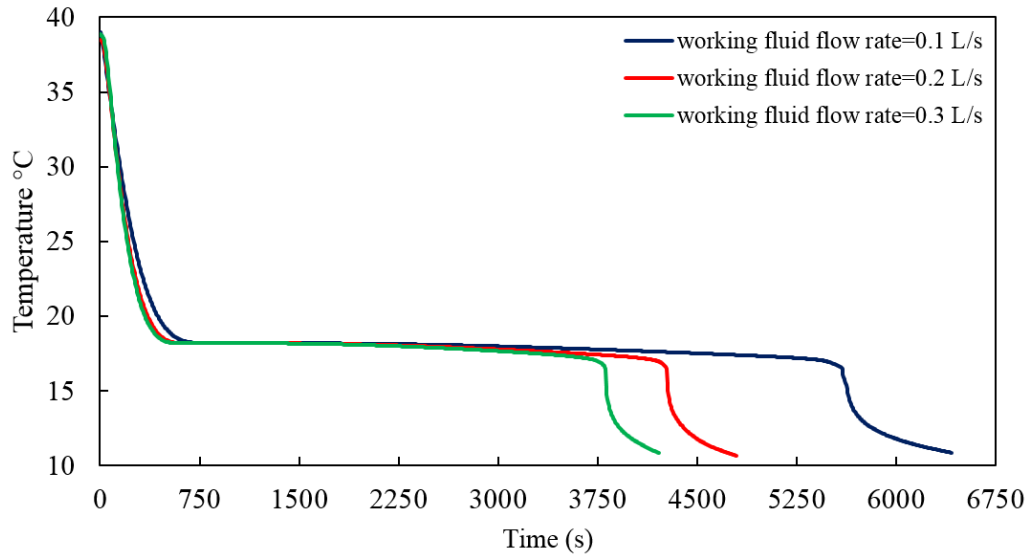


Figure 6.2. PCM discharging - the temperature at the middle of PCM HX for fixed inlet temperature ( $10^{\circ}\text{C}$ ) and different flow rates.

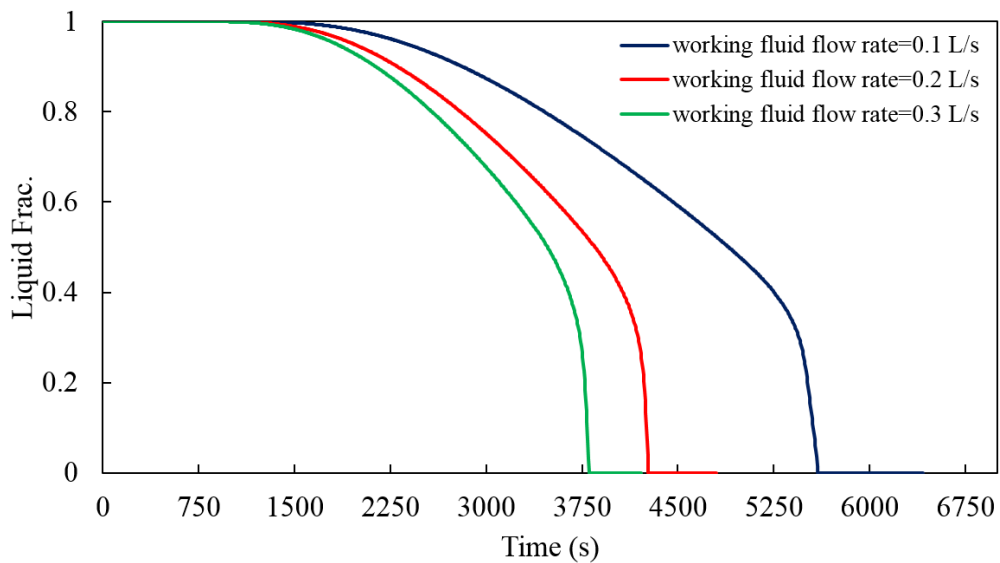


Figure 6.3. PCM discharging - mass fraction at the middle of PCM HX for fixed inlet temperature ( $10^{\circ}\text{C}$ ) and different flow rates.

For the PCM charging process, the initial PCM temperature inside the tank is set to  $10^{\circ}\text{C}$ . The temporal variations of PCM temperature and liquid fraction at the mid of tank can thus be simulated and are shown in Figure 6.4 and Figure 6.5 respectively. Similar to the discharging process, at each HTF flow rate, the phase transition period from solid to liquid dominant the whole discharging period. Meanwhile, the higher HTF flow rate can enhance the overall heat transfer during the phase change period and therefore speed up the charging process.

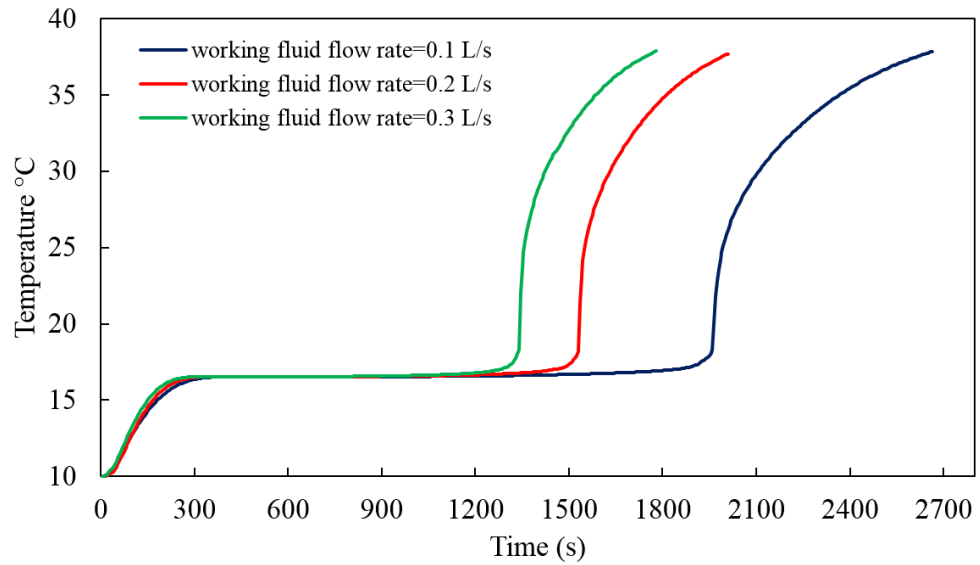


Figure 6.4. PCM charging- temperature at the middle of PCM HX for fixed inlet temperature (40°C) and different flow rates.

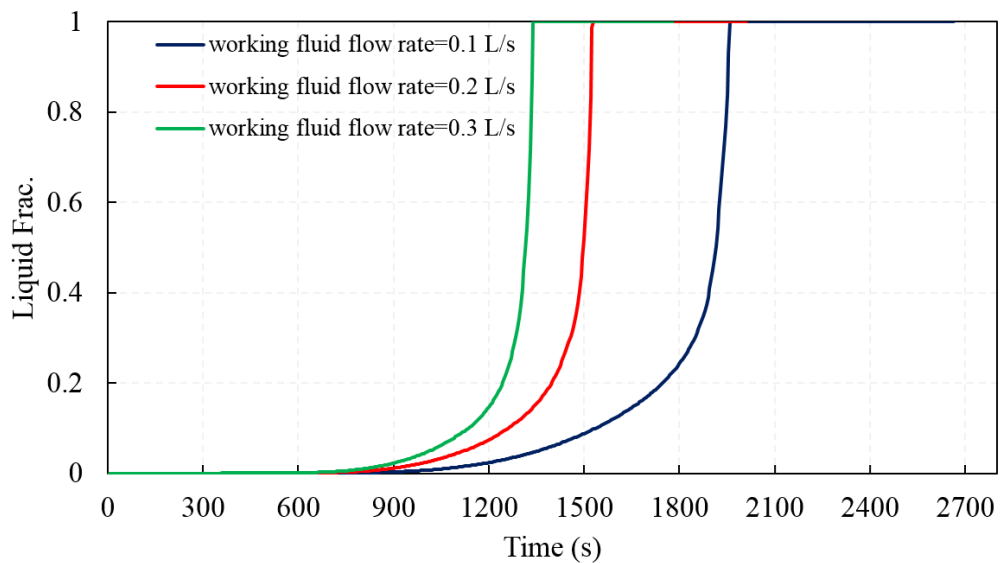


Figure 6.5. PCM charging – mass fraction at the middle of PCM HX for fixed inlet temperature (40°C) and different flow rates.

### 6.2.3. Effect of HTF inlet temperature variation

As another important application, the developed CFD model is used to simulate the PCM discharging and charging processes at constant HTF flow rate (0.1 kg/s) but varied inlet temperatures which are 5°C, 10°C and 15°C for discharging process and 30°C, 40°C and 50°C for charging process. The selections of these inlet temperatures are all applicable for the actual operation of indirect solar assistant heat pump system

where the PCM HX is integrated. For the discharging process, the initial PCM temperature is set to 40°C. The temporal variations of PCM temperature and liquid fraction at the mid of tank can thus be simulated and shown in Figure 6.6 and Figure 6.7 respectively. From these simulation results, due to the significant temperature difference between HTF and PCM and small sensible heat transfer involved, the PCM can all quickly approach to transition temperature point. Although the lower HTF inlet temperature can speed up a bit this process, it is compromised by the relatively small sensible energy stored. After that, at each HTF inlet temperature, the PCM starts to transit phase from liquid to solid by releasing larger latent heat to the HTF and thus taking longer time to complete the phase change. However, the lower fluid inlet temperature can lead to higher temperature difference between PCM and HTF and therefore increase the heat transfer rate. At constant PCM latent heat energy, the phase transition period can be greatly reduced with higher heat transfer rate or lower HTF inlet temperature. Once the PCM is solidified, the heat transfer process is much quicker considering the small sensible energy stored.

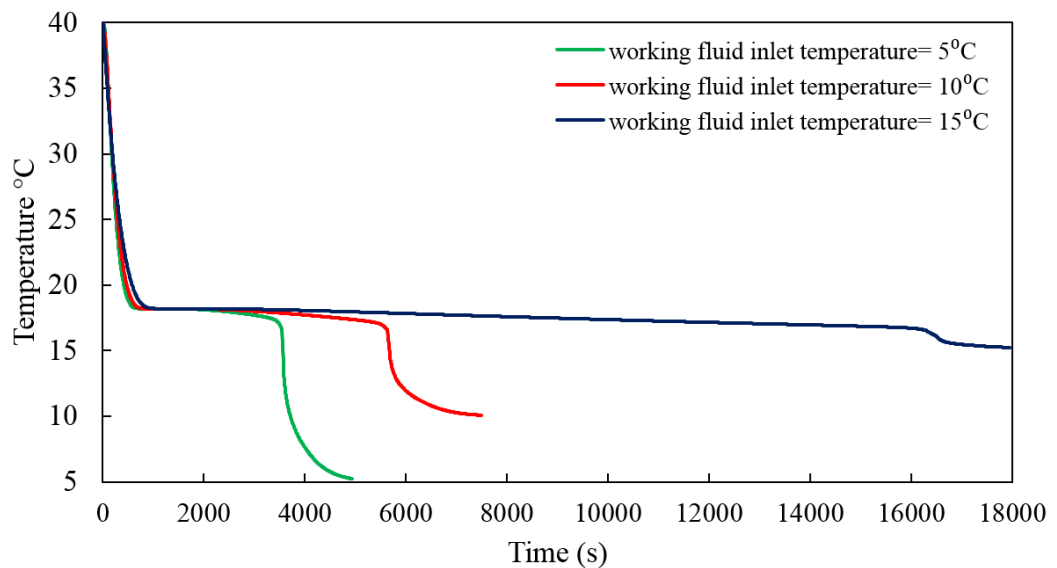


Figure 6.6. PCM discharging - the temperature at the middle of PCM HX for fixed inlet flow rate (0.1 kg/s) and different inlet temperature.

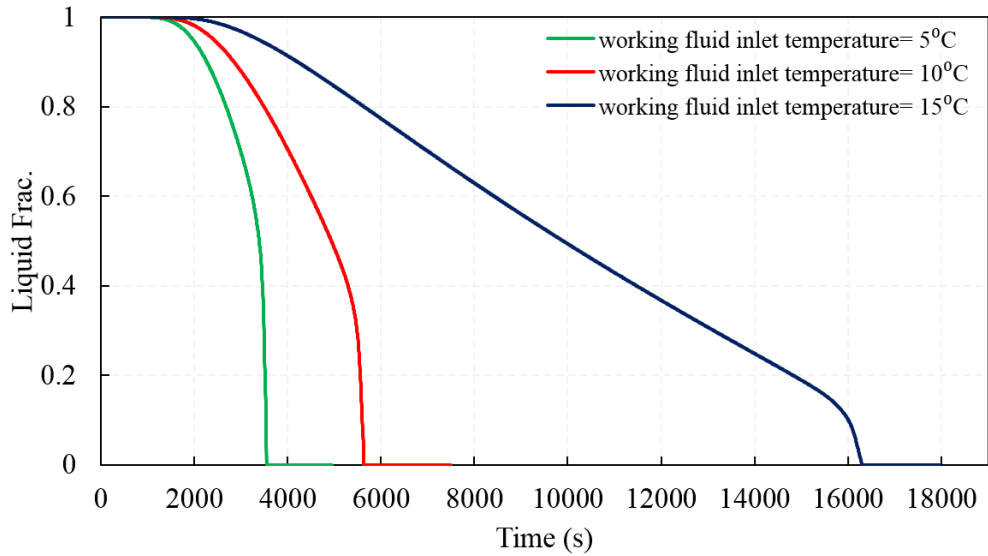


Figure 6.7. PCM discharging – mass fraction at the middle of PCM HX for fixed inlet flow rate (0.1 kg/s) and different inlet temperature.

For the PCM charging process, the initial PCM temperature inside the tank is set to 10°C. The temporal variations of PCM temperature and liquid fraction at the mid of tank can thus be simulated at constant fluid flow rate but different inlet temperatures, as shown in Figure 6.8 and Figure 6.9 respectively. Similar to the discharging process, at each HTF inlet temperature, the phase transition period from solid to liquid dominant the whole charging period. Meanwhile, the higher HTF inlet temperature can enhance the overall heat transfer during the phase changer period and therefore speed up the charging process.

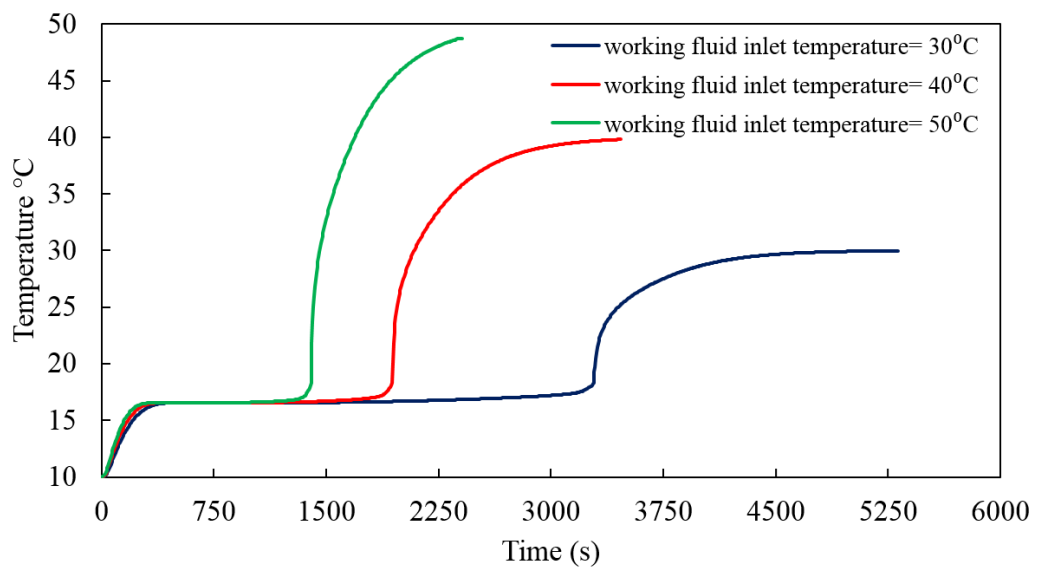


Figure 6.8. PCM charging - temperature at the middle of PCM HX for fixed inlet flow rate (0.1 kg/s) and different inlet temperature.

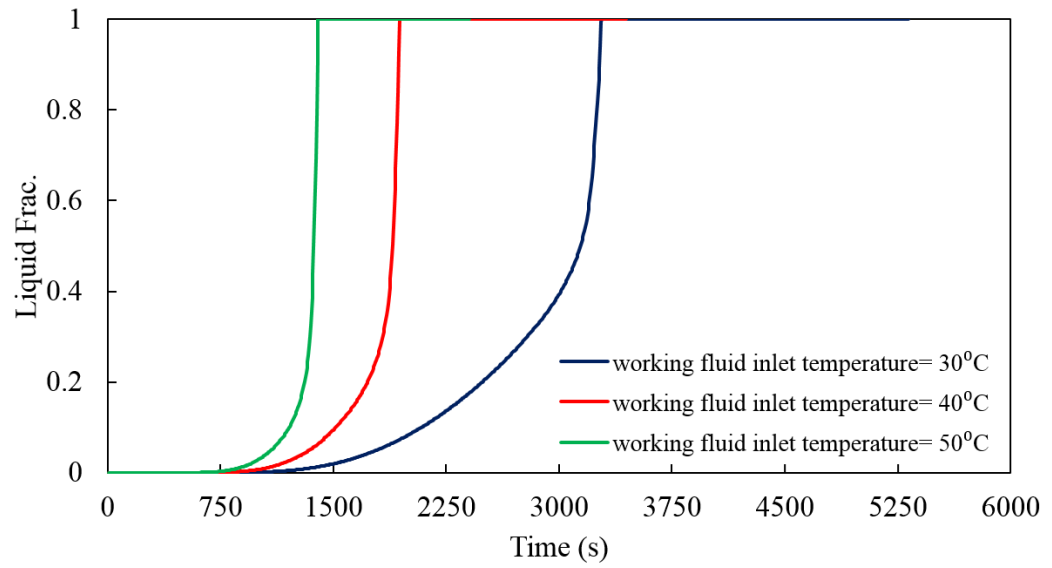


Figure 6.9. PCM charging – mass fraction at the middle of PCM HX for fixed inlet flow rate (0.1 kg/s) and different inlet temperature.

### 6.3. Coupled model case studies

Based on the proposed control strategy described in section 3.5.2 and the developed numerical model, the system was simulated in two different countries; Cairo-Egypt and Madrid-Spain. As one of the control parameters is the solar irradiance, it was important to study the system behaviour in hot locations. The load profile was set according to the DHW load profile described in section 2.2 for all simulated days. The delivered hot water temperature was at  $55^{\circ}\text{C}$  ( $\pm 2$ ) for all simulated days.

Four days were simulated in Cairo and Madrid, two during winter and two during summer for each location. As shown in Figure 6.10, the irradiance in Cairo during summer and winter were almost steady with a maximum value of  $751\text{ W/m}^2$  and  $1050\text{ W/m}^2$  respectively while the maximum value of the irradiance during summer and winter in Madrid were  $880\text{ W/m}^2$  and  $1053\text{ W/m}^2$  respectively. Figure 6.11 shows the variation of the ambient temperature during summer and winter in both locations. It was observed that the ambient temperature during summer was higher than the ambient temperature during winter by almost  $14^{\circ}\text{C}$  in Cairo and  $22^{\circ}\text{C}$  in Madrid. This will directly affect the feed water temperature and operation periods of the system as it will be explained further.

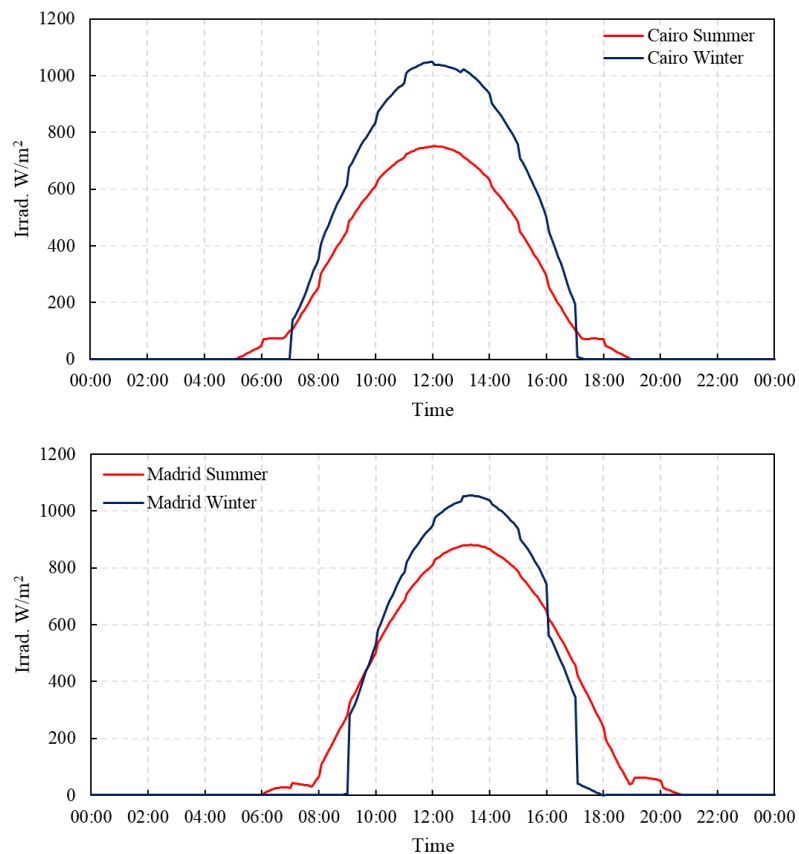




Figure 6.10. Typical irradiance during day in Cairo and Madrid for summer and winter

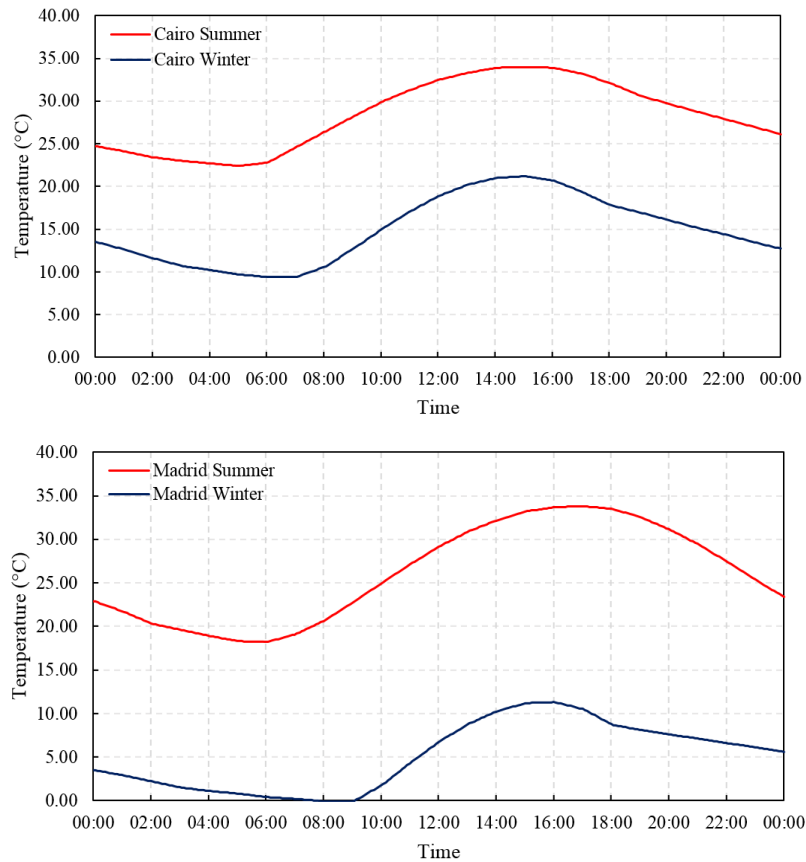


Figure 6.11. Typical ambient temperature during day in Cairo and Madrid for summer and winter

As illustrated in Figure 6.12 for the temperature development inside the WST in Cairo, the system could meet the DHW demand by supplying hot water flow from the top of the WST during summer with temperature between 52°C and 57°C while the range during winter was between 50°C and 57°C. On the other hand, as shown in Figure 6.13 for the temperature development inside the WST in Madrid, the system also could meet the DHW demand by supplying hot water flow from the top of the WST during summer with temperature between 52°C and 57°C but it was observed that the range was slightly different during winter for a value between 46°C and 57°C. The temperature at the bottom of the WST was found to have sharply dropped at around 7 am until the first operation of the heat pump. This was due to the load profile that was assigned to the WST at the beginning of this period. Moreover, the solar HX coil inside the WST is placed at the middle of the tank which makes the bottom tank temperature low. Due to the ambient temperature difference between summer and winter, the temperature at the bottom of the tank varied between the simulation days.

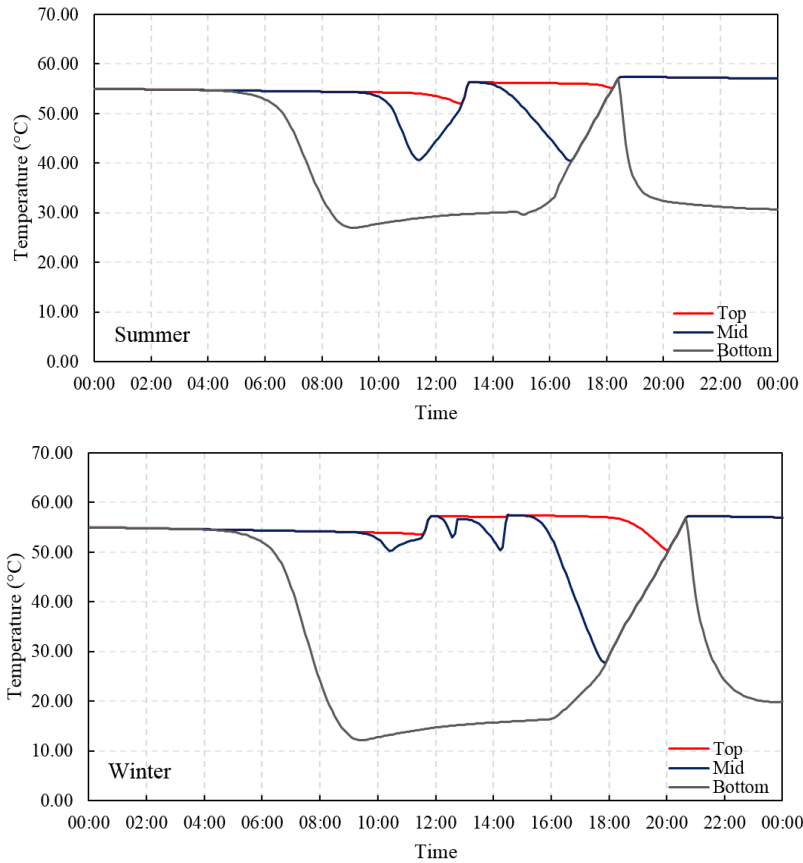


Figure 6.12. Variation WST water temperature during summer and winter in Cairo.

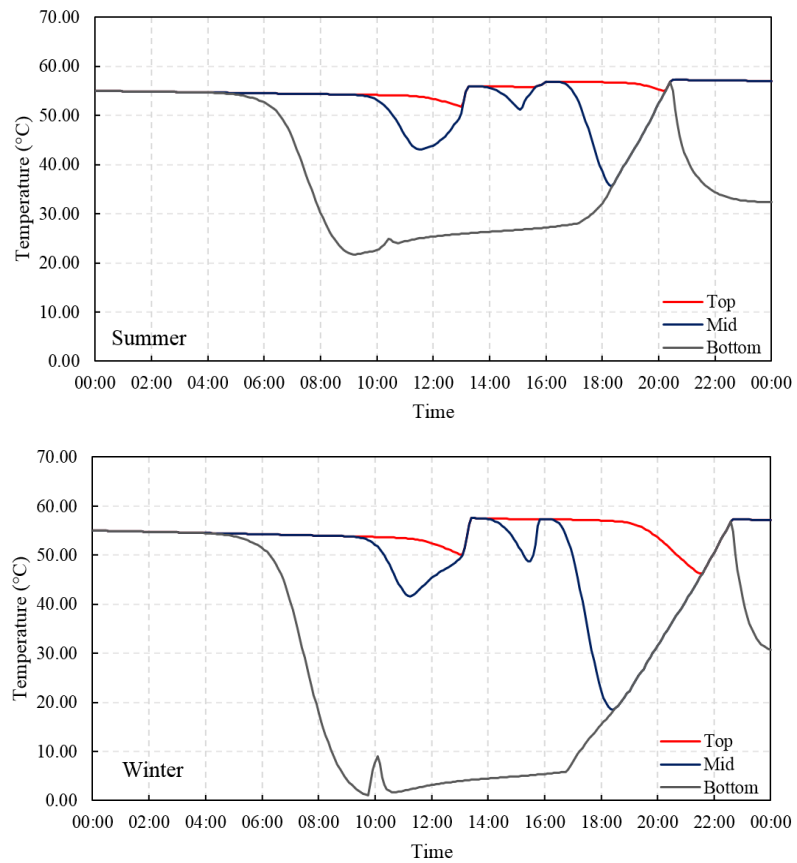


Figure 6.13. Variation WST water temperature during summer and winter in Madrid.

For the sunny simulated days in both locations, it was observed that the heat pump started only during the night. Therefore, the PCM HX stored enough energy during the day to cover the operation of the heat pump during the night. As it is shown in Figure 6.14, the PCM HX temperature dropped sharply from 17:10 and 18:50 in Cairo and Madrid respectively. This was because of the lack of the irradiance during the heat pump operation. After the heat pump was switched off, the ambient temperature outside was still above the melting point of the PCM. Therefore, the PCM HX was in the charging mode even during the night.

For the winter simulated days in both locations, at the start of the simulation, the PCM HX was not called 07:30 and 09:00 in Cairo and Madrid respectively. That explains the constant temperature that before this time was stored from the previous simulation. During the night, the PCM HX temperature was dropped due to the lack of solar irradiance during the operation of the heat pump. The temperature was maintained almost constant of the heat pump was switched off because the source circulation pump was switched off as the ambient temperature was below the PCM melting point.

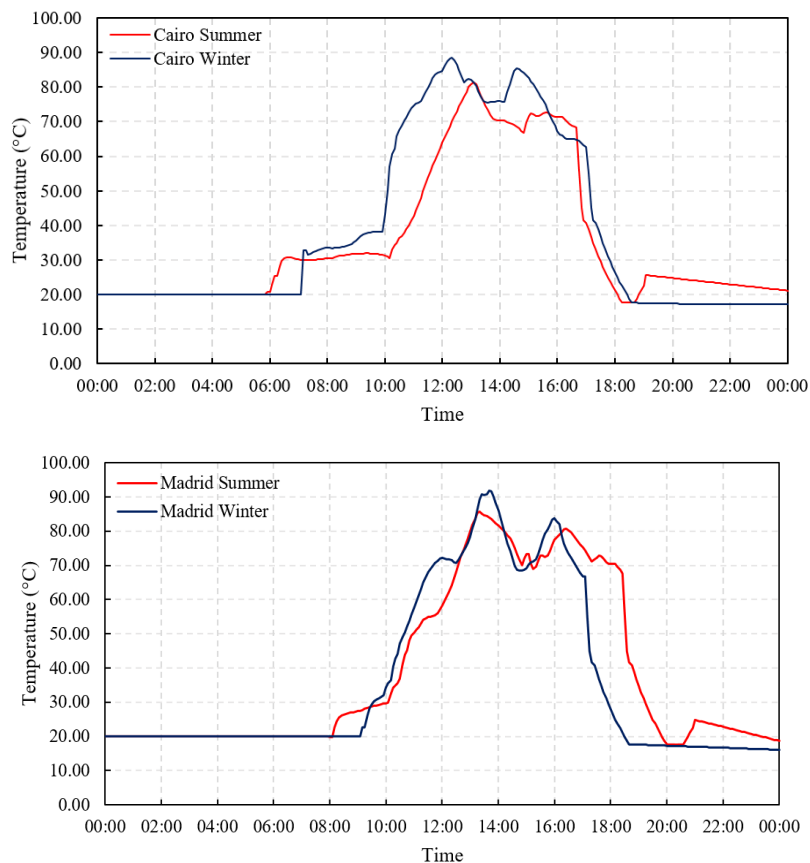


Figure 6.14. PCM HX inside temperature during summer and winter in Cairo and Madrid

The heat pump was operated for 20 minutes at almost 10:00 in during summer and winter in Madrid while the heat pump did not operate at all during daytime in Cairo. This was because the control was set to be in solar mode when the irradiance was above  $550 \text{ W/m}^2$  we respect of the dead-bands. This condition was satisfied in Cairo before the middle WST temperature drops below  $55^\circ\text{C}$  but it was not in Madrid. During daytime, as the irradiance was sufficient to operate the solar mode, the system utilized the DHW load demand via solar energy only with power consumption of 0.05 kW. During the night period, the heat pump was operated a single period in all simulated days. As shown in Figure 6.15 the maximum power consumption in Cairo during summer and winter is 1.62 kW and 1.85 kW respectively while the maximum power consumption in Madrid during summer and winter is 1.65 kW and 1.92 kW respectively. The AWHX was not called at any of the simulated days in both locations.

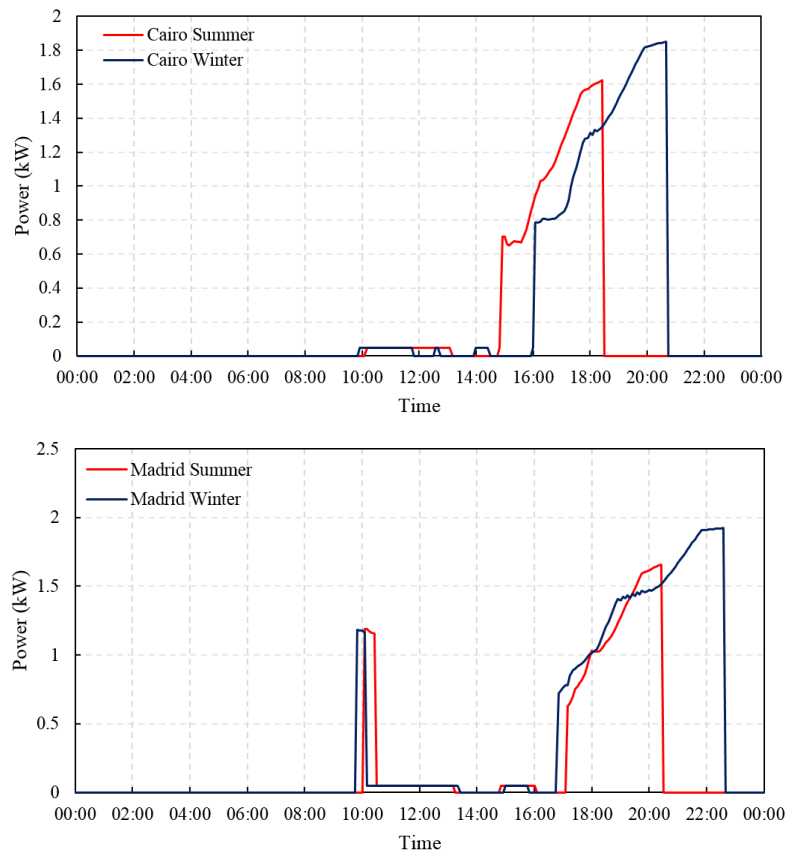


Figure 6.15. System power consumption during summer and winter in Cairo and Madrid

Figure 6.16 and Figure 6.17 shows the COP and SPF of the system in Cairo and Madrid respectively. For the sunny days in both locations, it was observed that system COP was increasing during the heat pump operation to reach a maximum value of 5.5 in both locations during summer. It was also observed that the SPF in Cairo during

summer was gradually increased to reach a value of 0.36; then it had a sharp increase to reach 0.69. This was because at the noontime the solar irradiance reaches the peak period when is the collector has the highest efficiency. Correspondingly, during summer in Madrid, the SPF had the same behaviour like in Cairo but the solar mode was operated for one additional period at 14:50 as the WST middle temperature dropped below 55°C. During winter in Cairo, the solar mode was fully able to utilize DHW load demand. However, due to the drop in the ambient temperature which was between 9.4°C and 21.2°C, the solar mode was called more than once during daytime. The maximum value of the COP and SPF were 5.3 and 0.83 respectively. As the second, third and fourth solar operational period was during the irradiance peak time, the SPF was increased. During winter in Madrid, the solar mode was operated for longer and continuous periods. That was because the feed water temperature was as low as ambient temperature with maximum and minimum value of 11.3°C and 0°C respectively, as it is shown in Figure 6.11. During the second solar operation period in this day, the SPF had a maximum value of 0.4, unlike the first period. This was because the irradiance dropped sharply during this period.

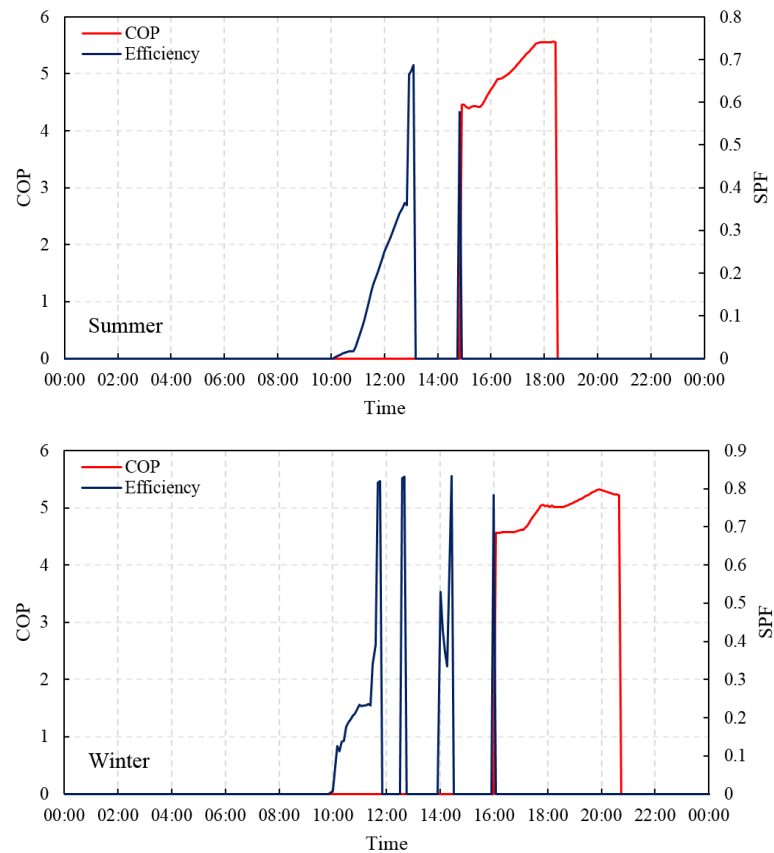


Figure 6.16. System COP and SPF during summer and winter in Cairo

Table 10. System Performance for the simulated days

	<b>Total heat added to WST (kWh)</b>	<b>Total power consumption (kWh)</b>
<i>Cairo Summer</i>	23.25	4.214237
<i>Cairo Winter</i>	35.79	6.358623
<i>Madrid Summer</i>	26.97	4.719712
<i>Madrid Winter</i>	47.28	8.843155

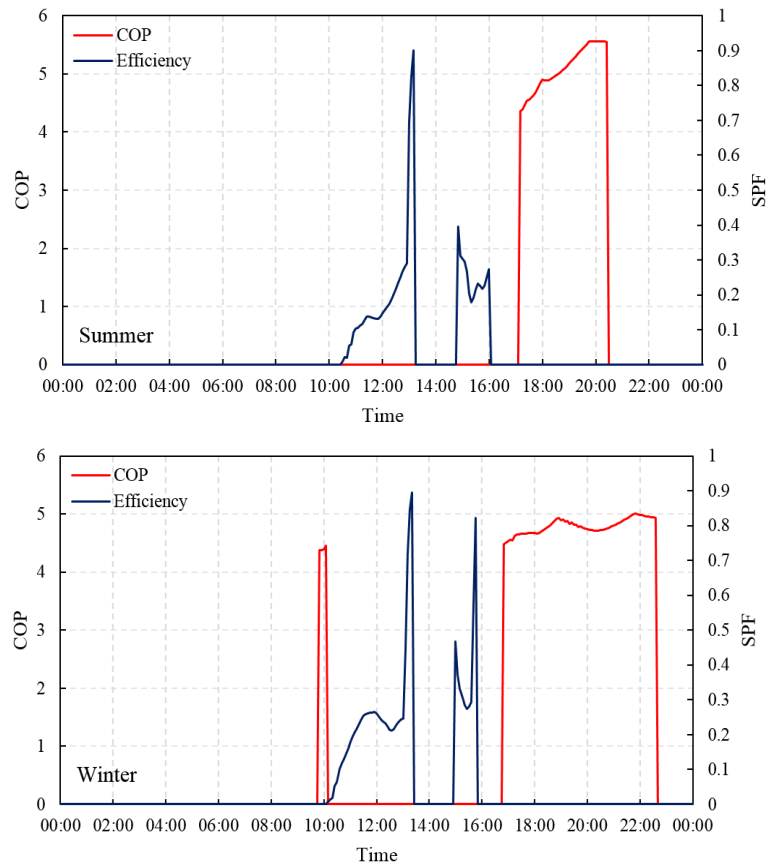


Figure 6.17. System COP and SPF during summer and winter in Madrid

The total power consumption and total heat added to the WST for all simulated days are listed in Table 10. The total heat added to the WST is calculated by the sum of the heat added during the solar mode and the heat pump mode. From the simulation, the summer simulated was found to have less energy input to the WST while winter simulated days' energy input was relatively higher. Also, it was noted that all simulated days have less power consumption and WST energy input compared with experimental results in London. This was mainly due to the variation of water feed temperature to the WST and solar was called during the daytime as primary heating. Moreover, the WST HX which is connected to the direct solar loop is placed at the middle of the WST. Consequently, during solar mode, the amount of water that will

be heated is almost half the amount compared to when the heat pump operated as a result of the tank stratification.

#### ***6.4. Summary of Chapter 6***

Latent TES technologies with PCMs are essential to be applied to solar thermal systems considering the intermittent nature of solar energy resource and requirement of system compactness. However, the PCM thermal conductivity needs to be greatly enhanced so as to speed up the processes of energy storage and release. Therefore, The CFD analysis for the PCM HX model has presented in this chapter as well as the case studies in Cairo and Madrid for the coupled model. The PCM HX CFD analysis included a visual analysis for the PCM behaviours as well as a comparison between different inlet flow rates and temperatures. The results showed that 0.1 kg/s is an ideal flow for the proposed application in terms of charging and discharging the PCM.

For the case studies of the coupled model, it was observed that the system can be more beneficial in warm location with high solar irradiance during the year. The direct solar loop was called more often in this location due to the sufficient irradiance during the daytime. This resulted in a significant saving in the total power consumption of the system.

The following chapter will include a summary of the outcome of this research and suggest recommendations for further studies based on this outcome.

---

***Chapter 7. Conclusion and Further  
Recommendation***

---



The main objectives of this study set in the beginning were to; create a novel configuration IDX-SAHP system, create control strategy of the designed system and investigated the control behaviour experimentally and numerically, size, design and manufacture an innovative PCM HX for excess solar energy storage, perform a CFD simulation for the designed PCM HX, validate both numerical models for whole system in TRNSYS and for PCM HX in CFD FLUENT with experiment results and simulate the system in TRNSYS in different location.

Therefore, an initial literature review was conducted to understand the system and the SAHP types following by intensive review on the current development of IDX-SAHP systems. The review continued to cover PCM in terms of types, selection criteria, advantages/disadvantages, heat transfer enhancement method and its applications in the solar sector. Accordingly, an experimental investigation was carried out to test the system performance and the reliability of the proposed control strategy. After analysing the experiment without the effect of the latent heat storage, an initial sizing for PCM required was conducted and following by detailed design for the PCM HX with a novel heat transfer enhancement method. The PCM HX when manufactured and installed in IDX-SAHP test rig for further experimentation. The final analysis of the experiment was conducted and the outcomes for this intensive experiment were published.

The system was then numerically modelled on TRNSYS without the latent heat storage application and validated with the experiment results. As the PCM HX is a novel application and it is not included at TRNSYS library, A CFD model for the PCM HX was developed and validated with the experiment. This work was submitted to Solar Energy Journal for publication. Both models TRNSYS and CFD were coupled together to study the performance of the system in different locations with high solar irradiance.

Therefore, based on the previous statement, the work conducted in this study fulfil the main objectives of the research that was set initially.

The work done during the project period can be summarized as follows:

- A literature review through the background concepts of SAHP, the types of the SAHP, the component configurations and IDX-SAHP development was presented in Chapter 2. Moreover, a brief review of PCM material was conducted in terms of its classification, selection criteria, advantages and disadvantages. Also, heat transfer enhancement techniques were reviewed in order to overcome the PCM poor thermal conductivity. Consequently, the literature of the previous use of latent heat storage for solar application was conducted.
- The experimental procedures, equipment, instrumentation, the design consideration and thermodynamic methodology used for the experimental investigation of this research were presented in Chapter 3. The objectives of this chapter were to; design and construct IDX-SAHP test rig, identify system operation modes, create and implement an optimal control strategy for the system, perform an investigation on PCM HX for excess solar energy storage. The outcome of this work was published (Youssef, Ge and Tassou, 2017)
- The findings of the performed experimental work and the control strategy behaviour of the different climate conditions during 24 hours for each tested day were presented in Chapter 4. Furthermore, the uncertainty analysis of the experimental finding was provided. The outcome of this work was published (Youssef, Ge and Tassou, 2017)
- The development of the numerical model of the whole system and PCM HX was presented in Chapter 5. The whole system was simulated in TRNSYS and PCM HX was simulated in CFD FLUENT then dynamically coupled to the TRNSYS model. A proposed heat transfer enhancement method for the PCM HX was illustrated in details in the same chapter. The outcome of this work was submitted to be published.
- The CFD analysis for the PCM HX model including a comparison between different inlet flow rate and temperature condition was presented in Chapter 6. The outcomes of this part were submitted to be published. Furthermore, a simulation for case studies in Cairo and Madrid for the coupled model was performed.

### ***7.1. Concluding remarks***

- The literature shows there is no optimal configuration yet for IDX-SAHP system. This is because of the lack of the control development in this area. The literature illustrated a clear understanding of the PCM types and selection criteria. As PCM poor thermal conductivity was a major challenge to its use, a focused literature was conducted on heat transfer enhancement techniques was performed; numerically and experimentally. The literature shows the radial fins solution was the most practical in terms of efficient heat transfer and cost-effective. Consequently, the literature of the previous use of latent heat storage was focused on SAHP applications.
- Experimentally, a new IDX-SAHP test system has been designed, built and instrumented. The DHW temperature was selected at 55°C as the minimum required for DHW operation temperature is 50°C according to the British standards. The system heating output capacity is 9 kW. The system is designed for large houses (4-5 bedrooms) or small buildings (2-3 apartments). The flow rate of the heat source loop and heat sink loop are 0.1 kg/s and 0.23 kg/s respectively. The solar collector efficiency is expected to be between 0.6-0.75 depending on the solar irradiance and operation temperature. For the heat pump operation, the condensation temperature is expected to be between 50-60°C. Meanwhile the evaporating temperature can vary depending on the selected heat source and operation time. For the PCM HX, the organic PCM material was selected for this project with a melting point at 16°C. The AWHX capacity is 10 kW. This capacity could be reduced by controlling the fan speed depending on the cooling capacity. The COP of the system reached 4.99 during the sunny tested day by using the PCM HX. There are three operational loops in the system including solar thermal, IDX-SAHP and load profile. A PCM HX tank was purposely designed and installed in the system solar thermal loop to absorb and store solar energy when applicable and release heat when required. The PCM HX was more compact and efficient compared to conventional WSTs used in IDX-SAHP systems. In addition, an air cooling HX was selected and also installed between the solar collector and the PCM HX in the solar thermal loop. It was controlled to be on when ambient air heat source was needed for the IDX-SAHP. A control strategy was intentionally designed and implemented with BMS so as to maintain

a constant temperature of hot water production and ensure high efficient system operations. Comprehensive measurements were carried out for four test days with different weather conditions (sunny and cloudy) and system structures (with and without PCM HX). The experimental results show that the designed IDX-SAHP system can meet the daily hot water load demand with constant hot water supply irrespective of weather conditions and system structures. In addition, the IDX-SAHP system could have various performance improvements at different weather conditions when PCM HX was integrated. Quantitatively, the average COP of the IDX-SHAP system with PCM HX could increase up to 6.1% and 14.0% on sunny and cloudy days respectively comparing to those systems without PCM HX integrations.

- For the CFD simulation, a PCM HX is purposely designed, manufactured and installed in an indirect solar assistant heat pump system. The PCM HX consists of eight spiral-wired tubes and enclosed with metal sheets in which organic PCM is charged on the outer tube side with wire fins while HTF flowing through the tube side. The PCM overall thermal conductivity was evaluated at  $11.07 \text{ W} \cdot (\text{m} \cdot \text{K})^{-1}$  including the contribution of the spiral wires. To fully understand the dynamic charging and discharging processes of the PCM HX, a 3D CFD model of the HX was developed and validated with experimental results. It is found from the simulation results that at specific operating conditions the charging time is much faster than the discharging time. This is due to the contributions of convection heat transfer and bouncing effect generated on the PCM side during charging or liquefying process. In addition, the HTF side temperature and flow rate can also affect the discharging and charging processes of the PCM HX. The higher HTF inlet flow rate can speed up both discharging and charging processes. Meanwhile, the lower and higher HTF inlet temperature can improve the discharging and charging processes respectively. However, the effects of these parameters' changes on the sensible heat storage and releasement are not significant. The simulation results can help to understand the dynamic charging and discharging processes of the PCM HX and instruct efficiently the operation of the HX and its integration with the solar system.
- For the coupled numerical model, in the case of the studies of the coupled model, it was observed that the system can more beneficial in warm location with high solar irradiance during the year. The direct solar loop was called more often in

this location due to the sufficient irradiance during daytime. This resulted in a significant saving in the total power consumption of the system.

### ***7.2. Recommendation and further work***

- As explained earlier in Chapter 3, the system has heat source loop and heat sink loop with HTF water/glycol and purified water respectively. Therefore, more experimental investigations to study the variation of the different flow rate are required in order to show the effect of this variation on the system performance.
- As an initial investigation of this novel system, the trend was to keep the cost as low as possible. Consequently, the heat pump used for the experiment was a custom-made heat pump with R-134a refrigerant which was recovered from another project. Therefore, further investigation of the system performance using different working refrigerant such as R744 (CO<sub>2</sub>) would be worth investigating as R-134a will be banned in the UK by 2022(Department for Environment, 2014).
- The system showed reliability and stability by maintaining the WST hot supply temperature at the control set point. Therefore, investigating the system ability for higher load demand can an interesting area of research.
- As mentioned earlier, the heat pump is custom made. Therefore, possible optimization can be employed to the system to make it more compact. Furthermore, managing the heat losses for the system by optimizing the system design would increase the COP of the system.
- As the proposed control strategy showed reliability and success, further investigation to test system in different seasonal conditions can be performed.
- The simulation in hot location showed that during the daytime, the temperature of the PCM ban reach 80°C. The energy is stored as sensible heat in the current design. Therefore, further investigation of attaching another PCM for higher melting point for direct heating of WST is expected to save more energy.
- As a novel system, the future trend is to commercialize such a system. In order to achieve that an economic analysis is required to be performed in order to compare the system with a conventional DHW and space heating systems.
- The developed numerical models can be used for further investigation in various applications.

---

*References*

---

- Abhat, A. (1981) 'Short term thermal energy storage', *Energy and Buildings*, 3, pp. 49–76.
- Abhat, A. (1983) 'Low temperature latent heat thermal energy storage: heat storage materials', *Solar Energy*, 30(4), pp. 313–332.
- Aguilar, C., White, D. J. and Ryan, D. L. (2005) *Domestic water heating and water heater energy consumption in Canada*.
- Agyenim, F., Eames, P. and Smyth, M. (2009) 'A comparison of heat transfer enhancement in a medium temperature thermal energy storage heat exchanger using fins', *Solar Energy*, 83, pp. 1509–1520. doi: 10.1016/j.solener.2009.04.007.
- Al-Abidi, A. A. *et al.* (2013) 'Internal and external fin heat transfer enhancement technique for latent heat thermal energy storage in triplex tube heat exchangers', *Applied Thermal Engineering*, 53(1), pp. 147–156. doi: 10.1016/j.applthermaleng.2013.01.011.
- Alva, G. *et al.* (2017) 'Thermal energy storage materials and systems for solar energy applications', *Renewable and Sustainable Energy Reviews*, 68, pp. 693–706. doi: 10.1016/j.rser.2016.10.021.
- Andrews, J. W. (1978) 'Development of a cost-effective solar assisted heat pump system', in *Meeting of the American Section of the International Solar Energy Society*, pp. 281–287.
- Assis, E. *et al.* (2006) 'Numerical and experimental study of melting in a spherical shell'. doi: 10.1016/j.ijheatmasstransfer.2006.10.007.
- AVX (2016) *NTC Thermistors, Notes*. doi: Cat.No.R44E-12.
- Ayompe, L. M. *et al.* (2011) 'Validated TRNSYS model for forced circulation solar water heating systems with flat plate and heat pipe evacuated tube collectors', *Applied Thermal Engineering*, 31, pp. 1536–1542.
- Bakirci, K. and Yuksel, B. (2011) 'Experimental thermal performance of a solar source heat-pump system for residential heating in cold climate region', *Applied Thermal Engineering*, 31(8–9), pp. 1508–1518. doi: 10.1016/j.applthermaleng.2011.01.039.
- Banister, C. J. and Collins, M. R. (2015) 'Development and performance of a dual



tank solar-assisted heat pump system’, *Applied Energy*, 149, pp. 125–132. doi: 10.1016/j.apenergy.2015.03.130.

Banister, C. J., Wagar, W. R. and Collins, M. R. (2014a) ‘Solar-assisted heat pump test apparatus’, *Energy Procedia*, 48, pp. 489–498. doi: 10.1016/j.egypro.2014.02.058.

Banister, C. J., Wagar, W. R. and Collins, M. R. (2014b) ‘Validation of a single tank, multi-mode solar-assisted heat pump TRNSYS model’, *Energy Procedia*, 48, pp. 499–504. doi: 10.1016/j.egypro.2014.02.059.

BEIS (2016) *Heat in buildings*. Available at: [https://www.gov.uk/government/uploads/system/uploads/attachment\\_data/file/575299/Heat\\_in\\_Buildings\\_consultation\\_document\\_v1.pdf](https://www.gov.uk/government/uploads/system/uploads/attachment_data/file/575299/Heat_in_Buildings_consultation_document_v1.pdf) (Accessed: 6 September 2017).

BEIS (2017a) *Energy consumption in the UK*. Available at: [https://www.gov.uk/government/uploads/system/uploads/attachment\\_data/file/633503/ECUK\\_2017.pdf](https://www.gov.uk/government/uploads/system/uploads/attachment_data/file/633503/ECUK_2017.pdf) (Accessed: 6 September 2017).

BEIS (2017b) *Energy consumption in the UK, department of business, energy and industrial strategy*. Available at: [https://www.gov.uk/government/uploads/system/uploads/attachment\\_data/file/633503/ECUK\\_2017.pdf](https://www.gov.uk/government/uploads/system/uploads/attachment_data/file/633503/ECUK_2017.pdf) (Accessed: 10 August 2017).

Bruno, F. (2004) ‘Using phase change materials (PCMs) for space heating and cooling in buildings’, in *the 2004 AIRAH performance enhanced buildings environmentally sustainable design conference*, pp. 26–31.

BS (2015) *Guide to the design, installation, testing and maintenance of services supplying water for domestic use within buildings and their curtilages - Complementary guidance to BS EN 806. BS 8558:2011, The British Standards Institution*.

BS (2017) *Heat pumps with electrically driven compressors — Testing and requirements for marking of domestic hot water units BS EN 161 17*.

Buker, M. S. and Riffat, S. B. (2016) ‘Solar assisted heat pump systems for low temperature water heating applications: A systematic review’, *Renewable and*

*Sustainable Energy Reviews*, 55, pp. 399–413. doi: 10.1016/j.rser.2015.10.157.

Çağlar, A. and Yamalı, C. (2012) ‘Performance analysis of a solar-assisted heat pump with an evacuated tubular collector for domestic heating’, *Energy and Buildings*, 54, pp. 22–28. doi: 10.1016/j.enbuild.2012.08.003.

Cai, J. *et al.* (2016) ‘Numerical simulation and experimental validation of indirect expansion solar-assisted multi-functional heat pump’, *Renewable Energy*, 93, pp. 280–290. doi: 10.1016/j.renene.2016.02.082.

Carbonell, D., Haller, M. Y. and Frank, E. (2014) ‘Potential benefit of combining heat pumps with solar thermal for heating and DHW preparation’, *Energy Procedia*, 57, pp. 2656–2665.

Chandrashekar, M. *et al.* (1982) ‘A comparative study of solar assisted heat pump systems for canadian locations’, *Solar Energy*. Pergamon, 28(3), pp. 217–226. doi: 10.1016/0038-092X(82)90160-8.

Chaturvedi, S. K. and Abazeri, M. (1987) ‘Transient simulation of a capacity-modulated, direct-expansion, solar-assisted heat pump’, *Solar Energy*, 39(5), pp. 421–428. doi: 10.1016/S0038-092X(87)80060-9.

Chaturvedi, S. K., Chen, D. T. and Kheireddine, A. (1998) ‘Thermal performance of a variable capacity direct expansion solar-assisted heat pump’, *Energy Conversion and Management*, 39(3–4), pp. 181–191. doi: 10.1016/S0196-8904(96)00228-2.

Chaturvedi, S. K., Chiang, Y. F. and Roberts, A. S. (1982) ‘Analysis of two-phase flow solar collectors with application to heat pumps’, *Journal of Solar Energy Engineering*. American Society of Mechanical Engineers, 104(4), p. 358. doi: 10.1115/1.3266330.

Chaturvedi, S. K. and Shen, J. Y. (1984) ‘Thermal performance of a direct expansion solar-assisted heat pump’, *Solar Energy*, 33(2), pp. 155–162. doi: 10.1016/0038-092X(84)90233-0.

Chow, T. T. *et al.* (2012) ‘Analysis of a solar assisted heat pump system for indoor swimming pool water and space heating’, *Applied Energy*, 100, pp. 309–317. doi: 10.1016/j.apenergy.2012.05.058.

Chu, J. and Cruickshank, C. a (2013) ‘Solar assisted heat pump systems: a review of

existing studies and their applicability to the Canadian residential sector’, *Journal of Solar Energy Engineering*, pp. 1–10. doi: 10.1115/1.4027735.

D’Antoni, M., Fedrizzi, R. and Sparber, W. (2012) ‘IEA – SHC task 44 / Annex 38 solar and heat pump systems’, *IEA-SHC*, June.

Danfoss (2014) *Pressure transmitter AKS 32*. doi: RI5GF222.

Dawson, K. (2012) *Heating trends by 2020*. Available at: <file:///acfs5/mepg/mepgwmy/Downloads/krystyna-dawson-presentation.pdf>.

Department for Environment, F. & R. A. (2014) *Bans on F gas in new equipment*. Available at: <https://www.gov.uk/guidance/bans-on-f-gas-in-new-equipment#refrigerants>.

DTI (2006) *Our energy challenge, power from the people*. Available at: <http://webarchive.nationalarchives.gov.uk/+http://www.berr.gov.uk/files/file27575.pdf>.

Edem N ’tsoukpoe, K. *et al.* (2009) ‘A review on long-term sorption solar energy storage’, *Renewable and Sustainable Energy Reviews*, 13, pp. 2385–2396. doi: 10.1016/j.rser.2009.05.008.

Element Energy (2008) *The growth potential for microgeneration in England, Wales and Scotland*. Available at: <http://webarchive.nationalarchives.gov.uk/20090609003228/http://www.berr.gov.uk/files/file46003.pdf>.

Energy Savings Trust (2008) ‘Measurement of domestic hot water consumption in dwellings’, *Energy Savings Trust*. Energy Saving Trust, pp. 1–62.

Fluent INC (2016) ‘Fluent User Guide 17.0’.

Fluke (2016) *Fluke 435 series II power quality and energy analyzer*.

Freeman, G. . (1997) *Indirect solar-assisted heat pumps for application in the Canada environment*. Queen’s University.

Freeman, T. L., Mitchell, J. W. and Audit, T. E. (1979) ‘Performance of combined solar-heat pump systems’, *Solar Energy*, 22(2), pp. 125–135. doi: 10.1016/0038-092X(79)90096-3.

- Fritsch, J. (2011) 'World renewables 2010, heat pumps in UK, a multi client study'. Available at: [http://www.gshp.org.uk/documents/HHIC BSRIA Summary UK Heat Pumps.pdf](http://www.gshp.org.uk/documents/HHIC_BSRIA_Summary_UK_Heat_Pumps.pdf).
- Gelažanskas, L. and Gamage, K. (2015) 'Forecasting hot water consumption in residential houses', *Energies*, 8(11), pp. 12702–12717. doi: 10.3390/en81112336.
- Gerin, O., Bleys, B. and Cuyper, K. De (2015) 'Domestic hot water consumption in apartment buildings', in *Symposium 2015*. Belgium.
- Hepbasli, A. and Kalinci, Y. (2009) 'A review of heat pump water heating systems', *Renewable and Sustainable Energy Reviews*, 13(6–7), pp. 1211–1229. doi: 10.1016/j.rser.2008.08.002.
- Ibrahim, N. I. *et al.* (2017) 'Heat transfer enhancement of phase change materials for thermal energy storage applications: A critical review', *Renewable and Sustainable Energy Reviews*, 74, pp. 26–50. doi: 10.1016/j.rser.2017.01.169.
- IEA (2016) 'Key world energy statistics', *International Energy Agency*,. Available at: <https://www.iea.org/publications/freepublications/publication/KeyWorld2016.pdf>.
- Incropera, F. P. *et al.* (2007) *Fundamentals of Heat and Mass Transfer*. 6th edn. John Wiley.
- Jegadheeswaran, S. and Pohekar, S. D. (2009) 'Performance enhancement in latent heat thermal storage system: A review', *Renewable and Sustainable Energy Reviews*, 13(9), pp. 2225–2244. doi: 10.1016/j.rser.2009.06.024.
- Jie, J. *et al.* (2015) 'Experimental study on the performance of solar-assisted multi-functional heat pump based on enthalpy difference lab with solar simulator', *Renewable Energy*, 75, pp. 381–388. doi: 10.1016/j.renene.2014.09.054.
- Jordan, R. C. and Threlkeld, J. L. (1954) 'Design and economics of solar energy heat pump system', *Heat., Piping Air Cond.; (United States)*, 26.
- Kalogirou, S. A. (2004) 'Environmental benefits of domestic solar energy systems', *Energy Conversion and Management*, 45(18–19), pp. 3075–3092. doi: 10.1016/j.enconman.2003.12.019.
- Kaygusuz, K. *et al.* (1993) 'Exergy analysis of solar-assisted heat-pump systems for

domestic heating', *Energy*. Pergamon, 18(10), pp. 1077–1085. doi: 10.1016/0360-5442(93)90056-J.

Kaygusuz, K. and Ayhan, T. (1999) 'Experimental and theoretical investigation of combined solar heat pump system for residential heating', *Energy Conversion and Management*, 40(13), pp. 1377–1396. doi: 10.1016/S0196-8904(99)00026-6.

Kaygusuz, K., Ayhan, T. and Arslan, F. (1993) 'Experimental investigation and a dynamic simulation of the solar-assisted energy-stored heat pump system', *Solar Energy*, 51(2), pp. 147–158.

Kaygusuz, K., Gültekin, N. and Ayhan, T. (1993) 'Solar-assisted heat pump and energy storage for domestic heating in Turkey', *Energy Conversion and Management*, 34(5), pp. 335–346. doi: 10.1016/0196-8904(93)90085-O.

Kenisarin, M. and Mahkamov, K. (2007) 'Solar energy storage using phase change materials', *Renewable and Sustainable Energy Reviews*, 11(9), pp. 1913–1965. doi: 10.1016/j.rser.2006.05.005.

Kipp & Zonen (2015) *SP Lite2 Silicon Pyranometer*.

Klein, S. A. *et al.* (2014) 'Mathematical reference Transient system simulation program', *Trnsys 17*, p. 474.

Klein, S. and Alvarado, F. (2016) 'Engineering equation solver', *F-Chart Software, Box*, pp. 1–363. Available at: [https://ceprofs.civil.tamu.edu/llovery/ees/ees\\_manual.pdf](https://ceprofs.civil.tamu.edu/llovery/ees/ees_manual.pdf).

Kong, X. Q. *et al.* (2011) 'Thermal performance analysis of a direct-expansion solar-assisted heat pump water heater', *Energy*, 36(12), pp. 6830–6838. doi: 10.1016/j.energy.2011.10.013.

Lane, G. . (1983) *Latent Heat Materials - Volume 1*. 1st edn. CRC Press.

Lior, N. (1977) 'Solar energy and the steam Rankine cycle for driving and assisting heat pumps in heating and cooling modes', *Energy Conversion*. Pergamon, 16(3), pp. 111–123. doi: 10.1016/0013-7480(77)90035-3.

Liu, Z., Sun, X. and Ma, C. (2005) 'Experimental investigations on the characteristics of melting processes of stearic acid in an annulus and its thermal conductivity enhancement by fins', *Energy Conversion and Management*, 46(6), pp. 959–969. doi:

- 10.1016/j.enconman.2004.05.012.
- Lomet, A., Suard, F. and Chèze, D. (2015) ‘Statistical modelling for real domestic hot water consumption forecasting’, *Energy Procedia*. Elsevier, 70, pp. 379–387. doi: 10.1016/j.egypro.2015.02.138.
- MacArthur, J. W. W., Palm, W. J. J. and Lessmann, R. C. C. (1978) ‘Performance analysis and cost optimization of a solar-assisted heat pump system’, *Solar Energy*. Pergamon, 21(1), pp. 1–9. doi: 10.1016/0038-092X(78)90110-X.
- Medrano, M. *et al.* (2009) ‘Experimental evaluation of commercial heat exchangers for use as PCM thermal storage systems’, *Applied Energy*, 86(10), pp. 2047–2055. doi: 10.1016/j.apenergy.2009.01.014.
- Meyer, J. P. and Tshimankinda, M. (1998) ‘Domestic hot water consumption in south african townhouses’, *Pergamon Energy Convers. Mgmt*, 39(7), pp. 679–684.
- Meyerl, J. P. (2000) ‘A review of domestic hot-water consumption in South Africa’, *R &D*, 16(3), pp. 55–61.
- Morgan, R. G. G. (1982) ‘Solar assisted heat pump’, *Solar Energy*. Pergamon, 28(2), pp. 129–135. doi: 10.1016/0038-092X(82)90291-2.
- Nhut, L. M. and Park, Y. C. (2013) ‘A study on automatic optimal operation of a pump for solar domestic hot water system’, *Solar Energy*, 98, pp. 448–457. doi: 10.1016/j.solener.2013.08.040.
- Nilufer Egrican, A. (1991) ‘Performance of a solar assisted heat pump system’, *Energy Conversion and Management*, 31(1), pp. 17–25.
- Omojaro, P. and Breitkopf, C. (2013) ‘Direct expansion solar assisted heat pumps: A review of applications and recent research’, *Renewable and Sustainable Energy Reviews*, 22, pp. 33–45. doi: 10.1016/j.rser.2013.01.029.
- Panaras, G., Mathioulakis, E. and Belessiotis, V. (2014) ‘A method for the dynamic testing and evaluation of the performance of combined solar thermal heat pump hot water systems’, *Applied Energy*, 114, pp. 124–134. doi: 10.1016/j.apenergy.2013.09.039.
- Parker, D. S., Fairey, P. W. and Lutz, J. D. (2015) ‘Estimating daily domestic hot-water use in North American homes’, in *2015 ASHRAE Conference*.

- Qu, S. *et al.* (2015) ‘System design and energy performance of a solar heat pump heating system with dual-tank latent heat storage’, *Energy and Buildings*, 105, pp. 294–301. doi: 10.1016/j.enbuild.2015.07.040.
- Rathod, M. K. and Banerjee, J. (2011) ‘Numerical investigation on latent heat storage unit of different configurations’, *International Journal of Mechanical, Aerospace, Industrial, Mechatronic and Manufacturing Engineering*, 5(3), pp. 652–557.
- Şevik, S. *et al.* (2013) ‘Mushroom drying with solar assisted heat pump system’, *Energy Conversion and Management*, 72, pp. 171–178.
- Shirazi, A. *et al.* (2016) ‘Solar-assisted absorption air-conditioning systems in buildings: Control strategies and operational modes’, *Applied Thermal Engineering*, 92, pp. 246–260. doi: 10.1016/j.applthermaleng.2015.09.081.
- Sontay (2012) *MW-S Screwed Water Meters Features : Specification : Part Codes :*
- Sporn, P. and Ambrose, E. R. (1955) ‘The heat pump and solar energy.’, in *Proceedings of the world symposium on applied solar energy*. Phoenix, Arizona, pp. 1–5.
- Sterling, S. J. and Collins, M. R. (2012) ‘Feasibility analysis of an indirect heat pump assisted solar domestic hot water system’, *Applied Energy*, 93, pp. 11–17. doi: 10.1016/j.apenergy.2011.05.050.
- Tassou, S. A. (2010) ‘Energy conversion technologies’, *Building Services Engineering MSc Programme*. London: Brunel University.
- Telkes, M. (1947) ‘Solar house heating, a problem of heat storage’, *Heating and Ventilating*, (44), pp. 68–75.
- The CCC (2016) ‘Annex 2. Heat in UK buildings today’, *The Committee on Climate Change*. Available at: <https://www.theccc.org.uk/wp-content/uploads/2017/01/Annex-2-Heat-in-UK-Buildings-Today-Committee-on-Climate-Change-October-2016.pdf>.
- Tian, Y. and Zhao, C. Y. (2011) ‘A numerical investigation of heat transfer in phase change materials (PCMs) embedded in porous metals’, *Energy*, 36, pp. 5539–5546. doi: 10.1016/j.energy.2011.07.019.
- Tyagi, V. V. and Buddhi, D. (2007) ‘PCM thermal storage in buildings: A state of

- art', *Renewable and Sustainable Energy Reviews*, 11(6), pp. 1146–1166. doi: 10.1016/j.rser.2005.10.002.
- Wang, Q. *et al.* (2011) 'Development and experimental validation of a novel indirect-expansion solar-assisted multifunctional heat pump', *Energy and Buildings*, 43(2–3), pp. 300–304. doi: 10.1016/j.enbuild.2010.09.013.
- Wang, S. K. (2000) *Handbook of air conditioning and refrigeration*. second Edi. McGraw-Hill.
- Waters, L., Wilkes, E. and Goodright, V. (2015) *Energy Consumption in the UK: Chapter 1: Overall energy consumption in the UK since 1970*, Department of Energy & Climate Change.
- Weiss, W. (2003) 'A Design handbook for solar combi-systems - IEA SHC task 26'. James & James Science Publishers, UK, p. 43.
- Yang, R. and Wang, L. (2012) 'Efficient control of a solar assisted ground-source heat pump system based on evaluation of building thermal load demand', in *North American Power Symposium (NAPS)*. Champaign, IL: IEEE. doi: 10.1109/NAPS.2012.6336400.
- Youssef, W., Ge, Y. T. and Tassou, S. A. (2017) 'Effects of latent heat storage and controls on stability and performance of a solar assisted heat pump system for domestic hot water production', *Solar Energy*, 150, pp. 394–407. doi: 10.1016/j.solener.2017.04.065.
- Zalba, B. *et al.* (2003) 'Review on thermal energy storage with phase change : materials , heat transfer analysis and applications', *Applied Thermal Engineering*, 23, pp. 251–283. doi: 10.1016/S1359-4311(02)00192-8.
- Zhai, Z. J. and Chen, Q. Y. (2005) 'Performance of coupled building energy and CFD simulations', *Energy and Buildings*, 37(4), pp. 333–344. doi: 10.1016/j.enbuild.2004.07.001.
- Zhang, Z. *et al.* (2007) 'Evaluation of various turbulence models in predicting airflow and turbulence in enclosed environments by CFD: part 2—comparison with experimental data from literature', *HVAC&R RESEARCH*, 13(6).
- Zhou, T. *et al.* (2017) 'Dynamic measurement of the thermal conductivity of phase



change materials in the liquid phase near the melting point', *International Journal of Heat and Mass Transfer*, 111, pp. 631–641. doi: 10.1016/j.ijheatmasstransfer.2017.04.020.

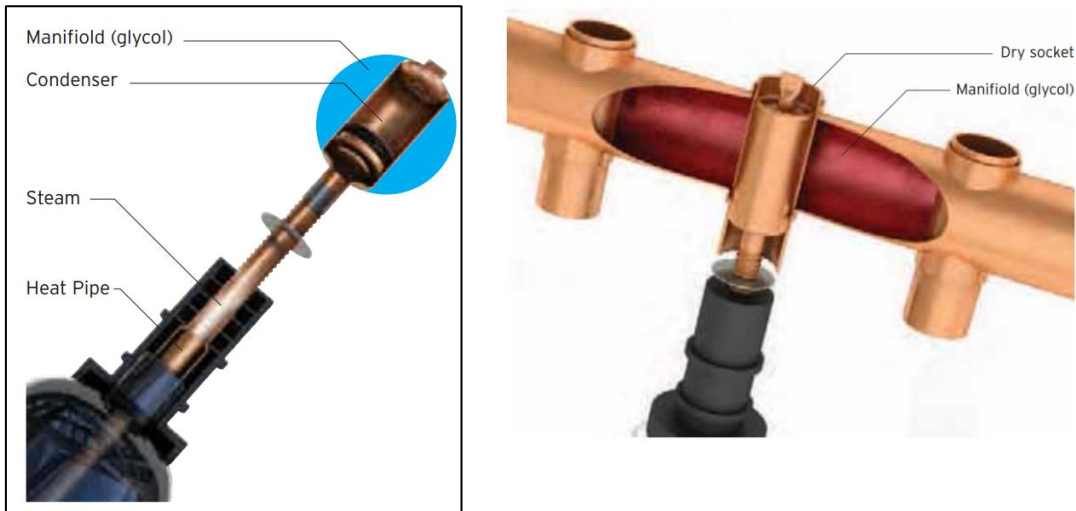
---

*Appendices*

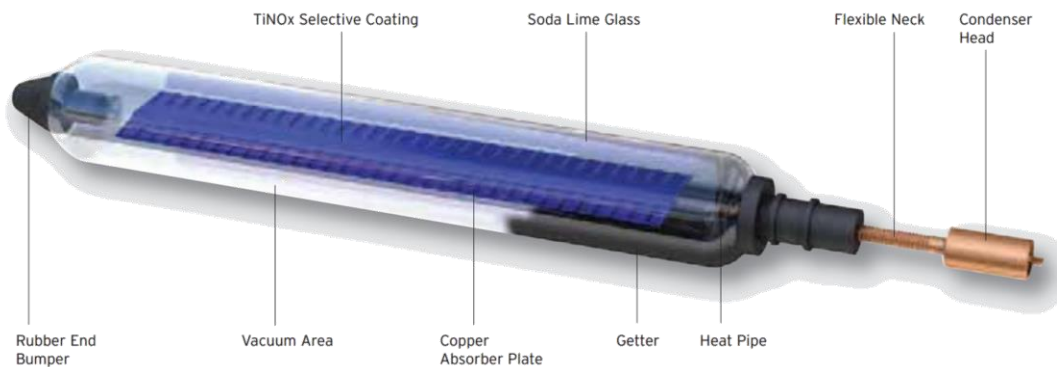
---

**Appendix A**

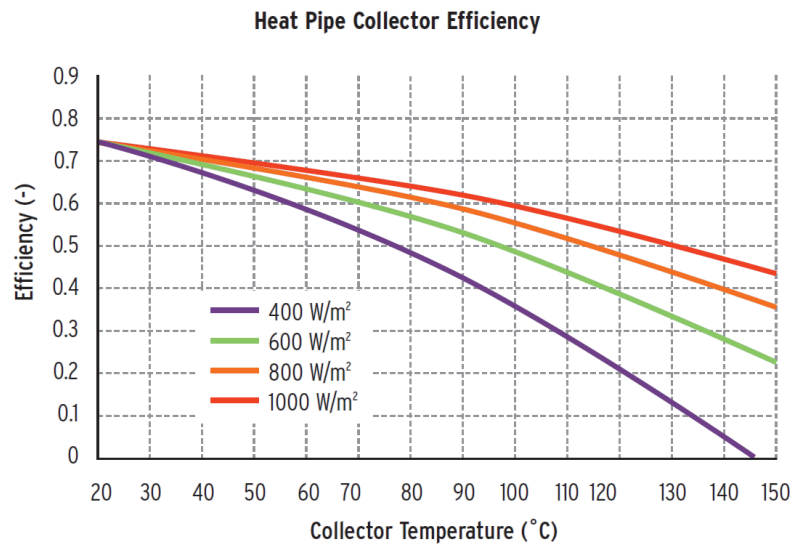
**Solar Collector**



*App-Fig 1. Evacuated tube collector heat pipe and manifold*



*App-Fig 2. Heat pipe details of single evacuated tube*

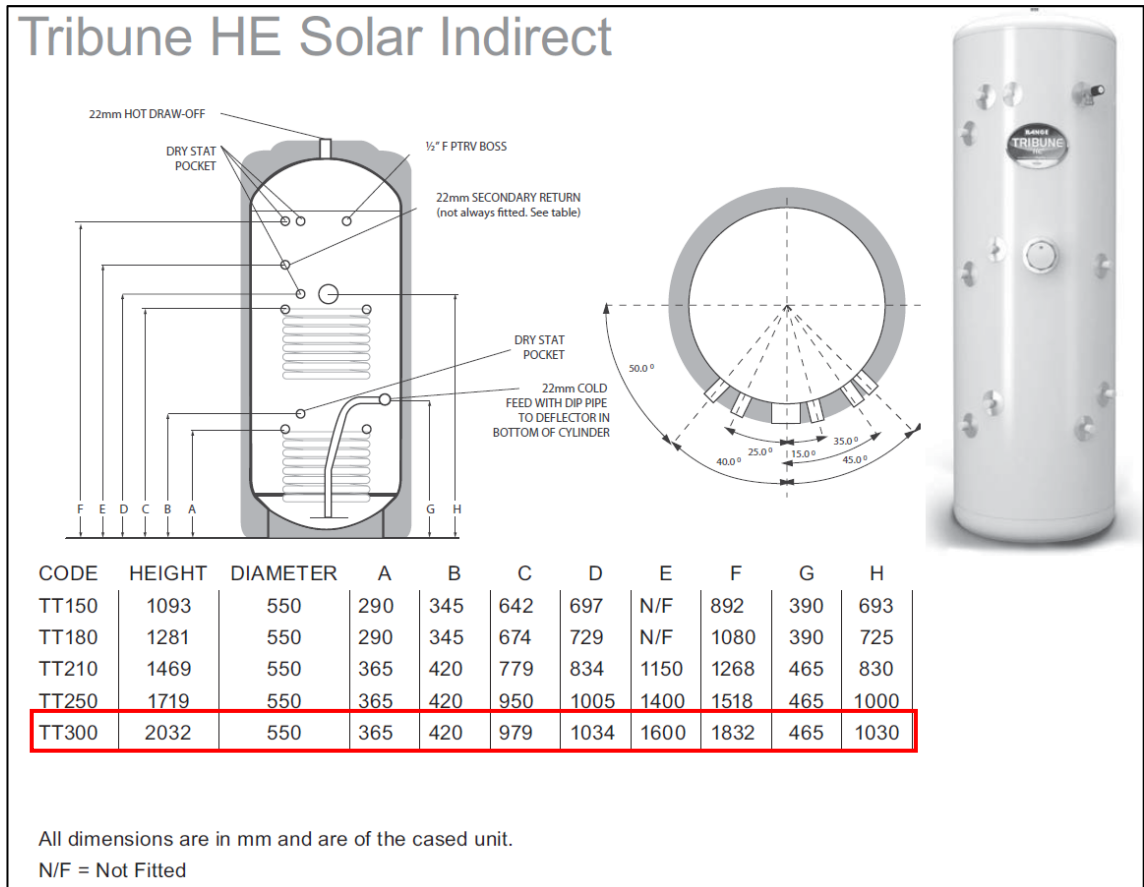


*App-Fig 3. Heat pipe collector efficiency by the manufacture*

*App-Tab 1. The proposed solar collector specifications (marked in red)*

<b>HP400 / HP450</b>	<b>2m<sup>2</sup></b>	<b>3m<sup>2</sup></b>
Number of tubes	20	30
<b>Dimensions</b>		
Absorber Area (m <sup>2</sup> )	2.01	3.021
Overall Dimensions (mm)	1952 x 1418 x 93	1952 x 2127 x 93
Width of Manifold (mm)	1418	2127
Length (tube and manifold) (mm)	1952	1952
Depth (mm)	93	93
Aperture Area (m <sup>2</sup> )	2.16	3.23
Fluid Volume (ltr)	1.2	1.7
Inlet and Outlet Dimensions (mm)	22	22
Weight (empty) (kg)	48	71
<b>Mounting</b>		
Recommended Inclination (°)	20-70	20-70
<b>Performance Data</b>		
Efficiency	Based on Aperture	Based on Aperture
Eta 0	0.75	0.75
a1 (W/m <sup>2</sup> K)	1.18	1.18
a2 (W/m <sup>2</sup> K <sup>2</sup> )	0.0095	0.0095
Solar Keymark Licence Numbers	HP400: 011-751793	
<b>Operating Data</b>		
<b>Flow Rate (ltr/h)</b>		
Rated	160	240
Minimum	120	180
Maximum	300	480
Maximum Operating Pressure	10 Bar	10 Bar
Stagnation Temperature (°C)	166	166
Heat Transfer Fluid	Water / Glycol	Water / Glycol
<b>Materials</b>		
Absorber	Copper	Copper
Coating	Selective Coating	Selective Coating
Absorbance (%)	95	95
Emissivity (5)	5	5
Mounting Frame and Clips	Stainless Steel, Aluminium, EPDM	Stainless Steel, Aluminium, EPDM
Glass	Low Iron - Transm. 0.92	Low Iron - Transm. 0.92
Vacuum	<10 <sup>-6</sup> mbar	<10 <sup>-6</sup> mbar
Temperature Limitation (°C)	90 / 135	90 / 135
Quality Certification / Solar Keymark	Yes	Yes

**Water storage tank (WST)**



*App-Fig 4. WST dimensions (in mm) and configuration*

**Water-glycol Specifications**

*App-Tab 2 the water-glycol properties used in the source load, heat sink loop and direct solar loop*

<b>Hydratech Product name</b>	<b>ThermaFlow DTX</b>	
	<b>(Non-Toxic, High Performance)</b>	
	-15°C requires 28% v/v -20°C requires 33% v/v	
<b>Density <math>\rho(\alpha,T)</math></b>	<b>28% (-15°C)</b>	
	<b>kg/m<sup>3</sup></b>	<b>Temp Deg C</b>
	1010	80
	1023	60
	1033	40
	1041	20
	1045	10
	1048	0
	1050	-10
	1050	-15
	<b>33% (-20°C)</b>	
	<b>kg/m<sup>3</sup></b>	<b>Temp Deg C</b>
	1018	80
	1031	60
	1042	40
1052	20	
1055	10	
1058	0	
1060	-10	
1061	-20	
<b>Specific Heat (cp)</b>	<b>28% (-15°C)</b>	
	<b>kJ/kg•K</b>	<b>Temp Deg C</b>
	3.91	80
	3.87	60
	3.83	40
	3.79	20
	3.78	10
	3.77	0
	3.76	-10
	3.76	-15
	<b>33% (-20°C)</b>	

	<b>kJ/kg•K</b>	<b>Temp Deg C</b>
	3.83	80
	3.78	60
	3.74	40
	3.70	20
	3.69	10
	3.67	0
	3.65	-10
	3.64	-20
<b>Kinematic Viscosity <math>\nu(\alpha,T)</math></b>		
	<b>28% (-15°C)</b>	
	<b>mm<sup>2</sup>/sec</b>	<b>Temp Deg C</b>
	0.66	80
	0.90	60
	1.34	40
	2.29	20
	3.17	10
	4.64	0
	7.27	-10
	9.69	-15
	<b>33% (-20°C)</b>	
	<b>mm<sup>2</sup>/sec</b>	<b>Temp Deg C</b>
	0.75	80
	1.04	60
	1.58	40
	2.75	20
	3.86	10
	5.72	0
	9.16	-10
	16.10	-20
<b>Thermal Conductivity (TC)</b>		
	<b>28% (-15°C)</b>	
	<b>W/m•K</b>	<b>Temp Deg C</b>
	0.508	80
	0.498	60
	0.488	40
	0.479	20
	0.475	10
	0.472	0
	0.467	-10
	0.464	-15
	<b>33% (-20°C)</b>	
	<b>W/m•K</b>	<b>Temp Deg C</b>
	0.480	80


## Appendices

---

	0.474	60
	0.468	40
	0.462	20
	0.459	10
	0.456	0
	0.454	-10
	0.452	-20



**Heat Pump Refurbishment order**



HRP Limited  
159 Edinburgh Ave  
Slough  
Berks, SL1 4UE  
T: 01753 495710  
F: 01753 495711  
VAT Reg No. GB 571

**PRO-FORMA INVOICE**

Company: Brunel University  
Contact: [Valid](#)

Your Reference: RA 46439  
Our Ref No: RA 46439


Date: 26.11.15

HRP Code	Description	Qty	Price (Each)	Total Price
470613	8540586 Capacitor 40MFD/370V	1	£33.54	£33.54
300019	06823346 TN2 R134A INT TEV Valve	1	£34.56	£34.56
300037	068-2007 Orifice 04 (T2 FL ON)	1	£12.68	£12.68
				£0.00
				£0.00
				£0.00
				£0.00
				£0.00
				£0.00
				£0.00
				£0.00
				£0.00
				£0.00
				£0.00
				£0.00

**Quotation Total Nett (excl. VAT):- £80.78**  
**VAT @ 20%:- £16.16**  
**Total:- £96.94**

*App-Fig 5. a quote of the required components to refurbishment the heat pump*

Initial quotations for the AWHX



**HC Coils Ltd**  
 Suite 175, Fareham Reach Business Park  
 Fareham Road, Gosport, Hants, PO13 0FW  
 Tel: +44 (0) 2392 501431 Fax: +44 (0) 2392 529272  
 Email: [sales@hccoils.com](mailto:sales@hccoils.com) Web: [www.hccoils.com](http://www.hccoils.com)

Date: 11 May 2015  
 Our Ref: APH/15/1013(0)/ 1.3.63 - Data 8 Expiry 30/06/2015  
 Your Ref:  
 Item: 1

**COOLER - GLYCOL REFRIGERANT: CM-20504, NC = 2**

<b>Duty(Wet):</b>	<b>5.00</b>	<b>kW</b>	<b>Medium:</b>	<b>EthGly 10%</b>
<b>Air Inlet Temp.:</b>	<b>5.6</b>	<b>°C</b>	<b>Medium On:</b>	<b>-3.0 °C</b>
Altitude:	0.0	m	<b>Medium Off:</b>	<b>3.0 °C</b>
Air Volume:	0.95	m <sup>3</sup> /s	Medium Flow Rate:	0.2 l/sec
E.S.P.:	0	Pa	Medium P.D.:	16.6 kPa
Air Throw:(Note 1)	11	m	<b>Noise level: (Note 2)</b>	<b>51 dB(A) @10 m</b>
No of Fans:	1		Defrost:	None
Supply:	240/1/50		Fan Power:	0.40 kW
Fan Diameter:	450	mm	Full Load Current:	1.80 A
Fan Speed:	1350	rpm		

**O/A Dimensions: 597H x 1272W x 515L mm**

Casing:	WP - White Powder Coated Galvanised Sheet Steel Casing			
Total Surface:	46	m <sup>2</sup>	Fins:	Aluminium
Internal Volume:	11	litres	FinPitch:	4.0 mm
Dry Weight:	58	kg	Tubes:	5/8" Copper
Max Work. Pressure:	6	barG	Test Pressure:	17 barG
Inlet + Outlet Conn.:	1xDN 20(28mm'Y'+4mm Cap)			
Connection Type:	PN16 Bimetal Flanges			

**No Off: 1**  
 Price: £ 990.00 each

**Total Price: £ 990.00Net + VAT, Delivered UK on scheduled transport**  
**Delivery: 6-7 weeks from approval of drawings**

Note 1: Air Throw is dependent on coldstore design, product loading and positioning of coolers.

Note 2: Noise levels are based on free field conditions without reflections. The noise levels are intended to be used as a guide. In practice the noise generated will be reflected within the room which may result in higher measured noise levels.

App-Fig 6. App-Fig 5. a quote of another AWHX



To: Brunel University Date: 27 / 05 / 2015  
Attn: Walid Youssef  
Your Ref: Air Cooler – 10kW  
From: Peter Hartley

No of Pages: 3

---

UK Exchangers Quotation Ref: P1505502

We thank you for your above referenced enquiry and in response we are pleased to forward the following quotation to supply an extended surface finned tube heat exchanger as requested.

Copper tubed, aluminium finned, fan cooled, extended surface tube matrix.  
Steel galvanised case work  
1 x axial fan with Single-phase electric IP65 motor, 6 poles, 240v/1ph/50 Hz  
Impeller in painted aluminium  
Protection, grill supporting motor, in steel painted with black epoxy powders  
Square mounting panel in steel - painted with black epoxy powders  
Blowing version: airflow from motor to impeller – horizontal

Model: FC-07  
Quantity: 1 off  
Price each: £1,070.00 – packed in crate, ex-works, excluding VAT  
Carriage: £60.00 – delivery withing England, excluding VAT  
Delivery: Please allow 2 working weeks  
Terms: 100% Payment prior to despatch  
Account holders – Net 30 days  
Validity 30 days

This quotation is based on our standard Terms and Conditions of Sale, a copy of which is available on request.

We trust that our offer is of interest. Should you require any further information, please do not hesitate to contact the undersigned.


Regards,

Peter Hartley  
[ph@ukeltd.com](mailto:ph@ukeltd.com)

---

Unit 55, Stilebrook Road, Olney, Buckinghamshire MK46 5EA  
Tel: (01234) 244320 Fax: (01234) 714978 e-mail: [sales@ukeltd.com](mailto:sales@ukeltd.com)

*App-Fig 7. Initial quote of the purchased AWHX (page 1)*

Heat Exchanger Matrix type	:	62AA 14T/4R/840L/P3/N4
Tube / fin material	:	Copper / Aluminium
Tube wall / fin thickness	:	0.35 mm wall / 0.12 mm thk.
Header material	:	<b>Copper with brass connections</b>
Frame material	:	Steel - galvanised
Frame construction	:	Channel & tray formed
Fin pitch (spacing)	:	3 mm
Tubes per row x no. of rows	:	14 x 4
Heat transfer area	m <sup>2</sup> :	51.7
Service connection size	:	1.0 inch.
Connection type fitted	:	BSPT male threaded (BS21)
Coil weight empty / volume	:	41.0 kgs / 11.8 litres
Heat Transfer Duty	kW :	10.00
Number of fans	:	1
Fan designation	:	560D - 6 pole
Motor supply required	:	240v / 1ph / 50 hz
Motor protection	:	IP65, class F insulation
Fan material	:	Aluminium
Motor side guard	:	Steel - Epoxy powder coated
Motor power	Watts :	456 (1.9 amps)
Air flow direction	:	Horizontal, across motor first
Air flowrate	m <sup>3</sup> /s :	1.6
Design inlet temp.	Deg C :	12
Tube side fluid description	:	Water with 15% Glycol
Tube side flowrate	l/s :	0.5
Tube side inlet temp.	deg C :	-1.0
Tube side outlet temp.	deg C :	4.0
Tube velocity	m/sec :	0.64
Tube side pressure drop	kPa :	11
<b>Dimensions using the attached sketch:</b>		
Length:		1005 mm
Height:		900 mm
Depth:		500 mm
 <p><b>UK EXCHANGERS LTD</b> the heat transfer specialists</p>		

App-Fig 8. Initial quote of the purchased AWHX (page 2)

Appendix B

NTC Thermistor tolerance

## NTC Thermistors General Characteristics



### 2.1.5. Further approximation of R (T) curve

The description of the characteristic R (T) can be improved by using a greater number of experimental points, and by using the equation:

$$\frac{1}{T} = A + B (\ln R) + C (\ln R)^2$$

The parameters A, B and C are determined by solving the set of equations obtained by using the measured resistances at three temperatures.

The solution of the above equation gives the resistance at any temperature:

$$\ln R (T) = \frac{1}{3} \left[ \sqrt[3]{\frac{27}{2} \left( \frac{A-1/T}{C} \right) + \frac{3}{2} \sqrt{3 \left( \sqrt{27 \left( \frac{A-1/T}{C} \right)^2 + 4 \left( \frac{B}{C} \right)^3} \right)}} \right. \\ \left. - \sqrt[3]{\frac{27}{2} \left( \frac{A-1/T}{C} \right) + \frac{3}{2} \sqrt{3 \left( \sqrt{27 \left( \frac{A-1/T}{C} \right)^2 + 4 \left( \frac{B}{C} \right)^3} \right)}} \right]$$

The precision of this description is typically 0.2°C for the range -50 to +150°C (A, B, C being determined with experimental values at -20, +50 and 120°C) or even better if this temperature range is reduced. The ratios R(T)/R(25°C) for each of the different materials shown on pages 29 to 33 have been calculated using the above method.

### 2.1.6. Resistance tolerance and temperature precision

An important characteristic of a thermistor is the tolerance on the resistance value at a given temperature.

This uncertainty on the resistance (ΔR/R) may be related to the corresponding uncertainty on the temperature (ΔT), using the relationship:

$$\Delta T = 100 \cdot \frac{\Delta R}{R} \cdot \frac{1}{\alpha}$$

Example: consider the thermistor ND06M00152J –

- R (25°C) = 1500 ohms
- Made from M material
- R (T) characteristic shown on page 23 gives: α = - 4.4%/°C at 25°C
- Tolerance ΔR/R = ±5% is equivalent to: ΔT = 5%/4.4%/°C = ±1.14°C

### 2.1.7. Resistance tolerance at any temperature

Any material used for NTC manufacturing always displays a dispersion for the R (T) characteristic.

This dispersion depends on the type of material used and has been especially reduced for our accuracy series thermistors.

Thus, the tolerance on the resistance (ΔR<sub>2</sub>/R<sub>2</sub>) at a temperature T<sub>2</sub> is the sum of two contributions as illustrated on Figure 1:

- the tolerance ΔR<sub>1</sub>/R<sub>1</sub> at a temperature T<sub>1</sub> used as a reference.
- an additional contribution due to the dispersion on the characteristic R (T) which may be called "Manufacturing tolerance" (Tf).

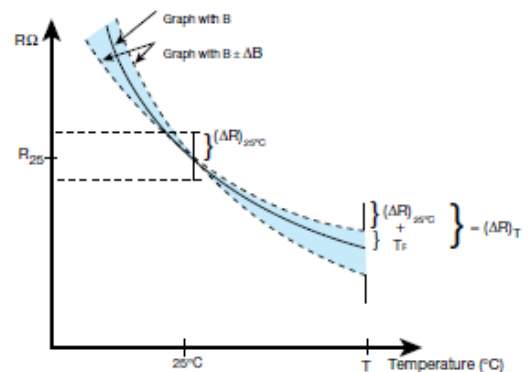


Figure 1

Differentiating the equation R = A exp (B/T), the two contributions on the tolerance at T can also be written:

$$\frac{\Delta R_2}{R_2} = \frac{\Delta R_1}{R_1} + \frac{1}{T_1} - \frac{1}{T_2} \cdot \Delta B$$

The T(f) values given with the resistance – temperature characteristics on pages 29 to 33 are based on a computer simulation using this equation and experimental values.

### 2.1.8. Designing the resistance tolerances

Using the fact that the coefficient α decreases with temperature (α = -B/T<sup>2</sup>), it is generally useful to define the closest tolerance of the thermistor at the maximum value of the temperature range where an accuracy in °C is required.

For example, let us compare the two designs 1 and 2 hereafter:

T (°C)	R (Ω)	α (%/°C)	Design 1		Design 2	
			ΔR/R(%)	ΔT(°C)	ΔR/R(%)	ΔT(°C)
0	3275	-5.2	3.5	0.7	5.0	1.0
25	1000	-4.4	3.0	0.7	4.5	1.1
55	300	-3.7	3.5	1.0	4.0	1.1
85	109	-3.1	4.1	1.3	3.4	1.1
100	69.4	-2.9	4.5	1.6	3.0	1.0

Only the Design 2 is able to meet the requirement T = 1°C from 25°C to 100°C.

App-Fig 9. NTC Thermistor tolerance

**Pressure Transmitter Specifications**

*App-Tab 3. Pressure Transmitter Specifications*

**Pressure transmitter, AKS 32 and AKS 33**



*Performance*

Accuracy (incl. non-linearity, hysteresis and repeatability)	± 0.3% FS (typ.) / ± 0.8% FS (max.)
Non-linearity BFSL (conformity)	< ± 0.2% FS
Hysteresis and repeatability	≤ ± 0.1% FS
Thermal zero point shift	≤ ± 0.1% FS / 10K (typ.)
	≤ ± 0.2% FS / 10K (max.)
Thermal sensitivity (span) shift	≤ ± 0.1% FS / 10K (typ.)
	≤ ± 0.2% FS / 10K (max.)
Response time	< 4 ms
Max. working pressure	See ordering table
Burst pressure	min. 300 bar

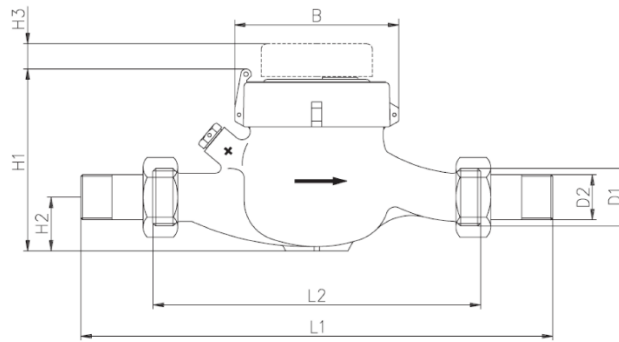
*Electrical specifications for AKS 32, 0 – 10 V DC output signal*

Rated output signal (short-circuit protected)	0 – 10 V DC
Supply voltage [U <sub>s</sub> ], polarity protected	15 – 30 V DC
Supply current consumption	< 8 mA
Supply voltage dependency	< 0.05% FS / 10 V
Output impedance	< 25 Ω
Load resistance, R <sub>L</sub>	R <sub>L</sub> ≥ 15 kΩ

*App-Tab 4. pressure transmitter operation range*

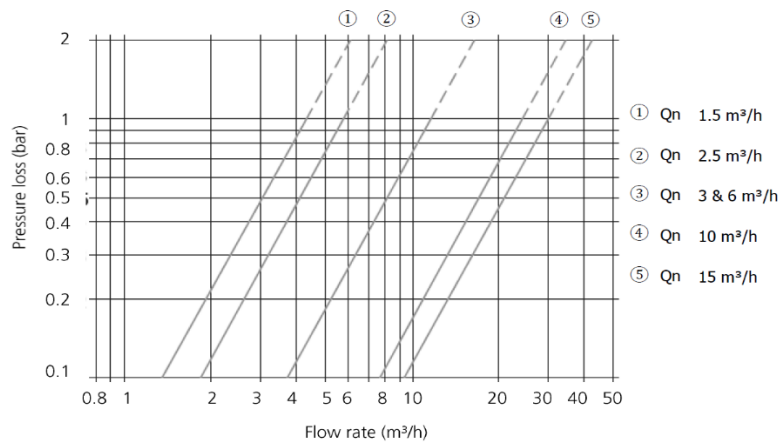
Operating range [bar]		Max. working pressure PB [bar]	Compensated temperature range [°C]
LP	-1 – 5	33	-30 – 40
	-1 – 9	33	-30 – 40
HP	-1 – 24	40	0 – 80
	-1 – 39	60	0 – 80

**Flow Meter details**

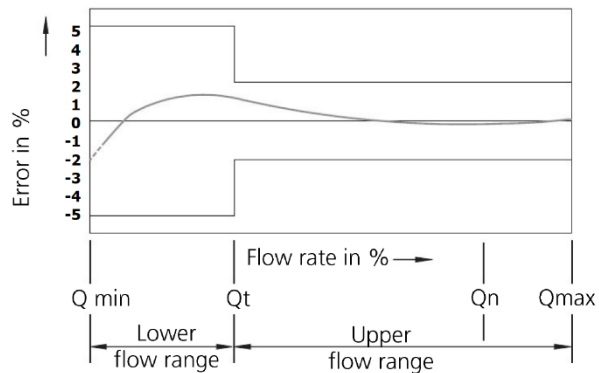


	MW-xS-15	MW-xS-20	MW-xS-25	MW-xS-32	MW-xS-40	MW-CS-50
L1	255	288	378	378	438	438
L2	170	190	260	260	300	300
D1 (")	¾	1	1 ½	1 ½	2	2 ½
D2 (")	½	¾	1 ¼	1 ¼	1 ½	2"
H1	120	115	140	140	170	190
H2	45	32	50	50	60	75
H3	15	15	15	15	15	15
B	95	95	100	100	131	165
Weight (kg)	1.7	1.8	2.7	2.7	5.4	5.4

App-Fig 10. Flow meter dimension



App-Fig 11. Flow meter pressure loss (bar)



App-Fig 12. Flow meter error margin

*Pyranometer (solar irradiance meter)*

*App-Tab 5. Sensitivity of the Pyranometer*

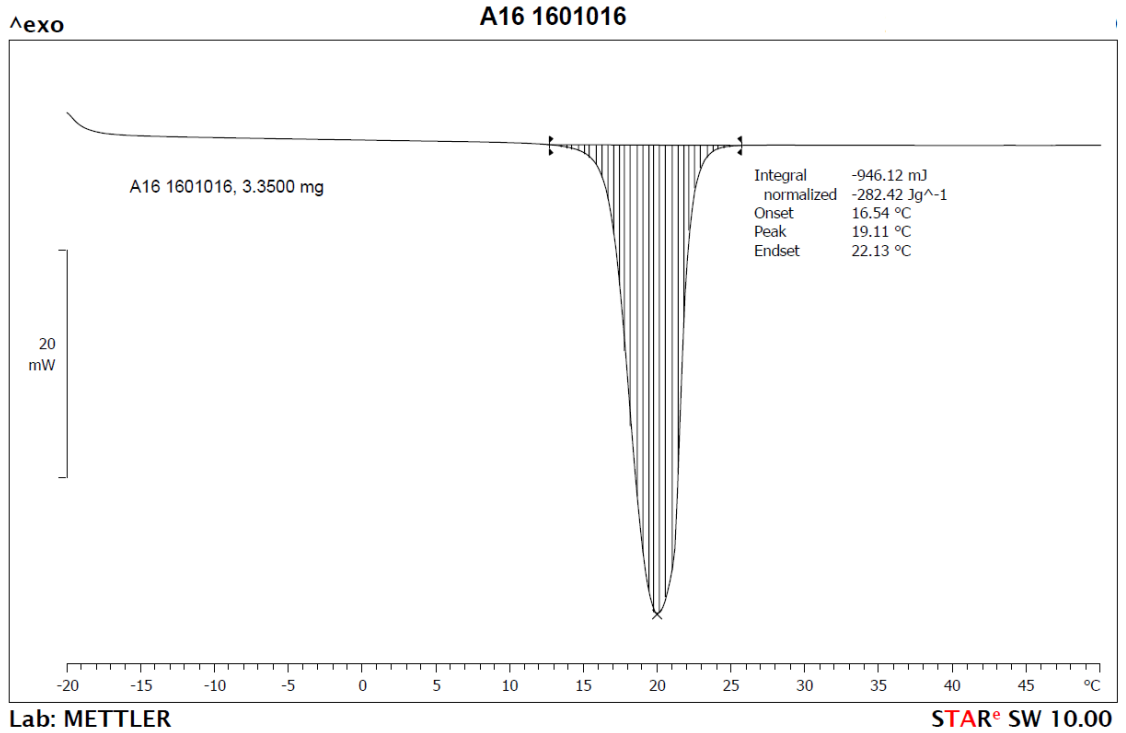


Sensor	Full scale	Sensitivity
CMP 3	2000 W/m <sup>2</sup>	5 .. 20 μV / W/m <sup>2</sup>
CMP 6	2000 W/m <sup>2</sup>	5 .. 16 μV / W/m <sup>2</sup>
CMP 11	4000 W/m <sup>2</sup>	7 .. 14 μV / W/m <sup>2</sup>
CMP 21	4000 W/m <sup>2</sup>	7 .. 14 μV / W/m <sup>2</sup>
CMP 22	4000 W/m <sup>2</sup>	7 .. 14 μV / W/m <sup>2</sup>
CM 4	4000 W/m <sup>2</sup>	7 μV / W/m <sup>2</sup>
SP Lite	2000 W/m <sup>2</sup>	60 .. 100 μV / W/m <sup>2</sup>
SP Lite *	4000 W/m <sup>2</sup>	9.5 .. 10.5 μV / W/m <sup>2</sup>
PAR Lite	10,000 μmol/m <sup>2</sup> s	4 .. 6 μV / μE/m <sup>2</sup> s
NR Lite	±500 W/m <sup>2</sup>	10 μV / W/m <sup>2</sup>
CUV 4	200 W/m <sup>2</sup>	1 mV / W/m <sup>2</sup>

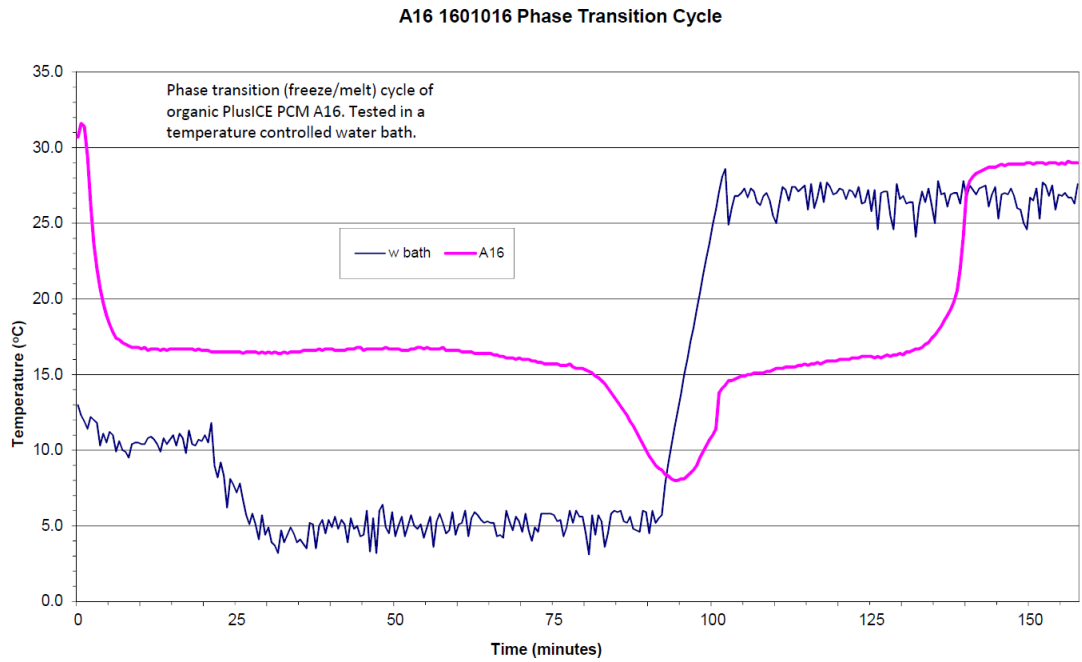


**Appendix C**

**PCM A16 specifications**



*App-Fig 13. PCM A16 temporal variation during melting/solidification cycle*



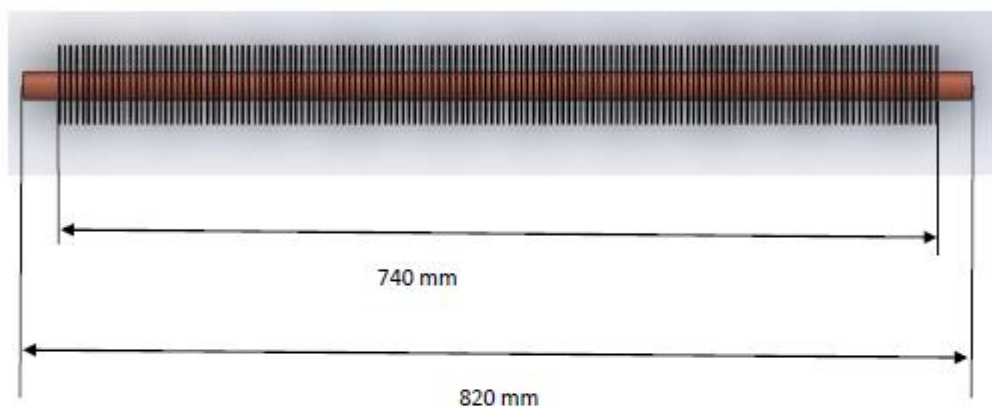
*App-Fig 14. PCM A16 phase change cycle*

PCM		PlusICE PCM (ORGANIC) (A) RANGE											2013-1	
PCM Type	Phase Change Temperature		Density		Latent Heat Capacity		Volumetric Heat Capacity		Specific Heat Capacity		Thermal Conductivity		Max Operating	Max Operating
	(°C)	(°F)	(kg/m <sup>3</sup> )	(lb / ft <sup>3</sup> )	(kJ/kg)	(Btu / lb)	(MJ/m <sup>3</sup> )	(Btu / ft <sup>3</sup> )	(kJ/kg K)	(Btu / lb*°F)	(W/m K)	(Btu / ft <sup>2</sup> h°F)	Temp (°C)	Temp (°F)
<b>ORGANIC PCM SOLUTIONS</b>														
A164*	164	327	1,500	93.8	230	125	435	11,875	2.42	0.573	nd	n/d	280	536
A155	155	311	900	56.2	100	43	90	2,418	2.2	0.521	0.230	0.133	250	482
A144	144	291	880	54.9	115	49	101	2,718	2.2	0.521	0.230	0.133	250	482
A133	133	271	880	54.9	126	54	111	2,978	2.2	0.521	0.230	0.133	250	482
A116**	118	244	1,450	90.5	340	148	493	13,232	2.7	0.640	nd	nd	300	572
A95	95	203	900	56.2	205	88	185	4,852	2.2	0.521	0.220	0.127	300	572
A82	82	180	850	53.1	155	67	132	3,536	2.21	0.524	0.220	0.127	300	572
A70	70	158	890	55.6	173	74	154	4,133	2.2	0.521	0.230	0.133	300	572
A62	62	144	910	56.8	145	62	132	3,542	2.2	0.521	0.220	0.127	300	572
A60H	60	140	800	49.9	212	91	170	4,552	2.15	0.509	0.180	0.104	400	752
A60	60	140	910	56.8	145	62	132	3,542	2.22	0.528	0.220	0.127	300	572
A58H	58	136	820	51.2	243	105	199	5,348	2.85	0.875	0.180	0.104	300	572
A58	58	136	910	56.8	132	57	120	3,224	2.22	0.528	0.220	0.127	300	572
A55	55	131	905	56.5	135	58	122	3,279	2.22	0.528	0.220	0.127	300	572
A53H	53	127	810	50.6	166	71	134	3,609	2.02	0.479	0.180	0.104	300	572
A53	53	127	910	56.8	130	58	118	3,175	2.22	0.528	0.220	0.127	300	572
A52	52	126	810	50.6	222	95	180	4,826	2.15	0.509	0.180	0.104	300	572
A50	50	122	810	50.6	218	94	177	4,739	2.15	0.509	0.180	0.104	300	572
A46	46	116	810	50.6	234	101	190	5,087	2.85	0.875	0.180	0.104	300	572
A46	46	115	910	56.8	155	67	141	3,788	2.22	0.528	0.220	0.127	300	572
A44	44	111	805	50.3	242	104	195	5,229	2.15	0.509	0.180	0.104	400	752
A43	43	109	780	48.7	165	71	129	3,454	2.37	0.581	0.180	0.104	300	572
A42	42	108	905	56.5	105	45	95	2,550	2.22	0.528	0.210	0.121	300	572
A40	40	104	810	50.6	230	99	186	5,000	2.43	0.578	0.180	0.104	300	572
A39	39	102	900	56.2	105	45	95	2,536	2.22	0.528	0.220	0.127	280	536
A37	37	99	810	50.6	235	101	190	5,109	2.85	0.875	0.180	0.104	300	572
A36	36	97	790	49.3	217	93	171	4,801	2.37	0.581	0.180	0.104	300	572
A32	32	90	845	52.8	130	58	110	2,848	2.20	0.521	0.210	0.121	300	572
A29	29	84	810	50.6	226	97	183	4,913	2.15	0.509	0.180	0.104	300	572
A28	28	82	789	49.3	155	67	122	3,282	2.22	0.528	0.210	0.121	280	536
A26	26	79	790	49.3	150	65	119	3,181	2.22	0.528	0.210	0.121	280	536
A25H	25	77	810	50.6	226	97	183	4,913	2.15	0.509	0.180	0.104	400	752
A25	25	77	785	49.0	150	65	118	3,180	2.26	0.535	0.180	0.104	280	536
A24	24	75	790	49.3	145	62	115	3,075	2.22	0.528	0.180	0.104	280	536
A23	23	73	785	49.0	145	62	114	3,055	2.22	0.528	0.180	0.104	280	536
A22H	22	72	820	51.2	216	93	177	4,754	2.85	0.875	0.180	0.104	400	752
A22	22	72	785	49.0	145	62	114	3,055	2.22	0.528	0.180	0.104	250	482
A17	17	63	785	49.0	160	65	118	3,180	2.33	0.538	0.180	0.104	250	482
A16	16	61	760	47.4	213	82	162	4,345	2.37	0.581	0.180	0.104	250	482
A15	15	59	790	49.3	190	58	103	2,758	2.26	0.535	0.180	0.104	250	482
A9	9	48	775	48.4	140	60	109	2,912	2.16	0.512	0.210	0.121	220	428
A8	8	46	773	48.3	150	65	116	3,112	2.16	0.512	0.210	0.121	220	428
A6	6	43	770	48.1	150	65	116	3,100	2.17	0.514	0.210	0.121	220	428
A4	4	39	766	47.8	200	89	153	4,112	2.18	0.518	0.210	0.121	220	428
A3	3	37	765	47.8	200	89	153	4,107	2.20	0.521	0.210	0.121	200	392
A2	2	36	765	47.8	200	89	172	4,818	2.20	0.521	0.210	0.121	200	392

PCM Products has a policy of continuous product and product data improvement and reserves the right to change design and specifications without notice

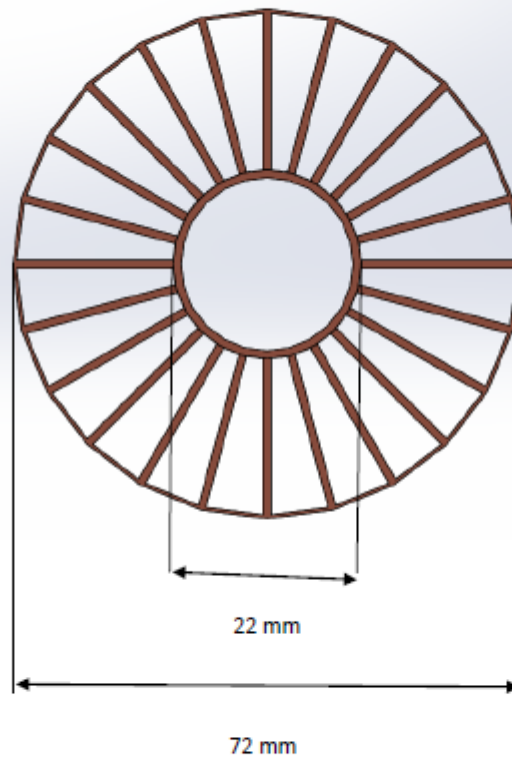
App-Fig 15. PCM A16 properties

## Spiral Tube Design



Brunel University London Kingston Lane, Uxbridge UB8 3PH UK  
Tel: 01895 267040, Fax: 01895 269777

*App-Fig 16. Copy of Heat transfer enhancement design report (page 1)*

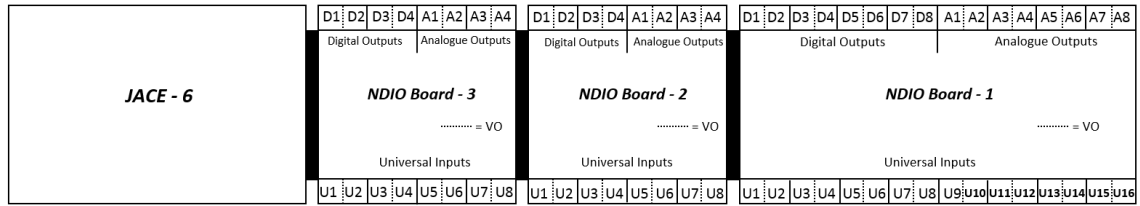


The dimensions of the requested tubes a following:

Spiral diameter	72 mm
Copper tube OD	22 mm
Spiral Length	740 mm
Total length of the tube	820 mm
Patch between spiral coils	4-6 mm (can be flexible)
No of wires in each spiral	24 - 30 ( can be flexible)
No of tubes	16 + 2 spare

**Appendix D**

**BMS control**



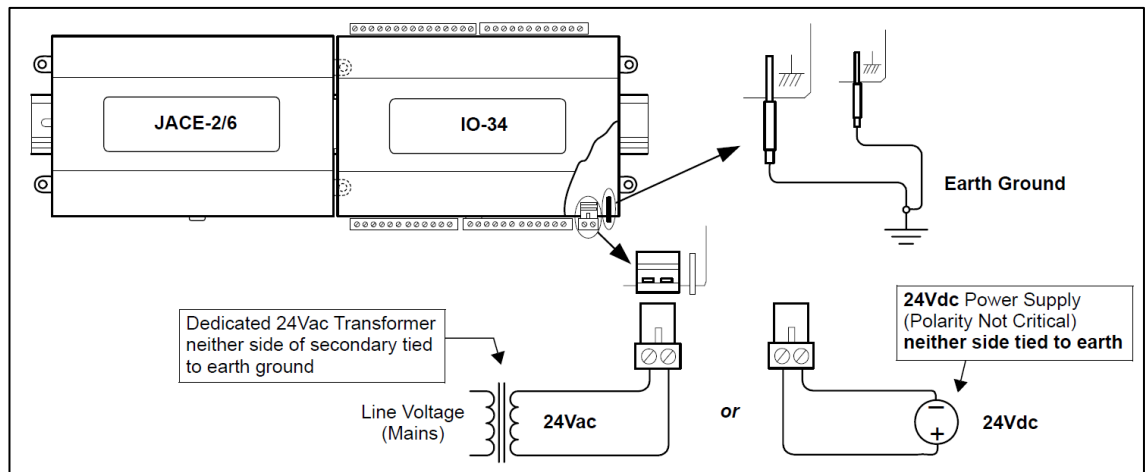
App-Fig 18. JACE-NDIO layout

App-Tab 6. Control box configuration

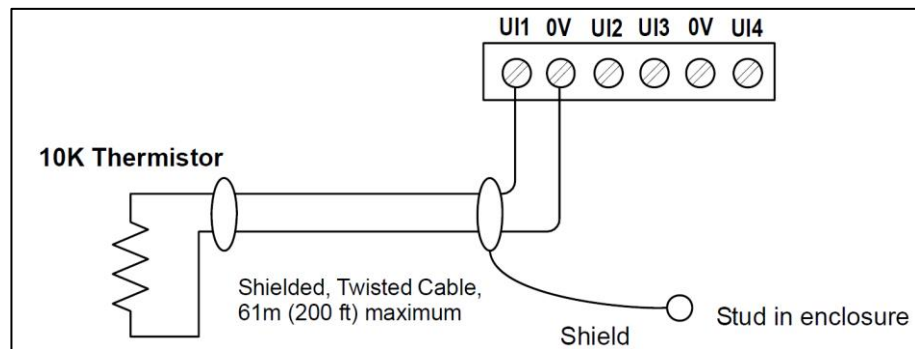
<b>NDIO board -1</b>			
<b>ID</b>	<b>Type</b>	<b>Address</b>	<b>Name</b>
U1	Resistive Input Point	1	T1
U2	Resistive Input Point	2	T2
U3	Resistive Input Point	3	T3 (ambient)
U4	Resistive Input Point	4	T4
U5	Resistive Input Point	5	T5
U6	Resistive Input Point	6	T6
U7	Resistive Input Point	7	T7
U8	Resistive Input Point	8	T8
U9	Resistive Input Point	9	T9
U10	Resistive Input Point	10	T10
U11	Resistive Input Point	11	T11
U12	Resistive Input Point	12	T12
U13	Resistive Input Point	13	T13
U14	Resistive Input Point	14	T14
U15	Resistive Input Point	15	T15
U16	Resistive Input Point	16	T16
D1	Boolean Output Point	1	Pump 9
D2	Boolean Output Point	2	Compressor
D3	Boolean Output Point	3	Pump 7
D4	Boolean Output Point	4	2-Way Valve
D5	Boolean Output Point	5	3-Way Valve after T4
D8	Boolean Output Point	8	AWHX & 3-Way Valve after T2
A1	Voltage Output Point	1	Pump 8
A2	Voltage Output Point	2	Fan cooler
<b>NDIO board -2</b>			
<b>ID</b>	<b>Type</b>	<b>Address</b>	<b>Name</b>
U1	Counter Input Point	1	Solar loop flow meter
U2	Counter Input Point	2	Heat sink loop flow meter
U3	Counter Input Point	3	Load simulation loop flow meter
U4	Voltage Input Point	4	Irradiance meter
U5	Voltage Input Point	5	Pressure transmitter after compressor

U6 Voltage Input Point 6 Pressure transmitter before compressor

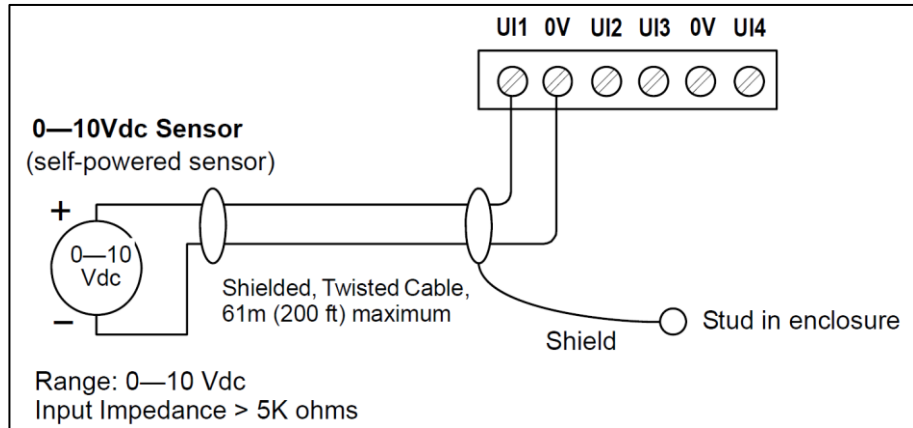
<b>NDIO board -3</b>			
<b>ID</b>	<b>Type</b>	<b>Address</b>	<b>Name</b>
U2	Thermistor Input Point	2	T-PCM (inside the HX)
U3	Thermistor Input Point	3	T-HX Top (PCM HX exterior surface)
U4	Thermistor Input Point	4	T-HX Bottom (PCM HX exterior surface)
U5	Thermistor Input Point	5	T-HX Mid 1 (PCM HX exterior surface)
U6	Thermistor Input Point	6	T-HX Mid 2 (PCM HX exterior surface)
U7	Thermistor Input Point	8	T-HX Mid 3 (PCM HX exterior surface)
U8	Thermistor Input Point	8	T-HX Mid 4 (PCM HX exterior surface)



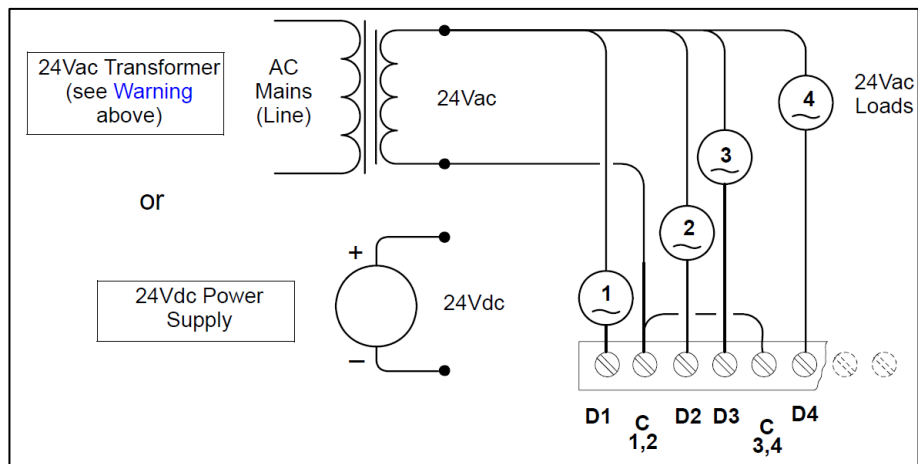
App-Fig 19. Earthling connection for the control box



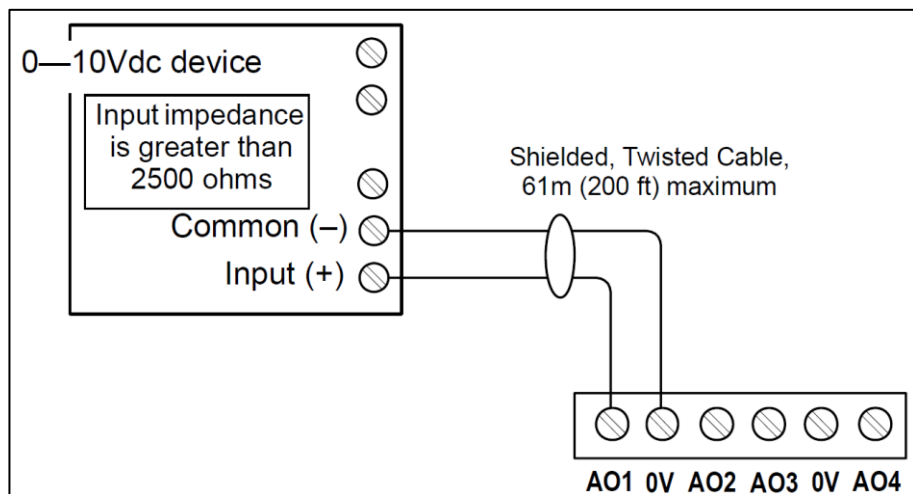
App-Fig 20. Thermistor input connection diagram



App-Fig 21. 0-10 voltage input connection diagram



App-Fig 22. Digital output connection diagram



App-Fig 23. Analogue output connection diagram

*Appendix E*

Uncertainties of Measured Variables

Enter a numerical value or variable name

Variable	Value	Units	Absolute Uncertainty	Relative Uncertainty
m_HP	0.217	kg/s		0.05
F[12]	1	bar		0.003
F[15]	1	bar		0.003
T[10]	1	C		0.01
T[11]	1	C		0.01
T[12]	1	C		0.01
T[13]	1	C		0.01
T[15]	1	C		0.01

OK Cancel

*App-Fig 24. Print screen of the error set up in EES*



Uncertainty Results		
Unit Settings: SI C bar kJ mass deg		
(Table 1, Run 42)		
Variable±Uncertainty	Partial derivative	% of uncertainty
<u><math>m_{ref} = 0.0468 \pm 0.004396</math> [kg/s]</u>		<u>± 9.31 %</u>
$m_{HP} = 0.217 \pm 0.01085$ [kg/s]	$\partial m_{ref} / \partial m_{HP} = 0.2157$	28.34 %
$P_{12} = 19.8 \pm 0.0594$ [bar]	$\partial m_{ref} / \partial P_{12} = 0.00121$	0.03 %
$P_{15} = 2.8 \pm 0.0084$ [bar]	$\partial m_{ref} / \partial P_{15} = 0$	0.00 %
$T_{10} = 62.4 \pm 0.624$ [C]	$\partial m_{ref} / \partial T_{10} = 0.004548$	41.68 %
$T_{11} = 52.11 \pm 0.5211$ [C]	$\partial m_{ref} / \partial T_{11} = -0.004548$	29.07 %
$T_{12} = 116.5 \pm 1.165$ [C]	$\partial m_{ref} / \partial T_{12} = -0.0002831$	0.56 %
$T_{13} = 66.76 \pm 0.6676$ [C]	$\partial m_{ref} / \partial T_{13} = 0.0003729$	0.32 %
$T_{15} = 10.88 \pm 0.1088$ [C]	$\partial m_{ref} / \partial T_{15} = 0$	0.00 %
<u><math>Q_H = 8.932 \pm 0.8351</math> [kW]</u>		<u>± 9.28 %</u>
$m_{HP} = 0.217 \pm 0.01085$ [kg/s]	$\partial Q_H / \partial m_{HP} = 41.16$	28.60 %
$P_{12} = 19.8 \pm 0.0594$ [bar]	$\partial Q_H / \partial P_{12} = 0$	0.00 %
$P_{15} = 2.8 \pm 0.0084$ [bar]	$\partial Q_H / \partial P_{15} = 0$	0.00 %
$T_{10} = 62.4 \pm 0.624$ [C]	$\partial Q_H / \partial T_{10} = 0.868$	42.07 %
$T_{11} = 52.11 \pm 0.5211$ [C]	$\partial Q_H / \partial T_{11} = -0.868$	29.34 %
$T_{12} = 116.5 \pm 1.165$ [C]	$\partial Q_H / \partial T_{12} = 0$	0.00 %
$T_{13} = 66.76 \pm 0.6676$ [C]	$\partial Q_H / \partial T_{13} = 0$	0.00 %
$T_{15} = 10.88 \pm 0.1088$ [C]	$\partial Q_H / \partial T_{15} = 0$	0.00 %
<u><math>COP = 5.223 \pm 0.4884</math></u>		<u>± 9.32 %</u>
$m_{HP} = 0.217 \pm 0.01085$ [kg/s]	$\partial COP / \partial m_{HP} = 24.07$	28.60 %
$P_{12} = 19.8 \pm 0.0594$ [bar]	$\partial COP / \partial P_{12} = 0$	0.00 %
$P_{15} = 2.8 \pm 0.0084$ [bar]	$\partial COP / \partial P_{15} = 0$	0.00 %
$T_{10} = 62.4 \pm 0.624$ [C]	$\partial COP / \partial T_{10} = 0.5076$	42.07 %
$T_{11} = 52.11 \pm 0.5211$ [C]	$\partial COP / \partial T_{11} = -0.5076$	29.34 %
$T_{12} = 116.5 \pm 1.165$ [C]	$\partial COP / \partial T_{12} = 0$	0.00 %
$T_{13} = 66.76 \pm 0.6676$ [C]	$\partial COP / \partial T_{13} = 0$	0.00 %
$T_{15} = 10.88 \pm 0.1088$ [C]	$\partial COP / \partial T_{15} = 0$	0.00 %

App-Fig 25. Print screen of the uncertainty analysis results in EES

**Appendix F**

**EES Transcript file**

{ Import inputs from the clipboard}

\$Import 'CLIPBOARD' T\_Source\_in, m\_Si, T\_Load\_in, m\_Li

Procedure cop\_q\_heating

(T\_Cond,COP35,COP37.5,COP40,COP42.5,COP45,COP47.5,COP50,COP52.5,COP55,  
,COP57.5,Q\_h\_35,Q\_h\_37.5,Q\_h\_40,Q\_h\_42.5,Q\_h\_45,Q\_h\_47.5,Q\_h\_50,Q\_h\_52.5,  
Q\_h\_55,Q\_h\_57.5:Q\_h,COP)

If (T\_Cond<=35) Then

COP=COP35

Q\_h=Q\_h\_35

Else

If (35<T\_Cond) and (T\_Cond<=37.5) Then

COP=COP37.5-((COP37.5-COP35)\*(37.5-T\_Cond))/2.5

Q\_h=Q\_h\_37.5-((Q\_h\_37.5-Q\_h\_35)\*(37.5-T\_Cond))/2.5

Else

If (37.5<T\_Cond) and (T\_Cond<=40) Then

COP=COP40-((COP40-COP37.5)\*(40-T\_Cond))/2.5

Q\_h=Q\_h\_40-((Q\_h\_40-Q\_h\_37.5)\*(40-T\_Cond))/2.5

Else

If (40<T\_Cond) and (T\_Cond<=42.5) Then

COP=COP42.5-((COP42.5-COP40)\*(42.5-T\_Cond))/2.5

Q\_h=Q\_h\_42.5-((Q\_h\_42.5-Q\_h\_40)\*(42.5-T\_Cond))/2.5

Else

If (42.5<T\_Cond) and (T\_Cond<=45) Then

COP=COP45-((COP45-COP42.5)\*(45-T\_Cond))/2.5

Q\_h=Q\_h\_45-((Q\_h\_45-Q\_h\_42.5)\*(45-T\_Cond))/2.5

Else

If (45<T\_Cond) and (T\_Cond<=47.5) Then

COP=COP47.5-((COP47.5-COP45)\*(47.5-T\_Cond))/2.5

Q\_h=Q\_h\_47.5-((Q\_h\_47.5-Q\_h\_45)\*(47.5-T\_Cond))/2.5

Else

If (47.5<T\_Cond) and (T\_Cond<=50) Then  
COP=COP50-((COP50-COP47.5)\*(50-T\_Cond))/2.5  
Q\_h=Q\_h\_50-((Q\_h\_50-Q\_h\_47.5)\*(50-T\_Cond))/2.5

Else

If (50<T\_Cond) and (T\_Cond<=52.5) Then  
COP=COP52.5-((COP52.5-COP50)\*(52.5-T\_Cond))/2.5  
Q\_h=Q\_h\_52.5-((Q\_h\_52.5-Q\_h\_50)\*(52.5-T\_Cond))/2.5

Else

If (52.5<T\_Cond) and (T\_Cond<=55) Then  
COP=COP55-((COP55-COP52.5)\*(55-T\_Cond))/2.5  
Q\_h=Q\_h\_55-((Q\_h\_55-Q\_h\_52.5)\*(55-T\_Cond))/2.5

Else

If (55<T\_Cond) and (T\_Cond<=57.5) Then  
COP=COP57.5-((COP57.5-COP55)\*(57.5-T\_Cond))/2.5  
Q\_h=Q\_h\_57.5-((Q\_h\_57.5-Q\_h\_55)\*(57.5-T\_Cond))/2.5

Else

If (T\_Cond>57.5) Then  
COP=COP57.5  
Q\_h=Q\_h\_57.5

Endif

Endif

Endif

Endif

Endif

Endif

Endif

Endif

Endif

Endif

Endif

End

Procedure m\_source\_in(m\_Si,T\_Source\_in,Q\_c,CP,Q\_loss:m\_S\_in,T\_Source\_out)

```
if(m_Si)>0 Then
m_S_in=m_Si
T_Source_out=T_Source_in - (Q_c-Q_loss)/((m_S_in/3600)*Cp)
```

```
Else
```

```
if(m_Si)=0 Then
m_S_in=0.0
T_Source_out=T_Source_in
```

```
Endif
```

```
Endif
```

```
End
```

```
Procedure m_load_in(m_Li,T_Load_in,Q_h,CP:m_L_in,T_Load_out)
```

```
if(m_Li)>0 Then
m_L_in=m_Li
T_Load_out=T_Load_in+(0.8*Q_h)/((m_L_in/3600)*Cp)
```

```
Else
```

```
if(m_Li)=0 Then
m_L_in=0.0
T_Load_out=T_Load_in
```

```
Endif
```

```
Endif
```

```
End
```

```
Call m_source_in(m_Si,T_Source_in,Q_c,CP,Q_loss:m_S_in,T_Source_out)
```

```
Call m_load_in(m_Li,T_Load_in,Q_h,CP:m_L_in,T_Load_out)
```

```
Call COP_Q_Heating
```

```
(T_Cond,COP35,COP37.5,COP40,COP42.5,COP45,COP47.5,COP50,COP52.5,COP55
,COP57.5,Q_h_35,Q_h_37.5,Q_h_40,Q_h_42.5,Q_h_45,Q_h_47.5,Q_h_50,Q_h_52.5,
Q_h_55,Q_h_57.5:Q_h,COP)
```

```
{ Calculation }
```

```
T_evap=T_Source_in
```

```
T_Cond=T_Load_in
```

```
COP35=-0.0006*(T_evap)^2+0.067*T_evap+3.058
```

$COP_{37.5} = -0.0006 \cdot (T_{evap})^2 + 0.067 \cdot T_{evap} + 3.148$   
 $COP_{40} = -0.0006 \cdot (T_{evap})^2 + 0.067 \cdot T_{evap} + 3.238$   
 $COP_{42.5} = -0.0006 \cdot (T_{evap})^2 + 0.067 \cdot T_{evap} + 3.328$   
 $COP_{45} = -0.0006 \cdot (T_{evap})^2 + 0.067 \cdot T_{evap} + 3.418$   
 $COP_{47.5} = -0.0006 \cdot (T_{evap})^2 + 0.067 \cdot T_{evap} + 3.508$   
 $COP_{50} = -0.0006 \cdot (T_{evap})^2 + 0.067 \cdot T_{evap} + 3.598$   
 $COP_{52.5} = -0.0006 \cdot (T_{evap})^2 + 0.067 \cdot T_{evap} + 3.688$   
 $COP_{55} = -0.0006 \cdot (T_{evap})^2 + 0.067 \cdot T_{evap} + 3.778$   
 $COP_{57.5} = -0.0006 \cdot (T_{evap})^2 + 0.067 \cdot T_{evap} + 3.868$   
 $Q_{h\_35} = -0.0015 \cdot (T_{evap})^2 + 0.1 \cdot T_{evap} + 3.5$   
 $Q_{h\_37.5} = -0.0015 \cdot (T_{evap})^2 + 0.1 \cdot T_{evap} + 4$   
 $Q_{h\_40} = -0.0015 \cdot (T_{evap})^2 + 0.1 \cdot T_{evap} + 4.5$   
 $Q_{h\_42.5} = -0.0015 \cdot (T_{evap})^2 + 0.1 \cdot T_{evap} + 5$   
 $Q_{h\_45} = -0.0015 \cdot (T_{evap})^2 + 0.1 \cdot T_{evap} + 5.5$   
 $Q_{h\_47.5} = -0.0015 \cdot (T_{evap})^2 + 0.1 \cdot T_{evap} + 6$   
 $Q_{h\_50} = -0.0015 \cdot (T_{evap})^2 + 0.1 \cdot T_{evap} + 6.5$   
 $Q_{h\_52.5} = -0.0015 \cdot (T_{evap})^2 + 0.1 \cdot T_{evap} + 7$   
 $Q_{h\_55} = -0.0015 \cdot (T_{evap})^2 + 0.1 \cdot T_{evap} + 7.5$   
 $Q_{h\_57.5} = -0.0015 \cdot (T_{evap})^2 + 0.1 \cdot T_{evap} + 8$

$W = Q_h / COP$   
 $Q_c = Q_h - W$   
 $C_p = 4.2$   
 $Q_{loss} = 5.7618 \cdot W - 3.0267$   
 $m_{S_o} = m_{S_{in}}$   
 $m_{L_o} = m_{L_{in}}$

{ TRNSYS outputs }

$out1 = T_{Source\_out}$   
 $out2 = m_{S_o}$   
 $out3 = T_{Load\_out}$   
 $out4 = m_{L_o}$   
 $out5 = COP$   
 $out6 = W$   
 $out7 = Q_h$

\$Export 'CLIPBOARD' out1,out2,out3,out4,out5,out6,out7

*Fluent Component modified code*

SUBROUTINE TYPE101 (TIME,XIN,OUT,T,DTDT,PAR,INFO,ICNTRL,\*)

!\*\*\*\*\*

\*\*\*\*\*

! Object: Call FLUENT

! Simulation Studio Model: Call FLUENT

!

! Author: Walid Youssef

! Date: Jan 10, 2017

!

! Revision history:

! 2006-05-25: DAA - In order to compile this type with IVF, the function SLEEP is found in the

!           portability library DFPORT.

!

! (Comments and routine interface generated by TRNSYS Studio)

!\*\*\*\*\*

\*\*\*\*\*

! Copyright © 2011 Solar Energy Laboratory, University of Wisconsin-Madison. All rights reserved.

! TRNSYS access functions (allow to access TIME etc.)

USE TrnsysConstants

USE TrnsysFunctions

USE DFPORT, ONLY: SLEEP

!-----

-----

! REQUIRED BY THE MULTI-DLL VERSION OF TRNSYS

!DEC\$ATTRIBUTES DLLEXPORT :: TYPE101

!-----

-----

!-----

-----

! TRNSYS DECLARATIONS

IMPLICIT NONE !REQUIRES THE USER TO DEFINE ALL  
VARIABLES BEFORE USING THEM

DOUBLE PRECISION XIN !THE ARRAY FROM WHICH THE INPUTS TO  
THIS TYPE WILL BE RETRIEVED

DOUBLE PRECISION OUT !THE ARRAY WHICH WILL BE USED TO  
STORE THE OUTPUTS FROM THIS TYPE

DOUBLE PRECISION TIME !THE CURRENT SIMULATION TIME -  
YOU MAY USE THIS VARIABLE BUT DO NOT SET IT!

DOUBLE PRECISION PAR !THE ARRAY FROM WHICH THE  
PARAMETERS FOR THIS TYPE WILL BE RETRIEVED

DOUBLE PRECISION STORED !THE STORAGE ARRAY FOR HOLDING  
VARIABLES FROM TIMESTEP TO TIMESTEP

DOUBLE PRECISION T !AN ARRAY CONTAINING THE  
RESULTS FROM THE DIFFERENTIAL EQUATION SOLVER

DOUBLE PRECISION DTDT !AN ARRAY CONTAINING THE  
DERIVATIVES TO BE PASSED TO THE DIFF.EQ. SOLVER

INTEGER\*4 INFO(15) !THE INFO ARRAY STORES AND  
PASSES VALUABLE INFORMATION TO AND FROM THIS TYPE

INTEGER\*4 NP,NI,NOUT,ND !VARIABLES FOR THE MAXIMUM  
NUMBER OF PARAMETERS,INPUTS,OUTPUTS AND DERIVATIVES

INTEGER\*4 NPAR,NIN,NDER !VARIABLES FOR THE CORRECT  
NUMBER OF PARAMETERS,INPUTS,OUTPUTS AND DERIVATIVES

INTEGER\*4 IUNIT,ITYPE !THE UNIT NUMBER AND TYPE NUMBER  
FOR THIS COMPONENT

INTEGER\*4 ICNTRL !AN ARRAY FOR HOLDING VALUES  
OF CONTROL FUNCTIONS WITH THE NEW SOLVER

INTEGER\*4 NSTORED !THE NUMBER OF VARIABLES THAT  
WILL BE PASSED INTO AND OUT OF STORAGE

CHARACTER\*3 OCHECK !AN ARRAY TO BE FILLED WITH THE  
CORRECT VARIABLE TYPES FOR THE OUTPUTS

CHARACTER\*3 YCHECK !AN ARRAY TO BE FILLED WITH THE  
CORRECT VARIABLE TYPES FOR THE INPUTS

```
!-----
-----

!-----
-----

! USER DECLARATIONS - SET THE MAXIMUM NUMBER OF PARAMETERS
(NP), INPUTS (NI),
! OUTPUTS (NOUT), AND DERIVATIVES (ND) THAT MAY BE SUPPLIED
FOR THIS TYPE
    PARAMETER (NP=4,NI=20,NOUT=20,ND=0,NSTORED=20)

!-----
-----

!-----
-----

! REQUIRED TRNSYS DIMENSIONS
    DIMENSION XIN(NI),OUT(NOUT),PAR(NP),YCHECK(NI),OCHECK(NOUT), &
        STORED(NSTORED),T(ND),DTDT(ND)
    INTEGER NITEMS,NO

!-----
-----

!-----
-----

! ADD DECLARATIONS AND DEFINITIONS FOR THE USER-VARIABLES
HERE

    INTEGER    ios, i_sleep, i
    LOGICAL    fileFound
    LOGICAL(4) bWait      !wait/no wait for new process to end
        LOGICAL    O_FLAG
        LOGICAL    scriptFound
    INTEGER*4  prochand,thrdhand
    CHARACTER (len=maxPathLength)  :: CMDLINE    !Command line to call
FLUENT
```



```

CHARACTER (len=maxPathLength)  :: scriptFileName,resultsFileName,textLine
      CHARACTER (len=maxPathLength)  ::
pathFluent,optionsFluent,pathFluentScrip
      CHARACTER (len=maxPathLength)  :: MSGFluent(2)

INTEGER mode      ! Mode
      INTEGER callingMode      ! Calling mode
INTEGER luScript  ! Logical unit number for script file at each time step
INTEGER luResults      ! Logical unit number of intermediate file that returns
the results from FLUENT
      INTEGER nResultsFluent ! Number of outputs read from FLUENT
      INTEGER nModifyBC      ! Number of variables to modify boundary conditions
DOUBLE PRECISION resultsFluent !Array with results from fluent
      DOUBLE PRECISION modifyBC      !Array with information to update
boundary conditions
      DIMENSION resultsFluent(NOUT)
      DIMENSION modifyBC(NOUT)

INTEGER      cf      ! Control function

DATA scriptFound /.true./
      DATA MSGFluent(1) /'Error opening script file.'/
DATA MSGFluent(2) /'Error opening results file.'/

!-----
-----
! SET THE VERSION INFORMATION FOR TRNSYS
IF(INFO(7).EQ.-2) THEN
      INFO(12)=16
      RETURN 1
ENDIF
!-----
-----

```

```
!-----  
-----  
! DO ALL THE VERY LAST CALL OF THE SIMULATION MANIPULATIONS  
HERE  
  IF (INFO(8).EQ.-1) THEN  
    IUNIT=INFO(1)  
    ITYPE=INFO(2)  
    RETURN 1  
  ENDIF  
!-----  
-----  
!-----  
-----  
! DO ALL THE VERY FIRST CALL OF THE SIMULATION MANIPULATIONS  
HERE  
  IF (INFO(7).EQ.-1) THEN  
  
! SET SOME INFO ARRAY VARIABLES TO TELL THE TRNSYS ENGINE  
HOW THIS TYPE IS TO WORK  
  NO    = JFIX(PAR(3)+0.1)    !Number of outputs  
  INFO(6) = NO  
  callingMode = JFIX(PAR(4)+0.1) !Calling mode  
    IF (callingMode == 1) INFO(9) = 1 !Dynamic coupling - Iterative calling  
    IF (callingMode == 2) INFO(9) = 2 !Static coupling - Call after all  
components have converged  
    INFO(10) = 0    !STORAGE FOR VERSION 16 HAS BEEN CHANGED  
  
! SET THE REQUIRED NUMBER OF INPUTS, PARAMETERS AND  
DERIVATIVES THAT THE USER SHOULD SUPPLY IN THE INPUT FILE  
! IN SOME CASES, THE NUMBER OF VARIABLES MAY DEPEND ON THE  
VALUE OF PARAMETERS TO THIS MODEL....  
  NIN    = JFIX(PAR(2)+0.1) + 1  
  NPAR   = NP
```

NDER = ND

! CALL THE TYPE CHECK SUBROUTINE TO COMPARE WHAT THIS  
COMPONENT REQUIRES TO WHAT IS SUPPLIED IN

! THE TRNSYS INPUT FILE

CALL TYPECK(1,INFO,NIN,NPAR,NDER)

! CALL RCHECK(INFO,YCHECK,OCHECK)

! SET THE NUMBER OF STORAGE SPOTS NEEDED FOR THIS COMPONENT  
NITEMS = 2 + NO

CALL setStorageSize(NITEMS,INFO)

! RETURN TO THE CALLING PROGRAM

RETURN 1

ENDIF

!-----  
-----

!-----  
-----

! DO ALL OF THE INITIAL TIMESTEP MANIPULATIONS HERE - THERE ARE  
NO ITERATIONS AT THE INTIAL TIME

IF (TIME < (getSimulationStartTime() + getSimulationTimeStep()/2.D0)) THEN

! SET THE UNIT NUMBER FOR FUTURE CALLS

IUNIT = INFO(1)

ITYPE = INFO(2)

!-----  
-----

! READ IN THE VALUES OF THE PARAMETERS IN SEQUENTIAL ORDER

mode = JFIX(PAR(1)+0.1) ! Mode - for future upgrades

NIN = JFIX(PAR(2)+0.1) + 1 ! Number of total inputs to the component

NO = JFIX(PAR(3)+0.1) ! Number of outputs

callingMode = JFIX(PAR(4)+0.1) ! Calling mode - 1 for Dynamic, 2 for  
Static

! CHECK THE PARAMETERS FOR PROBLEMS AND RETURN FROM THE  
SUBROUTINE IF AN ERROR IS FOUND

IF ((MODE < 1) .OR. MODE > 1 ) CALL TYPECK(-4,INFO,0,1,0)

IF ( NIN < 0 ) CALL TYPECK(-4,INFO,0,2,0)

IF ( NO < 0 ) CALL TYPECK(-4,INFO,0,3,0)

IF ((callingMode<1).OR.(callingMode>2)) CALL TYPECK(-4,INFO,0,4,0)

! --CALL FLUENT FOR THE FIRST TIME-----  
-----

! In this first call, Fluent may initialize the flow and create the output file needed  
! for the solution of the other components.  
! Fluent opens, solves the text script, creates a text file and closes.

!Open script file and write the information for the updated boundary conditions  
scriptFileName = TRIM(getLabel(IUNIT,3))

! if relative path (no colon in second position or backslash in first position), add path  
to script file

IF((.NOT.(index(scriptFileName,":")==2)) .and.

(.NOT.(index(scriptFileName,"\\")==1)) ) THEN

scriptFileName = trim(getTrnsysInputFileDir()) // "\\ " trim(scriptFileName)

ENDIF

luScript = getNextAvailableLogicalUnit()

OPEN (luScript, FILE = scriptFileName, STATUS = 'UNKNOWN')

CLOSE(luScript,STATUS='DELETE')

OPEN (luScript, FILE = scriptFileName, STATUS = 'NEW')

!Find results

resultsFileName = TRIM(getLabel(IUNIT,4))

! if relative path (no colon in second position or backslash in first position), delete path from results file

```
IF((index(resultsFileName,":")==2) .OR. (index(resultsFileName,"\")==1)) THEN
  resultsFileName =
  TRIM(resultsFileName(index(resultsFileName,'\',back=.true.)+1:maxPathLength))
ENDIF
```

```
! -----
! User defined 1.  INITIALIZATION OF FLUENT SIMULATION-----
-----
```

```
! -----
! Modify them according to the number of boundary condition data that needs to be updated
```

```
!Update boundary conditions
nModifyBC = 1                !Size of array that sends information to the
subroutine UPDATEBOUNDARY,
  modifyBC(1) = XIN(2)
```

```
nResultsFluent = 2          !Size of array that returns information from the
subroutine
```

```
!READ_FLUENT_RESULTS.
```

```
! -----
! -----
```

```
!Update boundary conditions
CALL UPDATEBOUNDARY
(luScript,nModifyBC,modifyBC,scriptFileName,resultsFileName)
CLOSE (luScript,STATUS='KEEP')
```

```
!Call fluent
pathFluent = getLabel(IUNIT,1)
optionsFluent = getLabel(IUNIT,2)
```

```

CMDLINE = TRIM(pathFluent) //" "//TRIM(optionsFluent)://"
"//TRIM(scriptFileName)
    bwait = .TRUE.
    CALL CALLPROGRAM(CMDLINE,bwait,prochand,thrdhand)

!Read the results from FLUENT
fileFound = .FALSE.
luResults = getNextAvailableLogicalUnit()

    i_sleep = 1
    ios = 1
    do i_sleep=1,10
CALL SLEEP(180)
        OPEN (luResults, FILE= resultsFileName, STATUS = 'OLD', IOSTAT = ios)
    IF (ios == 0) then
            EXIT
        ENDIF
    enddo

    IF (ios == 0) then
        OPEN (luResults, FILE= resultsFileName, STATUS = 'OLD')
        CALL READ_FLUENT_RESULTS
(luResults,nResultsFluent,resultsFluent)
        CLOSE (luResults,STATUS='DELETE')
    ELSE
        CALL MESSAGES(-1,MSGFluent(2),'fatal',IUNIT,ITYPE)
        RETURN 1
    ENDIF

! -----
! User defined 2. UPDATE THE OUTPUTS FOR THE COUPLING WITH THE
OTHER COMPONENTS-----
! -----

```

! PERFORM ANY REQUIRED CALCULATIONS TO SET THE INITIAL  
VALUES OF THE OUTPUTS HERE

!Modify these values according to the outputs from Fluent

OUT(1) = resultsFluent(1)

OUT(2) = resultsFluent(2)

! -----  
! -----

! PERFORM ANY REQUIRED CALCULATIONS TO SET THE INITIAL  
STORAGE VARIABLES HERE

NITEMS = 2 + NO

STORED(1)= luScript

STORED(2)= luResults

DO i = 1,NO

STORED(2 + i) = OUT(i)

ENDDO

! PUT THE STORED ARRAY IN THE GLOBAL STORED ARRAY

CALL setStorageVars(STORED,NITEMS,INFO)

! RETURN TO THE CALLING PROGRAM

RETURN 1

ENDIF

!-----  
-----

!-----  
-----

! \*\*\* ITS AN ITERATIVE CALL TO THIS COMPONENT \*\*\*

!-----  
-----

! RE-READ THE PARAMETERS IF ANOTHER UNIT OF THIS TYPE HAS BEEN  
CALLED SINCE THE LAST

```

! TIME THEY WERE READ IN
IF(INFO(1).NE.IUNIT) THEN
  !reset the unit number
    IUNIT = INFO(1)
    ITYPE = INFO(2)
  !REREAD THE PARAMETERS
  MODE = JFIX(PAR(1)+0.1)  ! Mode
  NIN  = JFIX(PAR(2)+0.1) + 1
  NO   = JFIX(PAR(3)+0.1)
ENDIF

!REREAD THE STORAGE VALUES
NITEMS = 2 + NO
  CALL getStorageVars(STORED,NITEMS,INFO)
luScript = STORED(1)
  luResults = STORED(2)

! READ THE INPUTS
cf      = JFIX(XIN(1) +0.1)

! -----
! User defined 3. UPDATE THE INPUTS FOR THE COUPLING WITH THE
OTHER COMPONENTS-----
! -----
! Modify this according to the special application
!Update boundary conditions
nModifyBC = 1
  modifyBC(1) = XIN(2)
nResultsFluent = 2
! -----
! -----

IF (cf >0.5) THEN
! Update boundary conditions and run simulations

```



```

!Open script file and write the information for the updated boundary conditions
scriptFileName = TRIM(getLabel(IUNIT,3))

! if relative path (no colon in second position or backslash in first position), add
path to script file
IF((.NOT.(index(scriptFileName,":")==2)) .and.
(.NOT.(index(scriptFileName,"\")==1))) THEN
    scriptFileName = trim(getTrnsysInputFileDir()) // '\//' trim(scriptFileName)
ENDIF

! Write boundary condition to modify
OPEN (luScript, FILE = scriptFileName, STATUS = 'UNKNOWN')
    CLOSE(luScript,STATUS='DELETE')
OPEN (luScript, FILE = scriptFileName, STATUS = 'NEW')

CALL UPDATEBOUNDARY
(luScript,nModifyBC,modifyBC,scriptFileName,resultsFileName)
CLOSE (luScript,STATUS='KEEP')

!Call fluent
pathFluent = getLabel(IUNIT,1)
optionsFluent = getLabel(IUNIT,2)
CMDLINE = TRIM(pathFluent) //' ' //TRIM(optionsFluent) //'
'//TRIM(scriptFileName)
    bwait = .TRUE.
    CALL CALLPROGRAM(CMDLINE,bwait,prochand,thrdhand)

!Read the results from FLUENT
fileFound = .FALSE.

i_sleep = 1
ios = 1
DO i_sleep=1,10

```

```

CALL SLEEP(180)
      OPEN (luResults, FILE= resultsFileName, STATUS = 'OLD', IOSTAT =
ios)
      IF (ios == 0) THEN
          EXIT
      ENDIF
ENDDO

IF (ios == 0) then
      OPEN (luResults, FILE= resultsFileName, STATUS = 'OLD')
      CALL READ_FLUENT_RESULTS
(luResults,nResultsFluent,resultsFluent)
      CLOSE (luResults,STATUS='DELETE')
      ELSE
          CALL MESSAGES(-1,MSGFluent(2),'fatal',IUNIT,ITYPE)
          RETURN 1
      ENDIF

! -----
! User defined 4. SET THE OUTPUTS FROM THIS MODEL IN SEQUENTIAL
ORDER AND GET OUT-----
! -----

      OUT(1) = resultsFluent(1)
      OUT(2) = resultsFluent(2)

! -----
! -----

! PUT THE STORED ARRAY IN THE GLOBAL STORED ARRAY
DO i = 1,NO
      STORED(2 + i) = OUT(i)
      ENDDO
CALL setStorageVars(STORED,NITEMS,INFO)

      ELSE

```

- ! Do not do anything if controlfunction is zero
- ! Keep the values of the outputs from the previous timestep

```
DO i = 1,NO
  OUT(i) = STORED(2+i)
ENDDO
ENDIF

RETURN 1
```

CONTAINS

```
! -----
! User defined 5. MODIFY THE SUBROUTINES UPDATEBOUNDARY AND
! READ_FLUENT_RESULTS-----
! -----
```

```
SUBROUTINE
UPDATEBOUNDARY(luScript,nModifyBC,modifyBC,scriptFileName,resultsFileNa
me)
```

- ! This subroutine writes the new information for the boundary conditions in FLUENT

```
USE TrnsysConstants
```

```
IMPLICIT NONE
```

```
INTEGER, INTENT(IN)      :: luScript
INTEGER, INTENT(IN)      :: nModifyBC
DOUBLE PRECISION, INTENT(IN) :: modifyBC
```

```
DIMENSION modifyBC(nModifyBC)
```

```
DOUBLE PRECISION v_boundary
```

```
CHARACTER (len=12) vStr
```

```
CHARACTER (len=maxPathLength) :: scriptFileName,resultsFileName
```

!Modify according to specific application

v\_boundary = modifyBC(1)

WRITE (vStr,'(F5.1)') v\_boundary

vStr = TRIM(ADJUSTL(vStr))

WRITE (luScript,'(A5)') "f/rcd" !File / read case data

WRITE (luScript,'(A9)') "fff.2.cas"

WRITE (luScript,'(A8)') "de/bc/vi" !Define/Boundary Conditions/Velocity

Inlet

WRITE (luScript,'(A)') " " !Zone ID (inlet)

WRITE (luScript,'(A)') " " !Domain ID (Mixture)

WRITE (luScript,'(A)') " " !Velocity Specification Method:

Magnitude and Direction [no]

WRITE (luScript,'(A)') " " !Velocity Specification Method:

Components [no]

WRITE (luScript,'(A)') " " !Velocity Specification Method:

Magnitude, Normal to Boundary [yes]

WRITE (luScript,'(A)') " " !Reference Frame: Absolute [yes]

WRITE (luScript,'(A)') " " !Use Profile for Velocity Magnitude? [no]

WRITE (luScript,'(A)') " " !Velocity Magnitude (m/s) [0.26]

WRITE (luScript,'(A)') " " !Use Profile for Supersonic/Initial Gauge

Pressure? [no]

WRITE (luScript,'(A)') " " !Supersonic/Initial Gauge Pressure (pascal)

[0]

WRITE (luScript,'(A)') " " !Use Profile for Temperature? [no]

WRITE (luScript,'(A4)') vStr !Temperature (c) [60]

WRITE (luScript,'(A)') " " !Turbulent Specification Method: K and

Epsilon [no]

WRITE (luScript,'(A)') " " !Turbulent Specification Method: Intensity

and Length Scale [no]

WRITE (luScript,'(A)') " " !Turbulent Specification Method: Intensity

and Viscosity Ratio [yes]

```

WRITE (luScript,'(A)') " "           !Turbulent Intensity (%) [5]
WRITE (luScript,'(A)') " "           !Turbulent Viscosity Ratio [10]
!WRITE (luScript,'(A4)') "s/it"      !Solve/iterate
!WRITE (luScript,'(A1)') "1"         !Number of Iterations
!WRITE (luScript,'(A7)') "s/s/t-s"  !solve/set/time-step
!WRITE (luScript,'(A4)') "0.01"     !Time Step Size
      !WRITE (luScript,'(A3)') "s/d"      !Solve/dual time
!WRITE (luScript,'(A2)') "10"        !Physical time steps (time=0.1 s)
      !WRITE (luScript,'(A)') " "        !Max number of time steps
!WRITE (luScript,'(A7)') "s/s/t-s"  !solve/set/time-step
!WRITE (luScript,'(A4)') "0.05"     !Time Step Size
      !WRITE (luScript,'(A3)') "s/d"      !Solve/dual time
!WRITE (luScript,'(A2)') "18"        !Physical time steps (time=1 s)
      !WRITE (luScript,'(A)') " "        !Max number of time steps
!WRITE (luScript,'(A7)') "s/s/t-s"  !solve/set/time-step
!WRITE (luScript,'(A3)') "0.1"       !Time Step Size
      !WRITE (luScript,'(A3)') "s/d"      !Solve/dual time
!WRITE (luScript,'(A2)') "10"        !Physical time steps (time=2 s)
      !WRITE (luScript,'(A)') " "        !Max number of time steps
!WRITE (luScript,'(A7)') "s/s/t-s"  !solve/set/time-step
!WRITE (luScript,'(A3)') "0.5"       !Time Step Size
      !WRITE (luScript,'(A3)') "s/d"      !Solve/dual time
!WRITE (luScript,'(A2)') "16"        !Physical time steps (time=10 s)
      !WRITE (luScript,'(A)') " "        !Max number of time steps
WRITE (luScript,'(A7)') "s/s/t-s"  !solve/set/time-step
WRITE (luScript,'(A2)') "30"        !Time Step Size
      WRITE (luScript,'(A3)') "s/d"      !Solve/dual times
WRITE (luScript,'(A2)') "10"        !Physical time steps (time=60 s)
      WRITE (luScript,'(A)') " "        !Max number of time steps
!WRITE (luScript,'(A7)') "s/s/t-s"  !solve/set/time-step
!WRITE (luScript,'(A1)') "30"       !Time Step Size
      !WRITE (luScript,'(A3)') "s/d"      !Solve/dual time
!WRITE (luScript,'(A2)') "18"        !Physical time steps (time=10 min)
      !WRITE (luScript,'(A)') " "        !Max number of time steps

```

```

!WRITE (luScript,'(A7)') "s/s/t-s" !solve/set/time-step
!WRITE (luScript,'(A4)') "0.01" !Time Step Size
    WRITE (luScript,'(A5)') "f/wcd" !File/Write case-data"
    WRITE (luScript,'(A)') " " !case/data file name ["pcmtank.cas"]
WRITE (luScript,'(A3)') "yes" !Overwrite?
WRITE (luScript,'(A7)') "plo/plo" !Plot/plot
WRITE (luScript,'(A3)') "yes" !Plot node values?
WRITE (luScript,'(A20)') resultsFileName !Filename
WRITE (luScript,'(A3)') "yes" !Order Points?
WRITE (luScript,'(A3)') "yes" !Y Axis direction vector?
WRITE (luScript,'(A1)') "0" !IX
WRITE (luScript,'(A1)') "1" !IY
WRITE (luScript,'(A1)') "0" !IZ
WRITE (luScript,'(A2)') "no" !X Axis direction vector? [no]
WRITE (luScript,'(A2)') "no" !X Axis curve length? [no]
WRITE (luScript,'(A1)') "m" !Domain - Mixture
WRITE (luScript,'(A11)') "temperature" !Cell Function - total-temperature
WRITE (luScript,'(A9)') "tc-outlet" !Surface id/name
WRITE (luScript,'(A10)') "tc-midtank" !Surface id/name
WRITE (luScript,'(A)') "" !Surface 2
    WRITE (luScript,'(A4)') "exit"

```

END SUBROUTINE UPDATEBOUNDARY

!-----

SUBROUTINE READ\_FLUENT\_RESULTS (luResults,Nresults,results)

USE TrnsysConstants

IMPLICIT NONE

INTEGER, INTENT(in) :: luResults, Nresults

DOUBLE PRECISION, INTENT(out) :: results

DIMENSION results(Nresults)

CHARACTER (len=maxPathLength) :: textLine

```
        READ (luResults,'(A)') textLine  !(title "Total Temperature (mixture) ")
        READ (luResults,'(A)') textLine  !(labels "Total Temperature (mixture) "
"Position")
        READ (luResults,'(A)') textLine  !
        READ (luResults,'(A)') textLine  !((xy/key/label "outlet")
!READ (luResults,'(A)') textLine  !((Ignore 1st line)
        READ (luResults,*) results(1)    !303.15      0.394
        READ (luResults,'(A)') textLine  !((Ignore 1st line)
        READ (luResults,'(A)') textLine  !((Ignore 1st line)
        READ (luResults,'(A)') textLine  !((Ignore 1st line)
        READ (luResults,*) results(2)    !303.15      0.394
END SUBROUTINE READ_FLUENT_RESULTS
```

END SUBROUTINE TYPE101

***TRNSYS Setup Description***

VERSION 17

\*\*\*\*\*

\*\*\*\*\*

\*\*\* TRNSYS input file (deck) generated by TrnsysStudio  
\*\*\* on Monday, March 27, 2017 at 21:40  
\*\*\* from TrnsysStudio project: C:\Trnsys17\MyProjects\WithPCM\WithPCM.tpf  
\*\*\*

\*\*\* If you edit this file, use the File/Import TRNSYS Input File function in  
\*\*\* TrnsysStudio to update the project.

\*\*\*

\*\*\* If you have problems, questions or suggestions please contact your local  
\*\*\* TRNSYS distributor or <mailto:software@cstb.fr>

\*\*\*

\*\*\*\*\*

\*\*\*\*\*

\*\*\*\*\*

\*\*\*\*\*

\*\*\* Units

\*\*\*\*\*

\*\*\*\*\*

\*\*\*\*\*

\*\*\*\*\*

\*\*\* Control cards

\*\*\*\*\*

\*\*\*\*\*

\* START, STOP and STEP

CONSTANTS 3

START=5760

STOP=5784

STEP=0.083333331



```

SIMULATION      START      STOP STEP ! Start time      End time      Time
step
TOLERANCES 0.001 0.001          ! Integration      Convergence
LIMITS 3000 5000000 5000          ! Max iterations      Max
warnings      Trace limit
DFQ 1          ! TRNSYS numerical integration solver method
WIDTH 80      ! TRNSYS output file width, number of characters
LIST          ! NOLIST statement
              ! MAP statement
SOLVER 0 1 1          ! Solver statement      Minimum relaxation
factor Maximum relaxation factor
NAN_CHECK 0          ! Nan DEBUG statement
OVERWRITE_CHECK 0          ! Overwrite DEBUG statement
TIME_REPORT 0          ! disable time report
EQSOLVER 0          ! EQUATION SOLVER statement
* User defined CONSTANTS

* Model "Solar evacuated heat pipe" (Type 71)
*

UNIT 2 TYPE 71      Solar evacuated heat pipe
*$UNIT_NAME Solar evacuated heat pipe
*$MODEL .\Solar Thermal Collectors\Evacuated Tube Collector\Type71.tmf
*$POSITION 114 518
*$LAYER Main #
PARAMETERS 11
1          ! 1 Number in series
5          ! 2 Collector area
4.035     ! 3 Fluid specific heat
1          ! 4 Efficiency mode
3.0       ! 5 Flow rate at test conditions
0.7       ! 6 Intercept efficiency
10        ! 7 Negative of first order efficiency coefficient

```

```

0.03      ! 8 Negative of second order efficiency coefficient
57        ! 9 Logical unit of file containing biaxial IAM data
5         ! 10 Number of longitudinal angles for which IAMs are provided
5         ! 11 Number of transverse angles for which IAMs are provided
INPUTS 10
4,1       ! source side pump:Outlet fluid temperature ->Inlet temperature
4,2       ! source side pump:Outlet flow rate ->Inlet flowrate
23,1      ! Type99-2:Ambient temperature ->Ambient temperature
23,18     ! Type99-2:total radiation on tilted surface ->Incident radiation
23,18     ! Type99-2:total radiation on tilted surface ->Incident diffuse radiation
23,16     ! Type99-2:angle of incidence on horizontal surface ->Solar incidence
angle
23,10     ! Type99-2:solar zenith angle ->Solar zenith angle
23,11     ! Type99-2:solar azimuth angle ->Solar azimuth angle
0,0       ! [unconnected] Collector slope
0,0       ! [unconnected] Collector azimuth
*** INITIAL INPUT VALUES
20.0 360 10.0 2160 2160 0.0 0.0 0.0 52 0
*** External files
ASSIGN "C:\Trnsys17\Examples\Data Files\Type71-EvacuatedTubeSolarCollector-
IAMData.dat" 57
*|? What file contains the 2D IAM data? |1000
*-----

* Model "Flow diverter-2" (Type 11)
*

UNIT 3 TYPE 11      Flow diverter-2
*$UNIT_NAME Flow diverter-2
*$MODEL .\Hydronics\Flow Diverter\Other Fluids\Type11f.tmf
*$POSITION 639 432
*$LAYER Main #

PARAMETERS 1
2             ! 1 Controlled flow diverter mode

```

INPUTS 3

11,1 ! Type31:Outlet temperature ->Inlet temperature

11,2 ! Type31:Outlet flow rate ->Inlet flow rate

MIXERsignal ! Equa:MIXERsignal ->Control signal

\*\*\* INITIAL INPUT VALUES

20.0 360 0

\*-----

\* Model "source side pump" (Type 114)

\*

UNIT 4 TYPE 114 source side pump

\*\$UNIT\_NAME source side pump

\*\$MODEL .\Hydronics\Pumps\Single Speed\Type114.tmf

\*\$POSITION 113 667

\*\$LAYER Main #

\*\$# SINGLE-SPEED PUMP

PARAMETERS 4

360 ! 1 Rated flow rate

4.035 ! 2 Fluid specific heat

216 ! 3 Rated power

0.0 ! 4 Motor heat loss fraction

INPUTS 5

12,1 ! Type31-2:Outlet temperature ->Inlet fluid temperature

12,2 ! Type31-2:Outlet flow rate ->Inlet fluid flow rate

SourcePumpSignal ! Equa:SourcePumpSignal ->Control signal

0,0 ! [unconnected] Overall pump efficiency

0,0 ! [unconnected] Motor efficiency

\*\*\* INITIAL INPUT VALUES

20.0 0.0 1.0 0.6 0.9

\*-----

\* Model "Thermal storage tank" (Type 60)

\*

UNIT 5 TYPE 60 Thermal storage tank

\*\$UNIT\_NAME Thermal storage tank

\*\$MODEL .\Thermal Storage\Detailed Fluid Storage Tank\Vertical Cylinder\Uniform  
Losses and Node Heights\1 Inlet, 1 Outlet\Type60d.tmf

\*\$POSITION 1113 446

\*\$LAYER Main #

PARAMETERS 56

2 ! 1 User-specified inlet positions  
0.3 ! 2 Tank volume  
2.032 ! 3 Tank height  
-1 ! 4 Tank perimeter  
0.1 ! 5 Height of flow inlet 1  
2.03 ! 6 Height of flow outlet 1  
-1 ! 7 Not used (inlet 2)  
-1 ! 8 Not used (outlet 2)  
4.190 ! 9 Fluid specific heat  
1000.0 ! 10 Fluid density  
1 ! 11 Tank loss coefficient  
2.16 ! 12 Fluid thermal conductivity  
0 ! 13 Destratification conductivity  
100.0 ! 14 Boiling temperature  
2 ! 15 Auxiliary heater mode  
1.0 ! 16 Height of 1st aux. heater  
1.25 ! 17 Height of 1st thermostat  
0 ! 18 Set point temperature for element 1  
0 ! 19 Deadband for heating element 1  
0 ! 20 Maximum heating rate of element 1  
1 ! 21 Height of heating element 2  
1 ! 22 Height of thermostat 2  
0 ! 23 Set point temperature for element 2  
5.0 ! 24 Deadband for heating element 2  
0 ! 25 Maximum heating rate of element 2  
0.0 ! 26 Overall loss coefficient for gas flue

20.0	! 27 Flue temperature
6	! 28 Fraction of critical timestep
0	! 29 Gas heater?
2	! 30 Number of internal heat exchangers
0	! 31 Equal sized nodes
0	! 32 Uniform tank losses
2	! 33 HX Fluid Indicator-1
0.7	! 34 Fraction of glycol-1
0.02	! 35 Heat exchanger inside diameter-1
0.022	! 36 Heat exchanger outside diameter-1
0.044	! 37 Heat exchanger fin diameter-1
0.878	! 38 Total surface area of heat exchanger-1
50	! 39 Fins per meter for heat exchanger-1
10	! 40 Heat exchanger length-1
500	! 41 Heat exchanger wall conductivity-1
500	! 42 Heat exchanger material conductivity-1
1.2	! 43 Height of heat exchanger inlet-1
1.2	! 44 Height of heat exchanger outlet-1
2	! 45 HX Fluid Indicator-2
0.7	! 46 Fraction of glycol-2
0.02	! 47 Heat exchanger inside diameter-2
0.022	! 48 Heat exchanger outside diameter-2
0.044	! 49 Heat exchanger fin diameter-2
0.878	! 50 Total surface area of heat exchanger-2
50	! 51 Fins per meter for heat exchanger-2
10	! 52 Heat exchanger length-2
500	! 53 Heat exchanger wall conductivity-2
500	! 54 Heat exchanger material conductivity-2
0.4	! 55 Height of heat exchanger inlet-2
0.4	! 56 Height of heat exchanger outlet-2
INPUTS 17	
10,1	! Type14b:Average water draw ->Flow rate at inlet 1
0,0	! [unconnected] Flow rate at outlet 1
0,0	! [unconnected] Not used (flow inlet 2)

0,0 ! [unconnected] Not used (flow outlet 2)  
0,0 ! [unconnected] Temperature at inlet 1  
0,0 ! [unconnected] Not used (temp inlet 2)  
23,1 ! Type99-2:Ambient temperature ->Environment temperature  
0,0 ! [unconnected] Control signal for element 1  
0,0 ! [unconnected] Control signal for element 2  
3,2 ! Flow diverter-2:Flow rate at outlet 1 ->Flow rate for heat exchanger -1  
3,1 ! Flow diverter-2:Temperature at outlet 1 ->Inlet temperature for heat  
exchanger -1  
0,0 ! [unconnected] Nusselt constant for heat exchanger-1  
0,0 ! [unconnected] Nusselt exponent for heat exchanger-1  
20,4 ! Type66c:Output-4 ->Flow rate for heat exchanger -2  
20,3 ! Type66c:Output-3 ->Inlet temperature for heat exchanger -2  
0,0 ! [unconnected] Nusselt constant for heat exchanger-2  
0,0 ! [unconnected] Nusselt exponent for heat exchanger-2  
\*\*\* INITIAL INPUT VALUES  
50.000399 -2 -1 -1 20.0 20.0 22.0 0 0 360 20.0 0.50 0.25 828 20.0 0.50 0.25  
DERIVATIVES 51  
55 ! 1 Initial temperature of node-1  
55 ! 2 Initial temperature of node-2  
55 ! 3 Initial temperature of node-3  
55 ! 4 Initial temperature of node-4  
55 ! 5 Initial temperature of node-5  
55 ! 6 Initial temperature of node-6  
55 ! 7 Initial temperature of node-7  
55 ! 8 Initial temperature of node-8  
55 ! 9 Initial temperature of node-9  
55 ! 10 Initial temperature of node-10  
55 ! 11 Initial temperature of node-11  
55 ! 12 Initial temperature of node-12  
55 ! 13 Initial temperature of node-13  
55 ! 14 Initial temperature of node-14  
55 ! 15 Initial temperature of node-15  
55 ! 16 Initial temperature of node-16

55	! 17 Initial temperature of node-17
55	! 18 Initial temperature of node-18
55	! 19 Initial temperature of node-19
55	! 20 Initial temperature of node-20
55	! 21 Initial temperature of node-21
55	! 22 Initial temperature of node-22
55	! 23 Initial temperature of node-23
55	! 24 Initial temperature of node-24
55	! 25 Initial temperature of node-25
55	! 26 Initial temperature of node-26
55	! 27 Initial temperature of node-27
55	! 28 Initial temperature of node-28
55	! 29 Initial temperature of node-29
55	! 30 Initial temperature of node-30
55	! 31 Initial temperature of node-31
55	! 32 Initial temperature of node-32
55	! 33 Initial temperature of node-33
55	! 34 Initial temperature of node-34
55	! 35 Initial temperature of node-35
55	! 36 Initial temperature of node-36
55	! 37 Initial temperature of node-37
55	! 38 Initial temperature of node-38
55	! 39 Initial temperature of node-39
55	! 40 Initial temperature of node-40
55	! 41 Initial temperature of node-41
55	! 42 Initial temperature of node-42
55	! 43 Initial temperature of node-43
55	! 44 Initial temperature of node-44
55	! 45 Initial temperature of node-45
55	! 46 Initial temperature of node-46
55	! 47 Initial temperature of node-47
55	! 48 Initial temperature of node-48
55	! 49 Initial temperature of node-49
55	! 50 Initial temperature of node-50

55 ! 51 Initial temperature of node-51

\*-----

\* Model "load side pump" (Type 114)

\*

UNIT 6 TYPE 114 load side pump

\*\$UNIT\_NAME load side pump

\*\$MODEL .\Hydronics\Pumps\Single Speed\Type114.tmf

\*\$POSITION 1003 603

\*\$LAYER Main #

\*\$# SINGLE-SPEED PUMP

PARAMETERS 4

828 ! 1 Rated flow rate

4.035 ! 2 Fluid specific heat

216 ! 3 Rated power

0.0 ! 4 Motor heat loss fraction

INPUTS 5

5,28 ! Thermal storage tank:Temperature of fluid exiting heat exchanger -2 -

>Inlet fluid temperature

0,0 ! [unconnected] Inlet fluid flow rate

HPSignal ! Equa:HPSignal ->Control signal

0,0 ! [unconnected] Overall pump efficiency

0,0 ! [unconnected] Motor efficiency

\*\*\* INITIAL INPUT VALUES

20.0 0.0 0 0.6 0.9

\*-----

\* Model "Type2d" (Type 2)

\*

UNIT 7 TYPE 2 Type2d

\*\$UNIT\_NAME Type2d



\*\$MODEL .\Controllers\Differential Controller w\_ Hysteresis\generic\Solver 0  
(Successive Substitution) Control Strategy\Type2d.tmf

\*\$POSITION 607 95

\*\$LAYER Main #

\*\$# NOTE: This controller can only be used with Solver 0 (Successive substitution)

\*\$#

\*\$#

\*\$#

\*\$#

\*\$#

\*\$#

\*\$#

\*\$#

\*\$#

PARAMETERS 2

5 ! 1 No. of oscillations

100.0 ! 2 High limit cut-out

INPUTS 6

0,0 ! [unconnected] Upper input value

5,48 ! Thermal storage tank:Temperature of node 1+-15 ->Lower input value

5,48 ! Thermal storage tank:Temperature of node 1+-15 ->Monitoring value

7,1 ! Type2d:Output control function ->Input control function

0,0 ! [unconnected] Upper dead band

0,0 ! [unconnected] Lower dead band

\*\*\* INITIAL INPUT VALUES

57 10.0 20.0 0 4 0

\*-----

\* Model "Type11d" (Type 11)

\*

UNIT 8 TYPE 11 Type11d

\*\$UNIT\_NAME Type11d

\*\$MODEL .\Hydronics\Flow Mixer\Other Fluids\Type11d.tmf

```

*$POSITION 714 688
*$LAYER Main #
PARAMETERS 1
3          ! 1 Controlled flow mixer mode
INPUTS 5
5,23      ! Thermal storage tank:Temperature of fluid exiting heat exchanger -1 -
>Temperature at inlet 1
0,0       ! [unconnected] Flow rate at inlet 1
20,1      ! Type66c:Output-1 ->Temperature at inlet 2
20,2      ! Type66c:Output-2 ->Flow rate at inlet 2
MIXERsignal      ! Equa:MIXERsignal ->Control signal
*** INITIAL INPUT VALUES
20.0 360 20.0 360 0
*-----

* Model "Type65d" (Type 65)
*

UNIT 9 TYPE 65      Type65d
*$UNIT_NAME Type65d
*$MODEL .\Output\Online Plotter\Online Plotter Without File\Type65d.tmf
*$POSITION 298 816
*$LAYER Main #
PARAMETERS 12
8          ! 1 Nb. of left-axis variables
0          ! 2 Nb. of right-axis variables
-30       ! 3 Left axis minimum
100       ! 4 Left axis maximum
0.0       ! 5 Right axis minimum
1000.0    ! 6 Right axis maximum
1         ! 7 Number of plots per simulation
12        ! 8 X-axis gridpoints
0         ! 9 Shut off Online w/o removing
-1        ! 10 Logical unit for output file

```

```
0          ! 11 Output file units
0          ! 12 Output file delimiter
INPUTS 8
2,1       ! Solar evacuated heat pipe:Outlet temperature ->Left axis variable-1
4,1       ! source side pump:Outlet fluid temperature ->Left axis variable-2
5,17      ! Thermal storage tank:Average tank temperature ->Left axis variable-3
20,1      ! Type66c:Output-1 ->Left axis variable-4
20,3      ! Type66c:Output-3 ->Left axis variable-5
5,5       ! Thermal storage tank:Temperature of outlet flow 1 ->Left axis variable-
6
23,1      ! Type99-2:Ambient temperature ->Left axis variable-7
3,3       ! Flow diverter-2:Temperature at outlet 2 ->Left axis variable-8
*** INITIAL INPUT VALUES
CollOutTemp CollInTemp AveTankTemp SourceOUTLET LoadTemp
OutletTankOutletTemp
AmbTemp SourceINLET
LABELS 3
"Temperatures"
"Heat transfer rates"
"Graph 1"
*-----
* Model "Type14b" (Type 14)
*
UNIT 10 TYPE 14   Type14b
*$UNIT_NAME Type14b
*$MODEL .\Utility\Forcing Functions\Water Draw\Type14b.tmf
*$POSITION 810 827
*$LAYER Main #
PARAMETERS 40
0          ! 1 Initial value of time
0          ! 2 Initial value of function
6          ! 3 Time at point
```

10	! 4 Value at point
7	! 5 Time at point
42	! 6 Value at point
8	! 7 Time at point
60	! 8 Value at point
9	! 9 Time at point
62	! 10 Value at point
10	! 11 Time at point
40	! 12 Value at point
11	! 13 Time at point
30	! 14 Value at point
12	! 15 Time at point
20	! 16 Value at point
13	! 17 Time at point
15	! 18 Value at point
14	! 19 Time at point
15	! 20 Value at point
15	! 21 Time at point
20	! 22 Value at point
16	! 23 Time at point
25	! 24 Value at point
17	! 25 Time at point
40	! 26 Value at point
18	! 27 Time at point
50	! 28 Value at point
19	! 29 Time at point
55	! 30 Value at point
20	! 31 Time at point
55	! 32 Value at point
21	! 33 Time at point
40	! 34 Value at point
22	! 35 Time at point
20	! 36 Value at point
23	! 37 Time at point

20 ! 38 Value at point  
24 ! 39 Time at point  
0 ! 40 Value at point

\*-----

\* Model "Type31" (Type 31)

\*

UNIT 11 TYPE 31 Type31

\*\$UNIT\_NAME Type31

\*\$MODEL .\Hydronics\Pipe\_Duct\Type31.tmf

\*\$POSITION 539 432

\*\$LAYER Main #

PARAMETERS 6

0.02 ! 1 Inside diameter

25 ! 2 Pipe length

3.0 ! 3 Loss coefficient

1000.0 ! 4 Fluid density

4.190 ! 5 Fluid specific heat

10.0 ! 6 Initial fluid temperature

INPUTS 3

C1 ! Equa-2:C1 ->Inlet temperature

13,2 ! Type1 1h:Outlet flow rate ->Inlet flow rate

0,0 ! [unconnected] Environment temperature

\*\*\* INITIAL INPUT VALUES

10.0 100.0 10.0

\*-----

\* Model "Type31-2" (Type 31)

\*

UNIT 12 TYPE 31 Type31-2

\*\$UNIT\_NAME Type31-2

\*\$MODEL .\Hydronics\Pipe\_Duct\Type31.tmf

\*\$POSITION 488 688

\*\$LAYER Main #

PARAMETERS 6

0.02 ! 1 Inside diameter

25 ! 2 Pipe length

3.0 ! 3 Loss coefficient

1000.0 ! 4 Fluid density

4.190 ! 5 Fluid specific heat

10.0 ! 6 Initial fluid temperature

INPUTS 3

8,1 ! Type11d:Outlet temperature ->Inlet temperature

8,2 ! Type11d:Outlet flow rate ->Inlet flow rate

0,0 ! [unconnected] Environment temperature

\*\*\* INITIAL INPUT VALUES

10.0 100.0 10.0

\*-----

\* Model "Type11h" (Type 11)

\*

UNIT 13 TYPE 11 Type11h

\*\$UNIT\_NAME Type11h

\*\$MODEL .\Hydraulics\Tee-Piece\Other Fluids\Type11h.tmf

\*\$POSITION 276 432

\*\$LAYER Main #

PARAMETERS 1

1 ! 1 Tee piece mode

INPUTS 4

14,1 ! Type11f:Temperature at outlet 1 ->Temperature at inlet 1

14,2 ! Type11f:Flow rate at outlet 1 ->Flow rate at inlet 1

19,1 ! Type6:Outlet fluid temperature ->Temperature at inlet 2

19,2 ! Type6:Outlet fluid flow rate ->Flow rate at inlet 2

\*\*\* INITIAL INPUT VALUES

20.0 100.0 20.0 100.0

\*-----

\* Model "Type11f" (Type 11)

\*

UNIT 14 TYPE 11    Type11f

\*\$UNIT\_NAME Type11f

\*\$MODEL .\Hydronics\Flow Diverter\Other Fluids\Type11f.tmf

\*\$POSITION 146 432

\*\$LAYER Main #

PARAMETERS 1

2                    ! 1 Controlled flow diverter mode

INPUTS 3

2,1                ! Solar evacuated heat pipe:Outlet temperature ->Inlet temperature

2,2                ! Solar evacuated heat pipe:Outlet flowrate ->Inlet flow rate

CoolerSignal        ! Equa:CoolerSignal ->Control signal

\*\*\* INITIAL INPUT VALUES

20.0 100.0 0

\*-----

\* Model "Type2d-2" (Type 2)

\*

UNIT 15 TYPE 2     Type2d-2

\*\$UNIT\_NAME Type2d-2

\*\$MODEL .\Controllers\Differential Controller w\_ Hysteresis\generic\Solver 0  
(Successive Substitution) Control Strategy\Type2d.tmf

\*\$POSITION 395 106

\*\$LAYER Main #

\*\$# NOTE: This controller can only be used with Solver 0 (Successive substitution)

\*\$#

\*\$#

\*\$#

\*\$#

\*\$#

\*\$#

\*\$#

\*\$#

\*\$#

PARAMETERS 2

5 ! 1 No. of oscillations

50000 ! 2 High limit cut-out

INPUTS 6

0,0 ! [unconnected] Upper input value

23,19 ! Type99-2:beam radiation on tilted surface ->Lower input value

23,19 ! Type99-2:beam radiation on tilted surface ->Monitoring value

15,1 ! Type2d-2:Output control function ->Input control function

0,0 ! [unconnected] Upper dead band

0,0 ! [unconnected] Lower dead band

\*\*\* INITIAL INPUT VALUES

2160 10.0 20.0 0 360 0

\*-----

\* EQUATIONS "Equa"

\*

EQUATIONS 10

HeatPumpOn = eql([15,1],0)

HPSignal = and([15,1],[7,1])

CoolerDemand = and([17,1],[7,1])

CoolerSignal = and([26,1],CoolerDemand)

NOTcolloutlet = not([27,1])

NOTtankdemand = not([7,1])

PCMchargingcondition = and(NOTcolloutlet,NOTtankdemand)

PCMchargingSignal = PCMchargingcondition

MIXERsignal = or(PCMchargingSignal,HPSignal)

SourcePumpSignal = or([7,1],PCMchargingSignal)

\*\$UNIT\_NAME Equa

\*\$LAYER Main



\*\$POSITION 511 212

\*-----

\* Model "Type2d-3" (Type 2)

\*

UNIT 17 TYPE 2      Type2d-3

\*\$UNIT\_NAME Type2d-3

\*\$MODEL .\Controllers\Differential Controller w\_ Hysteresis\generic\Solver 0  
(Successive Substitution) Control Strategy\Type2d.tmf

\*\$POSITION 320 95

\*\$LAYER Main #

\*\$# NOTE: This controller can only be used with Solver 0 (Successive substitution)

\*\$#

\*\$#

\*\$#

\*\$#

\*\$#

\*\$#

\*\$#

\*\$#

\*\$#

PARAMETERS 2

5            ! 1 No. of oscillations

50000       ! 2 High limit cut-out

INPUTS 6

0,0         ! [unconnected] Upper input value

23,19       ! Type99-2:beam radiation on tilted surface ->Lower input value

23,19       ! Type99-2:beam radiation on tilted surface ->Monitoring value

17,1        ! Type2d-3:Output control function ->Input control function

0,0         ! [unconnected] Upper dead band

0,0         ! [unconnected] Lower dead band

\*\*\* INITIAL INPUT VALUES

900 10.0 20.0 0 360 0

\*-----

\* Model "Type25c" (Type 25)

\*

UNIT 18 TYPE 25    Type25c

\*\$UNIT\_NAME Type25c

\*\$MODEL .\Output\Printer\Unformatted\No Units\Type25c.tmf

\*\$POSITION 1078 106

\*\$LAYER Main #

PARAMETERS 10

STEP            ! 1 Printing interval

START           ! 2 Start time

STOP            ! 3 Stop time

58              ! 4 Logical unit

0               ! 5 Units printing mode

0               ! 6 Relative or absolute start time

-1              ! 7 Overwrite or Append

-1              ! 8 Print header

0               ! 9 Delimiter

1               ! 10 Print labels

INPUTS 19

20,1            ! Type66c:Output-1 ->Input to be printed-1

20,2            ! Type66c:Output-2 ->Input to be printed-2

20,3            ! Type66c:Output-3 ->Input to be printed-3

20,4            ! Type66c:Output-4 ->Input to be printed-4

20,5            ! Type66c:Output-5 ->Input to be printed-5

20,6            ! Type66c:Output-6 ->Input to be printed-6

20,7            ! Type66c:Output-7 ->Input to be printed-7

5,5             ! Thermal storage tank:Temperature of outlet flow 1 ->Input to be  
printed-8

5,27 ! Thermal storage tank:Energy input from heat exchanger -2 ->Input to be printed-9  
 C1 ! Equa-2:C1 ->Input to be printed-10  
 CoolerSignal ! Equa:CoolerSignal ->Input to be printed-11  
 PCMinSideC ! Equa-3:PCMinSideC ->Input to be printed-12  
 23,1 ! Type99-2:Ambient temperature ->Input to be printed-13  
 5,32 ! Thermal storage tank:Tank temperature - top ->Input to be printed-14  
 5,48 ! Thermal storage tank:Temperature of node 1+-15 ->Input to be printed-15  
 5,73 ! Thermal storage tank:Temperature of node 1+-40 ->Input to be printed-16  
 23,18 ! Type99-2:total radiation on tilted surface ->Input to be printed-17  
 3,3 ! Flow diverter-2:Temperature at outlet 2 ->Input to be printed-18  
 5,28 ! Thermal storage tank:Temperature of fluid exiting heat exchanger -2 ->Input to be printed-19

\*\*\* INITIAL INPUT VALUES

TempSourceOut MFsource TempLoadOut MFload COP Work Heating TempLoad  
 EnergyInputLoad PCMTemp Coolersignal PCMinTemp AmbTemp TempTankTop  
 TempTankMid TempTankBottom Irradiance TempSourceIN TempLoadIN

\*\*\* External files

ASSIGN "\*\*\*\*.out" 58

\*|? Output file for printed results |1000

\*-----

\* Model "Type6" (Type 6)

\*

UNIT 19 TYPE 6 Type6

\*\$UNIT\_NAME Type6

\*\$MODEL .\HVAC\Auxiliary Heaters\Type6.tmf

\*\$POSITION 196 315

\*\$LAYER Main #

PARAMETERS 4

35999.997336 ! 1 Maximum heating rate

4.19 ! 2 Specific heat of fluid  
0.0 ! 3 Overall loss coefficient for heater during operation  
1.0 ! 4 Efficiency of auxiliary heater  
INPUTS 5  
14,3 ! Type11f:Temperature at outlet 2 ->Inlet fluid temperature  
14,4 ! Type11f:Flow rate at outlet 2 ->Fluid mass flow rate  
CoolerSignal ! Equa:CoolerSignal ->Control Function  
23,1 ! Type99-2:Ambient temperature ->Set point temperature  
23,1 ! Type99-2:Ambient temperature ->Temperature of surroundings

\*\*\* INITIAL INPUT VALUES

20.0 100.0 1 60.0 20.0

\*-----

\* Model "Type66c" (Type 66)

\*

UNIT 20 TYPE 66 Type66c

\*\$UNIT\_NAME Type66c

\*\$MODEL .\Utility\Calling External Programs\EES\First Input is a Control Signal\Set  
Outputs to Predefined Values when OFF\Type66c.tmf

\*\$POSITION 830 486

\*\$LAYER Main #

PARAMETERS 11

2 ! 1 Input mode  
2 ! 2 Output mode  
10000 ! 3 Allowable wait  
7 ! 4 Number of outputs  
0 ! 5 Value when OFF for output-1  
0 ! 6 Value when OFF for output-2  
0 ! 7 Value when OFF for output-3  
0 ! 8 Value when OFF for output-4  
0 ! 9 Value when OFF for output-5  
0 ! 10 Value when OFF for output-6  
0 ! 11 Value when OFF for output-7

INPUTS 5

HPSignal           ! Equa:HPSignal ->Control signal  
 3,3               ! Flow diverter-2:Temperature at outlet 2 ->Input-1  
 3,4               ! Flow diverter-2:Flow rate at outlet 2 ->Input-2  
 6,1               ! load side pump:Outlet fluid temperature ->Input-3  
 6,2               ! load side pump:Outlet flow rate ->Input-4

\*\*\* INITIAL INPUT VALUES

1 0 0 0 0

LABELS 2 2

c:\EES32\ees.exe

HPFULL3.ees

\*-----

\* Model "Type65d-2" (Type 65)

\*

UNIT 21 TYPE 65    Type65d-2

\*\$UNIT\_NAME Type65d-2

\*\$MODEL .\Output\Online Plotter\Online Plotter Without File\Type65d.tmf

\*\$POSITION 448 816

\*\$LAYER Main #

PARAMETERS 12

2               ! 1 Nb. of left-axis variables  
 2               ! 2 Nb. of right-axis variables  
 0.0            ! 3 Left axis minimum  
 2               ! 4 Left axis maximum  
 0.0            ! 5 Right axis minimum  
 2               ! 6 Right axis maximum  
 1               ! 7 Number of plots per simulation  
 12             ! 8 X-axis gridpoints  
 0               ! 9 Shut off Online w/o removing  
 -1             ! 10 Logical unit for output file  
 0               ! 11 Output file units  
 0               ! 12 Output file delimiter

INPUTS 4

HPSignal ! Equa:HPSignal ->Left axis variable-1  
CoolerSignal ! Equa:CoolerSignal ->Left axis variable-2  
PCMchargingSignal ! Equa:PCMchargingSignal ->Right axis variable-1  
NOTcolloutlet ! Equa:NOTcolloutlet ->Right axis variable-2

\*\*\* INITIAL INPUT VALUES

HPSignal CoolerSignal PCMcharging NOTcolloutlet

LABELS 3

"Temperatures"

"Heat transfer rates"

"Graph 1"

\*-----

\* Model "Type65d-3" (Type 65)

\*

UNIT 22 TYPE 65 Type65d-3

\*\$UNIT\_NAME Type65d-3

\*\$MODEL .\Output\Online Plotter\Online Plotter Without File\Type65d.tmf

\*\$POSITION 149 816

\*\$LAYER Main #

PARAMETERS 12

2 ! 1 Nb. of left-axis variables  
2 ! 2 Nb. of right-axis variables  
0.0 ! 3 Left axis minimum  
1000.0 ! 4 Left axis maximum  
0.0 ! 5 Right axis minimum  
1000.0 ! 6 Right axis maximum  
1 ! 7 Number of plots per simulation  
12 ! 8 X-axis gridpoints  
0 ! 9 Shut off Online w/o removing  
-1 ! 10 Logical unit for output file  
0 ! 11 Output file units  
0 ! 12 Output file delimiter

INPUTS 4

23,18 ! Type99-2:total radiation on tilted surface ->Left axis variable-1  
23,19 ! Type99-2:beam radiation on tilted surface ->Left axis variable-2  
0,0 ! [unconnected] Right axis variable-1  
0,0 ! [unconnected] Right axis variable-2

\*\*\* INITIAL INPUT VALUES

Total Beam label label

LABELS 3

"Temperatures"

"Heat transfer rates"

"Graph 1"

\*-----

\* Model "Type99-2" (Type 99)

\*

UNIT 23 TYPE 99 Type99-2

\*\$UNIT\_NAME Type99-2

\*\$MODEL .\Weather Data Reading and Processing\User Format\Type99.tmf

\*\$POSITION 96 52

\*\$LAYER Main #

PARAMETERS 3

59 ! 1 Logical unit  
5 ! 2 Sky model for diffuse radiation  
1 ! 3 Tracking mode

INPUTS 3

0,0 ! [unconnected] Ground reflectance  
0,0 ! [unconnected] Slope of surface  
0,0 ! [unconnected] Azimuth of surface

\*\*\* INITIAL INPUT VALUES

0.2 0.0 0.0

\*\*\* External files

ASSIGN "C:\Trnsys17\Examples\Data Files\Type99-UserFormat-London.99" 59

\*|? Weather data file |1000

```
*-----  
  
* Model "Type101" (Type 101)  
*  
  
UNIT 24 TYPE 101  Type101  
*$UNIT_NAME Type101  
*$MODEL .\Utility\Calling External Programs\Fluent\Type101.tmf  
*$POSITION 385 415  
*$LAYER Main #  
PARAMETERS 4  
1          ! 1 Mode  
1          ! 2 Number of inputs  
2          ! 3 Number of outputs  
2          ! 4 Calling mode  
INPUTS 2  
SourcePumpSignal      ! Equa:SourcePumpSignal ->Control function  
13,1          ! Type11h:Outlet temperature ->Input  
*** INITIAL INPUT VALUES  
1 0  
LABELS 4  
"C:\Program Files\ANSYS Inc\v162\fluent\ntbin\win64\fluent.exe"  
"-r16.2.0 3d -i"  
"scriptFluent.in"  
"fluentResults.txt"  
*-----  
  
* EQUATIONS "Equa-2"  
*  
EQUATIONS 1  
C1 = [24,1]-273.15  
*$UNIT_NAME Equa-2  
*$LAYER Main  
*$POSITION 460 411
```



```
*-----  
  
* Model "Type2d-4" (Type 2)  
*  
  
UNIT 26 TYPE 2      Type2d-4  
*$UNIT_NAME Type2d-4  
*$MODEL .\Controllers\Differential Controller w_ Hysteresis\generic\Solver 0  
(Successive Substitution) Control Strategy\Type2d.tmf  
*$POSITION 747 95  
*$LAYER Main #  
*$# NOTE: This controller can only be used with Solver 0 (Successive substitution)  
*$#  
*$#  
*$#  
*$#  
*$#  
*$#  
*$#  
*$#  
*$#  
*$#  
*$#  
  
PARAMETERS 2  
5          ! 1 No. of oscillations  
100.0      ! 2 High limit cut-out  
  
INPUTS 6  
0,0        ! [unconnected] Upper input value  
PCMinsideC      ! Equa-3:PCMinsideC ->Lower input value  
PCMinsideC      ! Equa-3:PCMinsideC ->Monitoring value  
26,1        ! Type2d-4:Output control function ->Input control function  
0,0         ! [unconnected] Upper dead band  
0,0         ! [unconnected] Lower dead band  
  
*** INITIAL INPUT VALUES
```

18 10.0 20.0 0 2 0

\*-----

\* Model "Type2d-5" (Type 2)

\*

UNIT 27 TYPE 2      Type2d-5

\*\$UNIT\_NAME Type2d-5

\*\$MODEL .\Controllers\Differential Controller w\_ Hysteresis\generic\Solver 0  
(Successive Substitution) Control Strategy\Type2d.tmf

\*\$POSITION 181 95

\*\$LAYER Main #

\*\$# NOTE: This controller can only be used with Solver 0 (Successive substitution)

\*\$#

\*\$#

\*\$#

\*\$#

\*\$#

\*\$#

\*\$#

\*\$#

\*\$#

PARAMETERS 2

5            ! 1 No. of oscillations

100.0       ! 2 High limit cut-out

INPUTS 6

0,0            ! [unconnected] Upper input value

2,1            ! Solar evacuated heat pipe:Outlet temperature ->Lower input value

2,1            ! Solar evacuated heat pipe:Outlet temperature ->Monitoring value

27,1           ! Type2d-5:Output control function ->Input control function

0,0            ! [unconnected] Upper dead band

0,0            ! [unconnected] Lower dead band

\*\*\* INITIAL INPUT VALUES

30 10.0 20.0 0 4 0

```
*-----  
  
* Model "Type2d-6" (Type 2)  
*  
  
UNIT 28 TYPE 2      Type2d-6  
*$UNIT_NAME Type2d-6  
*$MODEL .\Controllers\Differential Controller w_ Hysteresis\generic\Solver 0  
(Successive Substitution) Control Strategy\Type2d.tmf  
*$POSITION 843 95  
*$LAYER Main #  
*$# NOTE: This controller can only be used with Solver 0 (Successive substitution)  
*$#  
*$#  
*$#  
*$#  
*$#  
*$#  
*$#  
*$#  
*$#  
*$#  
  
PARAMETERS 2  
5          ! 1 No. of oscillations  
100.0      ! 2 High limit cut-out  
  
INPUTS 6  
0,0        ! [unconnected] Upper input value  
PCMinsideC      ! Equa-3:PCMinsideC ->Lower input value  
PCMinsideC      ! Equa-3:PCMinsideC ->Monitoring value  
28,1        ! Type2d-6:Output control function ->Input control function  
0,0         ! [unconnected] Upper dead band  
0,0         ! [unconnected] Lower dead band  
  
*** INITIAL INPUT VALUES  
20 10.0 20.0 0 2 0  
  
*-----
```

\* EQUATIONS "Equa-3"

\*

EQUATIONS 1

PCMinsideC = [24,2]-273.15

\*\$UNIT\_NAME Equa-3

\*\$LAYER Main

\*\$POSITION 479 330

\*-----

END